

## Digital Information Processing in Molecular Systems

Konrad Szaci#owski

*Chem. Rev.*, **2008**, 108 (9), 3481-3548 • DOI: 10.1021/cr068403q • Publication Date (Web): 27 June 2008

Downloaded from <http://pubs.acs.org> on December 24, 2008

### More About This Article

---

Additional resources and features associated with this article are available within the HTML version:

- Supporting Information
- Links to the 1 articles that cite this article, as of the time of this article download
- Access to high resolution figures
- Links to articles and content related to this article
- Copyright permission to reproduce figures and/or text from this article

[View the Full Text HTML](#)



ACS Publications  
High quality. High impact.

# Digital Information Processing in Molecular Systems

Konrad Szaciłowski\*

Uniwersytet Jagielloński, Wydział Chemii, ul. Romana Ingardena 3, 30-060 Kraków, Poland

Received November 8, 2007

## Contents

1. Introduction	3481
2. Boolean Logic and Logic Gates	3482
2.1. Basic Concepts of Boolean Logic	3483
2.2. One Input Logic Gates	3484
2.3. Multiple Input Logic Gates	3484
2.4. Combinatorial Logic Systems	3485
3. Molecular Logic Gates: Basic Concepts	3486
4. Simple Molecular Switches	3488
4.1. Chemically Driven Molecular Switches	3488
4.2. Light Driven Molecular Switches	3495
4.3. Redox Driven Molecular Switches	3502
4.4. Magnetic Switches	3503
4.5. Multistate Molecular Switches	3505
5. Two Input Chemical Logic Gates	3506
5.1. All-Chemical Logic Gates	3507
5.1.1. OR Gates	3507
5.1.2. AND Gates	3507
5.1.3. XOR Gates	3509
5.1.4. INH Gates	3511
5.1.5. Inverted Logic Gates (NOR, NAND, and XNOR)	3512
5.1.6. Reconfigurable and Superimposed Molecular Logic Devices	3514
5.2. All-Optical Logic Gates	3515
5.3. Electrochemical and Photoelectrochemical Logic Gates and Devices	3517
6. Combinatorial Logic Systems	3522
6.1. Multiple-Input Logic Gates	3522
6.2. Concatenated Chemical Logic Systems	3523
7. Molecular Arithmetic Systems	3527
7.1. Molecular-Scale Half-Adders	3528
7.1.1. Chemically Driven Molecular Half-Adders	3528
7.1.2. Optically Driven Molecular Half-Adders	3528
7.1.3. Mixed Signal Molecular Half-Adders	3530
7.2. Molecular-Scale Half-Subtractors	3531
7.3. Molecular-Scale Full Adders and Full Subtractors: Toward Arithmetical Processors	3532
8. Logic Devices Based on Biomolecules and Biosystems	3533
8.1. Boolean Processes in Natural Biosystems	3533
8.2. Protein-Based Molecular Logic Systems and Devices	3534
8.3. Nucleic Acid-Based Molecular Logic Systems	3536
9. Concluding Remarks	3541
10. List of Abbreviations	3541

11. Acknowledgments	3542
12. Note Added after ASAP Publication	3542
13. References	3542

## 1. Introduction

Digital electronics is so widely used in everyday life that it is almost impossible to find an electric device that does not make use of digital electronic components. On average, 85% of the circuitry in all the electronic devices is digital and only 15% is analog.<sup>1</sup> Due to the ease of construction, resistance to interference, and low cost, more and more electronic systems become digitalized. In digital systems, information is contained in series of zeros and ones, represented usually as low and high voltages (Figures 1a and 2), while in analog systems, the whole continuum of states must be considered (Figure 1b). Therefore, in contrast to analog systems, information processing in digital systems is straightforward and based on very simple principles of Boolean logic (vide infra).<sup>2</sup>

Digital systems are much less sensitive to any interference due to wide margins of allowed signal values (Figure 2a) resulting in turn from highly nonlinear characteristics. Any real digital device is characterized by signal rise time and signal fall time (Figure 2c). These times limit the rate of information processing, as the pulse duration (time required for one binary operation) cannot be shorter than the rise (or fall) time.

Currently used computers and other electronic digital devices are based on monolithic semiconductor structures fabricated on the surface of silicon wafers.<sup>3–7</sup> All these devices use binary logic for information transmission, processing, and storage, and utilize electric signals as information carriers. All the information is encoded in series of zeros and ones, represented as low and high potential values. Logic gates are basic elements processing information: they function as switches whose output (0 or 1) depends on input conditions. The development of these devices can be described using the empirical rule, also as known Moore's Law. It predicts that the economically feasible number of transistors per microchip (and hence the device performance) doubles every 18 months.<sup>8</sup> The increase of performance of any electronic device cannot proceed infinitely due to fundamental and technological barriers. The latter can be overcome by application of new materials (e.g., molecular wires<sup>9–13</sup> and other supramolecular  $\pi$ -conjugated systems,<sup>13–17</sup> functional dendrimers,<sup>18–22</sup> polymers<sup>21–27</sup> and other molecular materials of unusual electric properties,<sup>27–33</sup> nanoparticles,<sup>34–44</sup> nanotubes and nanowires,<sup>45–56</sup> and superconductors<sup>57–59</sup>), nanolithography and new surface patterning technologies,<sup>56,60–71</sup> new circuitry design,<sup>72–76</sup> utilization of electron spin as information carrier,<sup>77–84</sup> quantum effects<sup>85–90</sup> and so forth,

\* Corresponding author. Tel: +48 12 663 2208. Fax: +48 12 634 0515. E-mail: szacilow@chemia.uj.edu.pl.



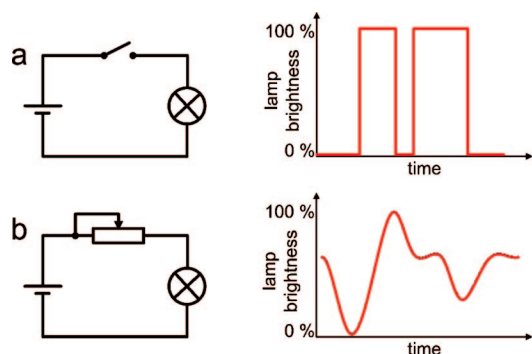
Konrad Szaciłowski was born in Kraków, Poland in 1971. He graduated from Jagiellonian University (Kraków) in 1995 (M.Sc., in cooperation with Professor Horst Kisch, Erlangen, Germany) and 2000 (Ph.D.) under the guidance of Professor Zofia Stasicka. He studied homogeneous catalysis with Professor Karl Anker Jørgensen (Århus, Denmark), EPR and NMR spectroscopy of iron nitrosyls with Professor Orazio Traverso (Ferrara, Italy), chemistry of molybdenum-sulfur clusters with Professor Michele Aresta (Bari, Italy), and high-pressure electrochemistry with Professor Rudi van Eldik (Erlangen, Germany). He spent one year with Professor John F. Endicott (Wayne State University, Detroit, USA) as a postdoc fellow working on synthesis, spectroscopy, magnetic properties, and electrochemistry of nickel complexes with macrocyclic ligands. Now, he is a member of Photochemistry of Coordination Compounds and Bioinorganic Chemistry Group, Centre for Inorganic Nanochemistry "nanolnchem", and Molecular Nanoelectronics Research Network "NanoMol". His research interests are focused mainly on surface engineering of nanocrystalline materials, microwave-assisted synthesis and (photo)electrochemistry of wide band gap semiconductors, information processing at the molecular level, and molecular nanoelectronics. Furthermore, he recently got involved in detailed spectroscopic investigations of doped chalcogenide semiconductors and quantum-chemical modeling of semiconductor nanoparticles.

while the fundamental limits define the ultimate computer performance.<sup>91–93</sup>

The fundamental limits of electronic device performance results from physical principles of quantum mechanics, thermodynamics, and electromagnetism. The basic factors describing the performance of any device are the time and the energy required for basic logic operation (Figure 3). The Heisenberg uncertainty principle imposes a fundamental limit on the performance of any logic gate (or other computing device). This principle states that the energy of a state with a lifetime of  $\Delta t$  can only be determined with a precision of  $\Delta E$  (eq 1).<sup>94</sup>

$$\Delta E \geq \frac{h}{\Delta t} \quad (1)$$

It also means that the quantum state with the  $\Delta E$  energy spread requires the time of  $\Delta t$  to evolve into an orthogonal



**Figure 1.** Examples of simple digital (a) and analogue (b) circuits. Adapted from ref 1.

(and hence distinguishable) state.<sup>94</sup> For very short switching times it also defines the minimum power required for a single switching operation (red line in Figure 3). The thermodynamic limit imposed on information transfer and processing is the minimal energy required for binary switching or transfer of one bit of information (eq 2).

$$E = k_B T \ln 2 \approx 3 \times 10^{-21} \text{ J bit}^{-1} \quad (2)$$

Equation 2 also defines the minimal value of entropy created when one bit of information is deleted. Electromagnetic limit simply expresses the fact that the rate of propagation of electromagnetic wave (and hence the rate of data transmission) cannot exceed the velocity of light in vacuum.<sup>95</sup>

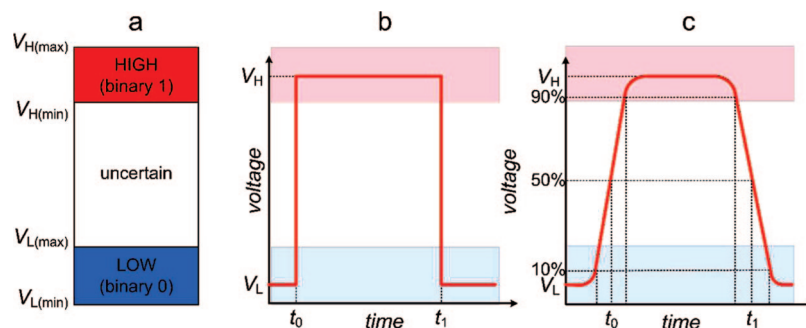
Other limitations are imposed by the material used, the device type used, the circuit concept, and the system configuration.<sup>93</sup> Material limits are related to the properties of semiconductor materials used for fabrication of the device: switching energy, transit time, thermal conductance, and a dopant fluctuation limit. Device, circuit, and system limitations are associated with heat dissipation, transition time, circuit latency, cross-talk and signal contamination, and the chip size.<sup>93</sup>

In order to sustain the development of telecommunication and information sciences, new technologies are needed to overcome at least some of the limitations.<sup>96–108</sup> One of the ideas was to apply the chemical structures for information processing. According to the opinion of some, this approach may be a way of bypassing, at least temporarily, the limitations of classical semiconductor technology and sustain the development of information technologies.<sup>96–100,102,104–106,108</sup>

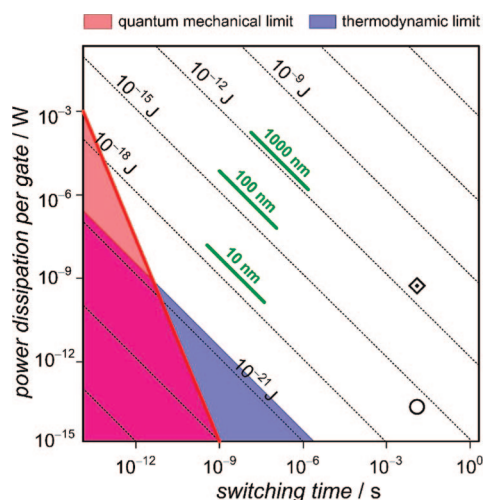
The most serious problem, however, is to address single molecules in a reproducible manner (and make more than two electric contacts with a single molecule), and this problem has not been efficiently solved so far. Therefore, molecular logic devices based on single molecules are mainly of academic interest. This should not discourage scientists to search for new information processing systems, as addressability of single molecules is not an absolute necessity for efficient chemical computing. Silicon-based microprocessors contain millions of transistors per chip. However, only several hundreds connections are sufficient to connect the inner circuitry with the macroscopic world of the users.<sup>109</sup> Furthermore, natural systems (brains and nervous systems of all of the animals) are the best example of molecular (or chemical) information processing systems, but the elemental information processing acts are not confined to single molecules.<sup>110,111</sup> Therefore the addressing of single molecules may not be necessary for efficient molecular information processing, and the control over the system can be achieved via self-assembly and molecular recognition.

## 2. Boolean Logic and Logic Gates

According to Charles S. Pierce and Charles W. Morris, we can define three levels of information: *syntactic* level, *semantic* level, and *pragmatic* level. Information on the syntactic level is concerned with the formal relationship between the elements of information, the rules of corresponding language, the capacity of communication channels, and the design of coding systems for information transmission, processing, and storage. The meaning of information and its practical meaning are neglected at this level. The semantic level relates information to its meaning, and semantic units (words and groups of words) are assigned



**Figure 2.** Voltage representation of logic zero and logic one (a), time profile of ideal pulse characteristics (b), and real pulse characteristics (c). Rise time is defined as the time required for increase of signal amplitude from 10% to 90% of pulse amplitude. Fall time is defined analogously. The signal is properly recognized only when it falls within the tolerance limits (shaded blue and red areas for '0' and '1', respectively). Adapted from ref.<sup>2</sup>



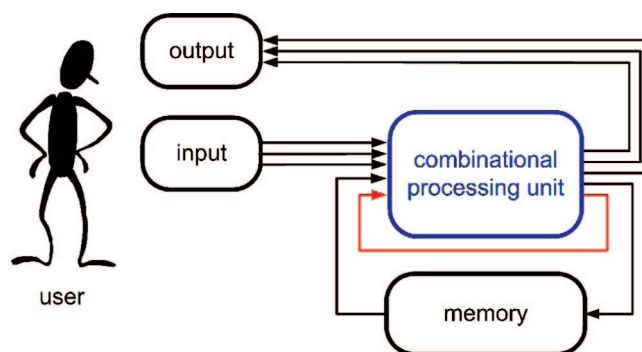
**Figure 3.** Performance of electronic digital devices presented as average dissipated power per gate versus transition delay time. The red area is inaccessible due to the fundamental limits of quantum mechanics while the blue area to the fundamental limits of thermodynamics. Green lines indicate the device limits for CMOS logic gates fabricated in 1000 nm, 100 nm, and (projected) 10 nm technologies. For comparison, estimated values for neuron ( $\diamond$ ) and synapse ( $\circ$ ) are indicated. Adapted from ref 94.

more or less precisely to their meaning. For correct information processing at the syntactic level, semantics is not necessary. On the pragmatic level, the information is related to the practical value of it. It strongly depends on the context and may be of economical, political, or psychological importance. Furthermore, at the pragmatic level the information value is time dependent, and its practical value decreases with time, while correct prediction of future information may be of high value.<sup>112</sup>

Any complex information processing device must then consist of several basic components: user interface for input and output of information, information processing unit, and memory for information storage. Moreover, every system must be equipped with proper channels for the transmission of information between components (Figure 4). The user translates the pragmatic level information into the semantic level; the input interface in turn translates it into the syntactic level. Information is then processed (and/or stored in memory), and the result is translated into usable semantic level information.

## 2.1. Basic Concepts of Boolean Logic

The mathematical logic, first established as a purely theoretical science,<sup>113</sup> was subsequently used in uncountable



**Figure 4.** Block diagram of sequential information processing device (an *automaton*). The simplest memory of the device can be realized in the feedback loop (red arrow), feeding one of the outputs of the device to the input.

electronic devices and became the most basic foundation of information science and digital electronics. It operates at the syntactic level. Nowadays, the concepts of Boolean logic are frequently used to describe behavior of various chemical systems. In many cases, chemical logic systems can be considered on all the three levels. The best example of the three-level information analysis can be shown on the example of chemosensors used in medical analysis. They perform logic operations (e.g., fluorescence is switched on upon the binding of corresponding analyte) on the syntactic level. The result of this operation on a semantic level reports the concentration of electrolytes, which in turn on a pragmatic level informs on the patient's condition.

A common representation of a Boolean logic is based on a basis set of characters and operators, union ( $\cup$ ,  $+$ ) and intersection ( $\cap$ ,  $\times$ ), and five axioms: commutativity, associativity, distributivity, existence of neutral elements, and existence of the complement. The union and intersection operators are usually called OR and AND operators (or logical sum and logical product), respectively.

The commutativity rule states that the order of variables in union and intersection operations is irrelevant (eqs 3 and 4).

$$a + b = b + a \quad (3)$$

$$a \times b = b \times a \quad (4)$$

The associativity rule states that the grouping of variables in union and intersection operations does not change the result (eqs 5 and 6).

$$a + (b + c) = (a + b) + c \quad (5)$$

$$a \times (b \times c) = (a \times b) \times c \quad (6)$$

The distributive law for three variables can be written as follows (eqs 7 and 8):

$$a \times (b + c) = a \times b + a \times c \quad (7)$$

and

$$a + (b \times c) = (a + b) \times (a + c) \quad (8)$$

It simply says that the logic product of a variable and a logic sum of variables is equal to the logic sum of two logic products (eq 7). Moreover, a sum of a variable and a product equals the product of two sums (eq 8).

There exist two neutral elements for logic sum (eq 9) and logic product (eq 10) operators, respectively:

$$a + 0 = a \quad (9)$$

$$a \times 1 = a \quad (10)$$

and a complementary element (eqs 11 and 12):

$$a + \bar{a} = 1 \quad (11)$$

$$a \times \bar{a} = 0 \quad (12)$$

Generation of a complement is usually called NOT operation.

These axioms of Boolean logic are complemented with two DeMorgan theorems. The first theorem states that the complement of a product of variables is equal to the sum of the complements of the variables (13), while the second theorem states that the complement of a product is equal to the sum of the complements of the variables (14).

$$\overline{a \times b} = \bar{a} + \bar{b} \quad (13)$$

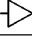

$$\overline{a + b} = \bar{a} \times \bar{b} \quad (14)$$

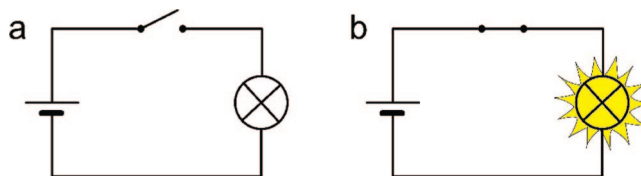
These rules allow the performance of any binary logic operations and all of the complex logic functions can be produced using the basic set of functions: OR, AND, and NOT. Electronic devices capable of performing Boolean operations on variables are called logic gates. A circuit comprising connected logic gates, devoid of feedback loops (memory), is a *combinatorial logic circuit*, a device whose output signal is a unique Boolean function of input variables (Figure 4). The combinatorial logic circuit with added memory forms a *sequential logic circuit*, often referred to as an *automaton* (cf. Figure 4). Memory function can be simply obtained by the formation of a feedback loop between output and input of individual gates within the circuit. The output state of the automaton depends on input variables and an inner state (memory) of the device.

## 2.2. One Input Logic Gates

There are four possible combinations of input and output values for one-input one-output logic gates (Table 1). The PASS 0 and PASS 1 gates yield 0 and 1 output, respectively, independently of the input value. The YES gate follows the input value to the output (Figure 5a). The gate functions as a simple switch, but in fact is very useful for signal amplification, connecting various devices, and signal transduction.


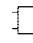
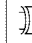
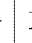
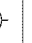
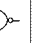
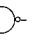
**Table 1. Truth Tables for Single Input Logic Gates**

output \ input	PASS 0	YES	NOT	PASS 1
	-			-
0	0	0	1	1
1	0	1	0	1



**Figure 5.** Simplest electric circuits representing the YES (a) and NOT (b) logic gates. Moving the switch (logical 1) turns on the light in the first system (YES gate), but turns it off in the second one (NOT gate).

**Table 2. Truth Tables for Two Input Logic Gates**

output \ input		OR	AND	XOR	INH	NOR	NAND	XNOR
								
0	0	0	0	0	0	1	1	1
0	1	1	0	1	1	0	1	0
1	0	1	0	1	0	0	1	0
1	1	1	1	0	0	0	0	1

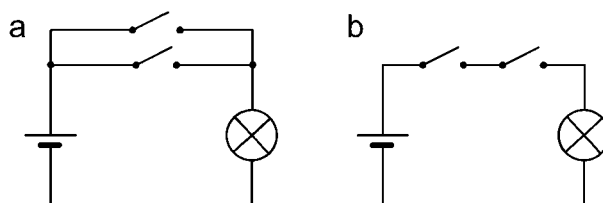
The inverter (NOT gate) performs inversion (complementation) of the input data (Figure 5b). It changes one logic level into the opposite: logic 0 (also called the low state, cf. Figure 2a) is converted into logic 1 (the high state) and vice versa. NOT is one of the principal Boolean operation, and very often, it is concatenated with multiple input gates (vide infra).

## 2.3. Multiple Input Logic Gates

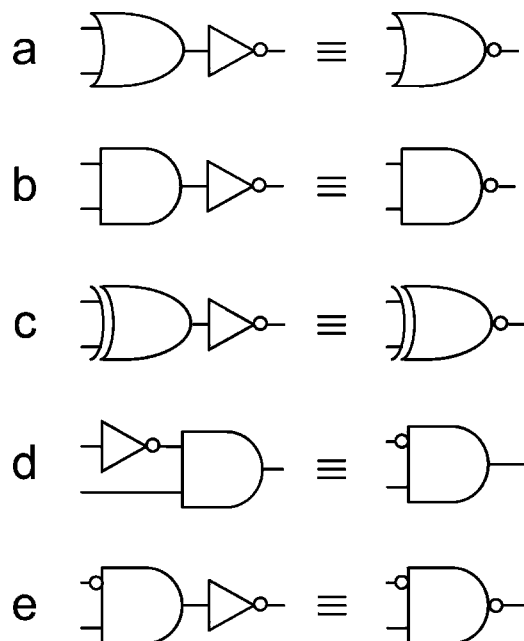
There are 16 various combinations of input and output signals for two-input logic gates, 8 of which are commonly used in electronics (Table 2): basic OR, AND, and XOR, and gates concatenated with NOT: NOR, NAND, and XNOR.<sup>114</sup> Usually, INHIBIT (INH) and NINH gates are regarded as simple logic gates as well.

The OR gate is one of the basic gates from which all other functions can be constructed. The OR gate produces high output when any of the inputs is in the high state, and the output is low when all the inputs are in the low state (Figure 6a). Therefore, the gate detects any high state at any of the inputs. It computes the logic sum of input variables, i.e., it performs the union operation.

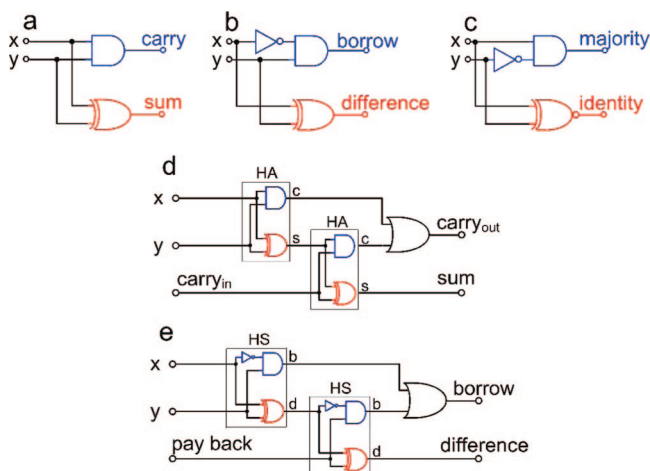
The AND gate is another of the principal logic gates; it has two or more inputs and one output. The AND gate produces high output (logical 1) only when all the inputs are in the high state. If any one of the inputs is in the low state, the output is also low (Figure 6b). The main role of the gate is to determine if the input signals are simultaneously true. In other words, it performs the intersection operation or computes the logic product of input variables.



**Figure 6.** Simplest electric circuits representing the OR (a) and AND (b) logic gates. Moving any of the switches turns on the light in the first system, but both switches must be moved to turn on the light in the second one.



**Figure 7.** Concatenation of various logic gates with the NOT gate results in NOR (a), NAND (b), XNOR (c), INH (d), and NOT-INHIBIT (e) logic gates.



**Figure 8.** Electronic diagrams for binary half-adder (a), half-subtractor (b), digital comparator (c), full adder (d), and full subtractor (e). HA stands for half-adder and HS for half-subtractor. In the case of subtractors,  $x$  stands for subtrahend and  $y$  for minuend.

A more complex logic function is performed by the exclusive-OR (XOR) gate. This is not a principal gate, but it is actually formed by a combination of the gates described above. However, due to its fundamental importance in numerous applications, this gate is treated as a basic logic element, and it has been assigned a unique symbol. The XOR gate yields the high output when two input values are different, but yields low output when the input signals are identical. The main application of the XOR gate is binary half-adder, simple electronic circuit enabling transition from Boolean logic to arithmetic (cf. Figure 8).

The whole family of logic gates is formed by concatenation of OR, AND, and XOR gates with the NOT gate, which can be connected to the input or output of any of the above gates. Various connection modes and resulting gates are shown in Figure 7. Gates resulting from concatenation with NOT are obviously not basic gates, but due to their

**Table 3.** Truth Table for Binary Half-Adder, Half-Subtractor, and Comparator

input		half-adder		half-subtractor		comparator
$x$	$y$	(c,s) <sup>a</sup>	decimal value	(b,d) <sup>b</sup>	decimal value	(i,m) <sup>c</sup>
0	0	(0,0)	0	(0,0)	0	(1,0)
0	1	(0,1)	1	(1,1)	-1	(0,0)
1	0	(0,1)	1	(0,1)	1	(0,1)
1	1	(1,0)	2	(0,0)	0	(1,0)

<sup>a</sup> (Carry, sum). <sup>b</sup> (Borrow, difference). <sup>c</sup> (Identity, majority).

**Table 4.** Truth Table for Full Adder and Full Subtractor

input			adder		subtractor	
$x$	$y$	$c/p$ <sup>a</sup>	(c,s) <sup>b</sup>	decimal value	(b,d) <sup>c</sup>	decimal value
0	0	0	(0,0)	0	(0,0)	0
0	0	1	(0,1)	1	(1,1)	-1
0	1	0	(0,1)	1	(1,1)	-1
0	1	1	(1,0)	2	(0,1)	-2
1	0	0	(0,1)	1	(1,0)	1
1	0	1	(1,0)	2	(0,0)	0
1	1	0	(1,0)	2	(0,0)	0
1	1	1	(1,1)	3	(1,1)	-1

<sup>a</sup> Carry/pay back. <sup>b</sup> (Carry, sum). <sup>c</sup> (Borrow, difference).

importance, they are usually treated as fundamental logic gates together with the NOT, OR, and AND logic gates.

## 2.4. Combinatorial Logic Systems

Single logic gates, even with multiple inputs allow only basic logic operations on single bits of information. More complex operations or on larger sets of bits require more complex logic systems. These systems, usually called combinatorial circuits, are the results of the connection of several gates. The most important are binary half-adder and half-subtractor, and full adder (Figure 8).<sup>114</sup> These circuits enable arithmetic operations on bits of information in binary fashion, which are one of the pillars on which the entire information technology has been built.

The half-adder is a device composed of two gates: AND and XOR. It has two inputs (two bits to be added) and two outputs (*sum* and *carry*). Half-subtractor is a related circuit (the only difference lies in one NOT gate at input), which performs a reverse operation: it subtracts the value of one bit from the other, yielding the bit of *difference* and a bit of *borrow* (Figure 8).

The most complex circuit presented here is full adder. It consists of two half-adders and an OR gate. The circuit performs full addition of three bits, yielding two-bit results. Similarly, full subtractor can subtract three one-bit numbers, yielding two-bit binary result. The truth tables for half-adder, half-subtractor, full adder, and full subtractor are shown in Tables 3 and 4.

An interesting device, closely related to the half-adder and half-subtractor, is the binary comparator. It takes two bit input ( $x$  and  $y$ ) and yields two bit output, which is determined by the relationship between the input quantities. If  $x = y$ , one output is set high (*identity* bit) and the other low (*majority* bit). If  $x > y$ , the identity bit is zero, while the majority bit equals 1. In the case of  $x < y$ , both output bits are 0 (Table 3 and Figure 8c).

There other numerous combinatorial logic devices, but their detailed analysis is out of the scope of this review. These and other combinatorial logic devices were imple-

mented in various molecular systems; some of them may contain tens of individual gates and may perform complex functions.

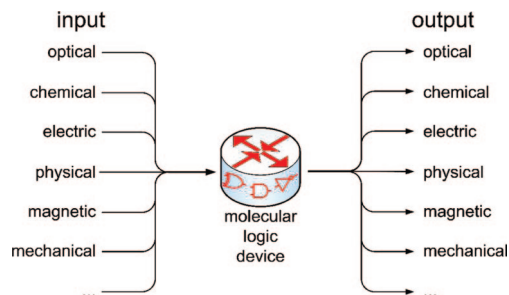
### 3. Molecular Logic Gates: Basic Concepts

Analogies are made possible by Nature's wonderful system of structural parallelism in which a physical element in one system may be represented by corresponding physical element in another.<sup>113</sup> Molecular information processing is a common feature of numerous biological and chemical systems. Living things have always processed information for purposes of survival.<sup>98</sup> Molecules and molecular assemblies are the information carriers and information processing devices in all of the biological systems. All of the regulatory processes in living cells, cellular signaling, and of course all of the neurobiological activities process information at the molecular level. Every biochemical bifurcate pathway undergoes Boolean logic rules at the molecular level in a sense that every single molecule can follow only one reaction path; therefore, its fate can be described in terms of Boolean algebra. The same concerns such complex biological processes as the synthesis of tetrapyrroles, cell replication, gene expression, or apoptosis.<sup>115,116</sup> Molecular recognition in biological systems, activation of enzymes by small molecules and signal transduction are also processes based on YES-NOT logic.<sup>117–119</sup> Although the collective response of the complex chemical or biochemical system is continuous (or, in other words, highly linear) on a macroscopic level, on the molecular level every single step is a discrete process, and its apparent linearity results from a combination (or averaging) of uncountable individual discrete processes of Boolean character. Every bifurcation on the chemical or biochemical reaction pathway at the single molecule level is a Boolean process: every molecule has to choose a reaction pathway according to its energy, conformation, and properties of its local environment. These processes are usually described using statistical thermodynamics, but the processes are Boolean in the sense that a single molecule cannot react on two or more reaction paths at the same time.

The molecular information processing structures are organized in a bottom-up fashion from the molecular to cellular level and beyond. Even the behavior of whole organisms under controlled conditions follows the Boolean logic, and for example, the movement of the amoeboid organism *Physarum polycephalum* can be used for the construction of logic gates.<sup>120</sup> Therefore, one should consider the bottom-up approach to construct devices for future IT industry.<sup>98,103</sup> This idea, first communicated by Richard P. Feynman,<sup>121</sup> resulted in tremendous development of nanoscience and nanotechnology.

The whole spectrum of input and output data encoding channels (Figure 9) should be considered. Classical electronic devices use electric input/electric output communication, but any other combination is possible.<sup>122</sup> Biological systems utilize various chemical stimuli for communication, while artificial systems use all possible combinations of input and output channels.

In principle, any chemical system that can exist in two quasi-stable states of different chemical or physical properties may be regarded as a molecular switch (or molecular logic gate) provided there are some physical or chemical stimuli that can (reversibly) change the state of the system. The simplest examples are colorimetric pH indicators, compounds

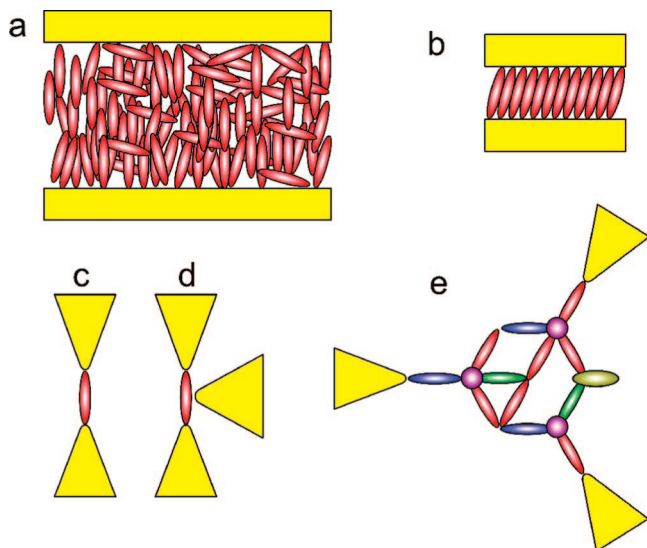


**Figure 9.** Input and output channels of molecular logic devices. These devices can be based on classical electronics paradigms (electric input/electric output) or utilize any nonclassical input/output configurations.

changing their color upon changes in proton concentration. They function as YES or NOT logic gates, depending on the property of the individual indicator and the assignment of input and output channels (e.g., pH values and colors). Furthermore, they are molecular devices that enable information transfer from the molecular level (presence of target molecules, e.g., protons) to the macroscopic level (observable change of optical properties). In order to perform any useful calculations, the switching process should be based on reversible chemical processes. There are, however, chemical logic systems that are based on irreversible reactions. These devices, not suitable for computing, have already found application in medicine as novel approaches toward anti-cancer therapy,<sup>123–125</sup> and other medical applications of molecular logic systems cannot be also excluded.<sup>102,126–129</sup>

The main difficulty with the construction of complex molecular logic devices results from the fact that they usually do not conform to some of the fundamental requirements for classical semiconductor logic devices. The requirements are as follows: nonlinear characteristics, signal amplification, concatenability, feedback prevention, and the performance of a complete set of Boolean operators.<sup>94</sup>

A nonlinear characteristic is an intrinsic feature of all digital logic systems (cf. Figure 2a), and it is required for the maintenance of sufficient signal-to-noise ratio. It is possible to build logic devices from linear elements (e.g., operational amplifiers),<sup>113</sup> but their signal-to-noise ratios greatly increases, especially in long chains of concatenated logic building blocks. Therefore, power amplification is necessary to maintain the signal level during logic processes over long chains of concatenated logic gates. It balances the signal losses that are unavoidable during processing (cf. Figure 2). Concatenability is required for efficient connection of logic gates into larger systems. It assures compatibility of input and output signals. If input and output do not belong to the same domain (e.g., optical input and electric output), a signal converter is necessary to connect gates into larger systems. Also, the signal intensities must be matched. In electronic systems, inputs and outputs of logic gates are matched in terms of domain (both are electrical) and signal intensities (cf. Figure 2). In the nervous system, in turn, outputs (released neurotransmitters) are compatible with inputs (receptors in postsynaptic neurons).<sup>94</sup> In molecular systems, due to high versatility of information carriers (cf. Figure 9) the compatibility problems are much more complex and change from one case to another. Most of the molecular logic systems cannot be concatenated due to the intrinsic properties of molecular species, while in other cases, e.g., in the case of enzymatic gates or ribozyme-based systems,



**Figure 10.** Schematic depiction of bulk molecular (a), hybrid molecular (b–d), and monomolecular electronic devices (e). Yellow bars and triangles symbolize conducting electrodes. See text for details. Adapted from ref 139.

the concatenation is virtually unlimited. Feedback prevention ensures a directed information flow through the system, which is necessary to perform any calculations. These calculations can be performed only if the complete set of instructions is available. The basic set of logic operators includes OR and NOT or AND and NOT functions.

As presented above, an information processing device (automaton) consists of user interfaces for data input and data output, combinatorial logic device for information processing, memory for data storage, and communication channels for data transmission between components of the automaton. Every abovementioned task can be performed in molecular systems, for example, molecular receptors and fluorophore fragments may function as input and output elements, respectively, various molecular switches and logic gates are capable of binary information processing, photochromic molecules can mimic the memory cells, and molecular wires can transmit information at molecular level. The most serious, and yet unsolved, problem consists in connecting all these molecular fragments into a usable device.

There are several different approaches toward the application of chemical systems to information processing. The oldest approach uses a classical electronics paradigm. It assumes the construction of molecular primitives that behave exactly like silicon-based semiconducting devices, but are just smaller and consisting of different materials. Input and output information is assumed to have a form of electric pulses. During the whole operation of the device, chemical bonds and molecular structure of the device are not changed.<sup>90,130–132</sup> This approach was initiated by theoretical works of Aviram and Rattner.<sup>133</sup> Various working devices based on organic semiconductors have been built.<sup>134,135</sup> Recently, memory chips containing molecular switches have just started to emerge.<sup>136,137</sup> This approach assumes facile connection of individual logic elements into larger logic systems using molecular wires, e.g., *p*-phenylene bridges.<sup>138</sup> Molecular electronic devices can follow three different construction patterns (Figure 10).<sup>139</sup> The simplest devices are based on bulk molecular systems of amorphous or polycrystalline structure (Figure 10a). In these devices, most

of the molecules form random contacts with other molecules and are not individually addressable. This type of molecular electronic system is usually applied in such devices as liquid crystal displays, OLEDs, and soft plastic transistors. Single molecular systems are in turn based on single molecules (Figure 10c and d) or perfectly ordered molecular films (Figure 10b); all of the molecules within the device are in direct contacts with electrodes. These devices can be divided into two classes: hybrid molecular devices, where every molecule is contacted with electrodes and monomolecular devices (Figure 10e), where individual molecular building blocks are connected at the molecular level, and electrodes are needed only for energy supply and for information exchange with the outside world.<sup>139</sup>

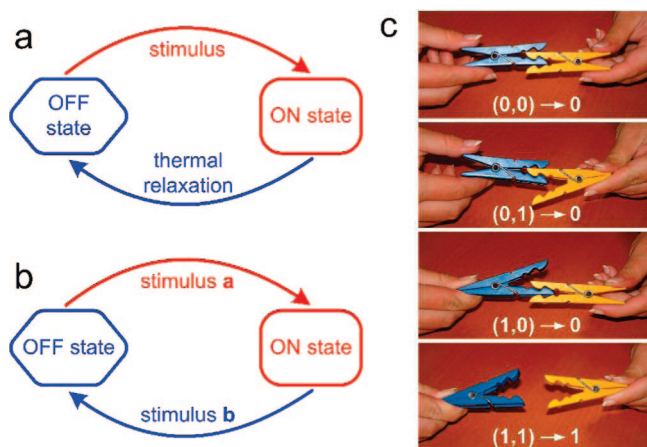
Another approach, which does not follow the classical electronics paradigm was initiated by A. P. de Silva in 1993.<sup>140</sup> Binary information processing in chemical systems has emerged from fluorescent sensor chemistry. Supplied information is usually chemical in nature (concentration of ions or other analytes), and output information is contained in the optical response of the sensor (light absorption or fluorescence). Some variation of these ideas were implemented in other substrate-recognition based devices, like logic gates based on ion pair formation,<sup>102,126</sup> various photoactive compounds,<sup>126,141–145</sup> nanocrystalline semiconductors,<sup>146–151</sup> or even DNA<sup>152</sup> and proteins.<sup>153</sup> In any of these chemical systems, information is supplied as chemical, optical, or electrical input. Upon processing, the result is directed into chemical, electrical, or optical output channels.<sup>154</sup> In the case of photoactive systems based on nitrosyl complexes, the chemical processes are usually irreversible, which is not very suitable for computing itself, but the processing usually follows Boolean algebra.

These chemical logic systems may be classified in an analogous way as the molecular electronic systems (cf. Figure 10). Most, if not all of the systems with chemical inputs discussed in this review, belong to the class of bulk molecular devices; sparse devices are based on thin ordered layers or other ordered structures. While there are no examples of artificial systems belonging to the class of monomolecular devices, the nervous systems of all the animals are perfect examples of all-molecular information processing systems based on chemical processes.<sup>110,111</sup>

A completely different approach toward information processing in chemical systems assumes the application of nonlinear dynamic processes in bulk media of high viscosity.<sup>155–164</sup> Propagation of chemical waves in gels may be used for classical binary information processing<sup>161–164</sup> or analog processing more related to the nervous system.<sup>155–157</sup>

Despite the apparent disutility of numerous molecular logic systems, their development is a great advance of science. First electric logic devices were also rather impractical, but in a short time, they became inherent elements of everyday life. In the future, the same may happen with molecular devices. At the moment, numerous information-processing molecules, such as fluorescent sensors, are commonly used in medical diagnostics, environmental analysis, and industry. Furthermore, studies on information processing in molecular systems (not necessarily with single molecules) may lead in the future to a better understanding of the human brain and nervous system operation.





**Figure 11.** Principle of operation of the monostable (a) and bistable (b) molecular switches. Combination of two simple switches results in the logic gate (c). See text for details. Adapted from ref 165.

#### 4. Simple Molecular Switches

Any chemical system that can exist in at least two forms of different spectral, electrochemical, or magnetic properties can be regarded as a molecular switch. Moreover, these forms should be relatively stable, and the transition of one into the other should not proceed spontaneously, but only upon stimulation with chemical, optical, electrical, or magnetic perturbation (Figure 11). If one state of the switch is assigned to logical 0 (ON) and the other to logical 1 (OFF), the switch should be regarded as one input logic gate: YES or NOT, depending on the state assignment and switching characteristics. The physicochemical processes behind may be very different: energy level rearrangement upon protonation/deprotonation, geometrical isomerization, proton transfer, changes in electron distribution (valence isomerism), spin state changes, bond formation/cleavage, which are the consequence of chemical reactions, photoexcitation, oxidation/reduction, or specific interactions with ions and molecules.

In principle, the switching from the OFF state to the ON state proceeds upon stimulation. The reverse process (from ON to OFF) may proceed instantaneously in the case of the monostable switch (Figure 11a) or upon stimulation with other stimuli (bistable switch; Figure 11b). Switching from ON to OFF state in many monostable switches is slow, but can be significantly accelerated by chemical or optical stimulation; therefore, depending on the discussed time scale, these switches can be regarded as monostable or bistable.

In order to consider a chemical system as a molecular switch, the two states must be easily distinguishable. In the case of fluorescence monitoring, the quantum yield should change from very small ( $\Phi \ll 1$ ) to high ( $\Phi \approx 1$ ), and in the case of absorbance monitoring, the spectral changes should be significant, and the shift of the absorption (or emission) band should be significantly larger than the corresponding band half-width. The same concerns changes in redox potentials, magnetic properties, or other physicochemical features of molecular systems.

These simple switches can be considered as one input logic gates. Depending on switching characteristics and arbitrary assignment of logic values to different states of the switch, they can be considered as YES or NOT logic gates. Furthermore, the bistable switches of sufficiently long lifetimes of both states should be regarded as molecular

memories, provided what the reading of the switch state does to induce switching. If the switching process relies not on a single stimulus but a combination of two or more physical or chemical triggers (e.g., concomitant change in pH and temperature), the system should be regarded as a molecular logic gate, if only the output can be described as a Boolean function of triggering signals. Any logic gate may be also generated from two independent switches driven by two distinct stimuli (cf. Figure 6). The way how they cooperate determines the Boolean response of the system. Figure 11c presents this idea for an extremely simple mechanical AND logic gate. Application of single stimuli does not change the state of the system, while cooperative interaction of two stimuli switches the system to its complementary state (Figure 11c).<sup>165</sup>

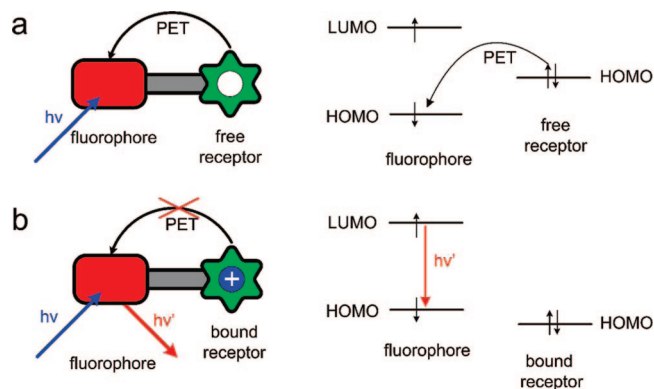
#### 4.1. Chemically Driven Molecular Switches

Numerous chemically driven molecular switches can be derived from chemosensors. They are molecules or molecular systems changing their optical or electrical properties upon interaction with small anions, cations, or neutral molecules. The use of fluorescence is the most popular due to very high sensitivity and relatively low price of measurement. They are the simplest tools that can transmit information on events occurring at a molecular scale to the macroscopic world.<sup>166</sup>

Chemically driven molecular switches usually molecules comprise three main building blocks: receptor moiety, linker (spacer), and the reporter moiety. Receptor moieties are specially designed binding sites for triggering ions or molecules. They should exhibit desirable selectivity and sensitivity toward selected triggers. The linker, in turn, should provide electronic communication between the receptor and reported moieties. There are three main ways of providing sufficient electronic communication: (i) bridge providing overlap of  $\pi$ -systems of both moieties, (ii) short  $\sigma$ -spacer enabling photoinduced electron transfer, or (iii) arrangement of receptor and reporter using some supramolecular interactions providing perturbation of electronic structure of the reported moiety.<sup>167</sup> The reporter moieties in turn should significantly (vide supra) change their photophysical, electrochemical, magnetic, or chemical properties to yield an easily recognizable signal. There are numerous review papers devoted to chemical sensors and switches;<sup>166–190</sup> therefore, only the basic principles of chemical switching and some relevant examples are briefly discussed here.

The most common are the systems where the interaction between the trigger and receptor results in the change of photophysical properties: changes in absorption and/or emission characteristics of the reporter moiety. It may also result in changes of redox potentials, translocation of molecular fragment within the supramolecular assembly (which may be also associated with changes in optical or electrochemical properties as well), chemical reactivity, or magnetic properties. There are numerous switchable systems of much simpler architecture: coordination compounds with free coordination sites or labile ligands show usually strong changes in optical and redox properties upon the binding of specific ligand.

Chemical switches with optical readout are usually based on the following photophysical phenomena: photoinduced electron transfer (PET), photoinduced charge transfer (PCT), electronic energy transfer (EET), excimer/exciple formation, and reorganization of electronic structure of transition-metal-based chromophore/fluorophore.

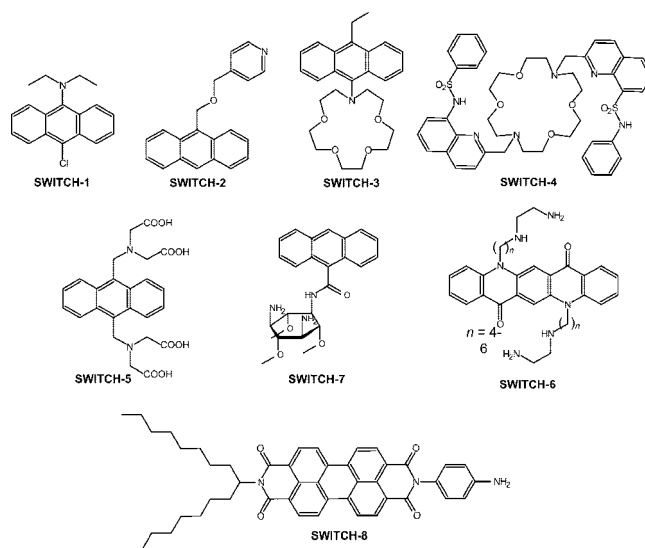


**Figure 12.** Principle of the PET chemically driven luminescent molecular switch. The HOMO level of the unbound receptor acts as an electron donor and effectively quenches the fluorescence of the reporter moiety (a). Upon coordination of the substrate, the energy of the HOMO level of the receptor is decreased because of electrostatic interaction with cationic species, and PET quenching is no longer possible (b). Reprinted from ref 128. Copyright 2005 American Chemical Society.

The principle of the PET-based chemical switch is shown in Figure 12. In most cases, the switch consists of a receptor, which selectively and reversibly binds a trigger, a fluorophore that provides optical communication between the switch and the environment, and a linker (even a virtual one)<sup>188</sup> that binds both components together and provides electronic communication between the receptor and the fluorophore (or chromophore) if the process is thermodynamically and kinetically feasible.<sup>166</sup> Importantly, the rate of electron transfer is much faster than the luminescence when PET is thermodynamically allowed (Figure 12a), and the luminescence of the fluorophore moiety is then quenched. Binding of the trigger to the receptor drastically alters the thermodynamics to the endoergonic situation (Figure 12b), and luminescence is not quenched any longer. PET-based luminescent switches may be triggered by various chemical and physical stimuli: protons, metal cations, anions, neutral organic molecules, and even nanoparticles. Depending on the desired spectral properties and lifetime of the fluorescent switch, the molecular assembly may include various organic (anthracene, pyrene, naphthalimides, pyromellitimide, coumarins, fluoresceins, pyrazolobenzothiazoles, and diphenylpyrazoles) or inorganic fluorophores (polypyridine Ru<sup>II</sup> complexes and lanthanide complexes).<sup>166,191</sup> Selectivity and sensitivity of the chemosensors are controlled in turn by careful design of the receptor part. The large diversity of possible organic ligands enables designing of the sensors suited for particular applications.

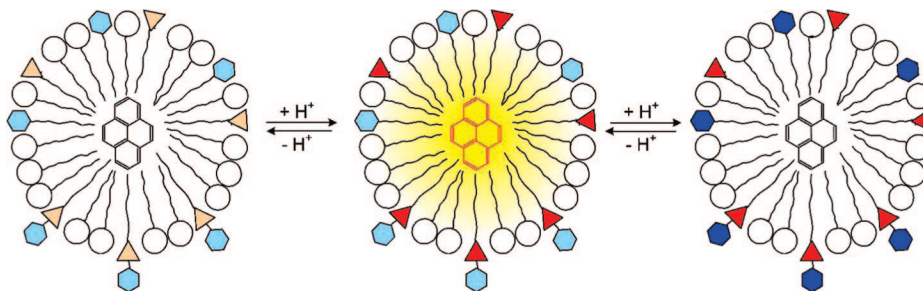
In the simplest case, the change of the energetics of the system is caused by electrostatic and electronic interactions between the receptor and the substrate. If the trigger ion is an open shell transition metal ion, the quenching occurs upon binding as PET involves the *d* orbitals of the metal center. Although most of the PET switches triggered by protons or closed shell cations work in OFF/ON fashion (i.e., fluorescence is switched on upon binding of the trigger), careful design of the receptor–fluorophore systems also gave the ON/OFF switch. Two anthracene-based switches show this phenomenon. Tertiary aliphatic amines are efficient quenchers of anthracene emission, upon the protonation of which the fluorescence is observed, as in the case of molecule SWITCH-1. Exchange of the aliphatic amine for pyridine moiety yields the ON/OFF switch: protonated amine becomes

an efficient quencher (SWITCH-2).<sup>192</sup> The fluorescence can also be easily switched on with lithium and other alkali metal cations (SWITCH-3).<sup>193</sup> Combination of *p*-toluenesulfonamido-quinoline with azacrown yields a very good switch responding selectively to Zn<sup>2+</sup> cations (SWITCH-4).<sup>194</sup> On the same principle, a PET-based switch activated with Cd<sup>2+</sup> was constructed from the anthracene fluorophore bearing two aminoacid side arms (SWITCH-5).<sup>195</sup> The opposite effect (ON/OFF switching on ion binding) was observed in the case of the fluorescent switch based on quinacridone skeleton with two diamine pendant arms (SWITCH-6).<sup>196</sup> The arms have long saturated flexible chains, and the amino groups are far away from the fluorophore. Coordination of metal ions (Cu<sup>2+</sup>, Hg<sup>2+</sup>, Zn<sup>2+</sup>, Co<sup>2+</sup>, and Ni<sup>2+</sup>) changes the geometry of the pendant arms, the metal ion localizes in close proximity of the central aromatic ring, and fluorescence is quenched due to photoinduced energy and/or electron transfer. A similar effect was observed in the case of the anthracene fluorophore linked via the amido bond with *all-cis*-2,4,6-triamino-1,3,5-trihydroxycyclohexane (SWITCH-7).<sup>197</sup>

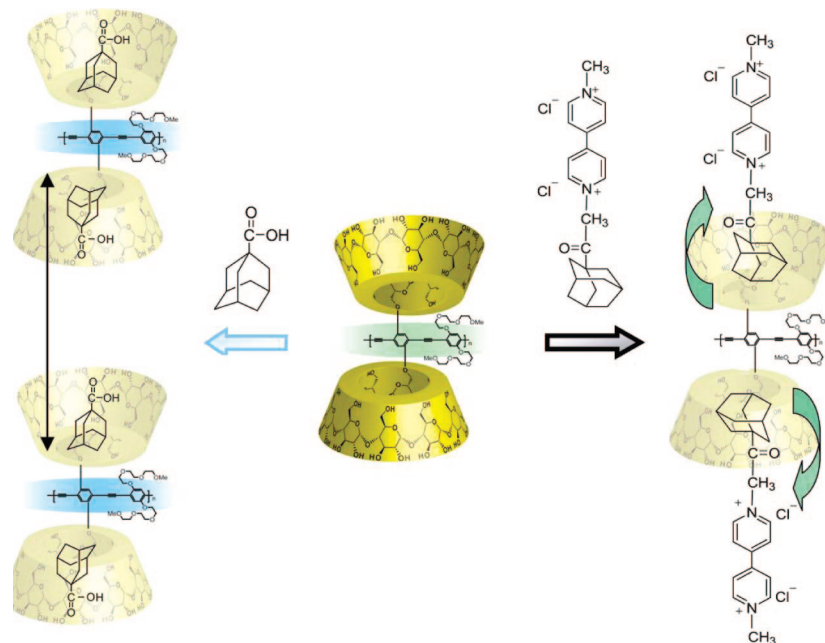


Extremely intense ( $\Phi \approx 0.99$ ) fluorescence of alkyl-substituted perylene tetracarboxyl bis-imide (SWITCH-8) can be effectively switched on by protonation of the aniline moiety. Furthermore, its fluorescence can be switched on upon interaction with various molecules and particles. Reaction with aldehydes or attachment to TiO<sub>2</sub> nanoparticles activates the fluorescence. Confocal fluorescence microscopy allows observation of fluorescence from single molecules of the molecular switch based on perylene bis-imide and tracking events at molecular level in real time.<sup>198</sup>

Fluorescence quenching by nonprotonated aliphatic amines and protonated pyridine moieties was used for the construction of three-state pH-controlled switches in micellar systems.<sup>199</sup> Triton X-100 micelles were doped with fluorescent probe (pyrene) and modified with a mixture of lipophilic aliphatic ternary amines (e.g., *N*-dodecyl piperidine, DPi) and lipophilic pyridines (e.g., 2-dodecylpyridine, DPy). Alternatively, compounds bearing both aliphatic and aromatic ternary amine groups were used (e.g., *N*-methyl, *N*-dodecyl-2-aminomethylpyridine). At high pH, all of the amino groups are deprotonated, and the fluorescence of pyrene is quenched by PET from ternary amino groups. Decreasing pH results in the protonation of aliphatic and then also aromatic nitrogen



**Figure 13.** Working scheme for the micellar pH-driven molecular switch. The upper part depicts micelles containing mixtures of two amines, while the lower part depicts the system with two amino groups within single lipophilic molecule. Amino groups are depicted as pink triangles, ammonium as red triangles, pyridine moieties as cyan hexagons, and pyridinium as dark blue hexagons. Adapted from ref 199.



**Figure 14.** Host-guest interactions of cyclodextrin-modified poly(phenyleneethylenes) resulting in diverse photophysical changes. Reprinted with permission from ref 200. Copyright 2006 The Royal Society of Chemistry. The original file was generously supplied by Professor Akira Harada.

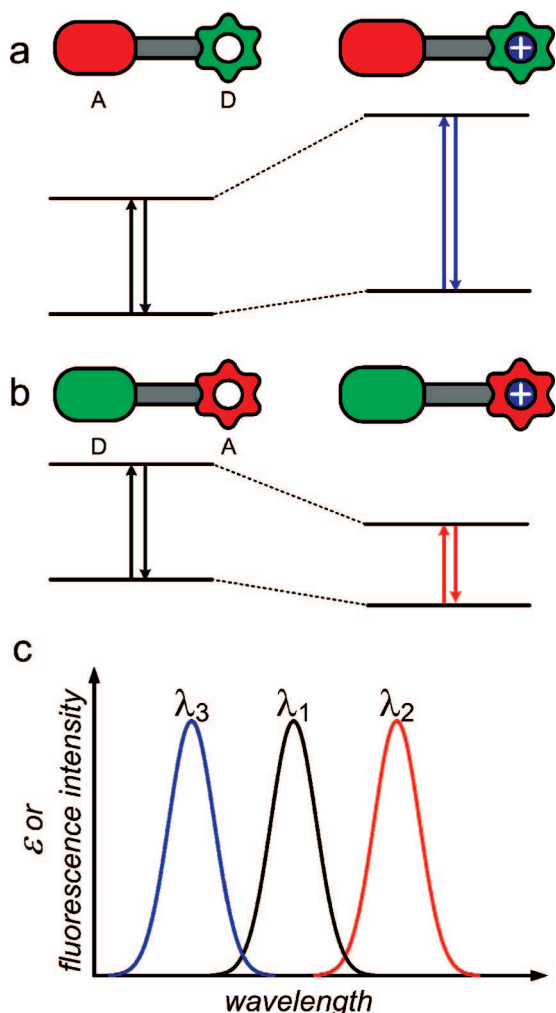
atoms. Protonation of aliphatic groups switches the pyrene fluorescence on, while further protonation switches it off again (Figure 13).

An interesting and potentially versatile fluorescent switch was reported very recently by Harada et al. (Figure 14).<sup>200</sup> The system is based on the poly(phenylene ethylene) modified with  $\beta$ -cyclodextrin moieties attached to the polymer backbone via ether linkers. The structure of the polymer is interesting as every phenylene group is flanked by two cyclodextrins, which makes it water soluble in contrast to unmodified poly(phenylene ethylene). The polymer easily aggregates in aqueous solutions via intermolecular  $\pi$ - $\pi$  stacking; it results in concentration-dependent dual fluorescence, 450 nm from unaggregated and 493 nm from aggregated material. Furthermore, polymer fluorescence can be drastically changed by the formation of inclusion complexes by cyclodextrin moieties. Incorporation of the methyl viologen derivative decorated with the adamantyl group results in efficient fluorescence quenching due to efficient PET. Incorporation of adamantane carboxylic acid or adamantylpyridinium cation results in turn in a hypsochromic shift of polymer emission due to deaggregation induced by electrostatic repulsion between charged host molecules. The system is especially interesting from the point of view of

molecular electronics. A combination of conducting polymer with a supramolecular host-guest system constitutes a bridge between molecular electronics and chemically driven molecular switches.

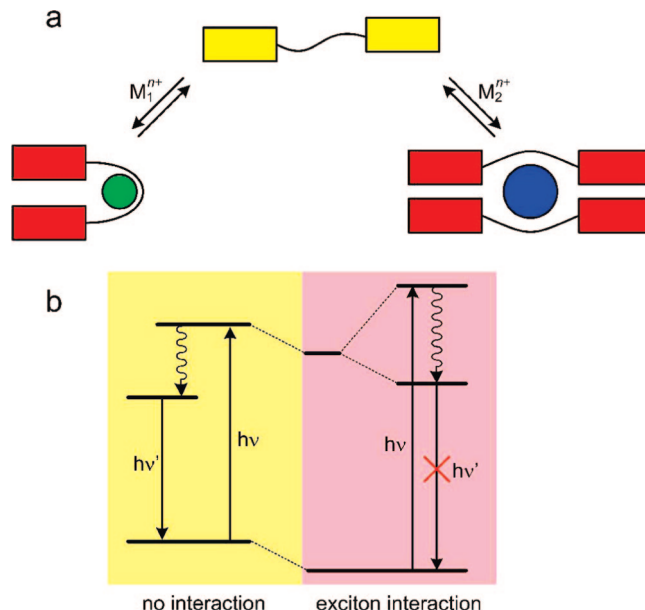
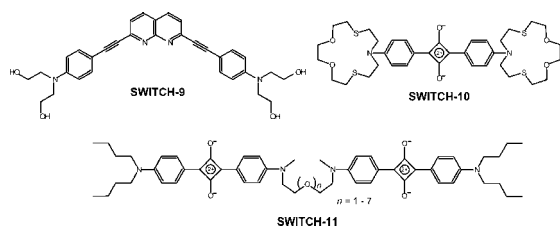
Another large category of chemically driven optical switches encompasses the PCT systems. In contrast to PET-based switches, the receptor and fluorophore (chromophore) moieties are connected in a way that provides extensive orbital delocalization between these two parts. One end of such a molecule is electron rich, while the other is electron poor; upon interaction with the environment, the electron distribution may significantly change, thus changing the optical properties of the switch. In such push-pull systems, excitation leads to redistribution of electron density and generation of dipole moment. If the receptor binds a charged trigger species, the additional charge interacts with the photogenerated dipole, thus modifying the fluorescence spectrum. Repulsive interaction results in the hypsochromic shift (Figure 15a) of absorption and emission bands, while attraction results in bathochromic shift (Figure 15b).

The main advantage of PCT switches over PET switches consists in the possibility of usage of several wavelengths to analyze the state of the switch, and it is essential in intracellular cation sensing. But from the Boolean logic point



**Figure 15.** Principle of the PCT chemically driven luminescent molecular switch based on the donor–spacer–acceptor architecture. Binding of cationic trigger to the donor (green) moiety results in the hypsochromic shift of absorption (emission) band (a), and binding of the same trigger to the acceptor moiety (red) results in bathochromic shift of the corresponding transition (b). The multi-receptor system may exhibit both bathochromic and hypsochromic shifts upon binding different trigger ions (c), which results in a multistate molecular switch.

of view, it enables parallel generation of several binary variables; in other words, it creates numerous independent information channels. In this context, the switches with pronounced concomitant absorption and fluorescence changes are of special interest. Numerous complex logic systems, including a molecular arithmetic device, have been built (*vide infra*). The only drawback of PCT-based systems consists in the necessity of triggering by charged molecules. It is a significant obstacle for the application of PCT switches as highly selective chemosensors, and it does not disturb Boolean systems at all.



**Figure 16.** Different self-assembly modes of the extended squaraine-based donor–acceptor chain with flexible polyether linker (a) together with corresponding energy diagrams (b). Adapted from refs 204 and 205.

PCT-based switches can be derived from well-known pH colorimetric indicators.<sup>201</sup> Very recently, similar systems, based on donor–acceptor–donor systems, as  $\text{Hg}^{2+}$  ion-driven molecular switches have been reported.<sup>202,203</sup> These switches bear central acceptor moieties: 1,8-naphthyridine (SWITCH-9) or squaraine coupled with two identical donor fragments, 1,4-dioxo-7,13-dithia-10-azacyclopentadecane (SWITCH-10) or diethanolamine (SWITCH-11), respectively.

The naphthyridine-based SWITCH-9 shows a strong absorption band at 450 nm. Binding of one mercury equivalent increases the asymmetry of electron distribution within the molecule, which in turn results in the bathochromic shift of the lowest energy absorption band. Binding of the second mercury ion results in turn in a hypsochromic shift of the low energy band due to interaction of bound cations with photoinduced dipole moments. This switch, due to low binding constant, requires high concentrations of triggering cation.<sup>202</sup> This type of switches, with at least three different states, is described in section 4.5. Dithiazacrown receptors are characterized by a very high affinity toward mercury ions, and even very low concentrations are sufficient to trigger optical changes of the squaraine-based switch (SWITCH-10). Binding of  $\text{Hg}^{2+}$  ions results in a gigantic hypsochromic shift from 650 to 285 nm.<sup>203</sup> Further extension of donor–acceptor chain results in structures such as SWITCH-11 as reported by Ajayaghosh and co-workers. Apart from typical PCT behavior, this molecule can be regarded as a chemomechanical switch due to cation-controlled folding and self-assembly (Figure 16a).<sup>204–207</sup> Formation of the foldamer or the sandwich dimer results in dramatic changes of spectral properties of the dye. These changes are due to the formation of H-like aggregated structure between chromophoric groups within the same molecule (foldamer) or belonging to two molecules linked via the calcium cation (sandwich dimer). Excitonic interaction brings about splitting of the excited-state energy levels, which in turn results in hypsochromic shift of the absorption band and decrease of fluorescence quantum yield (Figure 16b), as the transition from the lower excited state is

forbidden by theory.<sup>206</sup> Quite similar effects were reported for polythiophene and poly(*p*-phenyleneethynylene) with incorporated 12-crown-4 and 15-crown-5 moieties upon interaction with alkali metal cations.<sup>208–211</sup>

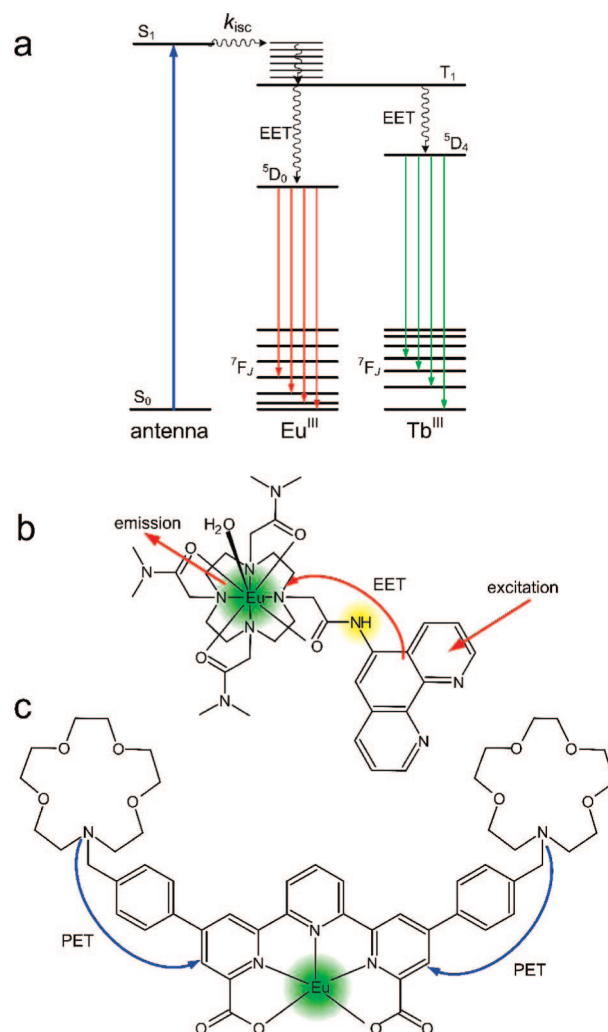
The changes in electronic configuration caused by chemical triggering are commonly observed in the case of coordination compounds of transition elements. Changes in the symmetry of the complex due to coordination of extra ligands or high spin/low spin transitions usually result in extensive changes of the spectroscopic signature; magnetic and/or electrochemical properties also alter significantly. The same concerns change in geometry with the preserved coordination sphere due to interaction of ligands with electron donors and electron acceptors. The latter is especially significant for cyanide and other pseudohalide complexes.<sup>212</sup> Up to now, however, these chromotropic systems based on metal complexes were not taken into the limelight of molecular logic devices.

An important group of molecular switches, sensors, and other devices is based on the electronic energy transfer (EET) process. The EET systems comprise three crucial elements: photonic antenna, linker, and fluorophore (usually a lanthanide complex). In order to make a fluorescent switch from the EET photonic device, a receptor group must be incorporated into the assembly. This receptor functionality may be just a labile coordination site at the lanthanide cation; integration of the receptor functionality with the antenna or the linker is also possible. Alternatively, the EET switch function may be based on trigger-controlled assembly of lanthanide fluorophore with efficient antenna.<sup>213</sup> The following examples illustrate the principle of EET switching in lanthanide-based systems. Excitation of the antenna moiety results in the formation of the  $S_1$  excited state of the organic chromophore. Intersystem crossing populates the  $T_1$  state, which in turn transfers the electronic energy to the europium(III)  $^5D_0$  or the terbium(III)  $^5D_4$  luminescent states (Figure 17a).

The first example is a switch containing the europium(III) ion complexed within tetraaza macrocyclic ligand with four amide pendant arms. One of the arms contains attached phenanthroline antenna (Figure 17b). Excitation of the phenanthroline moiety results in an efficient electronic energy transfer toward the europium(III) center, which in turn induces its bright luminescence. This process, however, is controlled by the redox potential of the phenanthroline fragment. Deprotonation of the amide linker (yellow circle) at high pH results in PET rather than in EET, thus leading to fluorescence quenching and Eu(III) reduction.<sup>214</sup> Another PET-based control over the EET process was observed by A. P. de Silva in the compound shown in Figure 17c.<sup>215</sup> In the case of unbound azacrown receptors, the efficient PET quenches the excited state of the polypyridyl ligand, and no fluorescence is observed. Upon binding of sodium cations (or potassium in 18-monoazacrown-6), the PET becomes endoergonic (cf. Figure 12), and EET from the ligand switches the europium fluorescence on.

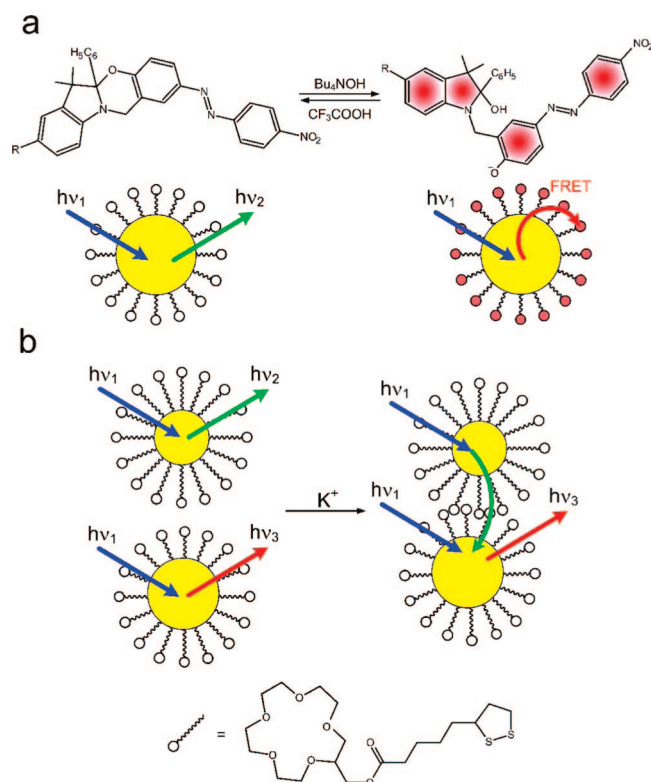
Quite recently, the EET processes were applied to trigger on and off the luminescence of semiconducting quantum dots, involving electronic energy transfer between the quantum dot and organic chromophore<sup>216,217</sup> or between quantum dots of different diameter.<sup>218</sup>

The [1,3]oxazine dye equipped with the methyl 5-(1,2-dithiolan-3-yl)pentanoyl linker (Figure 18a) can be easily attached to the CdSe/ZnS core/shell quantum dots. The dye



**Figure 17.** EET-based lanthanide molecular fluorescent switches: the Jablonski diagram (a) and two examples of the switches (b and c). See text for details. Partially adapted with permission from ref 213. Copyright 2005 Royal Society of Chemistry.

in the oxazine form does not interact with photoexcited quantum dots, and strong fluorescence is observed. Upon addition of a strong base (e.g., tetrabutylammonium hydroxide), the surface dye undergoes a reversible ring opening reaction yielding 4-nitrophenylazophenolate. Absorption spectrum of the resulting dye strongly overlaps with the emission spectrum of quantum dots. This leads to an efficient Förster energy transfer between quantum dots and 4-nitrophenylazophenolate, and thus fluorescence is quenched. The same linker was used to modify CdSe/ZnS quantum dots with 15-crown-5 moieties. This assembly allows potassium-induced aggregation of nanoparticles resulting in Förster energy transfer between quantum dots of two different sizes (Figure 18b). In the absence of potassium ions, solutions containing a mixture of two kinds of quantum dots show dual fluorescence. Upon the addition of  $K^+$  ion formation of sandwich-type complexes between  $K^+$  and 15-crown-5 moieties results in the formation of various aggregates. The average distance between individual quantum dots decreases allowing an efficient energy transfer.<sup>218</sup> Similar aggregation of gold nanoparticles via  $\pi$ - $\pi$  stacking of aromatic surface groups results in strong electronic coupling between individual nanocrystals.<sup>219</sup> Recently, systems involving EET between two organic fluorophores have been reported.<sup>220–222</sup>

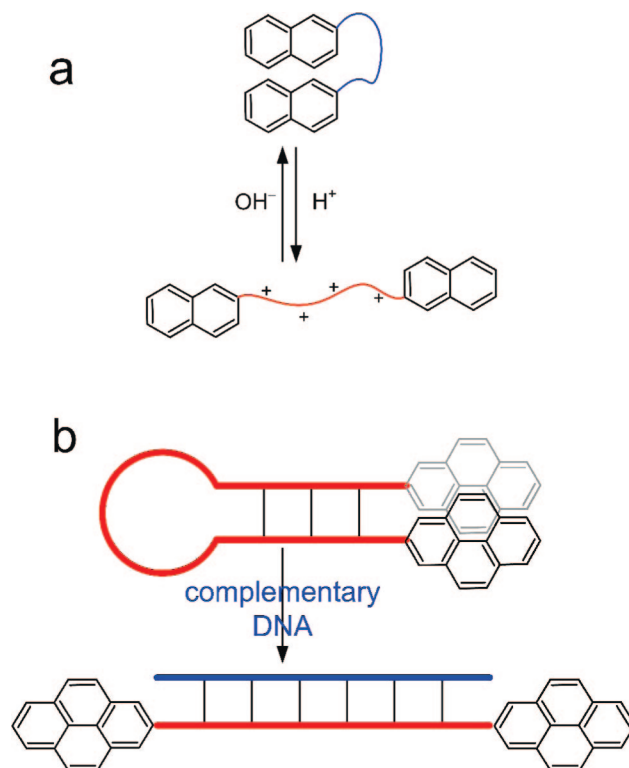


**Figure 18.** Reversible transformation of colorless [1,3]oxazine into strongly colored phenolate and corresponding photophysical processes involving oxazine and CdSe/ZnS core-shell quantum dot (a)<sup>216</sup> and potassium-induced aggregation of quantum dots resulting in Förster energy transfer.<sup>218</sup>

The efficiency of the EET process is modulated by the geometrical framework of the switch molecule.

The next category of chemically driven fluorescent switches falls into the excimer/excimer category. Various aromatic planar fluorophores, such as anthracene and pyrene, can form an excimer when an excited fluorophore molecule comes within close proximity of another molecule of the same kind within the excited-state lifetime.<sup>223</sup> Electronic configuration of an excited state includes half-filled molecular orbitals, which can overlap with orbitals of ground-state molecules. This  $\pi$ - $\pi$  interaction results in bathochromically shifted, broad, and featureless emission peaks. The broadness of the excimer emission is a consequence of Heisenberg's uncertainty principle: extremely shortly lived ground state gives a large peak broadening. By analogy, exciplex is formed when an excited molecule encounters a ground-state molecule of different structure. Formation of excimer/excimer is observed as dual fluorescence: together with an emission band characteristic for the undisturbed fluorophore, another one (usually broad and unstructured) can be seen at energies lower than that of the original fluorescence.

As excimer formation depends on the distance between the counterparts, the geometrical changes resulting from interaction between the receptor and the trigger are the key factors for the operation of the excimer-based molecular switch.<sup>178</sup> Therefore, the excimer-based switches should be assigned to the category of chemomechanical devices, i.e., molecular machines.<sup>96,224-227</sup> The prominent examples of the excimer-based fluorescent switches are molecules resulting from the incorporation of two anthracene moieties into the crown ether macrocycle,<sup>228</sup> naphthalene moieties tethered with aliphatic polyamine chains (Figure 19a),<sup>229,230</sup> or

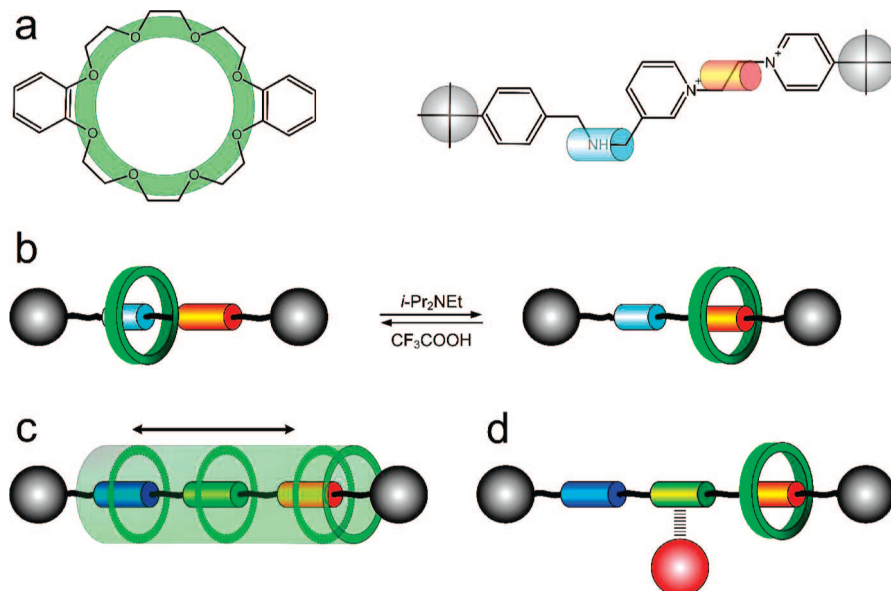


**Figure 19.** Switching between the excimer (up) and monomer emissions (bottom) in various molecular systems: naphthyl-labeled polyamine chains (a) and pyrene-labeled DNA (b).

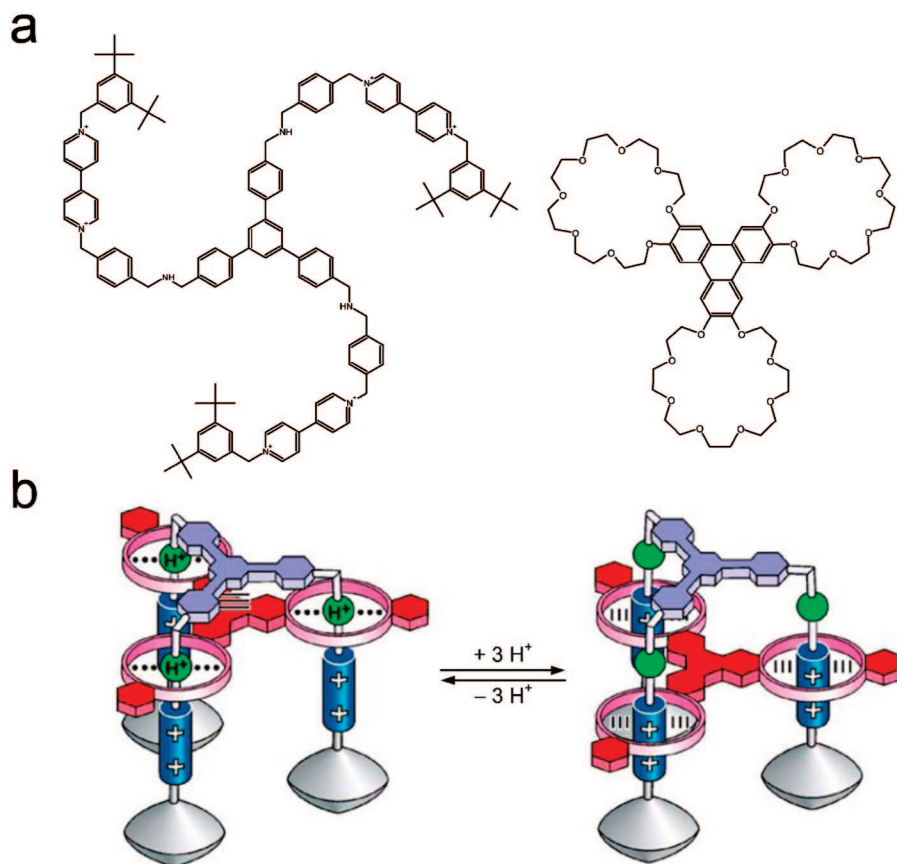
pyrene-labeled DNA (Figure 19b).<sup>231</sup> Changes in protonation of the polyamine chain causes geometrical changes resulting from electrostatic repulsion between two terminal naphthalene fluorophores. Furthermore, additional fluorescence control by protonation/deprotonation of secondary amino groups should be considered. As it was mentioned above, only protonated amines do not quench fluorescence due to PET process. Therefore, both monomer and excimer fluorescence occur only in a narrow pH window.<sup>229</sup> Similarly, DNA loops or hairpins equipped with pyrene fluorophores on both ends show excimer emission. In the presence of the cDNA chain, a hybrid two stranded DNA is formed, which results in a strong monomer emission with concomitant disappearance of the excimer emission.<sup>231</sup> An analogous system based on cyclic oligopeptides with pendant pyrene fluorophores was reported recently.<sup>232</sup>

Other numerous molecular switches depend on translocation of molecular fragments within molecules or supramolecular entities. As in the previous cases, the chemical stimulation changes (usually in a reversible manner) the affinity of some molecular fragments toward some other components of the system. Rotaxanes and catenanes containing various donor and acceptor moieties are the best examples of such switches. Let us consider a rotaxane composed of polyether macrocycle and a thread containing two stations: secondary aliphatic amine and bis(pyridine)ethane dication (Figure 20).<sup>233</sup> At low proton concentration, the polyether moiety interacts with cationic pyridinium fragment. On addition of strong acid, the secondary amine group gets protonated, and the macrocycle moves toward amine station. On addition of base, the thread is deprotonated, and the macrocycles move toward the pyridinium station.

Related systems were recently reported by Otera et al.<sup>234</sup> The [2]rotaxane comprises the polyether macrocycle and a



**Figure 20.** Components (a) and proton-driven switching (b) of the [2]rotaxane.<sup>233</sup> Coordination-controlled dynamic movements within the [2]rotaxane containing the central bipyridine unit. Uncoordinated rotaxane shows free movement of the macrocycle along the thread (c), while coordination of  $\text{Cu}^+$  results in inhibition of the translational movement (d).<sup>234</sup>



**Figure 21.** Structure of the guest (left) and host (right) components of a molecular elevator (a) and proton-induced switching (b). Partially reprinted from ref 236. Copyright 2006 American Chemical Society.

thread with two bipyridinium stations separated by the bipyridine station. The ring can freely move back and forth between all three stations. On coordination of copper(I) ion, the macrocycle must reside at one of the cationic centers, and its random movement is blocked.

One of the most complex switching system of that kind was reported recently by Vincenzo Balzani, Alberto Credi, and Fraser Stoddart with co-workers (Figure 21).<sup>235,236</sup> The

switching system comprises two molecular elements: triphenylene functionalized with three 24-crown-8 macrocycles (host) and triphenylbenzene-based trifurcated podand (guest) bearing three long arms incorporating secondary amine groups and  $N,N'$ -bipyridinium moieties (Figure 21a). Host and guest molecules in solution form a supramolecular assembly due to interactions between crown ether moieties of host and cationic bipyridinium fragments of the guest

molecule (Figure 21b). In the absence of acid, the crown ether moieties interact with bipyridinium cations. On protonation, the macrocyclic host molecule moves toward ammonium cations. This configuration is further stabilized by the  $\pi$ - $\pi$  stacking interaction between triphenylene and triphenylbenzene fragments.

There are other numerous switchable systems, which undergo spatial rearrangements upon chemical stimulation.<sup>224–227</sup> Another good example of the molecular switch based on polyether-cation interaction is closely related to the molecular elevator described above.<sup>237</sup> [2]Catenane composed of two interlocked rings bis-*p*-phenylene-34-crown-10 and asymmetrical *p*-cyclophane containing  $\pi$ -deficient bipyridinium and diazapyrenium cations can be switched by subsequent addition of aliphatic amines and trifluoromethanesulfonic acid. Initially, the diazapyrenium moiety resides inside the polyether macrocycle, while the bipyridinium stays outside. Aliphatic amines form strong charge transfer complexes with diazapyrenium, and the addition of hexylamine results in circumrotation; diazapyrenium moves outside the macrocycle, thus forming a CT complex with the base, while the uncomplexed bipyridinium moves inside. This process results in significant changes in absorption spectra as well as the electrochemical signature of the [2]catenane.<sup>237</sup> An analogous switch based on dimethylpyrenium and polyether macrocycle was reported this year.<sup>227</sup> Similar systems based on cucurbituril<sup>238–241</sup> and cyclodextrin<sup>242,243</sup> hosts were reported and reviewed recently.

## 4.2. Light Driven Molecular Switches

There is a plethora of well characterized chemical systems in which switching between two, more or less stable, states can be achieved via optical excitation. In this context, even generation of an excited state may be considered as switching, as ground and excited states exhibit significantly different spectroscopic and electrochemical properties as well as chemical reactivity. It is, however, well established in chemical literature that only molecules that undergo significant and long-lasting electronic, spectral, or structural changes upon light absorption are regarded as photochemical switches.

Three main photochemical processes should be considered in the context of light-driven molecular switches: photoisomerization of molecules with double bonds, light-induced ring opening and ring-closure reactions, and photoinduced electron transfer. The latter may result in valence tautomerism, which is the basic platform for various magnetic devices or translocation of components of a supramolecular assembly due to PET-induced changes in affinity of the components. The first two phenomena are usually associated with photochromic systems. Photochromism is defined as a reversible phototransformation of a molecule between two forms of different spectral properties. This process, however, may bring about other, not only spectral changes, e.g., refractive index, dielectric constant, dipole moment, oxidation/reduction potential, or geometry of a molecule. The reverse transformation may proceed upon excitation with light of different wavelength, on thermal pathway or in redox processes.

The most important photochromic system, which is also crucial for information processing is that based on rhodopsin. Rhodopsin is a small protein containing 11-*cis*-retinal bound via Schiff linkage with amino acid framework. Absorption

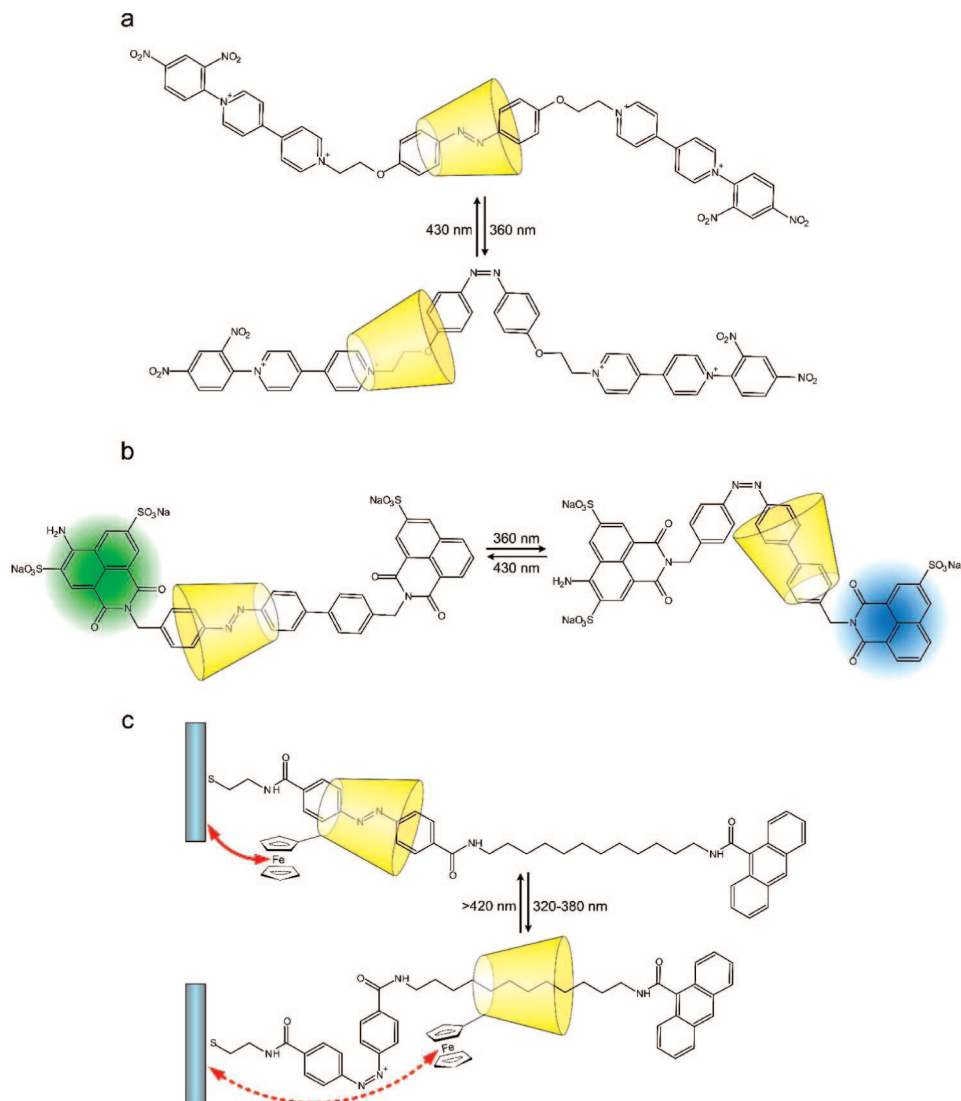
of visible light induces *cis*–*trans* photoisomerization. *Trans*-rhodopsin induces a cascade of reactions, which results in the vision process.<sup>244</sup> Protein similar to rhodopsin, a bacteriorhodopsin, is produced by some photosynthetic bacteria (e.g., *Halobacterium salinarum*) as light-harvesting antenna. Applications of bacteriorhodopsin as a switching molecule and a nanosensor have been reviewed recently.<sup>245,246</sup>

Other classical switching systems are also based on *cis*–*trans* isomerization of unsaturated systems: diazobenzenes and overcrowded alkenes with bulky aromatic substituents.<sup>247–249</sup> Their spectral properties and switching characteristics can be easily tuned via structural changes.<sup>250</sup> Photoactive liquid crystals<sup>251,252</sup> and photosensitive polymers<sup>253,254</sup> should be considered as the most interesting and easily applicable materials. Partial reduction of one phenyl rings in the azobenzene moiety should result in much higher photoisomerization quantum yields.<sup>255</sup>

Several rotaxanes with cyclodextrin host and azobenzene-based guest fragments were recently reported. *cis*–*trans* photoisomerization of azobenzene fragment induces a shift of the cyclodextrin host along the thread. This shift, in turn, results in the change of optical (circular dichroism, fluorescence) properties of the assembly together with absorption changes of the guest moiety. In the case of the symmetrical nonfluorescent guest (Figure 22a),<sup>256</sup> only CD and absorbance changes are observed. The nonchiral guest chromophore shows cyclodextrin-induced circular dichroism. The cyclodextrin in the complex with the *trans* isomer resides at the azobenzene moiety, which results in a strong dichroic signal within 350–450 nm. On 360 nm irradiation, photoisomerization occurs, and the cyclodextrin moiety moves toward the aliphatic bridge. This change is associated with the decrease of the CD signal associated with the absorption band of the azobenzene chromophore with concomitant increase of the CD signal associated with the absorption band of the 4,4'-bipyridinium moiety. The Janus-type rotaxane reported by Kaneda et al.<sup>257</sup> is based on the same principle. This molecular device is built from several hermaphroditic cyclodextrins, polyether-azobenzene threads with  $\alpha$ -cyclodextrin at one end. In solution, they undergo self-assembly, yielding long linear oligomers. Their length can be controlled via photoisomerization of azobenzene moieties. In this case, very strong changes in CD spectra are expected. Another system with dichroic activity was reported this year by Aida et al. Switching was based on photoisomerization of 4,4'-ethene-1,2-diylidipyridine and interaction of its *cis* isomer with zinc porphyrins linked with ferrocene moiety.<sup>258</sup>

Another clever application of the light-driven molecular shuttle with fluorescence output was reported recently by Tian and co-workers.<sup>259</sup> The switch consists of two naphthalimide fluorophores linked with the asymmetric azobenzene spacer and threaded through the  $\alpha$ -cyclodextrin cavity. In the *trans* form, the cyclodextrin moiety resides at diazo group. This results in hindered vibrations and rotations close to the green fluorophore (Figure 22b) and enhancement of the 520 nm fluorescence. Photoisomerization upon 360 nm irradiation results in relocation of cyclodextrin toward the second (blue) fluorophore, thus resulting in the increase of blue fluorescence with concomitant decrease in green emission. The same principle was utilized by Willner et al. to build the phototriggered electroactive system. The azobenzene-containing thread was immobilized onto a gold substrate via the thiolate anchor.<sup>260</sup> The cyclodextrin host fragment

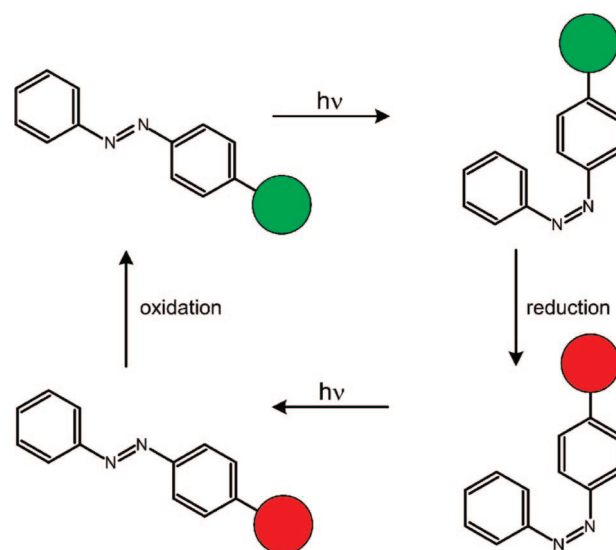




**Figure 22.** Optical switching of rotaxane-based molecular systems: switching of dichroic<sup>256</sup> (a), fluorescent<sup>259</sup> (b), and electrochemical<sup>260</sup> (c) properties.

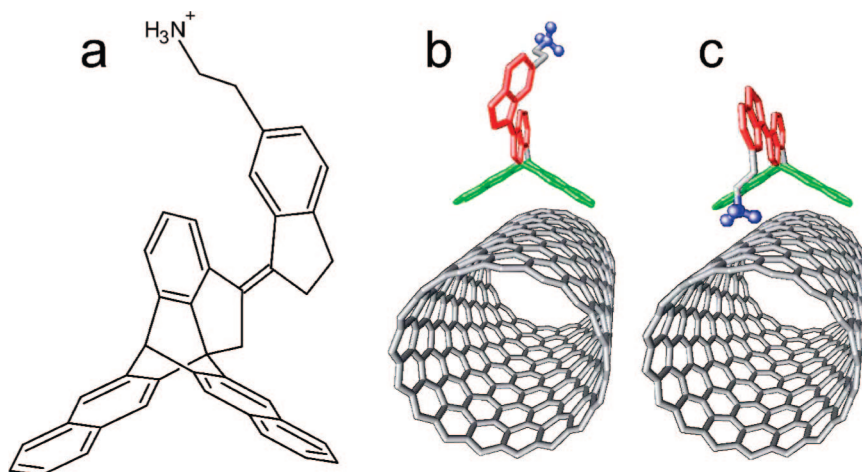
was additionally equipped with an electroactive ferrocene moiety (Figure 22c). In the *trans* isomer, the ferrocene moiety is located close to the surface of the gold electrode, which results in a high electron transfer rate. Photoisomerization of azobenzene fragment results in increased distance between the ferrocene moiety and the electrode surface. This in turn results in decreased electron transfer rate. These changes are observed as the change of the current intensities of anodic waves associated with ferrocene oxidation.

All of the chemical switches presented above use two different wavelengths for switching from *trans* to *cis* isomers and vice versa. A very interesting example of a molecular switch that undergoes *trans*-to-*cis* and *cis*-to-*trans* photoisomerization upon irradiation with single wavelength light came from the laboratory of Hiroshi Nishihara (Figure 23).<sup>261–263</sup> The switches are constructed from a photoswitchable moiety (azobenzene) coupled to a redox-active site (ferrocene,<sup>262</sup> Co(bpy)<sub>3</sub>,<sup>263</sup> and Cu(bpy)<sub>2</sub>).<sup>261</sup> It was observed, that depending on the redox state of the metal center irradiation with monochromatic light of fixed wavelength can induce both *trans*-*cis* and *cis*-*trans* photoconversion. Oxidation and reduction of a redox active moiety in the proximity of the azobenzene results in relative change in energies of  $\pi$ - $\pi^*$  and  $n$ - $\pi^*$  transitions,<sup>261–263</sup> which



**Figure 23.** Photochemical switch with redox-controlled switching characteristics. Colored circles represent the redox-active moieties in reduced (green) and oxidized (red) forms, respectively.

are responsible for *trans*-*cis* and *cis*-*trans* isomerization, respectively.<sup>264</sup> In all of the cases, the reduced form of



**Figure 24.** Molecular structure of the photoactivated switch for controlling electrical conductance of carbon nanotubes (a), its *trans* (b) and *cis* isomers attached to the carbon nanotube. The anchoring group, photoswitch, and the cationic moiety are marked in green, red, and blue, respectively. Adapted from ref 265.

studied complexes undergoes *trans-cis* photoconversion, while the oxidized one shows the *cis-trans* photoisomerization. In the case of the copper containing system, changes in the oxidation state of the central ion induce ligand exchange reactions due to steric hindrance,<sup>261</sup> while in the ferrocene containing system, the MLCT transition shows significant photoisomerization quantum yields.<sup>262</sup>

All of the light-driven switches presented above in principle can hardly be integrated with any classical or nanoelectronic circuitry. The only example of a light-driven nanoelectronic switch was reported (as a theoretical model) by Slava Rotkin and Ilya Zharov.<sup>265</sup> The designed system comprises a conducting carbon nanotube and biindalydene with an ammonium group on the aliphatic pendant arm. The photoswitchable chromophore is equipped with a 6,18-dihydropentacene group, which enables noncovalent attachment of the molecule to the carbon nanotube via  $\pi$ - $\pi$  interactions (Figure 24a). In the *cis*-form, the cationic group is relatively far from the surface of the nanotube (Figure 24b) and does not perturb its conducting properties. On photoisomerization, the cationic moiety approaches the nanotube surface (Figure 24c). Quantum chemical calculations (*ab initio* and DFT) indicate that this process creates an energy barrier within the carbon nanotube, thus decreasing the current intensity by 40%. This switch, although not demonstrated experimentally, constitutes an interesting combination of molecular switch and nanoelectronic device.

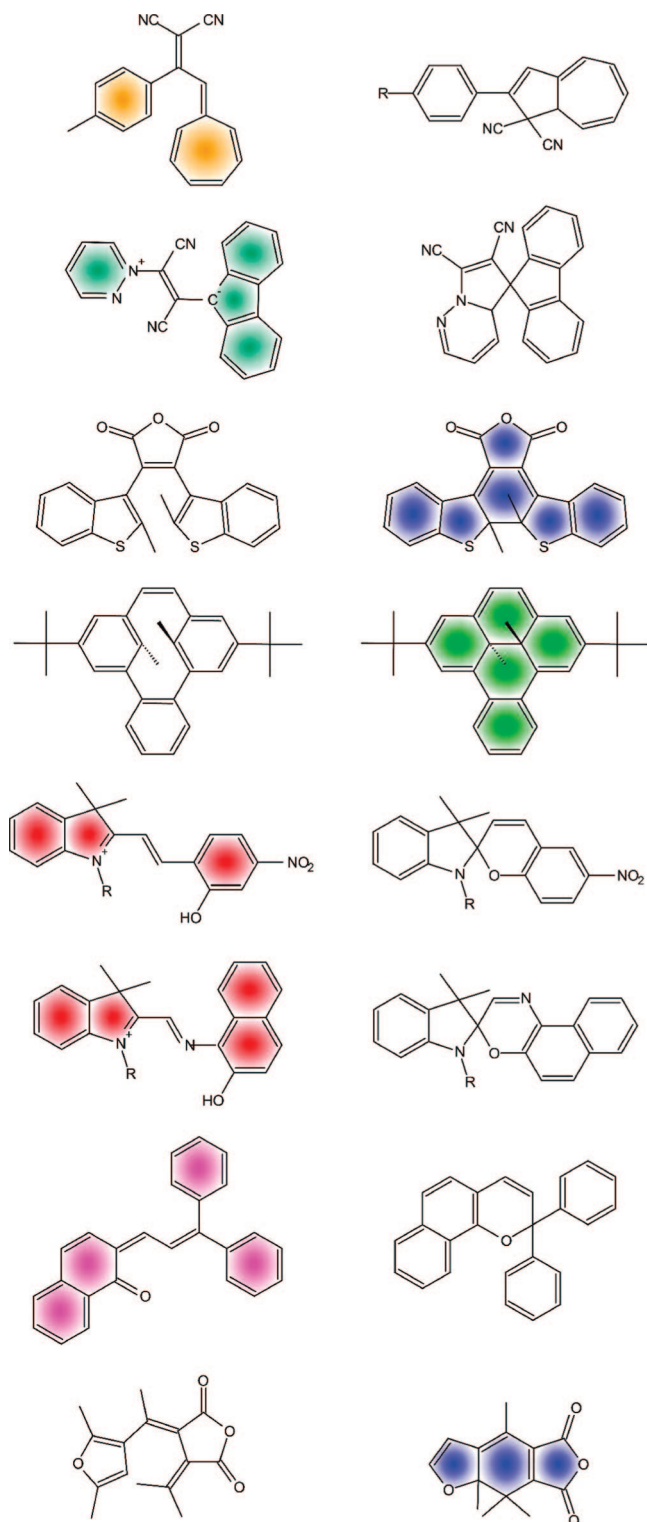
The second very large group of photochromic switches is based on the ring opening/ring closure reactions in photoinduced electrocyclic reactions. There are six main groups of compounds that have found numerous applications as switching molecules: dihydroazulenes and vinylheptafulvenes,<sup>266,267</sup> diarylethenes,<sup>268,269</sup> spiropyrans,<sup>270</sup> spiroxazines,<sup>270–272</sup> naphthopyrans,<sup>273</sup> dihydropyrenes,<sup>274</sup> fulgides, fulgimides, and related compounds (Figure 25).<sup>275</sup> There are many others examples of photoswitchable compounds, but these six classes of compounds are the most widely studied ones. Photoswitching of all of them involves reversible formation and opening of rings, and closed-ring forms of naphthopyrans, spiropyrans, spiroxazines, and fulgides are colorless, while the opened forms are strongly colored; in the case of diarylethenes and vinylheptafulvenes, the opened forms are colorless, and the closed forms are strongly colored. Photocyclization-based switches belong to monostable

and bistable switches: many molecules have been designed to achieve thermal stability, and they prospectively can be applied in molecular memories and as information carriers on other logic systems. However, numerous molecules undergo thermal back reactions. This process is disadvantageous from the point of view of long-term information storage, but for short-term storage and modeling of logic gates, it does not constitute any obstacle.

Various simple photochromic switches, based on the abovementioned structures, have been recently reviewed in the special issue of *Chemical Reviews* in 2000. Especially interesting are compounds that along with photochromism (reversible or irreversible) show other switching features, e.g., photocontrol of electron and energy transfer,<sup>276</sup> fluorescence modulation,<sup>269,277,278</sup> photoinduced polymer formation,<sup>279</sup> photoswitchable supramolecular receptors, photoswitchable organic magnets,<sup>269</sup> optically controlled receptors,<sup>280,281</sup> photoswitchable liquid crystalline phases,<sup>282</sup> and so forth. All of the abovementioned phenomena are usually the consequence of the reorganization of conjugated  $\pi$ -bond systems, which is especially evident in the case of diarylethenes and related species. Furthermore, numerous light-driven switches contain two or more photoswitchable chromophores, which results in multistate switches, e.g., multicolored photochromic systems.<sup>283</sup> Also the combination of photochromism and the formation of various coordination complexes results in complex switching patterns and cation-driven switching between positive and negative photochromism.<sup>284,285</sup> Many of these systems have been extensively reviewed; therefore, only the most recent systems relevant for molecular information processing devices are discussed.

Combination of photochromic spiropyrans reporter groups with azacrown and azathiocrown receptors results in compounds exhibiting complex and cation-dependent photoswitching patterns. Depending on the nature of the cation-receptor and the cation-photochromic unit interactions various processes have been observed: thermal isomerization, switching the photochromism off, reversal of photochromic reaction.<sup>284,285</sup> Similar effects were observed for diarylethene with pyridine receptor.<sup>286</sup> In general, behavior of these systems is closely related to the operation of PET-based chemosensors.

Especially promising, from the point of view of prospective applications in molecular logic systems, are molecules



**Figure 25.** Structures of opened (left) and closed (right) forms of various representatives of the photochromic switch families. From top to bottom: dihydroazulene, dihydroindolizine, diarylethene, dihydropyrene, spiroxazine, naphthopyran, and fulgide. Colored forms of photochromic compounds are marked with shading.

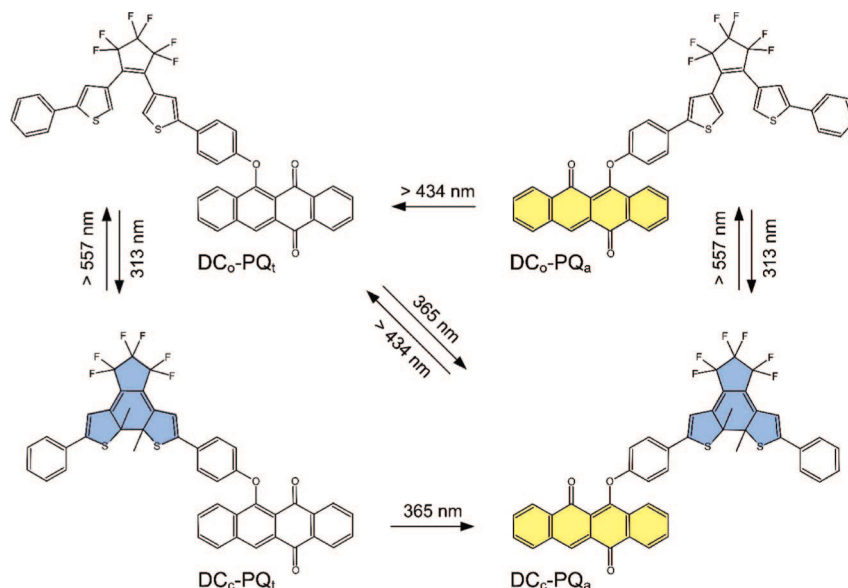
with covalently connected different photoswitchable chromophores. They may show multistate photoinduced switching and/or rerouting (or channeling) of excitation energy or electrons in conjugated frameworks. Similar effects can be

observed in molecular systems built from electron donor and electron acceptor moieties separated with a photochromic linker.

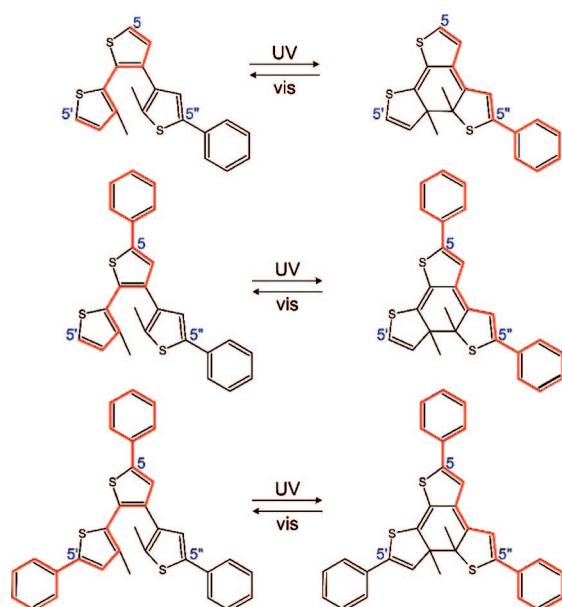
Two bichromophoric systems with three<sup>287</sup> and four<sup>288</sup> photochemically accessible states have been described recently. Multimode photochromism of a molecular dyad consisted of fused dithienylethene (DT) and dihydroazulene (DH) moieties.<sup>287</sup> Both chromophores undergo ring opening/closure reactions upon excitation. Three of four possible isomers have been detected and spectroscopically characterized. Due to thermal instability of the open ring form of dihydroazulene, the dyad is not very suitable for more complex switching devices.

The multiaddressable system of Branda and co-workers<sup>288</sup> comprises 1,2-dithienylcyclopentene and phenoxynaphthacenequinone (Figure 26). The components of this dyad exist in two distinctively different forms. Dithienylcyclopentene (DE) can exist in two thermally stable forms, opened (DE<sub>o</sub>) and closed (DE<sub>c</sub>), while phenoxynaphthacenequinone in *trans*- (PQ<sub>t</sub>) and *ana*- (PQ<sub>a</sub>) forms, respectively. Absorption spectra of the dyad are essentially equivalent to the spectra of isolated building blocks, thus indicating no significant electronic interaction between the two chromophores, but photochemical reactivity of the dyad is different from the reactivity of the 1:1 mixture of the components. Due to the thermal stability of all components of the dyad and weak electronic coupling between photochromic moieties, all possible forms of the DE-PQ dyad are stable and can be generated using only optical stimulation of proper spectral characteristics: DE<sub>o</sub>-PQ<sub>t</sub>, DE<sub>c</sub>-PQ<sub>t</sub>, DE<sub>o</sub>-PQ<sub>a</sub>, and DE<sub>c</sub>-PQ<sub>a</sub>. Due to the different spectral properties of the DE<sub>o</sub>, DE<sub>c</sub>, PQ<sub>t</sub>, and PQ<sub>a</sub> moieties, all four forms of the dyad can be easily detected spectroscopically. The most thermodynamically stable form is the DE<sub>o</sub>-PQ<sub>t</sub> isomer. Its irradiation with 313 nm light induces ring closure of the dithienylethene moiety resulting in the DE<sub>c</sub>-PQ<sub>t</sub> form. Irradiation with 365 nm light, in turn, induces both ring closure and photoisomerization of the naphthoquinone moiety. Further photochemical processes are depicted in Figure 26. Although the PQ cannot be addressed independent of the DE moiety, all four states can be photogenerated on the basis of different reaction quantum yields (hence different irradiation times are required to produce photostationary states related to the different chromophoric moieties). Due to the electrochemical activity of the naphthoquinone moiety, further development of the system resulting in more complex switching pattern should be possible.<sup>288</sup>

Various systems for routing of electron and electron transfer pathways have been designed and experimentally tested. A simple photochromic switch based on dithienylethene was reported by Kawai and co-workers from Kyushu University in Fukuoka.<sup>289</sup> The terthiophene moiety was further substituted with one, two, or three phenyl rings, thus resulting in a large  $\pi$ -conjugated framework. Photochemical ring closure reactions change the bonding pattern of the molecule, thus resulting in different double bond conjugation. In opened forms, double bond conjugated systems connect 5 and 5' carbon atoms and its aromatic substituents. On ring closure, the conjugation between these atoms is broken, while the other, between the 5 and 5'' carbon atoms, is formed. The authors suggest the application of these photonic rerouters as switching elements of logic gates (Figure 27).

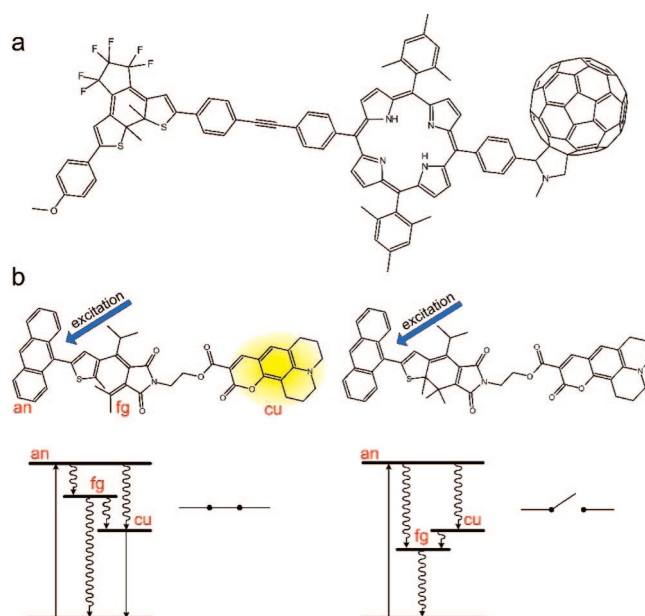


**Figure 26.** Photochemical reactions of the 1,2-dithienylcyclopentene-phenoxynaphthacenequinone dyad.<sup>288</sup>



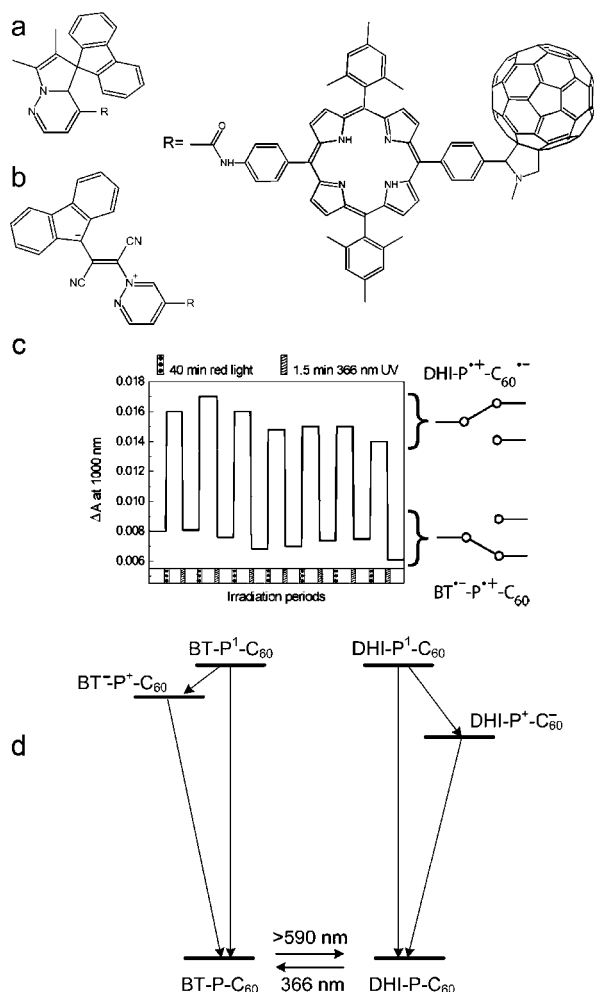
**Figure 27.** A series of photoswitchable molecular rerouters.<sup>289</sup> Frameworks of conjugated bonds are marked in red.

Much more promising photoswitching was observed in the case of the dithienylethene (DE)–porphyrin (P)–fullerene ( $C_{60}$ ) triad (Figure 28a) by Devens Gust and co-workers.<sup>290</sup> The triad does not show any significant porphyrin fluorescence in either open or closed forms due to a very efficient photoinduced electron transfer processes. When the DE is in the open form ( $DE_o$ ), the porphyrin singlet excited state generated by visible illumination undergoes photoinduced electron transfer with a time constant of 25 ps to the  $C_{60}$  unit to give  $DE_o\text{-P}^+-C_{60}^-$  with a quantum yield of unity, which decays to the ground state with a time constant of 3 ns. Upon excitation with UV light, dithienylethene undergoes ring closure reaction. When the DE is in the closed form ( $DE_c$ ), the porphyrin first excited singlet state generated by visible illumination is quenched by the energy transfer to the DE moiety within 2.3 ps, precluding significant electron transfer to the fullerene. Therefore, the switching unit controls the pathway of porphyrin excited-state deactivation between electron transfer and energy transfer, observed for opened



**Figure 28.** Structure of the DE-P- $C_{60}$  triad (a) and the structure and corresponding energy diagrams for the anthracene–fulgimide–coumarin triad (b).

and closed forms of the dithienylethene, respectively. The photonic switching of photoinduced electron transfer in the triad can be cycled many times and could prove useful in the construction of molecular-scale optoelectronic devices (*vide infra*). Other photoisomerizable moieties, such as dihydropyrene, yield similar results. Similar behavior of the molecular triad was observed by H. Port and co-workers from Stuttgart University.<sup>291</sup> The donor–acceptor system (anthracene and coumarin, respectively) was separated by a photoisomerizable fulgimide bridge (Figure 28b). In the case of the opened form of the fulgimide bridge, the molecular orbitals of all three subunits are decoupled. Upon excitation of the anthracene moiety, only the fluorescence of the coumarin unit is observed due to efficient electronic energy transfer. Upon photoisomerization of the fulgimide bridge, the first excited state of fulgimide is lower than the anthracene one, and it traps the excitation energy.



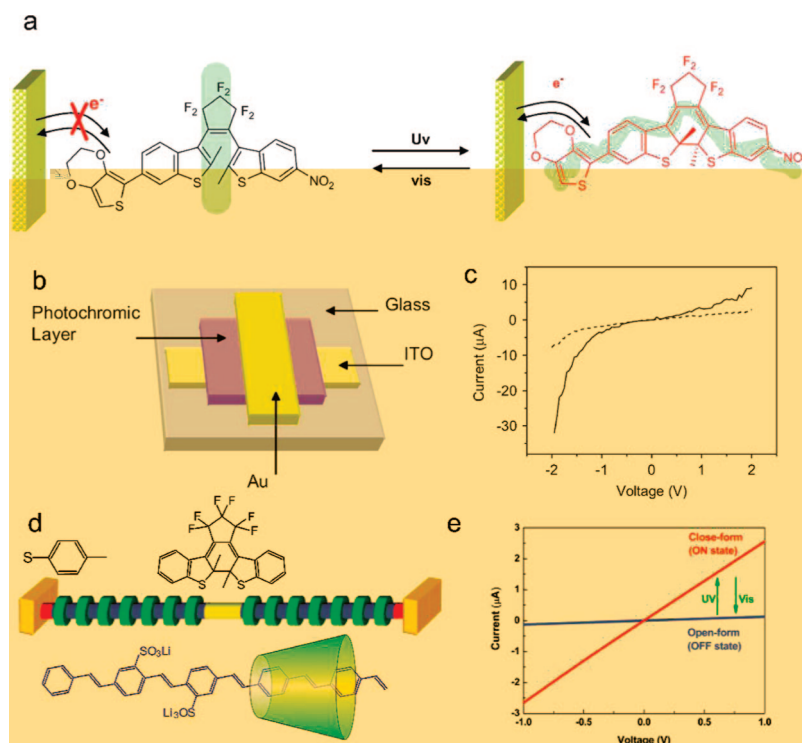
**Figure 29.** Structures of dihydroindolizine (a) and betaine (b) forms of the photoswitchable triad. Switching of the triad is shown as changes of transient absorption at 1000 nm (c). Energy diagram of the system (d) illustrates the photophysical behavior of the switch. Partially reprinted from ref 292. Copyright 2005 American Chemical Society.

A photoswitchable device, which is the closest to its electronic equivalent, was reported recently by Gust and co-workers. The idea of the device is similar to that shown in Figure 28, but instead of selecting the excited-state deactivation pathway, the system is capable of directing a photoinduced electron transfer reaction toward the desired electron acceptor. The switching molecule comprises three building blocks: porphyrin chromophore/electron donor (P), fullerene electron acceptor (C<sub>60</sub>), and a dihydroindolizine photoswitchable unit (DHI, Figure 29a).<sup>292</sup> Excitation of the porphyrin chromophore at 650 nm results in the generation of the DHI<sup>1</sup>P-C<sub>60</sub> excited state. Within a nanosecond, the photoinduced electron transfer proceeds, finally yielding the DHI-P<sup>+</sup>-C<sub>60</sub><sup>-</sup> charge separated state, characterized by absorption at 1010 nm, corresponding to the fullerene anion radical. UV irradiation (366 nm) results in photoisomerization of the dihydroindolizine (DHI) to the betaine (BT) form (Figure 29b). Subsequent irradiation at 650 nm does not produce the 1010 nm absorption, thus indicating the alternative electron transfer pathway that yields the BT-P<sup>+</sup>-C<sub>60</sub> product. The system can be thus regarded as a double throw switch (Figure 29c, d) directing flow of electrons toward two different destinations. Other photoactive electronic switches have been reviewed recently by Andrew

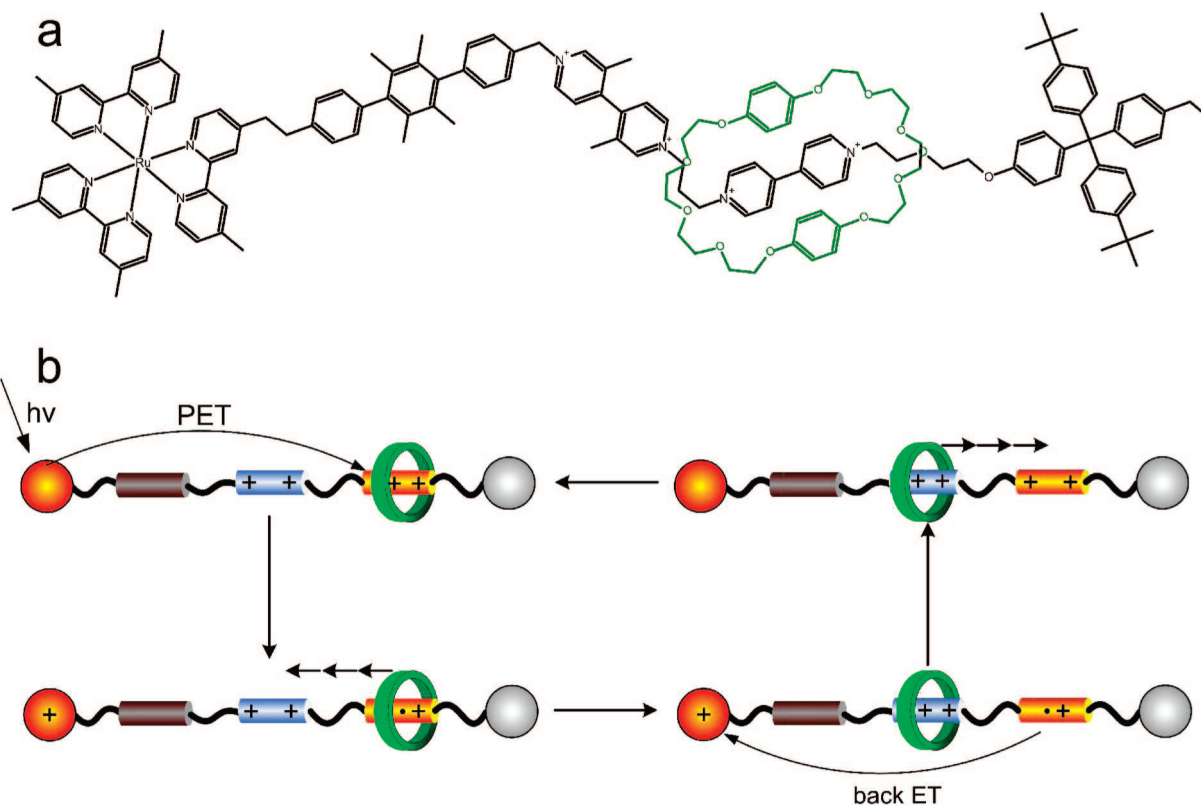
C. Benniston<sup>293</sup> and quantum chemical analysis of related switches was presented by Stanislav Nešpůrek and colleagues.<sup>294–296</sup>

A dithienylethene (DE) photoswitch reported by Kim et al. with attached donor (D) and acceptor (A) groups (Figure 30a) was used recently for the fabrication of the photoelectric switching device (Figure 30b).<sup>297</sup> The general structure of the switch resembles that of molecular photodiodes: donor and acceptor moieties are separated by an aromatic linker. In this case, however, the linker can change its electronic properties on demand: from nonplanar (and thus unconjugated) opened form and fully conjugated, planar closed form. In the closed form the conjugation extends on the two benzothiophene groups and to the donor and acceptor substituents. Introduction of donor and acceptor functionalities significantly influences the spectral properties of both forms and results in a bathochromic shift of the low energy absorption bands. Furthermore, the cyclization quantum yield is increased to 0.52 (0.34 for unsubstituted compound), while the ring opening quantum yield is decreased (0.01 vs 0.06 for unsubstituted one). Both compounds form stable and homogeneous dispersion in polystyrene yielding transparent composite films containing up to 30% of the photochromic dye. These films can be produced on conducting substrates (Figure 30b). Polymeric films containing the opened form of the dithienylethene switch are characterized by low electrical conductivity (Figure 30c). On irradiation, however, the conductivity significantly increases, and voltage-current characteristics shows typical rectifier behavior. Nanoscale versions of this device were reported recently.<sup>298–301</sup> The photoswitchable nanodevice (Figure 30d) comprises two polyrotaxane nanowires (poly *p*-phenylenethene +  $\alpha$ -cyclodextrin) equipped with thiolate alligator clips and photo-switchable unit (diarylethene). It was found that the electrical conductivity of the nanowire can be changed via optical stimulation: the opened form of the photoswitch results in high electric resistance of the nanowire, while on photochemical ring closure, the resistance decreases by 2 orders of magnitude.<sup>298</sup> Very similar effects were observed for arrays of gold nanoparticles bridged by thiol-terminated diarylethene.<sup>299</sup> Further miniaturization can be achieved when the photochromic moiety separates two electroactive centers, e.g., transition metal complexes, as shown by Akita and co-workers<sup>302</sup> or by bridging two carbon nanotubes with the photoswitchable unit.<sup>301</sup> Theoretical investigations on electrical conductivity through long diarylcyclopentene nanowires were reported recently by Yoshizawa and co-workers.<sup>303</sup>

A very special category of photoactive switches can be built on the basis of supramolecular complexes: rotaxanes and catenanes. These complexes are made from electron donor and electron acceptor subunits engaged in intermolecular charge transfer interactions. Furthermore, the supramolecular assemblies contain photosensitizers covalently attached to one of the counterparts of the assembly. Excitation of the photosensitizer results in PET reaction between the photoactive center and the electron acceptor. Ruthenium(II) bipyridine and rhenium(I) bipyridine carbonyl complexes are commonly used in these light-driven molecular switches. The photoswitchable supramolecular assembly presented in Figure 31 comprises the following building blocks: polyether *p*-cyclophane and a thread consisting of ruthenium bipyridine photosensitizer, rigid terphenyl spacer, two viologen-type electron acceptors, and a bulky stopper.<sup>304–306</sup> In the ground state,



**Figure 30.** Photoswitching of the D-DE-A triad results in increased electrical conductivity due to extension of bond conjugation (a). Structure of the thin film photocell consisting of the photochromic layer deposited between gold and ITO contacts (b). Voltage–current characteristics of the device before (dashed line) and after (solid line) irradiation (c). Nanoscale equivalent of photochromic electric switch equipped with thiol allegator clips (d) and its voltage–current characteristics (e). Reprinted with permission from ref 297. Copyright 2006 Elsevier. Reprinted from ref 298. Copyright 2006 American Chemical Society.



**Figure 31.** Structure of the photoswitchable rotaxane (a) and schematic representation of photoinduced shuttling movement of the polyether macrocycle between the two viologen-like stations (b).

the macrocyclic ring resides at the terminal viologen station due to strong charge transfer interactions. Photoexcitation of the ruthenium(II) moiety results in photoinduced electron transfer from  $Ru^{II}$  to the terminal

viologen station. Formation of the cation radical destabilizes the rotaxane and induces shuttling movement of the macrocycle toward the dimethylviologen station. Back electron transfer returns the electronic structure of the

thread component to the original state. As a consequence of electronic reset, the macrocycle moves back to the viologen station. This photocontrolled molecular shuttle is an example of a large class of molecular abaci developed recently. Other systems based on a similar principle were also reported<sup>307,308</sup> and reviewed recently.<sup>309,310</sup> The same approach can be used for rotation control of a catenane.<sup>311,312</sup> Related molecules have been successfully applied as molecular logic gates and in nanoelectronic circuits. Integration of optical switches with electronic devices is very important because of the development of optical devices in telecommunication networks.<sup>90,313</sup>

### 4.3. Redox Driven Molecular Switches

Electrochemically driven molecular switches are another large class of molecular systems with prospective application for information processing. There are numerous chemical systems in which the changes in optical properties (absorption, fluorescence) or molecular geometry/conformation can be controlled and/or switched by redox reactions.<sup>314</sup> There are three main categories of electrochemically switchable molecular systems: supramolecular assemblies in which translocation of molecular fragments is induced by electrochemical processes, electrochemical control over photoinduced energy/electron transfer, and electrochromic switches.

The supramolecular light-driven molecular switches based on donor–acceptor building blocks can be also addressed electrochemically: selective oxidation/reduction of some components results in identical changes in the supermolecule geometry. There are two main classes of electrochemically active compounds, which show geometrical/topologic changes upon oxidation/reduction. The first class encompasses various transition metal complexes containing two different sets of donor atoms within one supramolecular assembly. Upon change in oxidation state of the central metal ion, the geometry of the supermolecule rearranges to achieve the most favorable coordination environment around the metal ion. Such a system was reported recently by Abraham Shanzer and Anne-Marie Albrech-Gary et al.<sup>315</sup> The electroswitchable systems consisted of a large ligand incorporating two sets of tetraordinating cavities,  $N_2O_2$  and  $N_4$ , based on hydroxiquinoline and bipyridine moieties, respectively. The first cavity preferentially binds  $Cu^{2+}$  cations, while the latter binds  $Cu^+$ . Sequential reduction and oxidation of the metal center results in translocation of the copper ion between the two binding sites. Related systems were developed and reviewed by Jean-Pierre Sauvage et al. and are the basis for the nanometer scale model of muscles.<sup>316,317</sup>

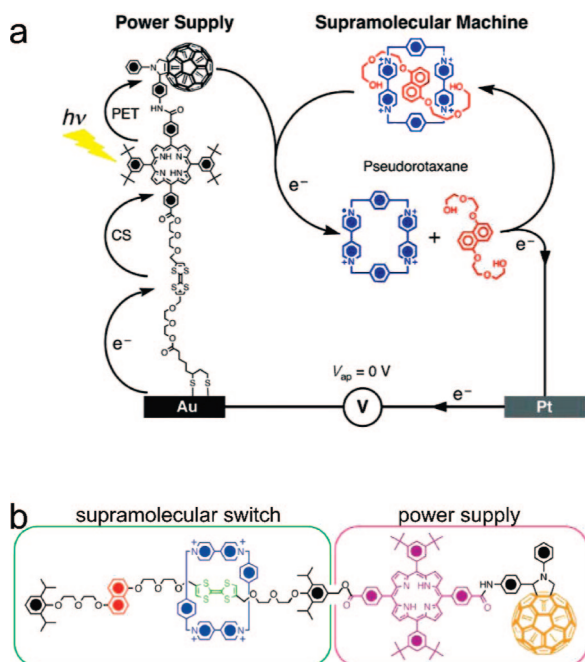
Frequently studied electroactive molecular switches are based on supramolecular assemblies containing donor and acceptor moieties incorporated into pseudorotaxanes, rotaxanes, or catenanes. Oxidation of donor or reduction of acceptor moieties results in weakening of interaction and subsequent dissociation or rearrangement of the supermolecule (cf. Figure 31b). This in turn dramatically changes the electrochemical and/or optical properties of the system. Commonly used electron donors include the following moieties: ferrocene, 1,5-naphthalenediol, 2,2'-bis(1,3-dithiolyldiene) (also known as tetrathiafulvalene), and others, while common electron acceptors are based on viologen framework. Some of these systems have found application in prototypical nanoelectronic devices. Most of these devices contained electrochemically active ro-

taxanes or catenanes deposited on conducting support and evaporated metallic contacts atop the supramolecular layer.<sup>318–323</sup> Changes in electric potential between the electrodes results in redox switching of the supramolecular entities. This switching results in geometrical rearrangements, which in turn affect the tunneling current.<sup>324–326</sup> Carbon nanotubes can also provide a support for polymer-bound supramolecular switches.<sup>327–329</sup> Even more complex devices can be made when the molecular switches are incorporated within the crossbar circuits.<sup>330,331</sup>

An interesting combination of an electrochemically driven molecular switch and molecular-scale power supply was presented recently by Jeffrey I. Zink and J. Fraser Stoddart.<sup>332</sup> The device is built from the photoactive tetrathiafulvalene–porphyrin–fullerene triad acting as light harvester and charge separation system and a electroswitchable pseudorotaxane (Figure 32).<sup>332</sup> Excitation of the dyad results in a photoinduced electron transfer reaction, yielding the charge-separated state with an electron localized on the fullerene moiety. Reaction of the fullerene anion radical with viologen-based cyclophane results in destabilization of the supramolecular entity and dethreading of the pseudorotaxane. This device is closely related to the photosensitized solar cells: the triad harvests light and generates photocurrent, while the cyclophane is a redox mediator regenerating the photoactive system.<sup>333,334</sup> A variation to this scheme was recently designed by Fraser Stoddart and Alberto Credi with co-workers.<sup>335</sup> The new system (Figure 32b) contains the photoactive charge generator and the switchable rotaxane integrated within single supermolecule. Preliminary experiments indicate, however, that the operation of these devices can be strongly perturbed by strong intramolecular charge transfer association and formation of various foldamers.<sup>335</sup>

Another combination of the electrical and optical activity of the molecular switch was presented recently by Ben. L. Feringa et al.<sup>336,337</sup> It was found that photoactive dithienylcyclopentenes can undergo oxidation-induced ring opening and ring closure reactions depending on the substituents in the central and terminal rings. Hexahydrodithienylcyclopentenes bearing aromatic pendant groups undergo the oxidative ring closure reaction along with typical photochemical ring opening and ring closure processes. Fluorination of the central ring changes the electrochemical reactivity of the molecule dramatically; oxidation results in the ring-opening reaction. Further modification of the molecule via introduction of methoxy groups into the pendant phenyls induces reversal or electrochemical reactivity. Similar coupling of photoisomerization and electroisomerization was found in the ferrocenyl derivative of hexahydrodithienylcyclopentene<sup>338</sup> and *N*-methylpyridinium substituted dithienylcyclopentenes.<sup>339</sup>

Electrochemical control of energy transfer processes in multiporphyrin arrays strongly resembled the control of electron flow through the electronic circuits. The studies systems comprising the light harvesting moiety (difluoroboron-dipyrrin) covalently linked with triporphyrinic array containing zinc porphyrin (ZnP), magnesium porphyrin (MgP), and free base porphyrin ( $H_2P$ ) connected in linear (SWITCH-12) or T-shaped fashion (SWITCH-13) via diphenylethyne bridges.<sup>340–342</sup> In the optoelectronic gate, a boron–dipyrrin chromophore (BDPY) plays a role in the input unit, the zinc porphyrin is the transmission unit, and a free base porphyrin is the output unit, while the magnesium porphyrin moiety controls the energy flow through the system. In the neutral state, excitation of the BDPY results in fast (17 ps) energy transfer to the ZnP fragment and further to the  $H_2P$  unit (45 ps). The same processes take place in the T-shaped system. In both cases, fluorescence is observed



**Figure 32.** Schematic representation illustrating how the light-driven power supply, the TTF–porphyrin–fullerene triad, provides the electrical energy to dethread a [2]pseudorotaxane. The curved arrows indicate the vectorial electron transfer (PET) from the photoexcited porphyrin chromophore to the C<sub>60</sub> component, followed by a charge shift to the TTF component, and finally a charge neutralization by the Au electrode in a closed circuit. Subsequently, the electron is transferred to the pseudorotaxane, leading to the dethreading reaction before the electron is passed onto the Pt counter electrode (a). The same device integrated into a single supermolecule (b). Reprinted with permission from ref 332. Copyright 2005 Wiley Interscience. Reprinted from ref 335. Copyright 2007 American Chemical Society.

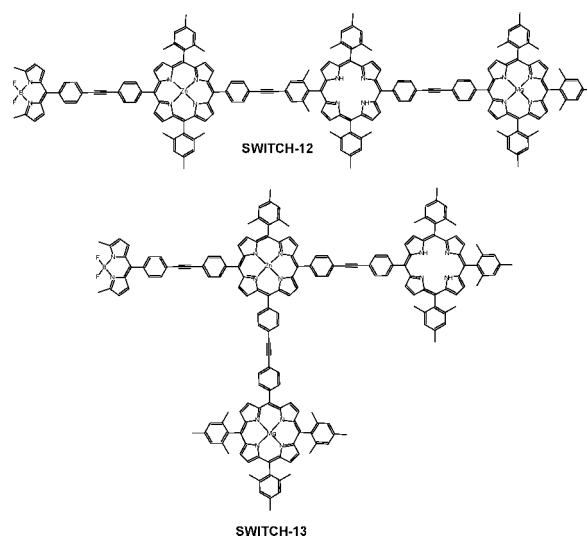
exclusively from the free base porphyrin fragment (Figure 33a and b). Oxidation of the magnesium porphyrin moiety results in lowering of the MgP energy level, which in turn results in almost complete fluorescence quenching (Figure 33c and d).

In contrast to previously discussed devices, which can be used for both information processing and storage, the numerous electrochromic systems can be used mainly for visualization purposes, e.g., in electrochromic displays. There is a great number of compounds showing electrochromic effects, but the most commonly used ones are Prussian blue and viologen derivatives as well as various polythiophene-based materials.<sup>343,344</sup> This subject is, however, out of the scope of this review.

#### 4.4. Magnetic Switches

Magnetic phenomena were one of the first bases for information storage in electronic devices.<sup>345,346</sup> Recent development of coordination chemistry, material science, and nanotechnology resulted in new magnetic materials<sup>347–350</sup> of prospective application in information storage and processing.<sup>351</sup> The most promising are the materials showing the spin crossover (SCO) phenomenon. Magnetic properties the SCO systems can be switched on and off upon thermal, optical, mechanical, or magnetic stimulation. Numerous systems showing SCO effects as well as various applications of inorganic SCO materials have been reviewed in three special issues of *Topics in Current Chemistry*<sup>352</sup> in 2004 and very recently in *Coordination Chemistry Reviews*,<sup>353–358</sup> *Angewandte Chemie*,<sup>359</sup> *Journal of Photochemistry and Photobiology*,<sup>360,361</sup> and *Chemical*

*Communications*.<sup>362,363</sup> Therefore, only a brief description of the SCO processes is given here.



Spin crossover systems can easily mimic the fundamental YES and NOT gates. This may be considered as a limitation, but as input and output do not need to share the same transmission channel, the SCO devices can transduce various chemical, magnetic, or optical signals into other information channels.

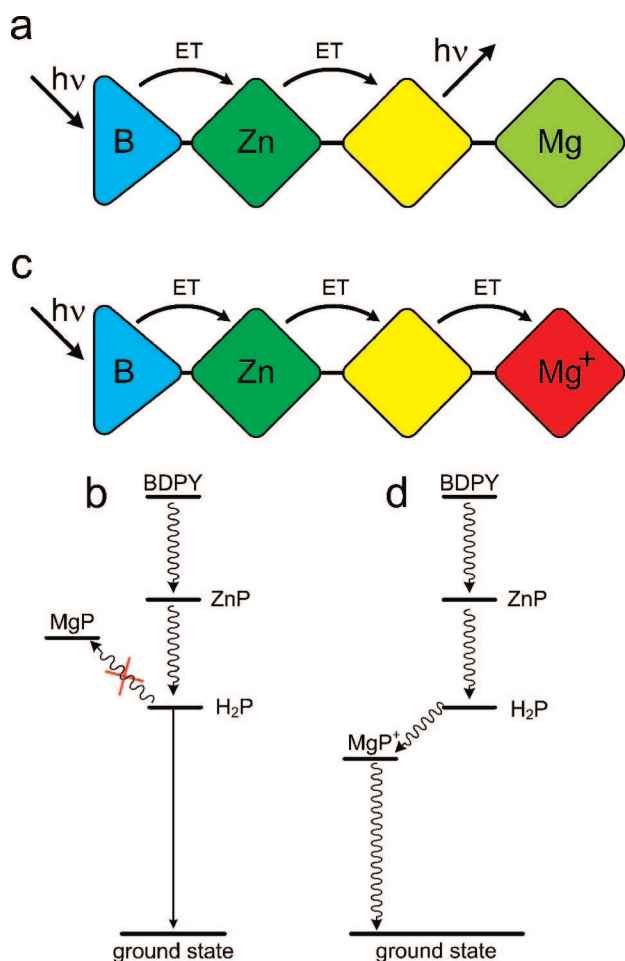
Spin crossover processes are mostly observed in transition metal complexes of  $d^4$ – $d^7$  electronic configuration as these ions (complexes) may be present in high spin or low spin configuration, depending on the competition between strength of the ligand field and electron pairing energy. Progressive change in the ligand field may result in the two spin states being almost equienergetic, and the electronic configuration may change with the application of external stimuli such as temperature, pressure, illumination, or magnetic field.<sup>364</sup> The most interesting, however, are the systems where switching can be induced by light or by magnetic field.

As light is a very convenient communication channel in molecular systems, optical switching of magnetic properties is especially interesting. It can involve two highly important processes: light-induced excited spin state trapping (LIESST) and ligand-driven light-induced spin change (LD-LISC). The LIESST process was first observed for the Fe(II) complex with propyltetrazole. The mechanism of LIESST for Fe<sup>II</sup> complexes is shown in Figure 34a.<sup>365</sup>

Excitation of the  $^1A_1$  ground state within the allowed transition yields the  $^3T_1$  ligand field excited state of the nanosecond lifetime. It can subsequently decay via two intersystem crossings to the  $^5T_2$  high spin state. As the  $^5T_2 \rightarrow ^1A_1$  transition is not spectroscopically allowed, the lifetime of this high spin excited state is long at low temperatures. Therefore, optical pumping of the low spin materials within the  $^1A_1 \rightarrow ^1T_1$  transition results in the population of the  $^5T_2$  state and formation of the high spin fraction. This metastable excited state can be converted to the  $^1A_1$  ground state either thermally or photochemically via irradiation within the  $^5T_2 \rightarrow ^5E$  transition (so called reverse-LIESST) (Figure 34a).

There are numerous molecular systems showing photomagnetic effects. To the most widely known belong Fe<sup>II</sup> complexes with nitrogen-containing heterocyclic ligands, transition metal complexes with TCNE and TCNQ ligands,<sup>366,367</sup> Prussian blue analogues, and other coord-



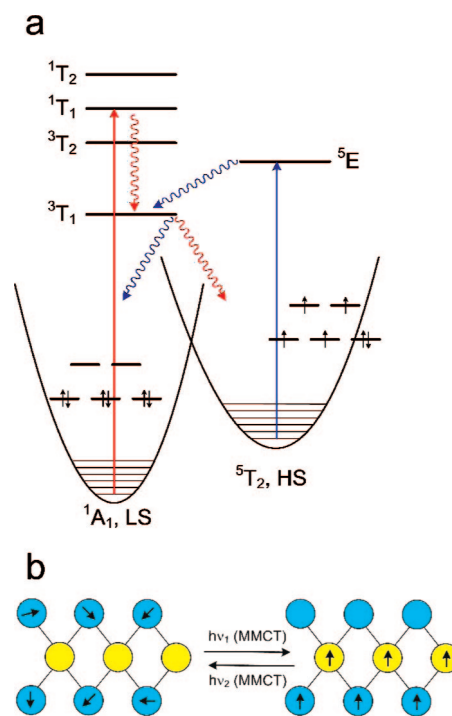


**Figure 33.** Representation of photophysical processes occurring in the linear porphyrinic optoelectronic gate in neutral (a) and oxidized form (c). Schematic energy level diagrams for the lowest excited states in the neutral (b) and oxidized (d) form of the gate. Adapted from ref 341.

dination polymers with cyanide and oxalate bridges.<sup>360,368</sup> Especially promising are cluster and polymeric systems, where photomagnetic effects are associated with MMCT transitions, and the magnitude of magnetization is amplified by magnetic ordering within these materials<sup>369–371</sup> resulting from efficient communication between paramagnetic centers.<sup>372</sup> Very good examples of such systems are polymeric cobalt(III) hexacyanoferrates(II)<sup>373</sup> and copper(II) octacyanomolybdates(IV).<sup>374</sup> The ground states of these materials can be described as diamagnetic  $\text{Co}^{\text{III}}\text{-N}'\text{C-Fe}^{\text{II}}$  and paramagnetic  $\text{Cu}^{\text{II}}\text{-N}'\text{C-Mo}^{\text{IV}}$  polymeric assemblies, respectively. On photoexcitation within the MMCT transition, metastable excited forms  $\text{Co}^{\text{II}}\text{-N}'\text{C-Fe}^{\text{III}}$  and  $\text{Cu}^{\text{I}}\text{Cu}^{\text{II}}\text{-N}'\text{C-Mo}^{\text{V}}$  are formed. Both excited forms show long-range ferrimagnetic ordering (Figure 34b).

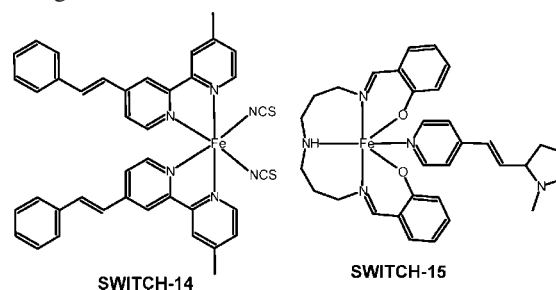
Other processes may include photoinduced electron transfer reactions between metal centers and redox-active ligands, such as catecholates and semiquinones, phenoxyls, triphenylmethyl radicals, nitroxides, and so forth.<sup>366,375–377</sup>

Photomagnetic phenomena are also observed in transition metal complexes with photoisomerizable ligands. These effects are based on the ligand-driven light-induced spin change (LD-LISC) phenomenon. The effect consists in modulation of the ligand-field strength of a suitable spin-crossover complex through a photochemical reaction on the ligand. It allows switching of the electronic spin state of the metal ion by means of light over a broad range of



**Figure 34.** Mechanism of LIESST (red arrows) and reverse LIESST (blue arrows) effects for Fe(II) complexes (a). Schematic representation of long-range magnetic ordering in copper octacyanomolybdate (b). Cu centers are marked in cyan, while Mo is in yellow.<sup>365,374</sup>

temperatures possibly including room temperature. Among the photochemical reactions capable of triggering the spin conversion reversibly, the *cis-trans* photoisomerization is the most studied one. The occurrence of the LD-LISC effect was shown in several iron(II) or iron(III) complexes (SWITCH-14, SWITCH-15). On varying the molecular components, the working temperature and excitation wavelengths were modulated so that the effect could be observed at room temperature upon irradiation of the sample with visible light.<sup>378</sup>



Much less common are systems that undergo spin cross-over upon magnetic field variations. In all of the SCO systems, application of the static magnetic field stabilized the high spin state. It usually demonstrates as a downward shift of the transition temperature, which can be described as a quadratic function of the magnetic field intensity, and significant spectral changes corresponding to low spin–high spin transition. The effect was observed for Fe<sup>II</sup>-thiocyanate complexes with phenanthroline and 4,4'-bis(1,2,4-triazole).<sup>379</sup>

Thermal and photoinduced switching of magnetic properties was also observed for various organic systems. As cross-linking of organic radicals is a strongly favored process, special care must be taken in designing organic molecular magnetic materials.<sup>366</sup> Reversible thermal switching of magnetic properties was observed for a series of dithiazolopyrazinyl radicals in solid state. Different crystal phases of different spin interactions

have been detected, and the mechanism of the spin transition is proposed. It is proposed that transition between the low temperature diamagnetic form (containing dimers of radicals) and the high temperature paramagnetic phase consists in slippage or a domino cascade-type of crystal structure rearrangement, depending on the structure of the radicals.<sup>380</sup> Photoswitching between dia- and paramagnetic forms was achieved in molecular systems containing two tetramethylimidazoline oxide oxyl radicals coupled with photochromic bis(benzothienyl)hexafluorocyclopentane (cf. section 4.2, Figure 25). In an opened form, two radical groups are independent, while in closed forms, unpaired electrons are efficiently coupled via the conjugated bond framework.<sup>381,382</sup>

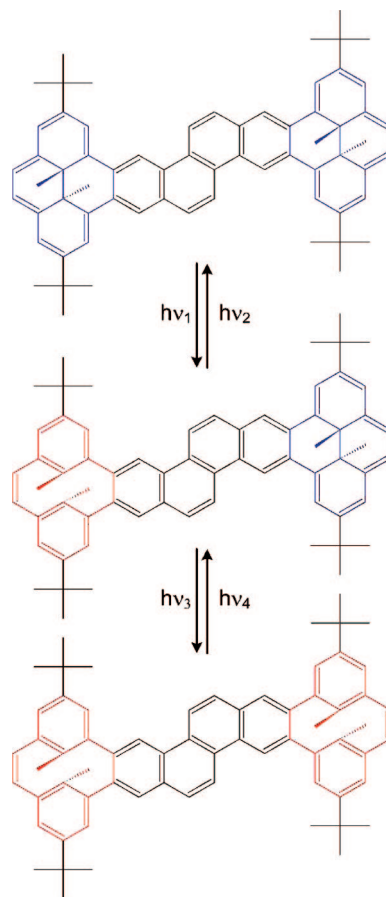
#### 4.5. Multistate Molecular Switches

The switchable molecules described so far exist in two stable forms of different spectral, electrochemical, or magnetic properties. They are direct analogues of simple electric switches existing in two easily distinguishable states, which can be denoted as ON and OFF states. It is possible, however, to find molecular systems that respond to stimulation in a more complex fashion. These molecules and molecular systems can exist in more than two distinguishable stable states and can therefore be related to multivalued logic systems. These multistate switches may be based on multichromophoric photochromic compounds, molecules undergoing orthogonal photochemical and electrochemical switching, supramolecular assemblies with equivalent or nonequivalent redox centers, fluorescent sensors capable of binding more than one target substrate or rotaxanes, and catenanes with a higher number of stations.

An interesting example of the three state photochromic switch was presented some time ago by R. H. Mitchell and co-workers.<sup>383</sup> The switching molecule contains two identical dimethyldihydropyrene photochromic switches linked with the chrysene moiety (Figure 35). Irradiation of the compound with full light of the tungsten lamp results in opening of both rings. Irradiation of the opened form within the chrysene absorption band (360 nm) results in photochemical closure of one ring. Prolonged irradiation or thermal reaction results in closure of the second ring. All three forms differ in the extension of the conjugated framework and therefore possess distinct optical and electrical properties.

An even more complex photochromic system with six stable states was reported the same year by F. Diederich.<sup>384,385</sup> In contrast to the previous example, the switching molecule contains two different photoisomerizable units: the dihydroazulene and tetraethylnethene. The switch is further complicated by the presence of the dimethylaniline moiety, protonation of which changes the photochemistry of the molecular assembly. Taking into account all possible forms of all of the components, it appears that there are eight possible forms of the switch (protonated and deprotonated, *cis* and *trans*, and opened and closed). Detailed spectroscopic analysis revealed the presence of six of them, and the detailed chemical transformations are shown in Figure 36.

Other systems showing complex switching pattern are based on the SP-MC photochromic couple and redox active TTF molecule. Photoisomerization changes many other chemical properties, such as redox potential,  $pK_a$  or coordinating properties of the SP-MC system. Combination of the photoswitchable SP unit and redox active tetrathiafulvalene (TTF) yielded an interesting four state molecular switch.<sup>386</sup> The photochemical activity of the SP unit within the SP-TTF dyad is almost unchanged as compared with the reference unsubstituted spiroopyran. Chemical oxidation with  $Fe^{3+}$  of the SP-TTF leads to



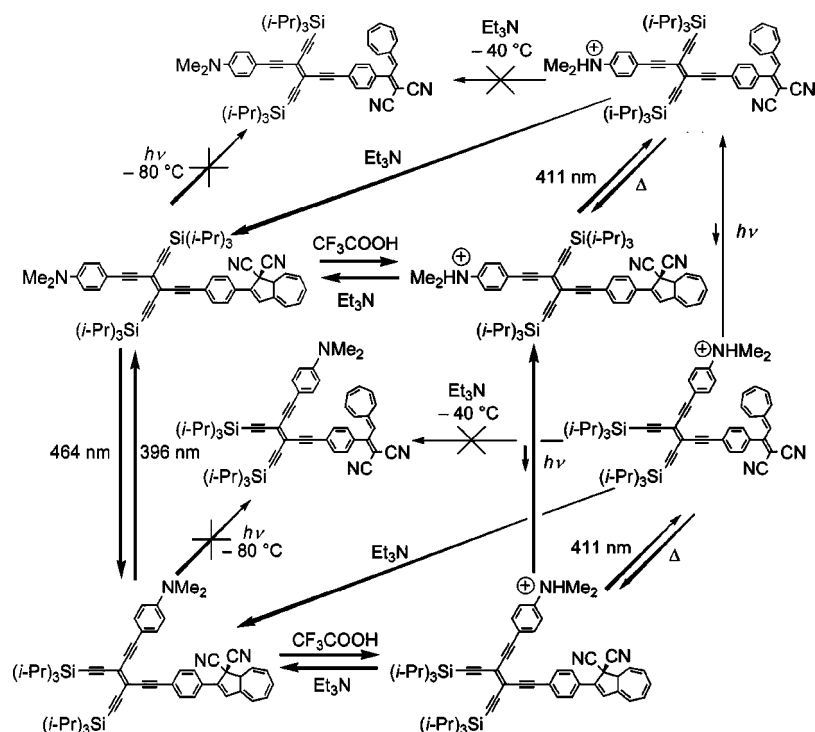
**Figure 35.** Three-state photochromic switch based on dihydropyrene (blue)–cyclophenadiene (red) photoisomerization. Adapted from ref 383.

immediate oxidation of the TTF moiety. Photoisomerization of the SP unit to the MC one results in back electron transfer, yielding  $Fe^{III}$  species, which are complexed in turn by the MC moiety, and TTF. In general, the redox state of the TTF unit within the TTF-SP dyad in the presence of ferric ions is controlled by the state of the photochromic moiety.

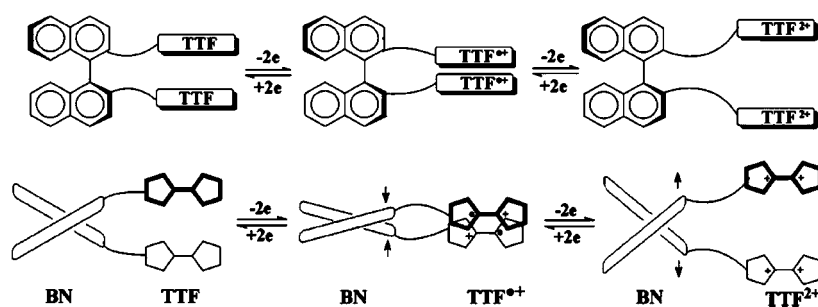
Other numerous spiroopyran–merocyanine systems have evolved into chemical logic gates or more complex systems and are described in detail in section 6. Other examples include dithienylethenes with the reactive 2-hydroxyphenyl substituent. Esterification of the OH group enables photochemical ring opening and closure reactions, while hydrolysis of ester stabilizes the opened form and prohibits photochemical ring closure, presumably due to efficient energy transfer to the hydroxyphenyl moiety.<sup>387</sup>

Multistate electrochemical switching, similar to photochemical switching, can be observed in systems containing several equivalent or nonequivalent redox centers. In the case of two redox centers, there are three possible distinct forms: fully oxidized, fully reduced, and the form where one redox center is oxidized and the other is reduced. The number of distinguishable states may be further increased taking into account protonation or other equilibria and processes involving some of the species.

A series of interesting systems containing up to four redox centers was reported recently by D. Zhu.<sup>388</sup> The switching molecule (Figure 37) combines the properties of the molecular building blocks: binaphthalene (BN) and tetrathiafulvalene (TTF). Absorption and CD spectral studies clearly indicate that the CD spectra resulting from axial chiral binaphthalene units can be modulated through the redox reactions of TTF units, which means new chiral molecular switches can be established on the basis of binaphthalene



**Figure 36.** Three dimensional switching diagram of the dihydroazulene–dimethylaniline–tetraethynylethene photochromic switch. Reprinted with permission from ref 384. Copyright 1999 Wiley-VCH.



**Figure 37.** Schematic illustration of the three states of the binaphthalene–tetrathiafulvalene switch showing different dihedral angles after partial and complete oxidation of the TTF units. Reprinted from ref 388. Copyright 2006 American Chemical Society.

molecules with TTF units.<sup>388</sup> In the fully reduced form of the switch (with two neutral TTF units), the two TTF units interact weakly due to  $\pi$ - $\pi$  stacking interaction, which results in a large dihedral angle ( $\sim 74^\circ$ ) between two naphthalene units. One electron oxidation of TTF units results in the cation radical, which exhibits very strong interaction.<sup>389</sup> The interaction decreases the dihedral angle, which results in an increase of dichroic absorption. Further oxidation yields the TTF dications, which strongly repulse each other. This in turn results in an increase of the dihedral angle between the BN units and a decrease of the dichroic signal. In addition, the manner of the CD spectrum modulation has been found to be dependent on the way TTF units are linked to the binaphthalene skeleton, in terms of linker length, the positions for substitution, and the number of TTF units.<sup>388</sup> Another TTF-based electroactive three-state molecular switch was described by Vincenzo Balzani and co-workers.<sup>390</sup> A supramolecular assembly of tetrathiafulvalene and viologen-based cyclophane is formed in solution containing both components (Figure 38a). Addition of 1,5-dinaphtho-[38]crown-10 (Figure 38b) does not change the properties of the systems, and the TTF guest stays within the cyclophane. Oxidation of TTF to the corresponding cation radical results in decomposition of the host–guest assembly due to

the decrease of charge transfer interaction between the components. Further oxidation of TTF to the dication yields the new supramolecular complex.  $\text{TTF}^{2+}$  is a good electron acceptor, and it forms a complex with the crown ether host (Figure 38c). Therefore, the state of this simple molecular switch can be easily controlled by potential (Figure 39d).

As envisioned by authors of the work, this simple molecular system can be further extended via the addition of chromophoric pendant groups to the molecular components. This would result in a system capable of controlling the photoinduced electron and/or energy transfer between the building blocks.

Other three state electroactive molecular switches with nonequivalent redox centers described recently are based on the terthiophene–fullerene dyad<sup>391</sup> and polychlorotriphenylmethyl-ferrocene assembly.<sup>392</sup>

## 5. Two Input Chemical Logic Gates

The idea of computation at the atomic or molecular level was first mentioned by Richard Feynman in 1959.<sup>121</sup> It took over 30 years for the first practical implementation of Feynman's ideas; the first molecular machines were reported in 1992 by Vincenzo Balzani and co-workers.<sup>393</sup> The work by Balzani et al. describes the first molecular devices based

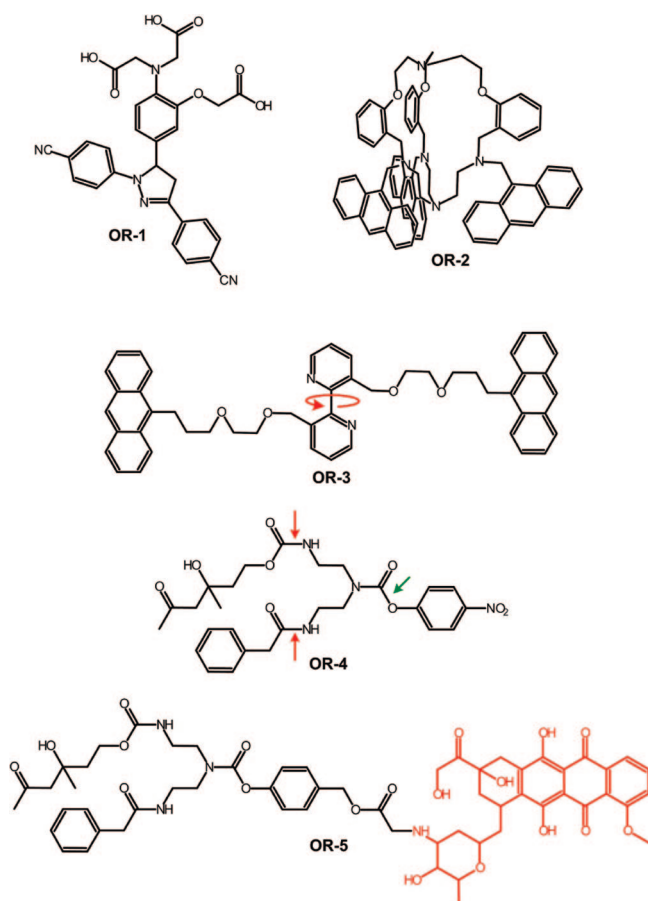
on molecular recognition and self-assembly. Nowadays, rotaxanes and catenanes are elements of molecular logic gates and nanoelectronic devices. Only a year later the first molecular logic gate was reported by A. Prasanna de Silva.<sup>140</sup> The first logic gate has emerged from fluorescent probes based on molecular recognition of target molecules.<sup>394–397</sup> These gates and other devices were controlled exclusively by chemical signals, while the output was observed as changes in fluorescence and absorption spectra.

During the last dozen or so years, great progress in the field of molecular logic gates was achieved. There are hundreds of chemical systems that are capable of complex information processing at the molecular level. Information can be fed in as chemical, optical, or electrical signals, while the result is retrieved in most cases as optical or electric signals. The next sections discuss in detail various kinds of simple chemical logic gates and more complex computational circuits based on molecular and nanocrystalline systems.

## 5.1. All-Chemical Logic Gates

### 5.1.1. OR Gates

The OR gate, which computes the logic sum of two input variables (cf. Table 2), is the easiest to be implemented in molecular systems. Most of the all-chemical OR gates described in the literature are based on fluorescent sensors that respond in the same way to at least two different molecular targets. Despite the simplicity of the chemical implementation of the OR function, only a few purely OR-type gates have been reported so far.



The OR-1 gate is based on the PET phenomenon. The tricarboxylate receptor part can successfully bind magnesium and calcium ions. This nonselectivity constitutes the basis

of OR operation. On ion binding, the electronic structure of the molecule is rearranged (cf. Figure 12), and fluorescence of the fluorophore is switched on.<sup>398</sup>

The same behavior was observed in the trianthryl cryptand system OR-2 and its analogues with different cage dimensions.<sup>399</sup> Fluorescence on the anthryl moieties is efficiently quenched due to PET from the nitrogen atoms within the cryptand, and only very weak exciplex emission is observed ( $\Phi \approx 0.0005–0.001$ ). Coordination of various metal ions within the cavity ( $\text{Mn}^{2+}$ ,  $\text{Fe}^{3+}$ ,  $\text{Co}^{2+}$ ,  $\text{Ni}^{2+}$ ,  $\text{Cu}^{2+}$ ,  $\text{Zn}^{2+}$ ,  $\text{Pb}^{2+}$ ,  $\text{Eu}^{3+}$ , and  $\text{Tb}^{3+}$ ) increases the fluorescence quantum yield of 1–3 orders of magnitude. Moreover, upon coordination of metal ions only monomer emission is observed. Surprisingly, some other heavy metal ions ( $\text{Hg}^{2+}$ ,  $\text{Tl}^{+}$ , and  $\text{Ag}^{+}$ ) do not affect the luminescent properties of the cryptand. Both gates can be brought to the initial state by the removal of cations from the reaction medium.

The output channel of the OR logic gate is not limited to the modulation of luminescence. Two other systems reveal Boolean control of chemical reactivity.

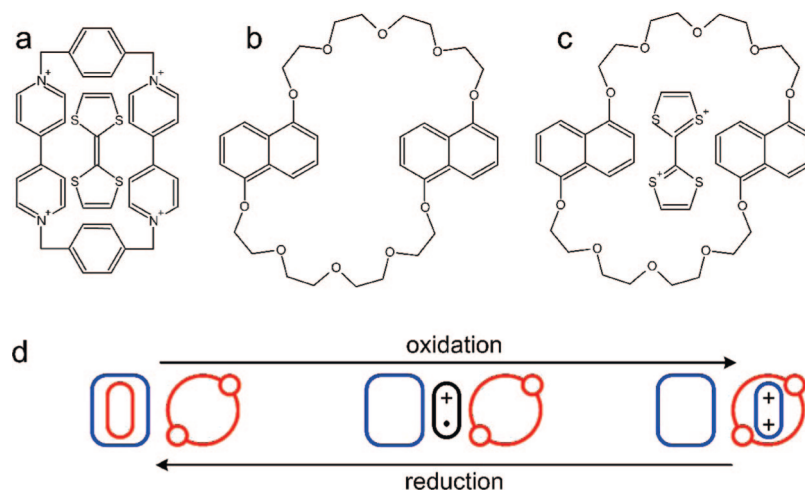
Compound OR-3 undergoes cation-induced rearrangement upon binding of metal ions to at least one of the receptor sites. Sodium ions are bound to the polyether chains, while  $\text{Hg}^{2+}$  is bound to the bipyridine unit. Irrespective of the cation, the molecule undergoes the same guest-enforced rearrangement, which greatly reduces the distance between two anthryl units and allows photoinduced dimerization. Return to the initial state must therefore include the removal of cations to unlock the rotation of the bipyridine unit and UV irradiation of the bianthryl moiety.<sup>400</sup>

Operation of all of the above OR logic gates may be extended to multi-input mode by selecting more than two triggering cations. The OR-2 already responds to 9 different cations and therefore can be regarded as a 9-input OR logic gate.

An important application of molecular logic gates was found recently in antitumor therapy. New generation anti-tumor drugs are based on various logic gate-like molecules.<sup>124,125</sup> Prodrugs of low general toxicity are metabolized selectively within or in the vicinity of malignant tissue due to a combination of various molecular signals including low oxygen concentration (hypoxia) and the presence of tumor-associated enzymes or antibodies. Two molecules representing this idea and operating as an OR gate were reported by D. Shabat and co-workers.<sup>123</sup> Model compound OR-4 contains two molecular targets, phenylacetamide and 4-hydroxy-4-methylhexan-2-one moieties, which can be selectively hydrolyzed by penicillin G amidase and 38C2 catalytic antibodies, respectively (red arrows). In the presence of any of the two biomolecules, one of the amido groups is cleaved, the free amino group catalyzes the cleavage of the second amido bond (green arrow), and 4-nitrophenol is liberated. Concentration of 4-nitrophenol can be used for diagnostic purposes or to monitor enzymatic activity. A more elaborated system (OR-5) contains an actual antitumor drug (marked in red), doxorubicin, bound to the OR trigger via the hydroxybenzyl linker. Enzymatic reaction liberates the active form of the drug. In vitro tests indicate good antitumor activity of the new generation drug against HEL and MOLT-3 cancer cells.

### 5.1.2. AND Gates

Most of the molecular AND logic gates are based on ditopic receptors and a fluorescent unit linked covalently



**Figure 38.** Molecular structure of the TTF-cyclophane inclusion complex (a), 1,5-dinaphtho-[38]crown-10 (b), and the crown-TTF<sup>2+</sup> inclusion complex (c). Host-exchange reactions as a consequence of sequential oxidation and reduction of tetrathiafulvalene guest (d). Electron donors are marked in red, while acceptors are in blue. Adapted from ref 390.

with both receptors. In contrast to the OR gate, fluorescence should be switched on when both receptors bind corresponding substrates. The first reported molecular logic gate was based on this approach (AND-1).<sup>140</sup> The gate consists of three structural elements: the cyanoanthryl fluorophore, azacrown cation receptor, and the tertiary amino group (proton acceptor). Upon excitation of the fluorophore, PET processes from azacrown and tertiary amine efficiently quench the fluorescence. Binding of sodium within the azacrown does not influence the luminescence of the compound as PET from amine can efficiently quench the fluorescence. Only simultaneous binding of two substrates to the receptors (i.e., sodium cations and protons) prohibits PET and switches the fluorescence on. The same approach of independent binding of protons and alkali metal cation was utilized in the design of AND-2 and other AND gates with the same molecular framework.<sup>401</sup> PET sensors with two identical receptors can be also regarded as molecular AND gates, but their operation relies only on the concentration of the triggering species (cations, anions, or sugar molecules).<sup>402–404</sup> Substitution of morpholine moiety in AND-2 with the C<sub>8</sub> aliphatic chain enables incorporation of resulting molecular logic gates into tetramethylammonium dodecylsulfate-based micelles. This is the first reported computational chemical system confined to the nanometer scale objects.<sup>405</sup> AND Boolean behavior was also observed for calcium selective chelator AND-3, but its operation is disturbed at very high acid concentration.<sup>406</sup> Structural rearrangement of the same building blocks results in a change of logic behavior of the system. A more sophisticated AND gate is based on molecule AND-4. Strong fluorescence of the anthracene fluorophores can be observed only in the presence of sodium cations and protons. Application of two crown receptors within one molecule was applied in AND-5. This result is a dual action device: a simple switch and a logic gate. Fluorescence of the anthryl moiety is observed in the presence of potassium cations (simple switch) or in the presence of protons and cesium cations (AND logic gate).<sup>407</sup> The recently reported two-receptor AND logic gate (AND-6) responds with intense fluorescence to the concomitant presence of sodium and thallium(I) cations.<sup>408</sup>

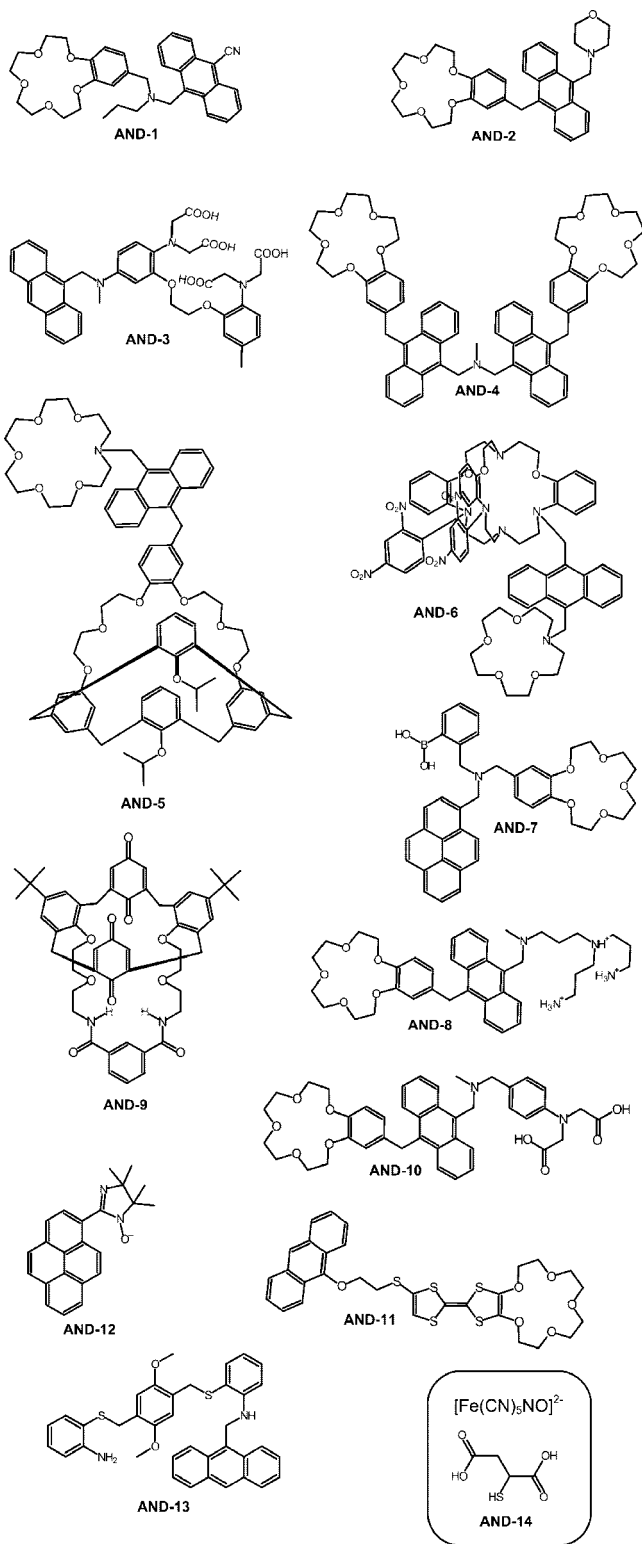
The next class of AND molecular logic gates is based on concomitant and/or cooperative binding of cations and anions by ditopic receptors. AND-7 selectively binds

potassium cations and fluoride anions, which results in fluorescence enhancement, while reactions with potassium cations (or fluoride anions) themselves does not significantly affect the fluorescence quantum yield.<sup>409</sup> On the same principle operates the AND-8 molecular gate. Reaction of AND-8 with Na<sup>+</sup> or H<sub>n</sub>PO<sub>4</sub><sup>n-3</sup> results in the binding of sodium cations and phosphate anions to the crown and ammonium moieties, respectively. It does not result, however, in a significant increase of fluorescence quantum yield. Concomitant complexation of Na<sup>+</sup> and H<sub>n</sub>PO<sub>4</sub><sup>n-3</sup> results in strong fluorescence, but due to the large separation between cation and anion binding sites, no cooperativity effects are observed.<sup>410</sup> Cooperative binding of potassium chloride ion pair was observed within ditopic calix[4]diquinone receptor AND-9.<sup>411</sup> NMR and UV-vis studies indicate the dramatic increase of potassium binding constant in the presence of chloride ions. Especially sensitive are protons from amide groups.

The most sophisticated AND gate based on the PET principle was developed in the laboratory of A. P. de Silva.<sup>412</sup> The AND-10 logic gate is constructed according to the principle of modular PET systems. The anthryl fluorophore is linked with three different receptor moieties into a linear array. The crown moiety binds sodium cations, amino acid side chain zinc cations, and tertiary amino group protons. This lab-on-a-molecule can be switched to fluorescent state only in the concomitant presence of these three triggers.

Fluorescence of the AND-11 compound is efficiently quenched by photoinduced electron transfer from the tetrathiafulvalene unit to the anthryl fluorophore ( $\Phi = 0.011$ ).<sup>413</sup> In the presence of Na<sup>+</sup>, fluorescence quantum yield of the anthryl fluorophore slightly increases ( $\Phi = 0.013$ ). In the presence of fullerene C<sub>60</sub>, fluorescence intensity is also slightly increased ( $\Phi = 0.019$ ). When both reagents are present, very strong emission from the anthryl group is observed ( $\Phi = 0.05$ ). This 5-fold increase of fluorescence quantum yield is a consequence of electrostatic inhibition of PET by Na<sup>+</sup> and competitive electron transfer between TTF and C<sub>60</sub>.

Dual mode quenching of the fluorescent excited state of pyrene is the photophysical basis for gate AND-12.<sup>414</sup> The

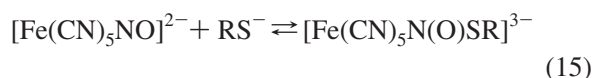


nitroxide group is well-known to efficiently quench the fluorescence of polyaromatic fluorophores.<sup>415</sup> This process is observed in the molecule AND-12. Furthermore, it contains another efficient quenched imidazole ring, which is an electron donor and can participate in the PET process. Therefore, switching the fluorescence of AND-11 must include reduction of the nitroxide functionality and protonation of the imidazole ring. AND-11 works as the AND gate taking as chemical inputs trifluoroacetic acid and cysteine. Reaction with these two reagents results in a 100-fold increase of fluorescence intensity, while any of the

reagents alone increases the fluorescence quantum yield only 5–10 times.

Open shell metal ions usually induce fluorescence quenching upon binding to fluorescent ligands. The AND-13<sup>416</sup> copper(II) system is an exception. The ligands itself is only weakly fluorescent, and its protonation only slightly increases the luminescence quantum yield. The same effect is observed upon addition of  $\text{Cu}(\text{NO}_3)_2$  solution. Surprisingly, complexation of  $\text{Cu}^{2+}$  ions by protonated ligand yields a strongly fluorescent compound. Therefore, AND-13 can be regarded as a molecular AND gate with  $\text{H}^+$  and  $\text{Cu}^{2+}$  inputs and fluorescence output.

The simplest from a chemical point of view is the AND logic gate based on the nitrosylpentacyanoferrate complex (*nitroprusside*) and mercaptosuccinic acid, AND-14.<sup>102,126</sup> In alkaline solution, nitroprusside reacts with thiolates yielding a dark red nitrosothiol complex of the type  $[\text{Fe}(\text{CN})_5\text{N}(\text{O})\text{SR}]^{3-}$ .<sup>417</sup>

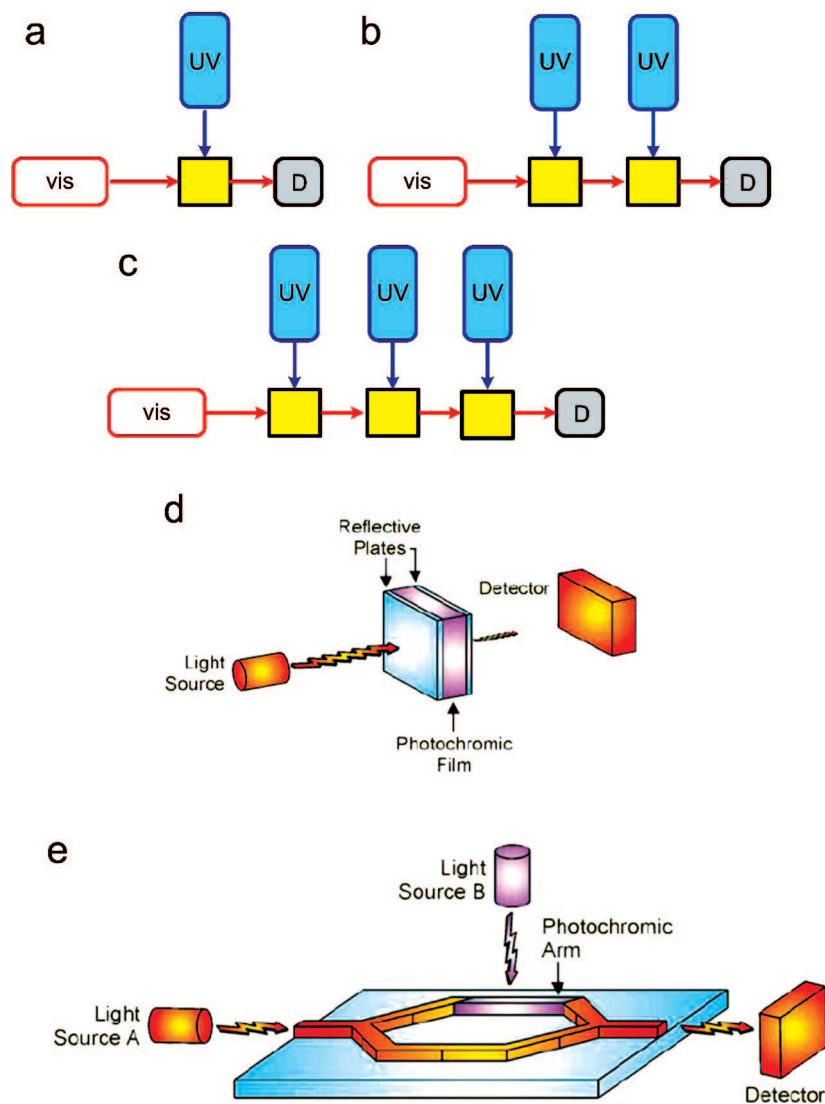


The absorption spectrum of the nitrosothiol complex is very different from the spectra of the parent compounds. The main absorption band, localized in the case of mercaptosuccinate at 526 nm, has dominant MLCT character with some MC contribution. The equilibrium (eq 15) is extremely sensitive to different stimuli, such as pH, cation type and concentration, temperature, pressure, and light. Increasing pH shifts the equilibrium to the right, while decreasing pH shifts it to the left. The pH dependence profile is almost identical with the titration curve of the specific thiol. The role of the cation consists primarily in the reduction of the electrostatic repulsion between anionic reagents, thus shifting the equilibrium (eq 15) to the right. Therefore, formation of strongly colored  $[\text{Fe}(\text{CN})_5\text{N}(\text{O})\text{SR}]^{3-}$  requires high pH and high electrolyte concentration. This corresponds to AND logic operation with pH and  $[\text{K}^+]$  as inputs and absorbance at 526 nm as an output. This system was used to create much more complex logic devices, integrating up to 20 AND and OR logic gates (cf. section 6.2).

### 5.1.3. XOR Gates

Implementation of the XOR gate in a chemical system is a difficult task. It requires a chemical system that responds to two different stimuli in a complex way: any of these two stimuli should switch the ion gate, while concomitant presence of both triggering molecules should leave the system in the OFF state. Most of the systems described so far are based not on single molecular systems but on mixtures of compounds or supramolecular assemblies. In most cases, two input chemicals react with each other, thus (0,0) and (1,1) inputs do not induce changes to the system. Usually they are just acid and base, which neutralize each other when added in stoichiometric proportions. There are only very few chemically driven molecular logic gates based on single molecules and operated with noncomplementary chemical inputs (vide infra).

The first XOR logic gate implemented in molecular systems was based of the controlled assembly of pseudorotaxane.<sup>311,418</sup> The  $N,N'$ -dibenzylidiazapyrenium cation was used as a guest and dinaphtho-30-crown-10 as a

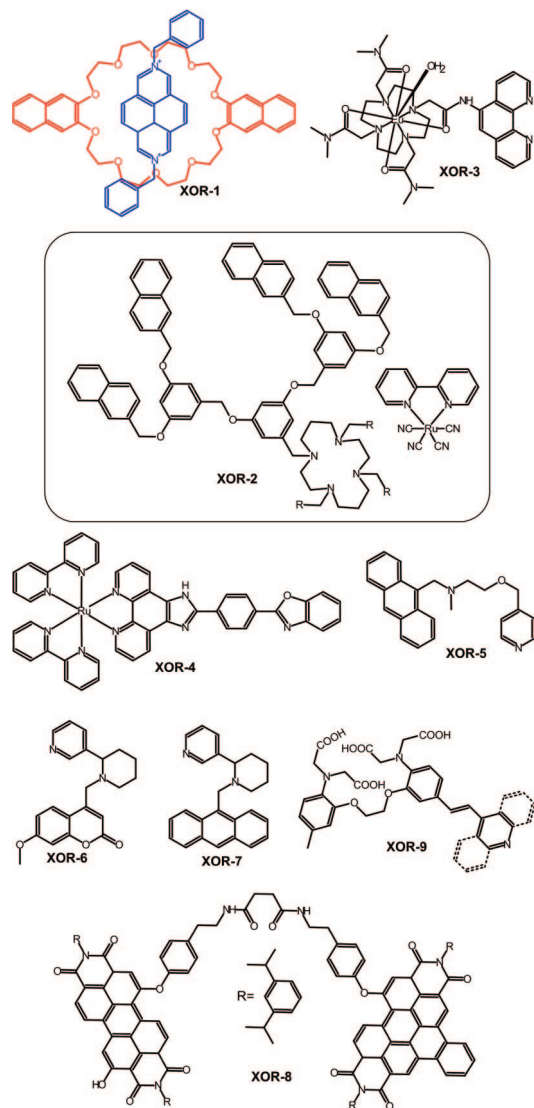


**Figure 39.** Construction of all-optical logic gates and other photonic devices from PHOTO-2 or PHOTO-3 photochromic dyes: NOT gate (a), two-input NOR gate (b), three input NOR gate (c), Fabry–Perot interferometer (d), and Mach–Zender interferometer (e). UV and vis denote the light sources, and switching cells and light detectors are shown as yellow and gray squares, respectively. Partially adapted with permission from ref 144. Copyright 2002 National Academy of Sciences. Partially reprinted with permission from ref 450. Copyright 2006 Wiley-VCH.

host molecule. In neutral  $\text{CH}_2\text{Cl}_2$ /acetonitrile solution, these two components undergo self-assembly, and the pseudorotaxane XOR-1 is formed. In the supramolecular assembly, the diazapyrenium moiety is sandwiched between two naphthyl rings. Strong charge transfer interaction between donor (red) and acceptor (blue) parts results in the formation of a new CT absorption band at 575 nm and complete quenching of the fluorescence of both components. Addition of strong acid (e.g., trifluoroacetic acid) results in protonation of the crown ether macrocycle and disassembly of the pseudorotaxane, which results in the recovery of the fluorescence of both the diazapyrenium part and the crown component. The pseudorotaxane can be also disassembled by the addition of tributylamine, which forms very strong charge-transfer complexes with the diazapyrenium cation. The later reaction results in the recovery of crown ether fluorescence. Concomitant addition and acid and base does not switch the fluorescence on as the two reagents react with each other, and tributylammonium trifluoroacetate is formed. If these two reagents are associated with the input data and fluorescence of the solution with the output, this simple

chemical system can be regarded as a model of the XOR gate. At the same time, the intensity of the CT band corresponds to the XNOR function.

On the same principle operates the XOR-2 system.<sup>419</sup> The supramolecular systems consists of ruthenium complex  $[\text{Ru}(\text{CN})_4(\text{bpy})_2]^{2-}$  and symmetrical cyclam-based dendrimer containing four naphthyl units in each arm (XOR-2). 2-Fold protonation of the cyclam central unit allows the formation of an ion-pair-like adduct. In this adduct, excitation of the naphthyl groups ( $\lambda_{\text{ex}} = 270$  nm) results in strong fluorescence from the ruthenium complex ( $\lambda_{\text{em}} = 680$  nm) due to efficient electronic energy transfer from peripheral antennas to the metal center. Disassembly of the supramolecular adduct leads to the recovery of naphthyl fluorescence at 350 nm and almost complete disappearance of ruthenium luminescence. The assembly can be disassembled by deprotonation of the cyclam moiety with a strong base (e.g., diazabicyclooctane) or protonation of the ruthenium complex with trifluoroacetic acid. Therefore, fluorescence changes at 350 nm (naphthyl group) correspond to the XOR logic and at 680 nm to the XNOR logic.<sup>420</sup>



Similar behavior was observed in the case monomolecular europium(III) and ruthenium(II) complexes (XOR-3 and XOR-4, respectively). The XOR-3 complex is strongly fluorescent within a pH range of 4–7. Deprotonation of the aqua ligand and/or the amide linker results in a change of photochemical properties of the complex: instead of efficient electronic energy transfer from phenanthroline antenna, an electron transfer occurs, and nonluminescent Eu(II) complex is formed. On the other side of the pH scale, the antenna group is protonated (at pH < 4), and its ability to populate the luminescent  $^5D_0$  state of Eu<sup>III</sup> is strongly reduced.<sup>214</sup>

Similar behavior was observed recently for the mixed ligand ruthenium(II) complex XOR-4.<sup>421</sup> Protonation of the oxazole ring results in a great increase of luminescence quantum yield, while protonation of the imidazole ring results in fluorescence quenching due to photoinduced electron transfer processes. Identical switching properties are observed for complexes containing two imidazole rings within the ligand.<sup>422</sup> pH-controlled PET processes are also the basis of operation of the XOR-5,<sup>423</sup> XOR-6<sup>424</sup> and XOR-7<sup>424</sup> gates. First protonation, which occurs at more basic aliphatic amine group, switches the fluorescence on due to inhibition of the PET process, while the second protonation at pyridine moiety

switches the fluorescence off by enabling the second PET process involving the pyridinium cation.

Annihilation of input signals constitutes the basis for the XOR-8 gate.<sup>425</sup> Excitation of the naphthoerythrin-bisimide moiety results in FRET and red emission ( $\lambda_{\max} = 580$  nm) from the hydroxyperylenebisimide unit. Protonation of the XOR-8 does not change the photophysics of the system, while deprotonation results in fluorescence quenching, which may be described, and INH logic operation. Much more interesting behavior is observed upon complexation of ferric ions by the succinamide unit of the XOR-8 molecule. In the neutral state, fluorescence is quenched by PET to the Fe<sup>3+</sup> center. Protonation of the succinamide units is followed by the translocation of the bound Fe<sup>III</sup> ion from the succinamide to the hydroxyperylenebisimide. The fluorescence of the naphthoerythrin-bisimide is not quenched while that of hydroxyperylenebisimide is by coordinated Fe<sup>III</sup>, and emission is observed predominantly at 527 nm. Alternatively, addition of base to the ferric complex results in a yellow emission at 527 nm, which was due to the fact that the FRET was switched off because the absorption band of hydroxyperylenebisimide was red-shifted due to interaction with Fe<sup>III</sup> ions. Upon concomitant addition of stoichiometric quantities of acid and base, no fluorescence at 527 nm is observed.<sup>425</sup>

The only chemically driven molecular XOR logic gates, which are not based on annihilation of input stimuli, were reported by A. P. de Silva and N. D. McClenaghan in 2002.<sup>426</sup> The XOR-9 molecule is a push–pull olefin with the top receptor containing four carboxylic acid anion groups capable of binding to calcium. The bottom part is a pyridine (quinoline and acridine) molecule, which is a receptor for hydrogen ions. The logic gate operates as follows. Without any chemical input of Ca<sup>2+</sup> or H<sup>+</sup>, the chromophore shows an absorption maximum at 390 nm. When calcium is introduced, a hypsochromic shift takes place, and the absorbance at 390 nm decreases. Likewise, addition of protons causes a bathochromic shift, and when both cations are in water, the net result is absorption at the original 390 nm. These systems represent a XNOR logic gate in absorption and a XOR logic gate in transmittance. The same molecular systems are elements of the first chemical arithmetical systems (vide infra).

#### 5.1.4. INH Gates

An INHIBIT (INH) logic gate is a result of concatenation of AND and NOT gates, but in contrast to other gates with concatenated NOT, the logic inversion concerns not the output but one of the inputs (cf. Figure 7). Numerous chemically driven INH gates can be based on simple molecular systems and supramolecular assemblies.

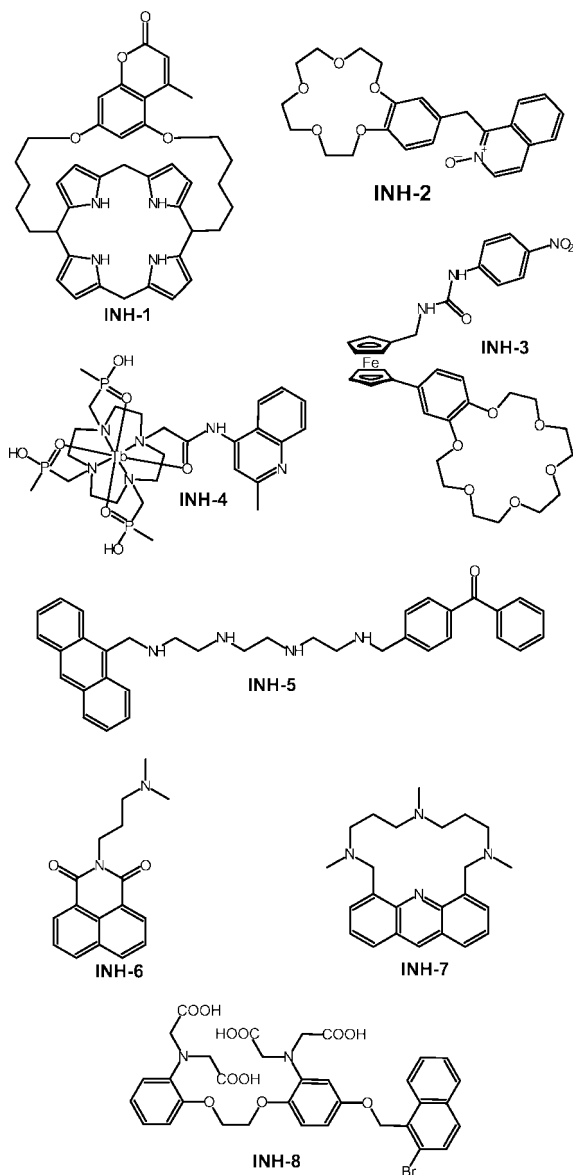
The nonfluorescent calix[4]pyrrole-coumarin assembly INH-1 can bind chloride anions within the calixpyrrole cavity and sodium cations via the carbonyl group. Association with chloride does not change the weak fluorescence. Binding of Na<sup>+</sup> cation, in turn, increases the fluorescence quantum yield. Concomitant binding of Na<sup>+</sup> and Cl<sup>-</sup> results in fluorescence quenching. This behavior is equivalent to the INHIBIT gate with sodium cations and chloride anions inputs and fluorescence output.<sup>427</sup>

Another example of ditopic receptor performing the action of INH gate is INH-2 fluorescence sensor based on isoquinoline N-oxide with an attached benzo-15-crown-5 recep-



tor.<sup>428</sup> Molecules based on this framework show dual fluorescence from locally excited and charge transfer states involving the benzocrown moiety. Charge-transfer fluorescence is observed only in the case of the protonated N-oxide moiety. Binding of cations by crown ether results in a decrease of HOMO energy of the donor, and CT fluorescence is not observed.

Ditopic receptor also constitutes the molecular basis for gate INH-3.<sup>429</sup> This chromogenic switch can bind potassium cations within the 18-crown-6 cavity and fluoride anions via the urea moiety. Only fluoride binding in the absence of potassium results in color change. This process is a consequence of chromogenic interaction between the ferrocene moiety and fluoride anions.



Another fluorescent INHIBIT gate is represented by macrocyclic Tb<sup>III</sup> complexes, INH-4.<sup>430,431</sup> Fluorescence of the Tb<sup>3+</sup> center can be observed only upon protonation of the quinoline moiety due to efficient electronic energy transfer from the quinolinium antenna to the terbium luminophore. However, terbium fluorescence is quenched by molecular oxygen. Therefore, the complex behaves like

the INHIBIT gate with proton and oxygen inputs and fluorescence output. Surprisingly, the analogous europium(III) complex does not show this interesting switching pattern.

Molecule INH-5 can bind protons and copper(II) cations to the polyamine chain.<sup>432</sup> This process can be regarded as a Boolean INHIBIT operation when anthracene fluorescence is considered as an output. The fully protonated polyamine chain keeps the anthracene and benzophenone fragments away, thus allowing high intensity fluorescence. Deprotonation results in closer contact of the aromatic fragments and fluorescence quenching due to anthracene  $\rightarrow$  benzophenone photoinduced electron transfer. Addition of Cu<sup>2+</sup> results in efficient fluorescence quenching of acidic solutions of INH-5. Coordination of Cu<sup>2+</sup> to the polyamine chain brings the two aromatic systems in proximity, thus creating spacial arrangement for efficient PET. Moreover, direct interaction of the anthracene excited state with copper cation leading to electronic energy transfer involving low energy *d* orbitals cannot be excluded.

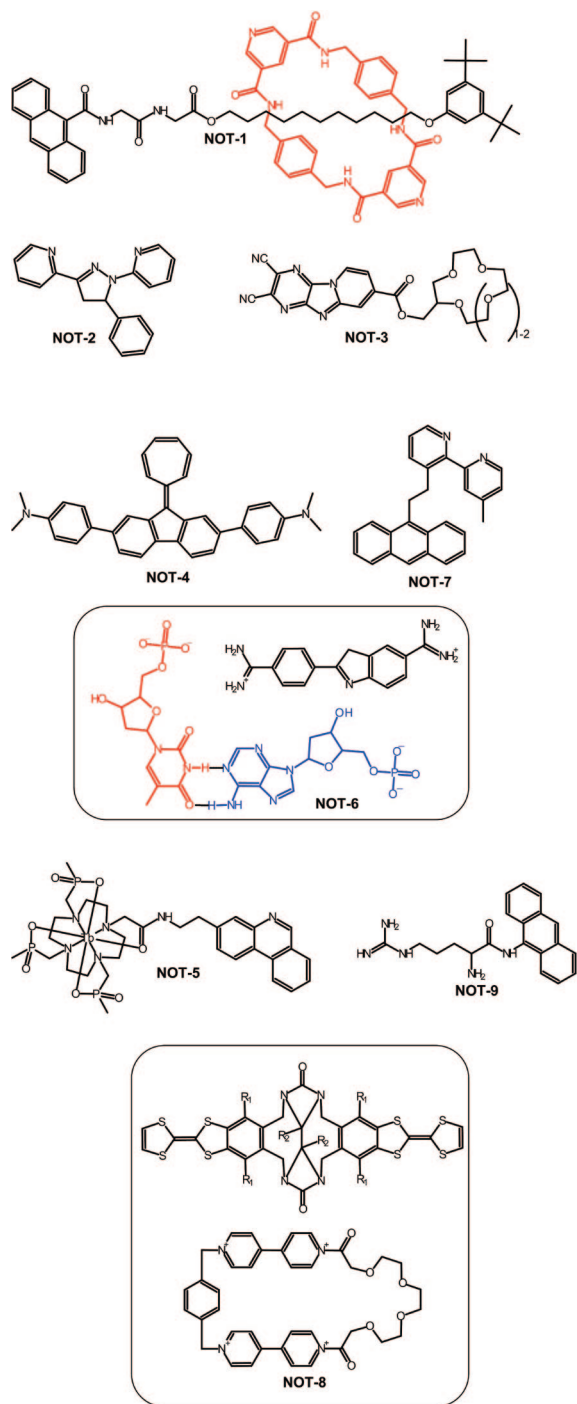
1,8-Naphthalimide INH-6 in acetonitrile solutions shows very weak fluorescence because of efficient PET quenching.<sup>433</sup> Interaction with Eu<sup>3+</sup> cations results in stronger luminescence of the naphthalimide as formation of the lanthanide complex inhibits the PET pathway. In the presence of oxygen, however, no red europium luminescence is observed. Only in the presence of europium(III) and rigorous absence of oxygen, luminescence from the <sup>5</sup>D<sub>0</sub> state is observed. Therefore, the systems can be regarded as chemically driven INH gate with Eu<sup>3+</sup> and O<sub>2</sub> inputs and red luminescence output.

The control of the INH-7<sup>434</sup> logic gate is closely related to XOR gates based on mutual neutralization of chemical inputs. This molecule is a selective zinc fluorescent sensor operating in aqueous solutions. Furthermore, its fluorescence spectrum strongly depends on proton concentration. The protonated form is strongly fluorescent, while in neutral and basic solutions its emission is weaker and blue-shifted. Therefore, addition of acid to the solution of INH-7 switches its fluorescence on, while addition of base or concomitant addition of acid and base does not change its fluorescence.

The only three-input INHIBIT molecular gate reported so far is the molecule INH-8.<sup>435</sup> It binds calcium via the four-armed amino acid receptor, which switches the phosphor to the on state. The phosphorescence of the 2-bromonaphthalene is, however, efficiently quenched by molecular oxygen via bimolecular triplet-triplet annihilation. Therefore, phosphorescence is observed only in rigorous absence of oxygen and upon complexation of the fluorophore within the cavity of  $\beta$ -cyclodextrin.

### 5.1.5. Inverted Logic Gates (NOR, NAND, and XNOR)

Concatenation of NOT gate with other logic gates results in inverted logic gates (NOR, NAND, XNOR, and NOT-INHIBIT; cf. Figure 7). There are two main approaches of mimicking these gates in chemical systems: application of complementary optical output (e.g., transmittance instead of absorption) or specific molecular design of the molecular switching element. The first approach corresponds to the switch from positive to negative logic (or vice versa), and some examples were described together with normal logic gates in preceding sections.



The supramolecular NON-INHIBIT logic gate based on NOT-1 rotaxane was recently reported.<sup>436</sup> The switching system is composed of a thread equipped with anthryl and di-*t*-butylphenyl stoppers and two solvophobic stations, glycyl-glycine and the C<sub>11</sub> alkyl chain. The amide macrocycle contains pyridine moieties that can quench the luminescence of the anthracene moiety. In nonpolar media, the macrocycle forms hydrogen bonds with the glycyl-glycine chain and resides close to the anthracene terminal. In strongly polar solvents (formamide and DMSO), the macrocycle moves toward the alkyl chain, and quenching becomes negligible. Protonation of the pyridine moieties switches on the anthracene fluorescence irrespective of the solvent polarity. This behavior can thus be described as the NOT-INHIBIT Boolean function.

NOR logic operations are performed by NOT-2 and NOT-7 molecules.<sup>435</sup> Upon ultraviolet irradiation, they fluoresce in the visible spectrum (blue and violet fluorescence, respectively). Protonation or complexation of transition metal cations (Hg<sup>2+</sup> and Zn<sup>2+</sup>, respectively) results in the quenching of fluorescence. Therefore, these molecules can be regarded as NOR molecular gates with chemical inputs and optical output.

Another NOR gate is represented by NOT-4.<sup>437</sup> This fluorenone derivative is fluorescent in the ambient form, but protonation of the dimethylamine groups enhances the PET process from the cycloheptatriene ring. Interaction of *N*-ethylpyridinium also results in fluorescence quenching due to the PET process. Reaction of the NOT-4:ethylpyridinium complex with a stronger electron donor triethylamine suppresses the charge transfer interaction and results in fluorescence enhancement. Acidification of the NOT-4:ethylpyridinium complex solutions results in decomposition of the CT complex but protonated NOT-4 is not fluorescent.

NOT-5 also functions as the NOR gate when excited at 375 nm.<sup>438</sup> Excitation within the absorption band of the phenanthridine moiety results in efficient energy transfer to the terbium(III) center. The phenanthridine triplet excited state is efficiently quenched by molecular oxygen. Furthermore, protonation of the aromatic chromophore changes the energy of the excited state (singlet), and in acidic media, it cannot be excited by 375 nm light. This behavior corresponds to NOR operation as fluorescence can be observed only in the absence of oxygen and acids.

NAND gates are the most ubiquitous in electronic systems since they can be treated as the simplest building blocks for any other logic gates. There are also several chemical implementations of the NAND functionality. Pyridoimidazolopyrazine derivative NOT-3 is a strong fluorophore.<sup>439</sup> Binding of alkali or alkaline earth metal cations by the crown ether moiety does not significantly influence the fluorescent properties. Interaction with alkali metal thiocyanates also has no effect on luminescence; electrostatic interaction between thiocyanate and cations is too weak to hold the anion in the proximity of the fluorophore. Calcium and barium cations efficiently bind to the crown moiety and can themselves coordinate thiocyanate, which in turn efficiently quenches the fluorescence in PET process.

Other NAND molecular gates are based on supramolecular interactions as well. The system of Baytekin and Akkaya (NOT-6)<sup>440</sup> comprises 4',6-diamidino-2-phenylindole (DAPI), DNA-binding fluorophore, and two nucleotides, deoxyadenosine phosphate and deoxythymidine phosphate. The fluorophore binds nucleotides electrostatically via the interaction of amidine groups with phosphate residues. Any of the nucleotides alone cannot efficiently suppress the 455 nm luminescence of the DAPI fluorophore. Formation of hydrogen-bonded Watson–Crick nucleotide dimer results in efficient quenching of fluorescence, which corresponds to the NAND operation (cf. Table 2). More sophisticated devices based on nucleotide interactions are discussed in section 8.3 of this review.

The NOT-8 NAND gate is also based on supramolecular interactions.<sup>441</sup> The gate is composed of two molecular fragments: a molecular clip with the tetrathiafulvalene side arms and a cyclophane with polyether chain. In acetonitrile solutions, these two components form a stable supramolecular host–guest assembly characterized by a charge transfer band at 533 nm. On interaction with cations (K<sup>+</sup>, NH<sub>4</sub><sup>+</sup>), or

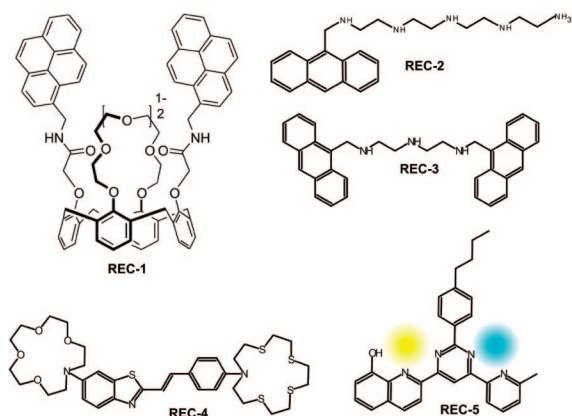
on heating, the complex disassembles into components, and the CT absorption band disappears. If these factors are considered as input stimuli and CT absorption as an output, the system can be described with the NAND function.

Supramolecular interactions are also the basis of the NOT-9 NAND gate, reported this year by Lu and co-workers.<sup>442</sup> The luminescence of the anthryl fluorophore is only slightly sensitive to pH (within pH range of 2 to 8), and in neutral solutions, it is also insensitive to the presence of ATP. Upon protonation, intermolecular interaction becomes much stronger ( $\pi$ - $\pi$  stacking + electrostatic interaction + hydrogen bonding), which results in significant quenching of the fluorescence due to PET from the adenosyl moiety. Therefore, if protons and ATP are considered as inputs and luminescence intensity as an output, the NOT-9 sensor behaves like the NAND gate.<sup>442</sup>

### 5.1.6. Reconfigurable and Superimposed Molecular Logic Devices

Reconfigurable logic devices are very important components of modern electronic devices. They usually are large arrays of logic gates, and the internal connections between particular elements can be changed on demand. Therefore, these electronic systems are very flexible and can be programmed (or configured) to fulfill numerous tasks.<sup>443</sup> There are numerous examples of similar devices in chemical systems. There are several molecular logic gates reported, the Boolean function of which depends on the chemical nature of input signals.

Superimposed logic devices are unprecedented devices found only in molecular systems. Their operation mode depends on the way information is read from the device, e.g., using different analytical wavelengths. They are conceptually somehow related to quantum logic gates, where the output state is a superposition of all possible output states.



Calixarene REC-1 with two pendant pyrene fluorophores and polyether receptor chain is a simple example of a reconfigurable logic device.<sup>444</sup> Strong pyrene emission is quenched by complexation of  $\text{Pb}^{2+}$  cations within the macrocyclic receptor due to efficient reverse-PET process from excited pyrene moieties to the electron-deficient amide groups. Strong acids and bases are also capable of fluorescence quenching. Protonation of the polyether chain creates a PET acceptor and results in fluorescence quenching. Deprotonation of the amide group (e.g., by addition of triethylamine) yields an electron donor and results in normal PET quenching. Concomitant addition of acid and base does

not change the fluorescence intensity. Therefore, the REC-1/acid/base system can be regarded as the molecular XNOR gate with fluorescence output. However, application of  $\text{Pb}^{2+}$  and triethylamine as inputs results in NOR Boolean function: fluorescence is quenched by any combination of inputs.

Another reconfigurable logic device is based on the anthracene fluorophore with a long polyamine tail (REC-2).<sup>445</sup> Fluorescence of this molecule is efficiently quenched by PET from the polyamine chain. Protonation or coordination of  $\text{Zn}^{2+}$  or  $\text{Cd}^{2+}$  cations inhibits the photoinduced electron transfer even at high pH and switches on the fluorescence. Coordination of some other cations ( $\text{Cu}^{2+}$  and  $\text{Ni}^{2+}$ ) results in fluorescence quenching of the partially protonated compound. Due to the diversity of responses of various chemical stimuli, this system should be regarded as a reconfigurable logic device with fluorescence output. Application of  $\text{Zn}^{2+}$  and  $\text{Cd}^{2+}$  as inputs yields an OR gate, while when the inputs are  $\text{Ni}^{2+}$  and  $\text{Cu}^{2+}$ , the anthracene derivative behaves as the NOR gate. Another logic operation can be performed when one input taken from the first group and the other from the second one (e.g.,  $\text{Zn}^{2+}$  and  $\text{Cu}^{2+}$ ). In this case, fluorescence can be observed only in the presence of  $\text{Zn}^{2+}$  and the absence of  $\text{Cu}^{2+}$ , which corresponds to INH operation.

The operation of the previous system was limited to one output channel as the energy of emission maximum does not strongly depend on the cation. This limitation was overcome in the REC-3 gate.<sup>446</sup> This fluorescent molecular device incorporates two anthryl fluorophores linked with the diethylenetriamine chain. The REC-3 molecule shows pH-dependent dual fluorescence. At low pH ( $\text{pH} < 9$ ), luminescence of isolated anthracene moieties (416 nm) is observed. On deprotonation, the two anthryl groups form a  $\pi$ - $\pi$  stacked complex. Its excitation within the ICT transition results in excimer emission at 520 nm. These two wavelengths are considered as two independent output channels of the molecular logic gate. Apart from protons, the REC-3 can interact with a series of transition metal cations including  $\text{Zn}^{2+}$ ,  $\text{Cd}^{2+}$ ,  $\text{Cu}^{2+}$ ,  $\text{Co}^{2+}$ ,  $\text{Ni}^{2+}$ ,  $\text{Hg}^{2+}$ , and  $\text{Ag}^{+}$ . These interactions affect both luminescence channels. Coordination of closed-shell cations ( $\text{Zn}^{2+}$  and  $\text{Cd}^{2+}$ ) at high pH results in switching on both the monomer emission and excimer emission. This is the result of cation-induced suppression of the PET process from the polyamine chain. Protonation of these complexes results in switching off the excimer emission due to geometrical changes, but the monomer emission remains unaffected. In this system, the monomer channel (416 nm) yields the OR function of the input data ( $\text{H}^{+}$  and  $\text{Zn}^{2+}$ ), while the excimer channel (520 nm) yields the NOT ( $\text{H}^{+}$ ) response. Open-shell cations completely quench the luminescence in both channels regardless of pH. In this case, the monomer luminescence can be observed only at low pH and in the absence of Cu ions, while the excimer luminescence can be observed only in the absence of both inputs. Therefore, the gate operating with  $\text{Cu}^{2+}$  and  $\text{H}^{+}$  inputs yields the INH function in the monomer channel and the NOR function in the excimer channel. Similar behavior is observed when  $\text{Ag}^{+}$  and  $\text{H}^{+}$  are applied as inputs. Monomer emission is observed at low pH irrespective of silver ions (YES gate). Excimer luminescence in turn is switched off by both protons and silver ions, which corresponds to the NOR operation. Mercury ions do not influence the excimer channel, but they quench the monomer emission in the presence of protons. Therefore, if  $\text{Hg}^{2+}$  and  $\text{H}^{+}$  are

considered as inputs, the monomer luminescence is described by INH and excimer luminescence by NOT ( $H^+$ ) functions.<sup>446</sup>

The next superimposed logic system is based on the benzothiazole derivative REC-4.<sup>447</sup> Solutions of REC-4 are yellow ( $\lambda_{\max} = 413$  nm) and only weakly fluorescent ( $\sim 500$  nm,  $\Phi = 0.05$ ). Interaction of the azacrown ether moiety with calcium ions results in a slight hypsochromic shift of the absorption band and a decrease of fluorescence intensity. The thiazacrown moiety can, in turn, interact with  $Ag^+$  cations. This reaction also induces a small hypsochromic shift of the absorption band and also a strong increase of the fluorescence quantum yield ( $\Phi = 0.27$ ). Concomitant presence of  $Ca^{2+}$  and  $Ag^+$  results in a strong hypsochromic shift of the absorption band and fluorescence quenching. If fluorescence at 500 nm and absorbance at 440 nm are taken as two outputs, they yield the NAND and INH responses, respectively.

Another reconfigurable and superimposed molecular logic system was reported by Jean-Marie Lehn and co-workers.<sup>448</sup> The systems are based on a ditopic ligand REC-5. It can coordinate mono ( $Cu^+$ ), di- ( $Zn^{2+}$ ,  $Cu^{2+}$ , and  $Pb^{2+}$ ), and trivalent ( $La^{3+}$ ) cations. Interaction of  $Cu^+$  is pH-independent, while  $Zn^{2+}$  can be bound only in the presence of  $OH^-$ . Spectral changes associated with the cation complexation are quite complex. Free ligand is almost colorless and shows only one strong band at  $\sim 330$  nm. Reaction with  $Cu^+$  results in increased absorption at 390 nm. Deprotonation of REC-5 in the presence of divalent cations results in complex formation with characteristic 480 nm absorption band. Concomitant binding of  $Cu^+$  and  $M^{n+}$  results in strong band at 555 nm and increased absorption at 390 and 480 nm. An AND gate can be therefore operated by  $M^{n+}$  and  $OH^-$ , the output should be associated with the absorbance at 480 nm. If all the analytical wavelengths are taken into account, the system behaves as three independent logic devices. The 390 nm output corresponds to the YES function controlled by  $Cu^+$  input, 480 nm output yields the AND function of ( $OH^-$  and  $M^{n+}$ ) inputs, and 555 nm output yields the AND ( $Cu^+$ ,  $OH^-$ , and  $M^{n+}$ ) function.

## 5.2. All-Optical Logic Gates

The previous section discusses molecular logic gates with chemical inputs. These systems can perform logic operation at the molecular level, but their main limitation consists of the necessity of the addition of chemical species in order to process information. These species diffuse to the target molecule and induce chemical reaction, which changes molecular structure and thus brings about information processing. These devices usually require fluid solutions, and their speed is limited by the time required for material transfer, diffusion and the rate of bimolecular reactions. The systems utilizing all-optical inputs and outputs are devoid of these limitations, and logic elements do not require access to triggering chemical or electric signals and in principle can operate on a much faster time scale and in rigid (or semirigid) media.<sup>449</sup> Furthermore, these devices are especially promising in the context of optical control of optical signals (i.e., optical equivalent of a transistor). Nowadays, optical networks transfer huge amounts of data, but this transmission relies on the cooperation of optoelectronic devices with optical fibers, and signal routing requires numerous steps of optoelectronic and electrooptical signal conversion, which is the

bottleneck of the development of optical networks.<sup>144</sup> Therefore, novel optically controlled logic devices for handling optical signals are essential for further development of optical data transfer and processing.

Despite quite a large number of light-driven chemical switches, there are, however, only a few all-optical logic gates; most of the light-triggered logic devices require some additional (mostly chemical) inputs. These all-optical information processing molecular systems can be divided into three main categories based on the operation mode. Their operation can be based on (i) simple (reversible) photophysical and/or photochemical processes, (ii) photophysical processes involving two-photon transitions and higher excited states, (iii) and holographic (and other optical) effects in photoisomerizable (photochromic) rigid media.

One of the simplest all-optical logic gate was reported F. Pina and colleagues in 2000.<sup>141</sup> The gate was based on acidic solution containing *trans*-chalcone PHOTO-1 and  $K_3[Co(CN)_6]$  complex. On 365-nm irradiation, *trans*-chalcone isomerizes to the *cis* form, which in acidic medium undergoes a ring-closure reaction yielding strongly colored (and fluorescent) flavylum species. Prolonged irradiation induces photoaquation of the cyanocobaltate, and the released cyanide anions increase the pH of the mixture, thus resulting in decomposition of the flavylum species. If pulsed laser irradiation is applied, the first pulse results in increased absorbance, and the second in decreased absorbance. This behavior corresponds to XOR logic operation, but in contrast to classical logic gates that take both input signals at the same time, this system requires sequential data input. Because of this feature, it can be regarded as the simplest chemical system reproducing the basic properties of neurons.

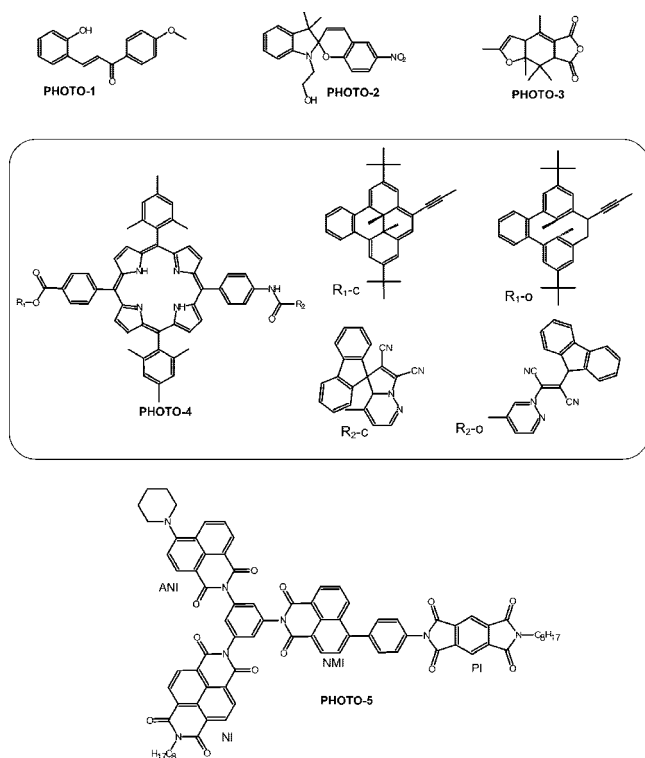
Simple spiropyran derivative PHOTO-2 was used for the construction of very complex all-optical switches.<sup>144</sup> The colorless, closed form of the switch undergoes extremely fast photoinduced ring opening upon UV excitation yielding purple-colored merocyanine (cf. section 4.2, Figure 25). Therefore, the PHOTO-2 based switch can, in principle, operate in optical devices with picosecond time resolution.

An optical network consisting of one cell containing the PHOTO-2 solution and UV and vis light sources works as the all-optical NOT gate (Figure 39a). Visible light is transmitted through the switching cell almost without decrease of intensity. Upon UV stimulation, the absorbance of switching solution increases, and the signal is strongly attenuated (at least 2 orders of magnitude, depending on path length and concentration). When the UV source is off, the dye isomerizes rapidly back to the colorless state, and the visible signal at the output gains its initial value.

More complex logic systems (e.g., NOR gates) can be easily achieved in systems containing more switching elements (Figure 39b and c). Application of two switching cells placed in series into the light beam results in a two-input NOR logic gate (Figure 39b), while three cells yield the three-input NOR gate (Figure 39c). Identical logic devices can be built with the PHOTO-3 switch. Apart from these logical devices, some other assemblies of potential use in optoelectronics have been built on the basis of photochromic materials (Figure 39d and e).<sup>450</sup>

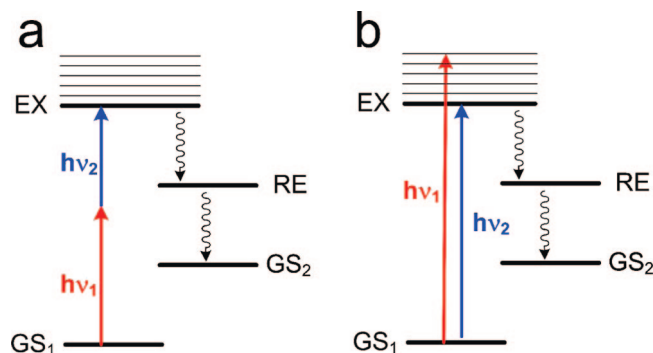
Incorporation of a photochromic film (polymethacrylate doped with PHOTO-3) between reflective plates of a Fabry–Perot interferometer results in a light-switchable device. Opened form of the PHOTO-3 switch is colorless and upon 366-nm irradiation converts into the colored, closed

form, which in turn undergoes photochemical ring opening on irradiation at 515 nm. The Fabry–Perot interferometer tuned to 515 nm and simultaneously illuminated at 366 and 515 nm yields complex output depending on light intensities at both wavelengths. Another optical device, the Mach–Zender interferometer, can also be supplied with the photochromic switch (Figure 39e). In this system, a high output signal is obtained when materials at both arms have an identical refractive index. It was already demonstrated that photochromic dyes incorporated into polymers may modulate their refractive index; therefore, this device can be used as a light-driven light modulator and an all-optical XOR logic gate. These photoactive interferometers can be connected in larger optical systems and used as model systems for all-optical computing and information storage.<sup>450</sup>



The classical single-molecule all-optical logic gate is the system PHOTO-4.<sup>449</sup> This logic gate is based on two different photochromic groups (dihydropyrene and dihydroindolizine) and free base porphyrin fluorophore. Two photochromic groups can be addressed independently, therefore all possible combinations of isomers ( $R_1$ -o,  $R_2$ -o;  $R_1$ -o,  $R_2$ -c;  $R_1$ -c,  $R_2$ -o;  $R_1$ -c,  $R_2$ -c) can be generated via the proper sequence of irradiations. Only the ( $R_1$ -o,  $R_2$ -c) form of the compound is fluorescent. UV irradiation results in ring closure of the cyclophenadiene ( $R_1$ -o) to dihydropyrene ( $R_1$ -c), but to ring opening of the dihydroindolizine ( $R_2$ -c), which yields the colored betaine form ( $R_2$ -o). Visible irradiation opens the ring of dihydropyrene, and visible or IR irradiation of the betaine form results in formation of dihydroindolizine. On this basis, two different logic devices with fluorescent input can be built.

Assignment of input signals to IR and red irradiations results in the AND gate. The starting form ( $R_1$ -c,  $R_2$ -o) is not fluorescent. Irradiation with red light yields the nonfluorescent form ( $R_1$ -o,  $R_2$ -o). However, IR irradiation yields the nonfluorescent ( $R_1$ -c,  $R_2$ -c). Only simultaneous (or sequential) application of red and IR irradiation results in the fluorescent ( $R_1$ -o,  $R_2$ -c) form. Application of UV and red

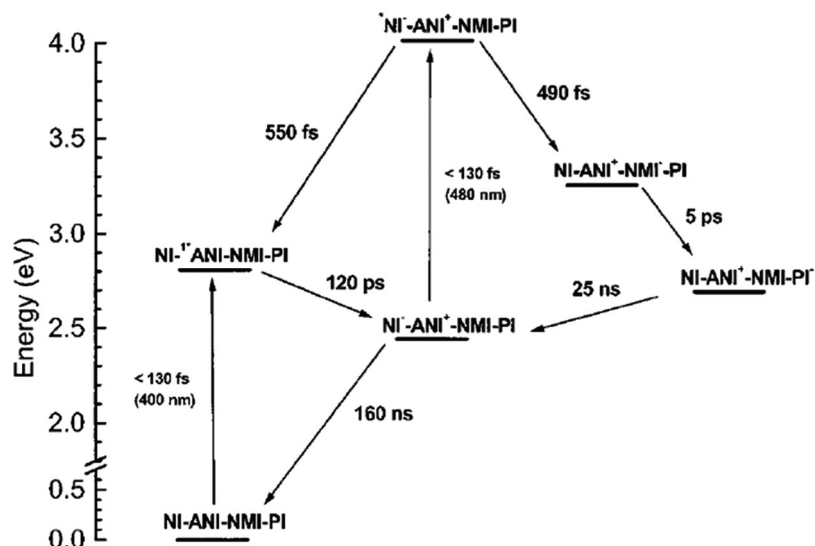


**Figure 40.** A schematic representation of the four-level AND (a) and OR (b) single molecule logic gates. Adapted from ref 454.

light as inputs and the ( $R_1$ -c,  $R_2$ -c) initial state results in an INHIBIT gate. The same chromophore equipped with fulgimide (FG) and dithienylethene photochromes (cf. Figure 29) mimics the XOR and NOR logic gates,<sup>451</sup> while application of 532 and 1064 nm inputs results in the two channel demultiplexer (cf. Figure 47).<sup>452</sup> Two output channels are associated with porphyrin fluorescence at 720 nm and betaine absorption at 572 nm. When the 1064-nm input is set to off, one fluorescence output follows the state of the 532-nm data input. Upon switching the 1064-nm input on, fluorescence is switched off, but the absorbance output follows the input data. The demultiplexer does not require chemical or electrical inputs, and can cycle through its operational sequences multiple times.<sup>452</sup> Change in the assignment of the input signals results in the binary 2:1 multiplexer.<sup>453</sup>

Another type of optical logic devices can be based on almost any photoisomerizable system.<sup>454</sup> Furthermore, this approach allows integration of AND and OR logic gates within a single molecule. The concept of these logic gates is based on a four-level energy diagram (Figure 40). The switchable molecule is first pumped from its ground state ( $GS_1$ ) to the spectroscopically accessible excited state (EX), but it does not have to be the lowest excited state. Subsequently, the molecule should rearrange to the RE state in a radiationless process and via conical intersection finally yield the product ground state ( $GS_2$ ), which may be stable or can thermally return to the  $GS_1$ . The AND operation is therefore realized in two-photon excitation to the RE state, and the energy of these two photons must be equal to the energy of the reactive excited state (Figure 40a). If the absorption band associated with the  $GS_1 \rightarrow RE$  transition is broad, photons of significantly different energies can be used for excitation, which corresponds to the OR gate (Figure 40b).<sup>454</sup> An AND gate based on this principle can be based, e.g., on IR-UV double-resonance of nitric acid.<sup>455</sup> Concomitant excitation of  $HONO_2$  with IR and UV pulses results in luminescence of photogenerated  $*NO_2$ . The same approach can be used for construction of much more complex logic and arithmetic devices (vide infra).

The molecule PHOTO-5 can exist in two, relatively long-lived charge-separated states:  $NI^- - ANI^+ - NMI - PI$  and  $NI - ANI^+ - NMI - PI^-$ . The first of these states can be generated upon single excitation (Figure 41), while generation of the state with unpaired electron located at the pyromellitimide moiety required sequential excitation with two photons, which corresponds to the AND logic operation.<sup>456</sup> These systems can be also considered as light-driven routers. An electron from the ANI electron donor can be directed to two different acceptors: NI upon single excitation and subse-



**Figure 41.** Energy diagram of single molecule AND logic gate with a routing properties. Reprinted with permission from ref 456. Copyright 2001 American Chemical Society.

quently to PI if the second photon of appropriate energy is absorbed within the lifetime of the charge separated state.

Bacteriorhodopsin belongs to one of the most studied photochromic molecules and has found some applications in all-optical logic gates and in the information storage devices.<sup>245</sup> This protein occurs naturally in membranes of photosynthetic bacteria and is responsible for the photogeneration of the proton gradient across the membrane. In the presence of lipids it forms two-dimensional crystalline structures containing trimeric assemblies of bacteriorhodopsin molecules (Figure 42a).<sup>457</sup>

The ground state absorption spectrum of bacteriorhodopsin shows an intense maximum at 570 nm.<sup>458,459</sup> Excitation with 570-nm light induces the whole series of chemical processes usually called the bacteriorhodopsin photocycle (Figure 42b).<sup>459–461</sup> These reactions include photoisomerization of covalently bound retinal moiety and proton transfer steps. These reactions are accompanied by complex spectral changes (Figure 42c).<sup>461</sup>

The simplest bacteriorhodopsin-based logic gates utilize the spectral changes following the 570-nm excitation. Assignment of 570 nm light as input and transmittance at 640 nm as output result in the NOT gate; excitation results in temporary darkening of the bacteriorhodopsin films and decrease of output intensity. More sophisticated devices utilize two independent laser pulses at 570 nm. In the simplest case, the Boolean analysis leads to the NOR gate; even single pulse at 570 nm results in strongly decreased transmission of 640-nm light. Properly defined threshold level allows application of the same systems as the all-optical NAND gate.<sup>462</sup> The same mode of operation can be used with other compounds showing strong excited-state absorption, e.g., Pt-ethynyl complexes.<sup>463</sup>

Photogeneration of holographic diffraction gratings together with degenerate four wave mixing (DFWM) is another phenomenon that allows mimicking of logic devices using bacteriorhodopsin films.<sup>464</sup> Red irradiation of the bacteriorhodopsin films with coherent light results in saturation of  $R_{570} \rightarrow M_{410}$  transition first in the places of constructive interference, and subsequently, light scattering induces saturation also in the regions of destructive interference. Analogously, irradiation with blue light saturates the whole film in the  $R_{570}$  state. When two light sources operate at the

same time, a complex pattern of two independent holographic gratings is formed, which results in the DFWM signal. Similar effects can be observed in methyl orange-doped polyvinyl alcohol films.<sup>465</sup> Bacteriorhodopsin films were also successfully applied as holographic memories and other photonic devices.<sup>461</sup>

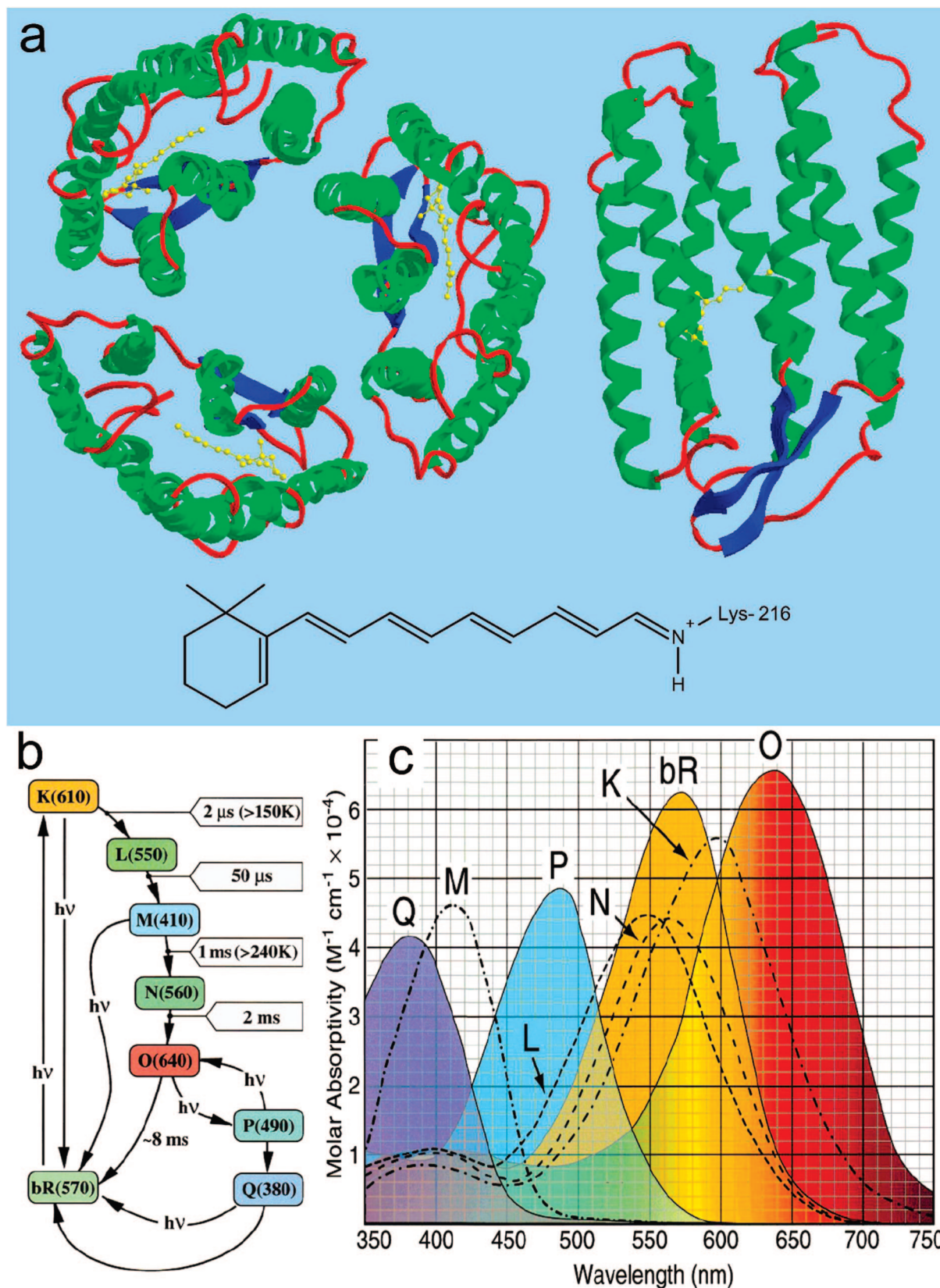
### 5.3. Electrochemical and Photoelectrochemical Logic Gates and Devices

In contrast to the plethora of chemical and optical logic gates, there are only few reports on electrochemical logic devices, and in fact almost none of them can be regarded as purely electrochemical logic gate. Much more reports can be found on photoelectrochemical devices based on organic monolayers or surface-modified wide band gap semiconductors.

The only purely electrochemical device, which is somehow related to CHEMFET transistors, was reported recently by Berggren and co-workers.<sup>466</sup> The device operates with electric input and electric output. The operation of the transistor is based on oxidation/reduction of the poly(3,4-ethylenedioxythiophene):poly(styrene sulfonic acid) blend (PEDOT:PPS) in the form of thin film electrodes. Similar to the classical field effect transistor, the electrochemical device has three electrodes: source, drain, gate, and an active PEDOT:PPS channel. Application of the voltage between the gate and source electrodes modulates the redox state of the polymer and thus the impedance of the channel, which in turn affects the source-drain current. These transistors can be easily connected to larger circuits, like logic gate ring oscillators and other devices.

Another electrochemical universal device is a microfluidic diode reported by Crooks et al.<sup>467</sup> The electrochemical microfluidic system comprises poly(dimethylsiloxane) (PDMS) channels and three indium tin oxide electrodes patterned onto glass using standard photolithographic methods. The PDMS microfluidic system contains three input channels and a common outlet (Figure 43). The output of the device is electrical (microfluidic diode) or electroluminescence (OR and NAND logic gates).

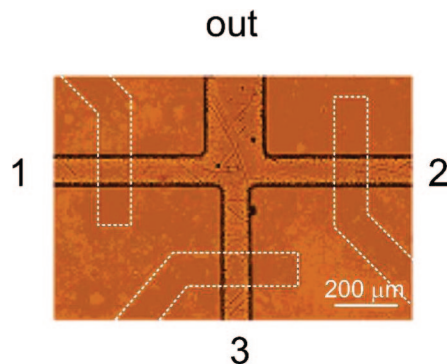
In order to mimic the behavior of a diode, aqueous solutions of  $[\text{Ru}(\text{NH}_3)_6]^{3+}$ ,  $[\text{Ru}(\text{bpy})_3]^{2+}$ , and supporting electrolyte are passed through channels 1, 2, and 3, respec-



**Figure 42.** X-ray structure of the bacteriorhodopsin trimer (PDB entry 1brr) and a side view of bacteriorhodopsin monomer (a). Lipid molecules are removed for clarity.<sup>457</sup> Photochemical cycle of bacteriorhodopsin (b) and ambient temperature absorption spectra of the most important bacteriorhodopsin forms.<sup>459–461</sup> Partially reprinted with permission from ref 461. Copyright 1999 American Chemical Society.

tively, at the same flow rate. These three fluids move under laminar flow conditions and exit the device through the large channel at the top of the device. When a forward bias of 1.5 V is applied between electrodes 1 and 2 ( $E_{1,2}$ ), where

electrodes 1 and 2 are configured as the cathode and anode, respectively, and electrode 3 is at open circuit, the  $[\text{Ru}(\text{NH}_3)_6]^{3+}$  complex is reduced, and the  $[\text{Ru}(\text{bpy})_3]^{2+}$  complex oxidized. This processes result in current flow



**Figure 43.** Micrograph of the PDMS microfluidic electrochemical device. The channels are  $100\ \mu\text{m}$  wide and  $17\ \mu\text{m}$  high. The dashed lines depict the ITO electrodes. Reprinted with permission from ref 467. Copyright 2003 American Chemical Society.

between the electrodes. Reverse polarization results in a current of 2 orders of magnitude lower.

When the same device is fed with the  $[\text{Ru}(\text{NH}_3)_6]^{3+}$  complex to inputs 1 and 2, but  $[\text{Ru}(\text{bpy})_3]^{2+}$  and tripropylamine to input 3, it can mimic the OR logic gate with electric inputs and electroluminescence output. In this configuration, potential can be applied to 1,3 and/or 2,3 electrode pairs. In any case, positive polarization of electrode 3 results in electroluminescence from electrode 3 due to electrochemical generation of  $^*\text{[Ru}(\text{bpy})_3]^{2+}$ , which directly corresponds to the OR function. Other logic functions require more complex systems of several electrically connected microfluidic cells.

Very similar devices were built using paired band electrodes immersed in various electrolytes containing redox-active substrates.<sup>468</sup> These electrochemical models of neurons can be configured to mimic the behavior of logic gates.

The photoelectrochemical logic gates are devices that are much more common. There are two different classes of these devices: layer organic structures and surface-modified nanocrystalline semiconductors. In both cases, the material is deposited/immobilized onto the surface of the transparent electrode and immersed in proper electrolyte solution. In most cases, the output signal has the form of photocurrent pulses, while the inputs include light pulses of desired wavelengths and photoelectrode potentials.

The very first report on photoelectrochemical switching devices comes from the laboratory of Tokuji Miyashita.<sup>469</sup> The device comprised gold electrode covered with four Langmuir–Blodgett layers of *tert*-pentacrylamide covalently modified with chromophores, electron donors, and electron acceptors. A layer containing the phenanthrene chromophore was deposited at the gold surface. The next layers contained electron acceptors (dinitrobenzene moieties), electron donors (dimethylaniline moieties), and anthracene chromophore. Illumination of the electrode within absorption of one chromophore (300 or 380 nm for phenanthrene and anthracene, respectively) resulted in weak cathodic photocurrents. Concomitant excitation of both chromophores results in over 2-fold increase of photocurrent intensity. This can be applied for AND function; only illumination of both chromophores (both inputs in high state) results in high photocurrent intensity. The mechanism of operation of this device is shown in Figure 44a.

The same device devoid of the donor layer constitutes the photoelectrochemical XOR gate (Figure 44b).<sup>470</sup> Illumination within the phenanthrene absorption results in electron transfer from *phen* moieties to the acceptor layer, which in turn

results in cathodic photocurrents ( $\sim 500\ \text{pA}$ ). Excitation of the anthracene-containing polymer also results in electron transfer to the acceptor layer, but due to the geometrical constraints, anodic photocurrent is observed. Concomitant irradiation of both chromophores results in null net photocurrent. The same approach was later explored by Kimura et al., but these devices yielded even lower photocurrent intensities ( $50\text{--}100\ \text{pA}$ ).<sup>471</sup> The latter results, however, can be strongly perturbed by photoelectrochemical response resulting from local heating of the chromophore-modified gold surface; therefore, the reliability of the device is highly questionable.<sup>472</sup>

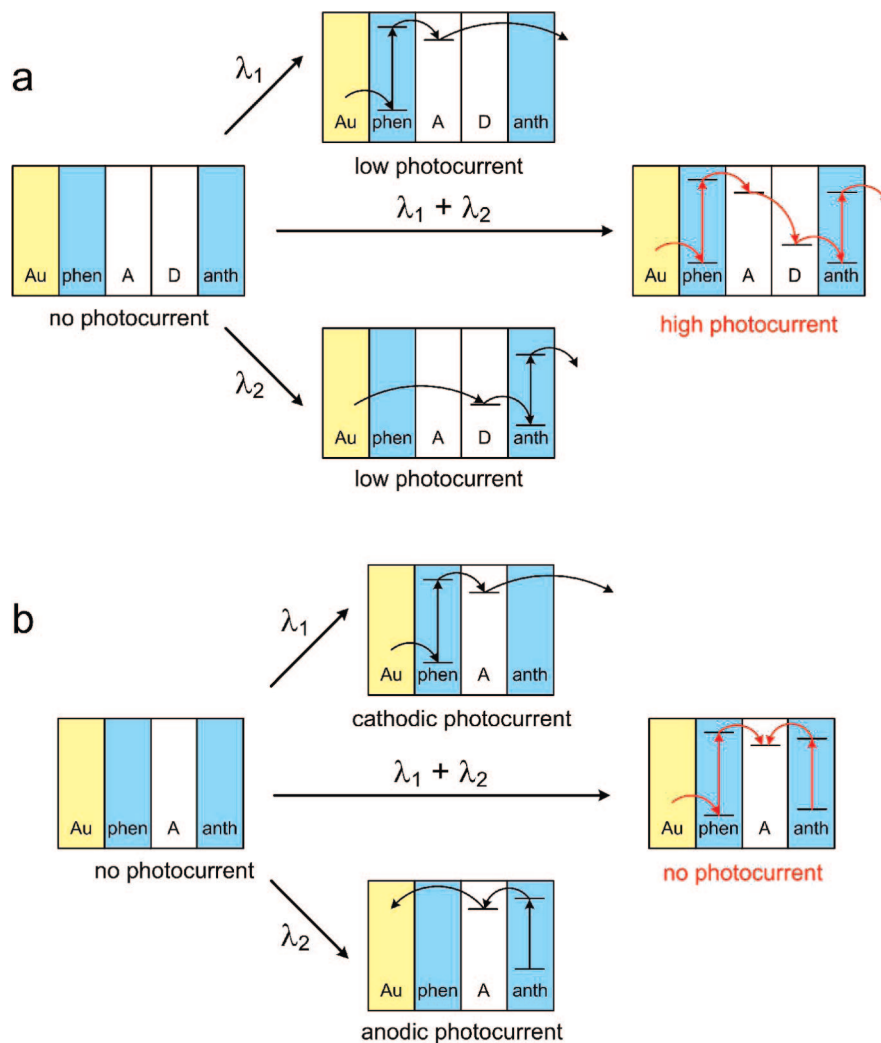
More efficient photoelectrochemical devices were reported by Yamada et al. (Figure 45).<sup>473,474</sup> The device comprised gold electrode covered with chromophores bound via alkyl chains terminated with thiol groups. As chromophores, palladium(II) phthalocyanine and  $[\text{Ru}(\text{bpy})_3]^{2+}$  complex covalently linked with viologen moiety were used (Figure 45a), and the electrolyte contained electron acceptor (methyl viologen,  $\text{MV}^{2+}$ ) and sacrificial electron donor (triethanolamine, TEA). Excitation of the ruthenium species results in photoinduced electron transfer toward the viologen moiety, which in turn transfers the electron to the gold substrate. The ruthenium complex is subsequently reduced by triethanolamine. Upon excitation of phthalocyanine, an electron is transferred to the electron acceptor ( $\text{MV}^{2+}$ ) present in the electrolyte, and cathodic photocurrent is observed. Therefore, illumination of the electrode with blue light yields anodic photocurrent, while excitation with red light results in cathodic photocurrent (Figure 45b). Both currents reach approximately  $0.5\ \text{nA}$ . Simultaneous illumination with blue and red light results in null net photocurrent due to complete compensation of photoanodic and photocathodic responses. This behavior corresponds to the XOR gate.

Photoelectrochemical properties of wide band gap semiconductors have been utilized in numerous photoelectrochemical logic gates.<sup>146,148,149,475–480</sup> These devices are characterized by much higher photocurrent intensities; therefore, these devices are much less susceptible to interference from other processes, like local electrode heating or diffusive currents.<sup>472</sup> Most of the semiconductor-based photoelectrochemical logic gates are based on photoelectrochemical photocurrent switching (PEPS effect). This effect is characteristic for wide band gap semiconductors modified on the surface with redox-active species. It was observed for titanium dioxide modified with acetate-bridged ruthenium(II) cluster with pyridine and pyrazine ligands,<sup>149</sup> carotene,<sup>481</sup> hexacyanoferrate (HCF),<sup>147</sup> pentacyanoferrates (PCF),<sup>475,477</sup> Prussian blue,<sup>478</sup> ferrocene derivatives,<sup>479</sup> and folic acid.<sup>480</sup> In these devices, photoelectrodes generate photocurrent, the polarization of which depends on photoelectrode potential, and/or wavelength of incident light.

The best example of such a device consists of the  $\text{TiO}_2$  photoelectrode modified with hexacyanoferrate and two LEDs acting as light sources.<sup>148,476</sup> Cyanoferrate is deposited onto  $\text{TiO}_2$  via formation of Ti–N–C–Fe framework. These materials are characterized by intense MMCT( $\text{Fe}^{\text{II}} \rightarrow \text{Ti}^{\text{IV}}$ ) transition.<sup>482</sup>

At potentials ensuring complete oxidation of the surface species (e.g.,  $+400\ \text{mV}$  vs  $\text{Ag}/\text{AgCl}$ ), pulsed irradiation of the  $\text{HCF}/\text{TiO}_2$  material with violet light (LED  $\lambda_{\text{max}} = 400\ \text{nm}$ ) results in anodic photocurrent pulses, while irradiation with blue light (LED  $\lambda_{\text{max}} = 460\ \text{nm}$ ) does not generate any photocurrent. Simultaneous irradiation with two LEDs yields





**Figure 44.** Mechanism of operation of the photoelectrochemical AND (a) and XOR (b) photoelectrochemical logic gates. (Au, gold substrate; phen, phenanthrene-doped polymer; A, acceptor polymer; D, donor polymer; anth, anthracene-doped polymer). Partially adapted with permission from ref 469. Copyright 2003 Wiley Interscience.

the same effect as the violet diode alone (Figure 46a, signal at 400 mV, output 1). Electrochemical reduction of the surface species is achieved at lower potentials. Excitation of this material with violet and blue diodes leads to the generation of cathodic photocurrent. Simultaneous irradiation by both diodes results in a higher intensity of photocurrent. Such behavior of the photoelectrode at  $-200$  mV vs Ag/AgCl corresponds to the OR logic gate (Figure 46a, signal at  $-200$  mV, output 3).

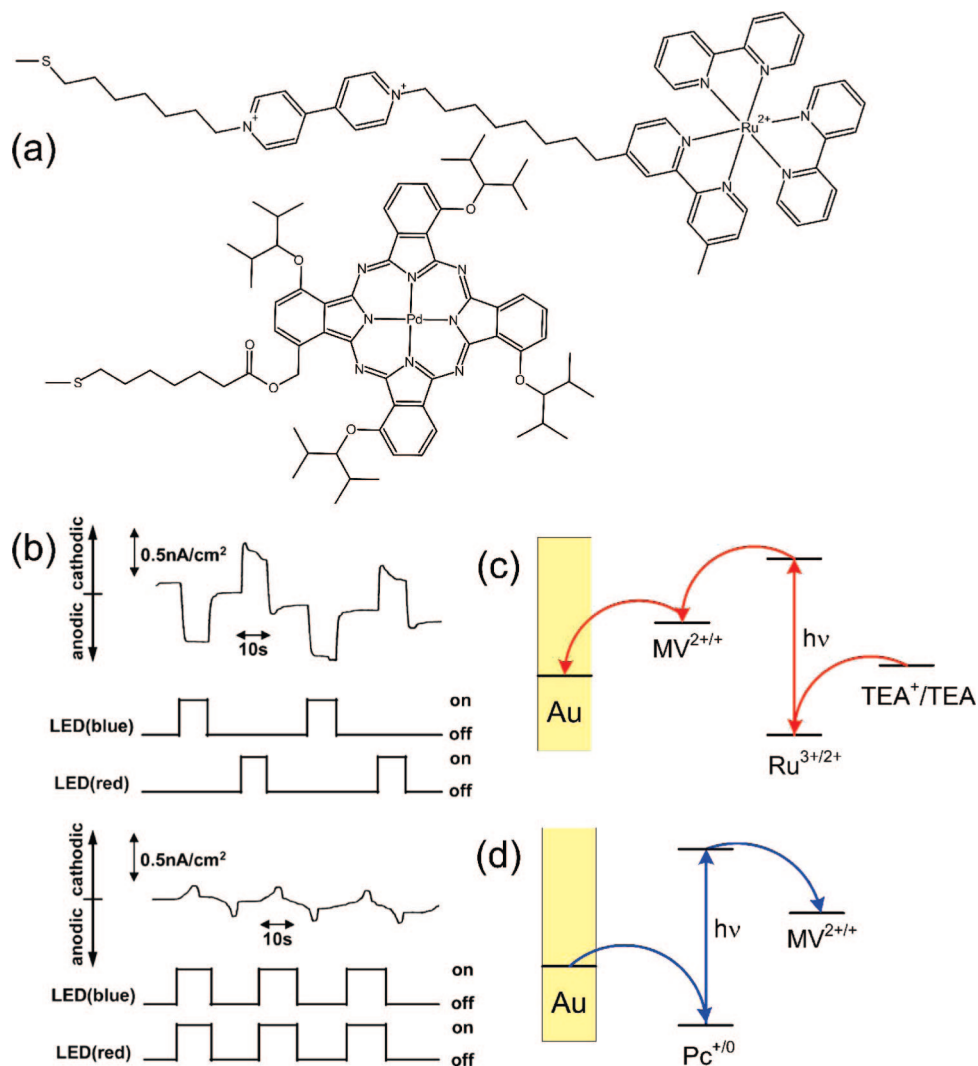
Much more interesting photocurrent profiles were recorded upon partial oxidation of the surface complex (e.g., at 250 mV). Irradiation with 400 nm light results in the generation of anodic photocurrent, which is consistent with excitation of the inner part of semiconductor particles. Irradiation with 460 nm light results in the generation of cathodic photocurrent. Simultaneous irradiation with two diodes gives null net current as anodic and cathodic photocurrents compensate effectively (Figure 46a, signal at 250 mV, output 2). This behavior analyzed in terms of Boolean logic corresponds to the XOR gate. The photocurrent compensation, however, requires such adjustment of light intensity of both sources that absolute values of anodic and cathodic photocurrents are equal. This can be easily achieved here by adjustment of diode supply current.

The logic device based on semiconducting photoelectrodes shows another important feature. It should be noted that the

logic analysis of this system can be much more complex if photoelectrode potential is considered as the third input channel. In this context, the logic system described here is a chemical model of a reconfigurable logic device, the function of which can be programmed by the user.<sup>318,443</sup> Changes in applied potential can switch the logic behavior of the photoelectrode between three different regimes: (i) transmission of the input 1 signal to the output neglecting input 2 (YES), (ii) computation of the XOR function of two input values, and (iii) computation of the OR function of two input values (Figure 46b, Table 5).

Different modes of action were found for some PCF@TiO<sub>2</sub> materials (e.g., with thioethers<sup>475</sup> and thiamine<sup>477</sup> as axial ligands), Prussian blue-titanium dioxide,<sup>478</sup> and ferrocenitania<sup>479</sup> composites as well as folate-modified titania.<sup>480</sup> Variation of the potential results in photocurrent polarity reversal. Similar effects were also observed for bulk heterojunction materials such as *n*-BiVO<sub>4</sub>/*p*-Co<sub>3</sub>O<sub>4</sub>,<sup>483</sup> *n*-TiO<sub>2</sub>-*N/p*-CuI,<sup>484</sup> *n*-TiO<sub>2</sub>/*p*-Se,<sup>485</sup> or *n*-TiO<sub>2</sub>/*p*-polythiophene composites.<sup>486,487</sup> This effect can be utilized for the construction of optoelectronic demultiplexers and other switching devices.<sup>488</sup>

At potentials higher than the switching threshold (positive polarization), the electrodes generate anodic photocurrent, while at lower potentials (negative polarization), cathodic photocurrents are observed. One can assign the logic values



**Figure 45.** Molecular structures of components of the photoelectrochemical switch (a), photoelectrochemical characteristics of the device (b), and mechanisms of generation of anodic (c) and cathodic (d) photocurrents. Partially reprinted with permission from ref 473. Copyright 2005 American Chemical Society.

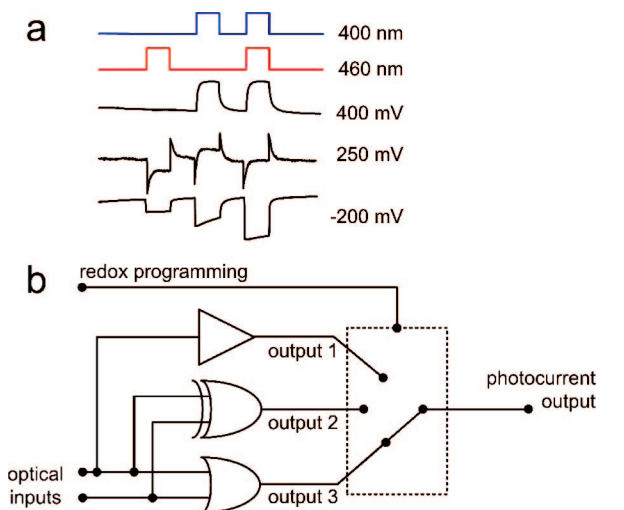
of 0 and 1 to the negative and the positive polarization of the photoelectrode, respectively. The switching characteristics allows one to use it as an optoelectronic two channel demultiplexer (data selector). This device collects information in the form of light pulses and converts it into photocurrent pulses. Furthermore, the polarity (direction) of photocurrent pulses depends on the photoelectrode potential. In other words, information in the form of photocurrent pulses can be directed into two output channels: cathodic or anodic. An electronic equivalent of this logic device is composed of two AND and NOT logic gates (Figure 47). The input data signal (light pulses) is applied to one input of both AND gates, the control signal goes to one AND gate directly and to the other via an inverter. In this configuration, one of the AND gates is in the ON state and the other in the OFF state.<sup>147,478–480</sup> Thus, a signal applied to the data input is always transmitted by one of the AND gates and thus directed into one of the output channels.

Alternative approach to the photoelectrochemical information processing is represented by the logic gate reported by Bigozzi and co-workers.<sup>146</sup> The device consists of electrodes covered with porous TiO<sub>2</sub> subsequently modified with the [Ru(bpy')<sub>2</sub>(CN)<sub>2</sub>] complex, in which every bipyridine ligand contains two carboxylic groups in 4,4' positions (Figure 48a). The complex itself is luminescent, and excita-

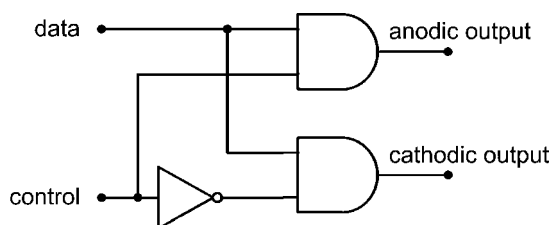
tion at 467 nm results in strong emission at 668 nm. Upon its chemisorption onto TiO<sub>2</sub>, the luminescence can be switched on and off reversibly by application of appropriate potentials and by changes in the electrolyte composition.

At positive bias, the photoluminescence of the ruthenium complex is quenched due to efficient electron injection into the conduction band of the semiconductor (Figure 48b). Upon addition of the external electron acceptor (e.g., Cu<sup>2+</sup> ions), two photoinduced electron transfer processes compete, resulting in efficient quenching of the ruthenium complex luminescence (Figure 48c). Negative polarization of the photoelectrode (i.e., application of potential lower than the Fermi level potential) results in inhibition of electron injection into the conduction band, and the only quenching mechanism involves PET to the external electron acceptor (Figure 48d). In the absence of the quencher, ruthenium luminescence can be observed (Figure 48e). Therefore, these systems can be regarded as NOR logic gate with potential and [Cu<sup>2+</sup>] inputs and fluorescence output.

These two families of semiconductor-based photoelectrochemical devices are, among all the chemical switches and logic devices, the closest to their silicon-based counterparts. Very much like monolithic semiconductor devices, these logic circuits utilize light and electricity for transmission and processing of information, the output of which is also



**Figure 46.** Photocurrent transients recorded for  $[\text{Fe}(\text{CN})_6]^{4-}$ -modified titanium dioxide photoelectrodes during pulsed irradiation with violet (400 nm) and blue (460 nm) LEDs (a). Electronic equivalent circuit for reconfigurable logic system based on modified titanium dioxide electrode (b). Output 1 follows the input 1 signal, and output 2 computes the XOR function of input data, while output 3 corresponds to the logic sum (OR) of input data. Programming input and three-position switch represent programming of the device through the photoelectrode potential. Adapted from ref 148.



**Figure 47.** Electronic equivalent circuit of surface-modified titania photoelectrode working as two channel optoelectronic demultiplexer. Adapted from ref 478.

**Table 5. Truth Table for Logic Gates Based on  $[\text{Fe}(\text{CN})_6]^{4-}$  Modified Titanium Dioxide Photoelectrodes<sup>a</sup>**

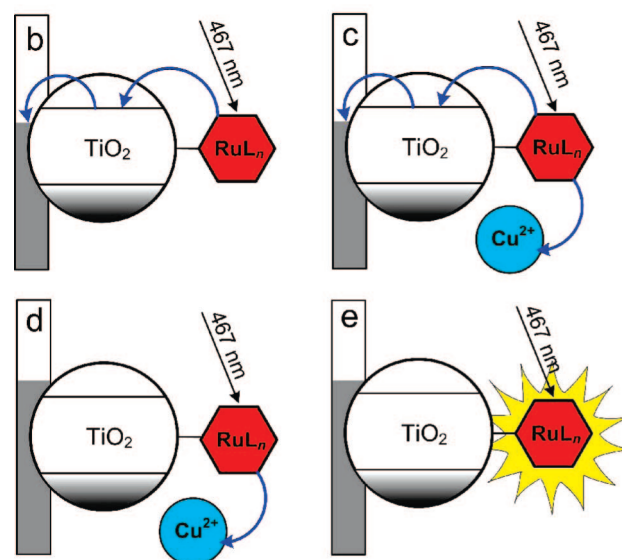
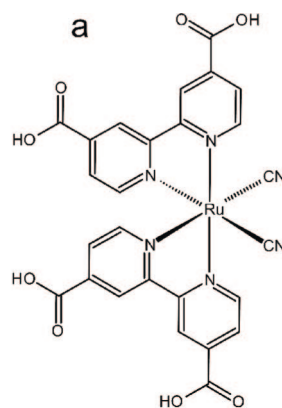
input 1 400 nm light	input 2 460 nm light	output 1 400 mV	output 250 mV	output 3 -200 mV
0	0	0	0	0
0	1	0	1	1
1	0	1	1	1
1	1	1	0	1
		YES	XOR	OR

<sup>a</sup> Outputs 1, 2, and 3 refer to photocurrent responses at given potentials.

communicated by means of light or electric pulses. Therefore, in principle there should be no obstacles to concatenate these devices into larger computing circuits. For any other class of molecular devices described in this review this goal is extremely difficult to achieve, except for some logic systems based on biomolecules (cf. section 8).

## 6. Combinatorial Logic Systems

Simple logic gates (cf. Tables 1 and 2) can perform only basic logic operations. Practical application of any logic device requires much more complex logic structure including complex logic functions performed on large data sets, multiplexing, and demultiplexing of data streams, arithmetic operations, and so forth. Molecular logic systems presented so far are not complex enough to fulfill these requirements.

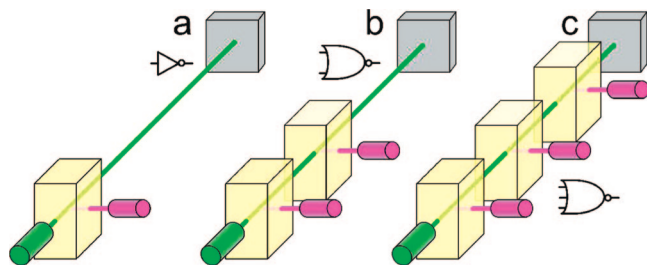


**Figure 48.** Design and operating principles of the photoelectrochemical logic gate based on  $[\text{Ru}(\text{bpy})_2(\text{CN})_2]$ -modified titanium dioxide.<sup>146</sup> Molecular structure of ruthenium fluorophore (a), luminescence quenching pathways due to the PET to the semiconductor (b and c), luminescence quenching pathways due to the PET to the external electron acceptor (b and d), and luminescence under negative bias of the photoelectrode (e).

However, there are molecular systems capable of more complex data processing or processing of larger number of input parameters in parallel. The first of these tasks is performed by concatenated logic devices, while the latter by multiple-input logic gates and other devices.

### 6.1. Multiple-Input Logic Gates

There are very few chemical logic systems that can be described as elementary multi-input logic gates. Easily expandable multi-input OR molecular logic device was designed by Raymo and Giordani.<sup>144</sup> The system is based on an array of cells containing photochromic spiropyran acting as a light switch. Colorless SP upon irradiation with UV light is converted into strongly colored merocyanine dye (cf. Figure 25). Therefore, the cell containing the SP solution may act as a light-controlled filter: in the absence of UV illumination, the visible light is transmitted, while upon switching the UV source strong visible absorption occurs. This is the basis of the photonic NOT gate (Figure 49a). Extension of the system via introduction of a larger number of the cells results in the NOR gate, as visible light is transmitted through the series of cells only if all the UV



**Figure 49.** Construction of NOT (a), two-input NOR (b), and three-input NOR (c) logic gates. Visible light sources are marked in green, while UV sources are in purple. Adapted from ref 144.

sources are switched off. The number of inputs directly corresponds to the number of photoactive cells arranged in series (Figure 49b and c).

The three-input AND gate, also based on spiropyran as the switching unit, was proposed by Zhu et al.<sup>489</sup> The gate is based on the spiropyran–perylenebisimide conjugate (Figure 50a). At high pH and in the absence of ferric ions, the luminescence quantum yield is very low ( $\sim 0.01$ ) due to strong electronic coupling of perylenebisimide (PI) with spiropyran, which leads to PI fluorescence quenching. UV irradiation leading to spiropyran ring opening (Figure 50b) or SP protonation (Figure 50d) results only in a minor increase of the luminescence intensity. Also, the addition of  $\text{Fe}^{3+}$  ions does not influence the luminescence intensity. Protonation of the opened (merocyanine) form of the conjugate and reaction with ferric ions (Figure 50f) induces 30-fold increase in luminescence quantum yield due to the electron-withdrawing property of ferric ions leading to effective decoupling of merocyanine and PI units. Therefore, the system can be regarded as a three input AND gate, with 365 nm light, protons, and  $\text{Fe}^{3+}$  ions as input stimuli and luminescence at 560 nm as an output.

Other more complex molecular logic systems cannot be regarded as multiple input logic gates as they perform more complex functions, and their inputs are not commutative. They can be described as concatenated logic circuits.

## 6.2. Concatenated Chemical Logic Systems

Simple concatenated logic systems are based on luminescent or chromogenic sensor-derived molecules, which can change their state upon stimulation with more than two different stimuli or systems with dual luminescence. Systems with complex photochemical or photophysical behavior are also suitable for implementation of complex logic systems.

First, complex logic systems based on photoactive compounds were reported by F. M. Raymo and co-workers in 2001.<sup>142,490,491</sup> The photoactive spiropyran can exist in three forms of very different optical properties (Figure 51a): colorless spiropyran (SP), purple merocyanine betaine (ME), and yellow protonated merocyanine (MEH).<sup>142,492</sup>

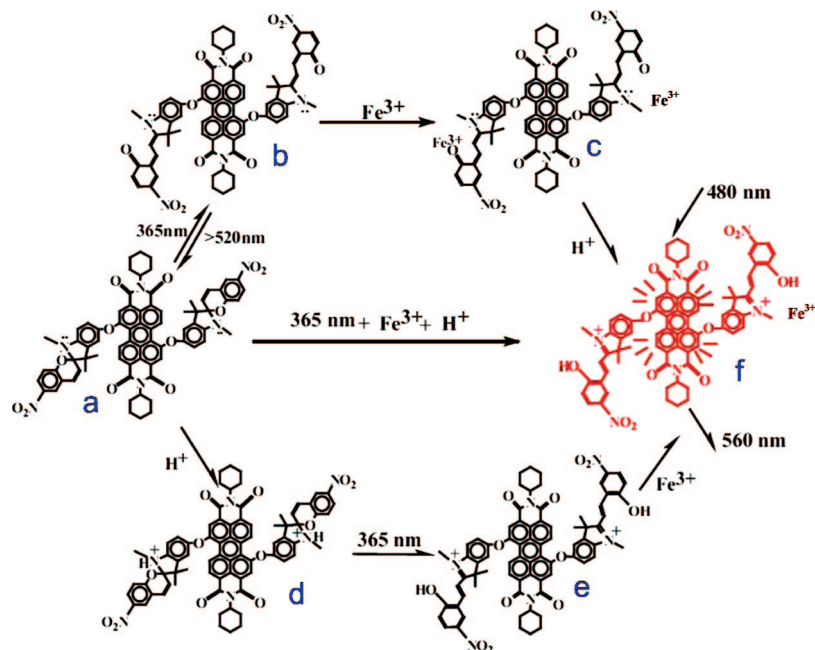
The absorption spectrum of a colorless acetonitrile solution of the SP form does not show any absorption bands in the visible range of the electromagnetic spectrum. Upon irradiation of this solution with ultraviolet light, the colorless SP is converted into the purple ME form. This process is accompanied by the appearance of a strong absorption band at 563 nm. Upon addition of 1 equivalent of trifluoroacetic acid, the purple ME protonates yielding the yellow-green MEH, and the absorption band at 563 nm disappears. An absorption band at 401 nm is observed instead. Upon visible irradiation, the MEH form is completely converted to SP.

Upon addition of 1 equivalent of  $\text{CF}_3\text{COOH}$  to a colorless solution of SP maintained in the dark, the yellow-green MEH is obtained, which makes the whole cycle perfectly reversible. This three-state molecular switch can thus detect three different input signals: ultraviolet light ( $\text{in}_1$ ), visible light ( $\text{in}_2$ ), and protons ( $\text{in}_3$ ). As a response to these stimulations, the system generates two output signals: the absorption band at 401 nm of MEH ( $\text{out}_1$ ) and that at 563 nm of ME ( $\text{out}_2$ ). This leads to a very complex logic structure of the device, the truth table of which is presented in Table 6. The combinational logic circuit (Figure 51b) illustrates the complexity of the logic structure of the three-state device. It is worth noticing that nine logic elements are necessary to reproduce the functions performed by a single molecule.<sup>142</sup> In this circuit, the three chemical and optical input signals  $\text{in}_1$ ,  $\text{in}_2$ , and  $\text{in}_3$  are processed through a series of AND, NOT, and OR gates yielding the two optical output signals  $\text{out}_1$  and  $\text{out}_2$ . The eight possible combinations of input data are transduced into three of the four potential strings of output data. The logic circuit excludes the output string (1,1), which is never produced. Indeed, the two output signals cannot be on simultaneously. They correspond to two distinct states of the molecular switch that cannot coexist in solution.<sup>142</sup>

Introduction of another molecule to the SP-ME-MEH system may result in information transfer (communication) at the molecular level.<sup>490,491</sup> Addition of a fluorescence probe (perylene, PY) to the SP solution results in decreased photoluminescence at 373 nm (336 nm excitation) intensity due to coabsorption of excitation light. Upon conversion of SP into ME or MEH, the PY fluorescence intensity further decreases due to strong overlap of PY emission and ME (MEH) absorption, and thus reabsorption of the fluorescence light.<sup>490</sup> Detailed Boolean analysis of fluorescence intensity as a function of input data (UV and VIS irradiation, acid concentration) is presented as  $\text{out}_3$  in Table 6. The system described above integrates three input channels, three output channels, and 16 elementary AND, OR, and NOT gates into one complex logic circuit. This is one of the most complicated logic networks reported so far in the chemical literature.

Further development of the fluorescent reporter-type device was achieved by spatial separation of the switch from the reporter and construction of an optical network for data transmission.<sup>493</sup> This network consisted of two cells and three light sources (Figure 52a). As a light source, a cell containing solutions of three fluorescent hydrocarbons, naphthalene, anthracene, and tetracene, was used. The fluorescence light was that directed to the switching cell containing the SP-ME-MEH photoswitch. This cell was equipped with two light sources: UV and VIS. The naphthalene fluorescence (335 nm) is absorbed completely by all the forms of the photoswitch; therefore, this channel is excluded from further considerations. The anthracene fluorescence (401 nm) is absorbed by ME and MEH forms, while the tetracene emission (544 nm) is only by the ME. Assignment of UV light, visible light, and addition of acid as input channels ( $\text{in}_1$ ,  $\text{in}_2$  and  $\text{in}_3$ , respectively) and anthracene ( $\text{out}_1$ ) and tetracene ( $\text{out}_2$ ) emissions as output channels lead to the complex logic device (Figure 52b) containing 5 AND, OR, and NOT logic gates. This device can be further developed in a way similar to the three-input NOR gate (cf. Figure 49) and is a model of the optically controlled router of optical signals.<sup>493</sup>

Addition of a chromogenic proton acceptor *N,N*-dimethyl-4-[(*E*)-pyridin-2-ylidiazenyl]aniline (*azopyridine*, AZ) to the



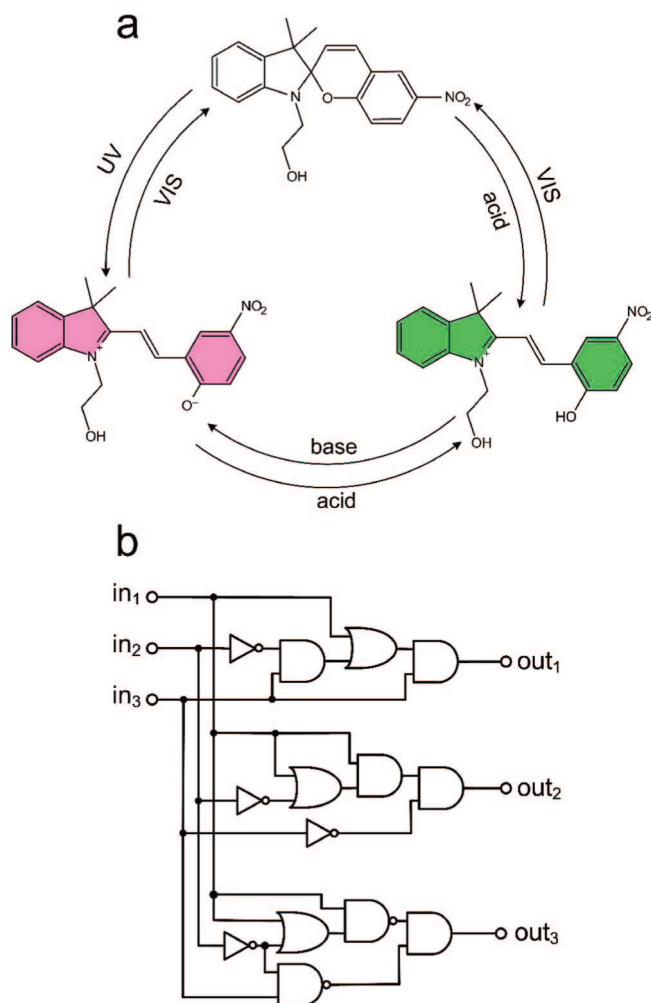
**Figure 50.** Interaction of the spiropyran–perylene–bisimide conjugate with light, protons, and  $\text{Fe}^{3+}$  ions responsible for the cooperative control of fluorescence: three-input AND logic gate. The fluorescent form is marked in red. Reprinted with permission from ref 489. Copyright 2004 Wiley-VCH.

SP based system results in the logic network containing a memory element. The AZ dye exists in acetonitrile solution in two colored forms: orange free base form ( $\lambda_{\text{max}} = 422$  nm) and purple-red protonated form, AZH ( $\lambda_{\text{max}} = 556$  nm). As photoisomerization of SP to ME controls its basicity, the photoinduced intermolecular photon transfer can be observed during photolysis of AZH+SP mixtures.<sup>491</sup> Upon UV irradiation ( $\text{in}_1 = 1$ ), the photogenerated base (ME) resulting from photoisomerization of SP can deprotonate the AZH acid. Conversely, VIS irradiation ( $\text{in}_2 = 1$ ) of the MEH+AZ mixture results in photoisomerization of merocyanine and back proton transfer, resulting in the SP+AZH mixture (Figure 53a). The proton transfer process reduces the number of SP-ME-MEH states to two, but introduces a memory element due to the inhibition of thermal recovery of the merocyanine form. Therefore, the system in the absence of light ( $\text{in}_1 = 0$  and  $\text{in}_2 = 0$ ) remembers the last state. The memory element is represented by the feedback loop connecting the output of the device with one of the inputs (Figure 53b and cf. Figure 4).

Complex logic devices can also be derived from simple fluorescent sensor or elementary logic gates (e.g., XOR-8).<sup>426</sup> This molecule operates in transmittance mode as a XOR gate with protons and alkali earth metal cations. Therefore, application of  $\text{Ba}^{2+}$ ,  $\text{Sr}^{2+}$ , and  $\text{H}^+$  as inputs results in a combinatorial circuit with three inputs:  $\text{Ba}^{2+}$ ,  $\text{Sr}^{2+}$  feed the OR gate, the output of which is connected with one input of concatenated XOR. The other input of XOR is  $[\text{H}^+]$ .<sup>426</sup>

The most common approach to the concatenated molecular logic devices includes molecular receptors of low selectivity (i.e., several different chemical species can interact with the receptor) and multiple output channels (e.g., dual emission, emission, and absorption, etc.).

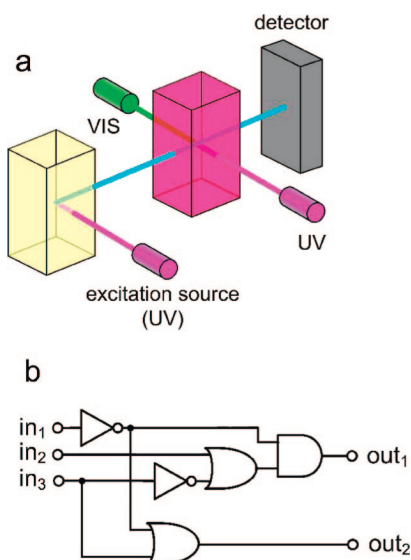
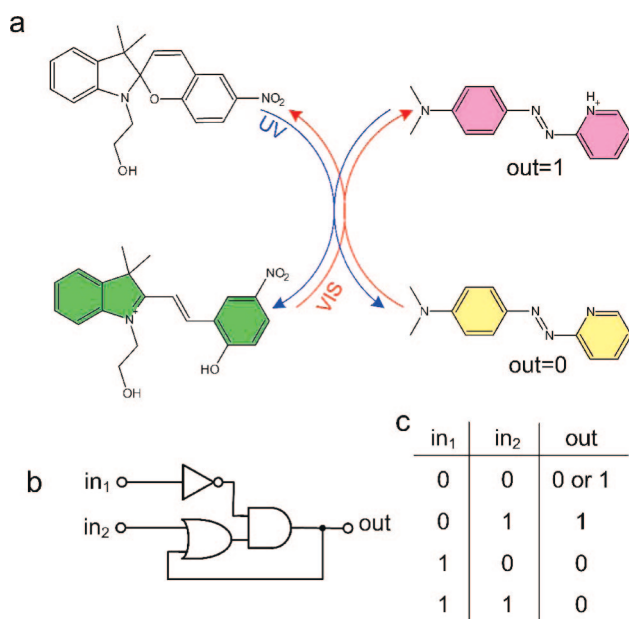
Very complex sensing behavior is observed in the case of the CON-1 sensor.<sup>494</sup> Binding of most of the transition metal ions ( $\text{Ag}^+$ ,  $\text{Cd}^{2+}$ ,  $\text{Cu}^{2+}$ ,  $\text{Hg}^{2+}$ , and  $\text{Zn}^{2+}$ ) within the azacrown receptor does not influence the characteristics of the charge transfer band involving aniline donor and tricya-



**Figure 51.** The switching cycle associated with the three states SP, ME, and MEH (a). The logic circuit equivalent of the three-state molecular switch transducing the  $\text{in}_1$ ,  $\text{in}_2$ , and  $\text{in}_3$  into the  $\text{out}_1$ ,  $\text{out}_2$ , and  $\text{out}_3$  outputs through the logic network of AND, NAND, NOT, and OR operations. Adapted from refs 142 and 490.

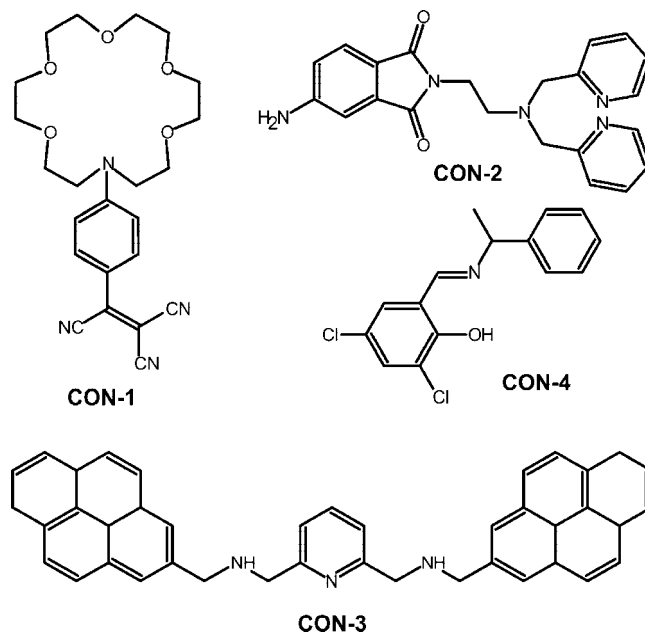
**Table 6. Truth Table for the Three-State Molecular Device from Figure 51<sup>142</sup>**

inputs			outputs		
in <sub>1</sub> (254 nm light)	in <sub>2</sub> (524 nm light)	in <sub>3</sub> (CF <sub>3</sub> COOH)	out <sub>1</sub> (abs@401 nm)	out <sub>2</sub> (abs@563 nm)	out <sub>3</sub> (fl@373 nm)
0	0	0	0	0	1
0	0	1	1	0	0
0	1	0	0	0	1
0	1	1	0	0	0
1	0	0	0	1	0
1	0	1	1	0	1
1	1	0	0	1	0
1	1	1	1	0	0

**Figure 52.** Optical network employed to implement digital transmission on an ensemble of communicating molecules (a) and the combinational logic circuits of the device. Adapted from ref 493.**Figure 53.** Switching cycle of the SP/PY combined molecular switch (a), corresponding electronic circuit (b), and the truth table (c). Adapted from ref 491.

noethene acceptor moieties. A color variation from red-pink to yellow-orange (hypsochromic shift from 520 to 475 nm) was observed upon addition of the Pb<sup>2+</sup> cation. Furthermore,

a 3-fold decrease of the band intensity was recorded. The correct combination of ring and cation size would result in a suitable coordination to the nitrogen atom of the macrocyclic subunit, thus inducing the hypsochromic shift of the charge-transfer band. In turn, the presence of Fe<sup>3+</sup> results in strong decrease of the absorption band intensity and a small hypsochromic shift of approximately 10 nm. Addition of other metals such as Ag<sup>+</sup>, Cu<sup>2+</sup>, Cd<sup>2+</sup>, Hg<sup>2+</sup>, Ni<sup>2+</sup>, and Zn<sup>2+</sup> to acetonitrile solutions of CON-1 ligand gave no change in the color of the solutions.<sup>494</sup>



Fluorescence of the CON-1 sensor is also sensitive to the nature of the metal cation, but the observed changes are not compatible with the changes in absorption spectra. For Pb<sup>2+</sup>, the emission fluorescence enhancement is remarkable and is most likely associated with a strong metal coordination to the anilinium nitrogen, which is also supported by the changes in absorption spectra. However, quenching was observed with the redox-active metal cations Fe<sup>3+</sup> and Cu<sup>2+</sup>, for which electron-transfer processes involving the *d*-orbitals of the metals and the excited state of the fluorophore can occur.<sup>494</sup>

Not only spectral but also electrochemical properties of the sensor are modified with cation binding. The CON-1 ligand undergoes two reversible one-electron processes: reduction of the tricyanoethene moiety at -0.70 V (vs SCE) and oxidation of the aniline moiety (at +1.2 V). Most of the studied cations (Hg<sup>2+</sup>, Zn<sup>2+</sup>, Pb<sup>2+</sup>, and Fe<sup>3+</sup>) induce a notably large anodic shift of the reduction wave. Moreover, Pb<sup>2+</sup> is the only cation capable of inducing a significant anodic shift of the oxidation peak, strongly suggesting coordination of the Pb<sup>2+</sup> cation with the anilinium nitrogen, in agreement with the chromogenic results. Ag<sup>+</sup> and Cu<sup>2+</sup> cations gave negligible variations of the electrochemical behavior of CON-1.<sup>494</sup>

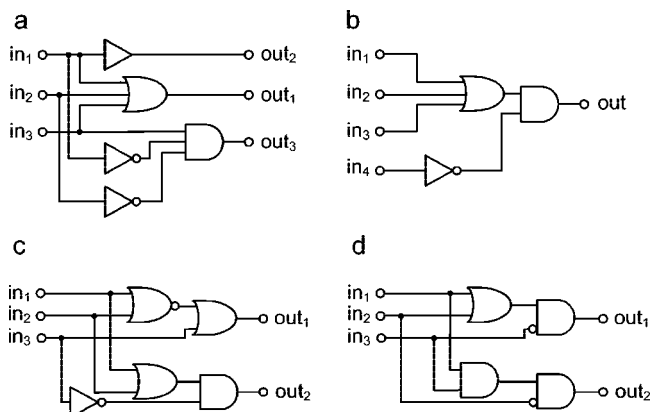
All these complex responses of CON-1 in three independent channels (absorbance, emission, redox potential) lead to rather complex logic structure of the chemical logic device. Let us consider a device operated with three input signals: Pb<sup>2+</sup> (in<sub>1</sub>), Hg<sup>2+</sup> (in<sub>2</sub>), and Fe<sup>3+</sup> (in<sub>3</sub>), and considering three outputs, change in redox potential (out<sub>1</sub>), color change (out<sub>2</sub>), and fluorescence quenching (out<sub>3</sub>). Detailed response of the

**Table 7. Triple Input Logical Truth Table Associated with the CON-1 Molecular Device<sup>a</sup>**

inputs			outputs		
in <sub>1</sub>	in <sub>2</sub>	in <sub>3</sub>	out <sub>1</sub>	out <sub>2</sub>	out <sub>3</sub>
0	0	0	0	0	0
0	0	1	1	0	1
0	1	0	1	0	0
0	1	1	1	0	0
1	0	0	1	1	0
1	0	1	1	1	0
1	1	0	1	1	0
1	1	1	1	1	0

<sup>a</sup> Adapted from ref 494.**Table 8. Triple Input Logical Truth Table Associated with the CON-3 Molecular Device<sup>a</sup>**

inputs			outputs	
in <sub>1</sub>	in <sub>2</sub>	in <sub>3</sub>	out <sub>1</sub>	out <sub>2</sub>
0	0	0	1	0
0	0	1	1	0
0	1	0	0	1
0	1	1	1	0
1	0	0	0	1
1	0	1	1	0
1	1	0	0	1
1	1	1	1	0

<sup>a</sup> Adapted from ref 496.**Figure 54.** Electronic equivalent logic diagram of the CON-1 (a), CON-2 (b), CON-3 (c), and CON-4 (d) molecular devices.

systems are given in Table 7, while the electronic equivalent of the device is depicted in Figure 54a.<sup>494</sup>

A similar strategy was applied in the device CON-2.<sup>495</sup> This fluorescent sensor responds with high intensity fluorescence (out) to several heavy cations including Zn<sup>2+</sup> (in<sub>1</sub>), Cd<sup>2+</sup> (in<sub>2</sub>), and Pb<sup>2+</sup> (in<sub>3</sub>). This strong fluorescence is observed only in the absence of strong acids (in<sub>4</sub>). The logic device based thereon integrates one three-input OR, two-input AND, and NOT gates (Figure 54b).

One device based on dual emission (monomer and excimer) was already described in section 5.1.6 (REC-3). Another with more complicated response characteristics was described recently by Zhu and co-workers.<sup>496</sup> The CON-3 switch may emit upon excitation both the monomer and the excimer luminescence, depending on the mutual orientation of the pyrene moieties. In the fully protonated CON-3 molecule, the two pyrene fluorophores are separated due to electrostatic repulsion of cationic fragments, and only monomer emission can be observed. The same is observed upon coordination of Zn<sup>2+</sup> by the three nitrogen donor atoms. Addition of triethylenetetramine (TETA) results in the full recovery of excimer emission due to deprotonation of the CON-3 switch and/or chelation of Zn<sup>2+</sup>. Assignment of the three inputs to trifluoroacetic acid (in<sub>1</sub>), Zn<sup>2+</sup> (in<sub>2</sub>), and TETA (in<sub>3</sub>) and output channels to excimer (out<sub>1</sub>) and monomer (out<sub>2</sub>) emissions results in a complex logic device (Table 8 and Figure 54c).

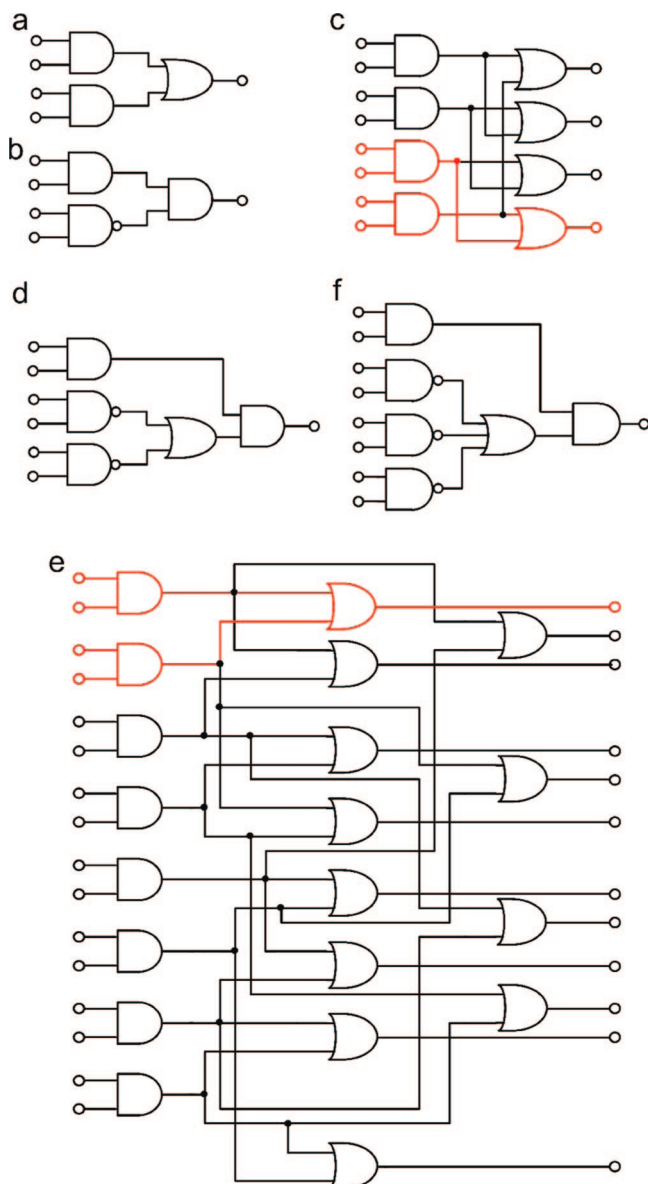
The Schiff base *N*-3,5-dichloro-salicylidene-*(S)*-*R*-phenylethylamine (CON-4) can serve as a dual-output (absorbance at 323 and emission at 460 nm, out<sub>1</sub> and out<sub>2</sub>, respectively) logic device with OH<sup>-</sup>, Zn<sup>2+</sup>, and UV light (254 nm) inputs.<sup>497</sup> The initial form of the compound showed only weak absorbance at 323 nm and is not luminescent. Deprotonation at the phenolic group changes the absorption

spectrum significantly, but the out<sub>1</sub> value remains low. The deprotonated form is also not luminescent; therefore, out<sub>2</sub> remains low as well. Addition of Zn<sup>2+</sup> ions results in formation of the 2:1 CON-4:Zn<sup>2+</sup> complex, which shows remarkably high emission at 460 nm, is pH-independent. Irradiation of the CON-4 switch results in photoisomerization to the keto form, which upon deprotonation strongly absorbs at 323 nm. Irradiation of the CON-4:Zn<sup>2+</sup> complex also results in the same process, which is accompanied by zinc release of switching off the 460 nm fluorescence. Boolean analysis of these processes result in quite complex logic circuits consisting of one AND, one OR, and two INH gates (Figure 54d).<sup>497</sup> Alternative assignment of the absorbance output (e.g., at 380 or 430 nm) should result in further complication of the logic structure of this device.

These logic devices (Figure 54), although relatively complex, have severe drawbacks as compared with the initial photonic chemical devices described by Raymo et al.<sup>142,144,490,491</sup> They do not support any chances of further development without redesigning the molecular structure of the switch. Therefore, more flexible systems are needed, which would allow the combination of numerous gates into large circuits without changes at the molecular level. The idea of cell array presented by Raymo<sup>144,493</sup> was further developed by Szaciłowski<sup>126</sup> in 2004.

A series of devices was based on one-, two-, and three-dimensional arrays of cells containing the nitroprusside-mercaptosuccinate switch.<sup>102</sup> Potassium concentration and pH was set as an input to each cell. The readout of the state was performed using low intensity green light (absorption mode) or high intensity green light (capable of inducing photochemical reaction of the [Fe(CN)<sub>5</sub>N(O)SR]<sup>3-</sup> complex).<sup>498,499</sup>

The simplest logic system with real data flow between logic gates can be achieved when two or more cells containing the switching system are placed in series, as was previously proposed by Raymo and co-workers.<sup>144,493</sup> The connection between logic gates can be realized using a light beam ( $\lambda = 520$  nm) passing through all of the cells in line. The simplest is the system containing two identical cells. Every cell in the set works as a single AND gate with [K<sup>+</sup>] and pH inputs and absorbance output. The set of the cells has low absorbance only when all the cells have low absorbance, i.e., when equilibrium (eq 15) is shifted to the left in all of them. High absorbance can be in turn achieved when in at least one cell the equilibrium is shifted to the right, which corresponds to OR operation on two outputs of AND gates (Figure 55a). As the logic state of any individual



**Figure 55.** Electronic equivalents of the logic devices based on the  $[\text{Fe}(\text{CN})_5\text{NO}]^{2-}$  switching system: one-dimensional (a and b), two-dimensional (c and d), and three-dimensional (e and f) optical networks working in absorption (a, c, and e) and in the photoreaction (b, d, and f) model. Basic sets of one OR and two AND gates are marked in red. Adapted from ref 126.

cell depends on two parameters (pH and  $[\text{K}^+]$ ), the set on  $n$  cells in series can simultaneously process  $2n$  bits of input data.

Photochemical reaction upon visible irradiation in the last cell in series occurs only when this cell is in the ON state, while all the preceding cells are in the OFF state. For the two-cell system, the Boolean analysis yields the circuit shown in Figure 55b.

Further complication of the system can be achieved by increasing the cell number and changing the geometry of the set of cells. The simplest two-dimensional system of this kind consists of four identical switching cells placed in four edges of the square. Four light sources and four detectors ensure easy information readout. Every cell responds to switching with pH and cation concentration, as in the previous case. Four independent outputs may be associated with light absorption in every row and column of the cell matrix. There are 256 different combinations (8 input bits,

$2^8 = 256$ ) of input parameters, and the system exists in  $2^4 = 16$  different states. If light absorption at 520 nm is assigned to be the output parameter, the system behaves like its electric equivalent shown in Figure 55c. On every edge of the square, light is absorbed if at least one of the cells is in the ON state. Four edges connecting four cells correspond to four 2-input AND gates (one gate for every cell in the system) and four OR gates (one gate for every edge of the square). Like in the previous case, photochemical reaction in the cell requires specific arrangement of ON and OFF cells, which is described as a circuit in Figure 55d. There is one cell in the system, which is not irradiated directly, but through other cells. The occurrence of photochemical reaction in this cell depends on two factors: (i) absorbance of the solution in this cell and (ii) absorption of the solutions in other cells. The cell in which photoreaction is to occur must be switched to the ON state, and other cells must be in the OFF state. It corresponds to the set of 5 logic gates connected as shown in Figure 55d. Any larger  $N \times N$  matrix can be described in the same way, with larger number of individual gates and more complicated network of connections.<sup>126</sup>

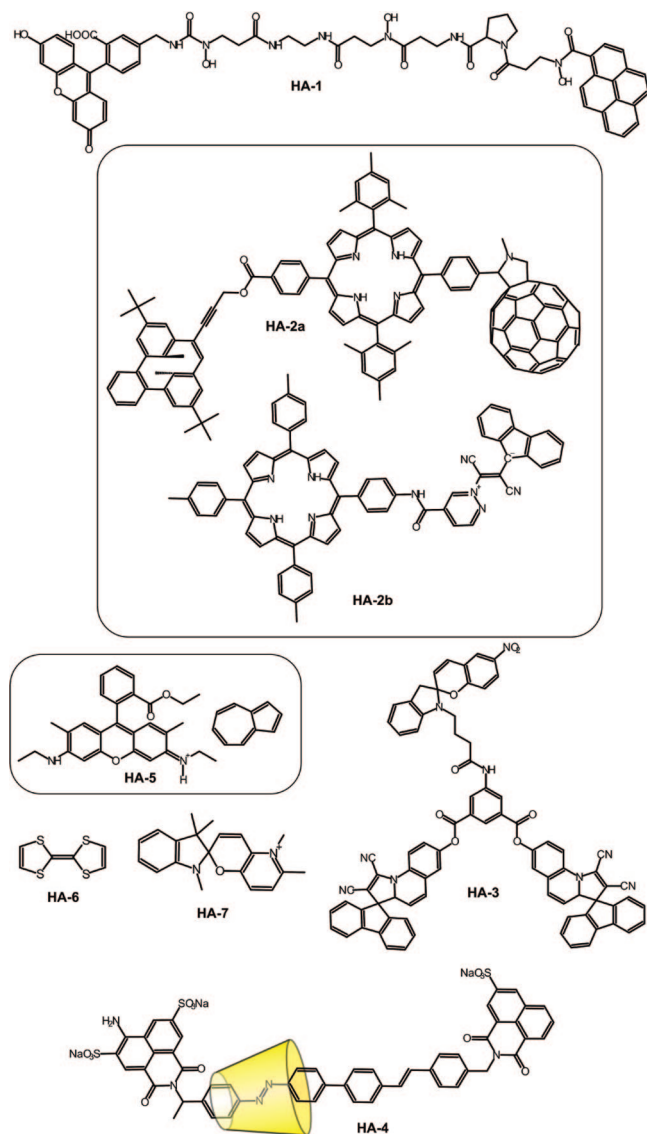
Maximal complexity of logic behavior can be achieved in the three-dimensional system. It consists of eight identical cells with switching compound placed at the corners of the cube, 12 light sources, and 12 detectors; light is guided along all 12 edges of the  $2 \times 2 \times 2$  cube. The system has 16 data inputs (8 cells with two inputs each) and 12 outputs (12 edges of the cube). Logic structure of this system is much more complicated, as compared with previous systems. There are  $2^{16} = 65536$  different combinations of input parameters, and 256 different sets of 12-bit outputs. Every edge of the cube, as in the previous case, works like a circuit containing two AND and one OR gate. The electronic equivalent of the system is shown in Figure 55e. The circuitry looks very complicated, but it is a set of simple components connected in parallel (cf. red elements in Figure 55c and e).

One cell in the cubic set cannot be irradiated directly, but the light beam must pass through other cells first. Photochemical reaction induced by visible light irradiation can occur only when this cell is in the ON state, and at least one of the cells on the common cube edges is in the OFF state. The electronic equivalent of this system is shown in Figure 55f. Three NAND gates correspond to three edges of the cube, which must be transparent at 520 nm (in OFF state) in order to enable light transmission to the ON cell (depicted in turn as the AND gate). The OR gate illustrates that only one transparent edge is enough to supply light to the ON cell. The last AND gate (at the output) checks if both conditions are fulfilled: the cell is illuminated and is in the ON state. Larger  $N \times N \times N$  arrays or other geometrical arrangements of the cells lead to increased complexity of logic operation that can be performed with the system, but the basic principles of the device remain unchanged.

## 7. Molecular Arithmetic Systems

Performance of arithmetic operation (addition, subtraction) requires the connection of several basic logic gates (cf. Table 2) into more complex circuits, namely, half-adder and half-subtractor (cf. Table 4). Depending on the size of binary representation of the numbers to add (or to subtract), the corresponding half-adders (or half-subtractors) must be connected in series and equipped with auxiliary gates to process the carry (or borrow) bits (cf Figure 8 and Table 5).<sup>1,2</sup>



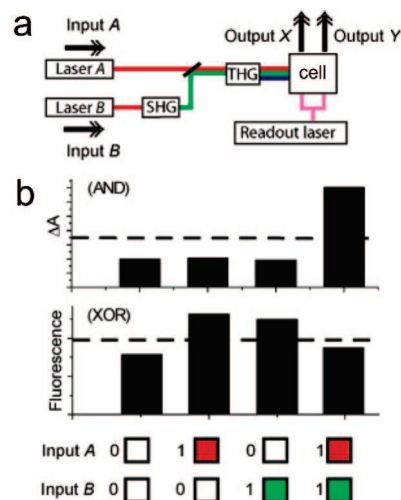


There are numerous molecular implementations of binary half-adders, half-subtractors, full adders, and full subtractors.<sup>500,501</sup> The most complex systems integrate both functions in a single molecular system and are called *molecularators* (molecular calculators).<sup>502</sup>

## 7.1. Molecular-Scale Half-Adders

### 7.1.1. Chemically Driven Molecular Half-Adders

The first molecular half-adder was reported by in 2000 A. P. de Silva.<sup>503,504</sup> The system was based on previously reported AND-3 and XOR-8 with quinoline moiety molecular logic gates mixed in one solution and operating on the same chemical inputs. The binary input numbers were encoded in  $[H^+]$  and  $[Ca^{2+}]$ , respectively. The AND gate operated in fluorescence mode, yielding high fluorescence intensity in the presence of both  $H^+$  and  $Ca^{2+}$ . The XOR gate, in turn, operated in transmittance mode, yielding high transmittance of violet light in the presence of acid or calcium ions. This molecular half-adder conceptually resembles the electronic equivalents: both molecular gates share the same inputs, and the outputs are independent. This system, however, cannot be further developed into full adder due to incompatibility of inputs and outputs.



**Figure 56.** Half-adder and molecule-based logic gates. The experimental setup of the half-adder (a) and the absorbance and fluorescence outputs (b). Reprinted from ref 506. Copyright 2004 American Chemical Society.

The only monomolecular chemically driven binary half-adder-like system was reported by Margulies et al. in 2004.<sup>505</sup> The HA-1 device is based on a modified bacterial siderophore equipped with two fluorophores: fluorescein and pyrene. The central siderophore unit has three hydroxamic groups and exhibits high affinity toward  $Fe^{3+}$  ions. Excitation of the HA-1 in its native form results in strong green emission from the fluorescein unit due to FRET from the pyrene moiety. Upon protonation, the blue emission from pyrene is observed. Iron binding completely quenches the fluorescence of both fluorophores due to efficient PET processes. Addition of ethylenediaminetetraacetic acid ( $H_4EDTA$ ) to the  $Fe^{III}$ -HA-1 complex protonates the fluorescein group and removes iron ions from the siderophore ligand. This results in exclusive emission from the pyrene moiety at 390 nm. Addition of a base, in turn, causes ionization of the fluorescein, but without the removal of iron so that a faint green emission is observed. Only when both inputs are present, namely, the solution is basic and the iron is removed, an intense green emission of the fluorescein at 525 nm can be observed. Consequently, by monitoring the emission signals at 525 nm, an AND logic gate is obtained.

The XOR gate can be mimicked in the same molecular systems using strong acid and a strong base as chemical inputs. Protonation of the  $Fe^{III}$ -HA-1 complex results in iron decomplexation, which results in blue pyrene emission being switched on. However, addition of base deprotonated the fluorescein unit and resulted in weak green emission. Therefore, if emission from the HA-1 molecule is considered, the system behaves as a XOR gate; addition of both acid and base results in fluorescence switching. The HA-1 system thus integrates the AND and XOR logic gates within a single molecule, but due to different input operation, these two gates cannot be regarded as fully functional molecular half-adders.

### 7.1.2. Optically Driven Molecular Half-Adders

The all-optical half-adder based on the mixture of two photochromic switches was reported by Andréasson et al.<sup>506</sup> The system consists of two Nd:YAG pulsed lasers, second harmonic generator (SHG), third harmonic generator (THG), a 650 nm-readout laser, and a cell containing the switching mixture (Figure 56a). This molecular system is based on two

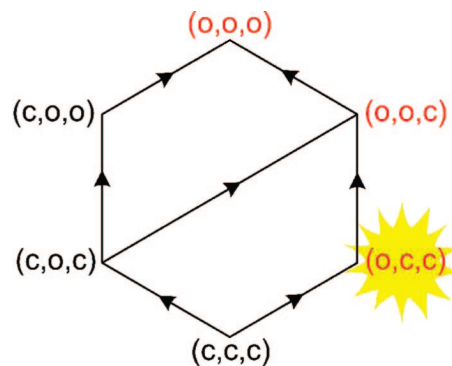
porphyrins equipped with photochromic units: the dihydropyrene–porphyrin–fullerene triad (HA-2a) and the porphyrin–dihydroindolizine dyad (HA-2b). The laser system may irradiate the cell at either 1064 nm (input A) or 532 nm via a second-harmonic generator (SHG, input B). When both inputs are on, the sample is irradiated with 355 nm light from the third-harmonic generator (THG). Outputs X (AND gate) and Y (XOR gate) are the transient absorbance of the fullerene radical anion and porphyrin fluorescence, respectively (Figure 56b).

The AND gate is based on the HA-2a switch. If the photochromic moiety is in the opened form (cyclophanedienene, CPD), excitation of the porphyrin moiety yields only the short-lived charge separated state  $\text{CPD-P}^+-\text{C}_{60}^-$ . Long-lived charge separated state  $\text{DHP}^+-\text{P-C}_{60}^-$ , characterized by strong absorption at 1000 nm (output of the AND gate), can be generated only from the closed form of the HA-2a. Photochemical closure of the CPD to the DHP moiety can proceed only upon UV irradiation, which is available when both lasers are on the third harmonic of Nd:YAG line is generated. Therefore, this system can be regarded as a photonic AND gate.

A porphyrin moiety linked to a photochromic dihydroindolizine (P-DHI dyad, HA-2b) acts as a photonic XOR gate. Excitation of the porphyrin moiety within the dyad in the closed form (cf. Figure 29a) results in strong fluorescence at 720 nm (output signal of the XOR gate). Irradiation of the closed form of the HA-2b switch with 355 nm-light (3rd harmonic) results in the formation of the opened betaine form (BT). In this situation, porphyrin excitation results in the charge separated state  $\text{P}^+-\text{BT}^-$ , which results in fluorescence quenching. BT can be transferred back to the DHI form upon visible (532 nm, second harmonic) or IR (1064 nm) irradiation. Therefore, the HA-2b molecule working in the laser system in Figure 56 behaves as a photonic XOR gate. Integration of the two molecular logic gates operating with the same photonic inputs and two different output channels results in the light-powered binary half-adder.<sup>506</sup>

A very similar laser setup was used to mimic the binary half-adder within a single molecule.<sup>507</sup> In this case, two input channels are set to the third harmonic of the Nd:YAG laser, 355 nm. The switching molecule HA-3 contains three photochromic moieties (one spiropyran and two dihydroindolizines) linked with the central benzene core. The thermally stable form of the switch has all three photochromic systems in colorless closed form. The spiropyran in its closed, thermally stable form may be photoisomerized with ultraviolet light (e.g., 355 nm) to an open merocyanine form, which closes back thermally. Each dihydroindolizine moiety also exists in a thermally stable closed form. Photoisomerization with ultraviolet light (e.g., 355 nm) produces an open, zwitterionic form that closes thermally. The HA-3 molecule can therefore exist in numerous forms, the stable  $[\text{c},\text{c},\text{c}]$  isomer and a series of thermally unstable, (partially) opened forms:  $[\text{c},\text{c},\text{o}]$ ,  $[\text{c},\text{o},\text{c}]$ ,  $[\text{o},\text{c},\text{c}]$ ,  $[\text{o},\text{o},\text{c}]$ ,  $[\text{o},\text{c},\text{o}]$ ,  $[\text{c},\text{o},\text{o}]$ , and  $[\text{o},\text{o},\text{o}]$ ; Figure 57. At ambient temperatures, the opened forms are thermally converted into the  $[\text{c},\text{c},\text{c}]$  form within minutes.

Merocyanine is the only fluorescent moiety within the system ( $\lambda_{\text{max}} = 659$  nm, output of the XOR gate). However, the betaine form absorbs the merocyanine emission and acts as an efficient quencher. Therefore, only the  $[\text{o},\text{c},\text{c}]$  isomer is fluorescent. Furthermore, only the forms  $[\text{o},\text{c},\text{c}]$ ,  $[\text{o},\text{o},\text{c}]$ ,



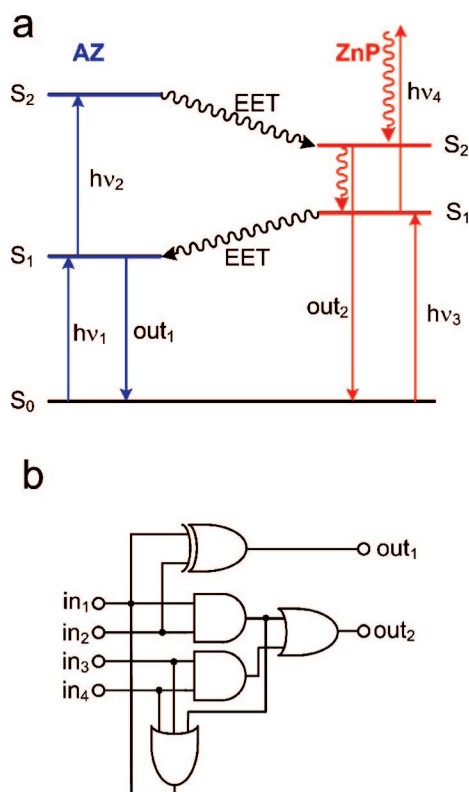
**Figure 57.** Graph of isomerization pathways for HA-2. Net photochemical isomerization under the influence of UV light occurs in the direction of the arrows. Thermal isomerization and photoisomerization promoted by visible light occurs in the opposite direction. Colored isomers are marked in red, and the only fluorescent isomer is marked in yellow. Adapted from ref 506.

$[\text{o},\text{c},\text{o}]$ , and  $[\text{o},\text{o},\text{o}]$  show characteristic merocyanine absorption at 579 nm (output of the AND gate).

Irradiation of the HA-3 generates all possible opened forms, the ratio of which depends on a subtle interplay of the rate of their population (thus the light flux) and the thermal recovery of the stable  $[\text{c},\text{c},\text{c}]$  form controlled by temperature and properties of the solvent. Irradiation at 355 nm leads to net isomerization in the direction of the arrows in Figure 57, whereas thermal reversion results in net isomerization in the opposite direction. In the dark, the entire population is in the  $[\text{c},\text{c},\text{c}]$  state, which is represented by a point at the bottom of the hexagon. Under UV irradiation, the center of the population distribution rises toward the top of the hexagon; at steady-state, the center of this distribution is determined by the equilibria between the thermal and photochemical reactions. Therefore, the maximal intensity of merocyanine absorption increases with increasing light flux, as the distribution of HA-3 forms approaches the top corner of the hexagon (Figure 57). In the laser system, this situation is obtained with two concomitant pulses from both lasers, which corresponds to AND operation. However, the fluorescence of the  $[\text{o},\text{c},\text{c}]$  form reaches its maximum at moderate light flux, which can be achieved only with the single laser pulse. Thus, fluorescence output can be associated with XOR function. As in the previous case, integration of AND and XOR gates in one system (here also in one molecule) results in the photonic half-adder.<sup>506</sup>

Another optically controlled binary half-adder was reported by Tian and co-workers.<sup>508</sup> The system is based on [2]rotaxane HA-4. The thread of this rotaxane contains two photoswitchable moieties, azobenzene and stilbene; both ends are terminated with fluorescent reporters, 4-amino-1,8-naphthalimide-3,6-disulfonate ( $\lambda_{\text{em}} = 520$  nm) and 1,8-naphthalimide-5-sulfonate ( $\lambda_{\text{em}} = 395$  nm), respectively. In the thermally stable  $[\text{E}_{\text{N}=\text{N}}, \text{E}_{\text{C}=\text{C}}]$  isomer, the cyclodextrine macrocycle can freely move along the thread; this isomer is weakly emissive (at both fluorophores) due to vibrational and rotational energy dissipation by methylene spacers. The  $[\text{Z}_{\text{N}=\text{N}}, \text{Z}_{\text{C}=\text{C}}]$  isomer is an even weaker emitter, and the macrocycle resides trapped between the azobenzene and stilbene moieties (cf. Figure 22).

Two photoswitchable units of the HA-4 switch can be selectively addressed: photoisomerization of stilbene to the Z isomer proceeds at 313 nm (back reaction at 280 nm), while the azobenzene moiety is isomerized on irradiation at 380 nm (back reaction at 450 nm). Thermal equilibration in



**Figure 58.** Energy diagram for azulene-zinc porphyrin molecular half-adder (a) and corresponding electronic circuit (b).

darkness also yields the  $[E_{N=N}, E_{C=C}]$  form. In the  $[E_{N=N}, Z_{C=C}]$ , the cyclodextrin macrocycle resides at the *E*-azobenzene moiety, and the fluorescence intensity of the neighboring fluorophore (green emitter) is strongly enhanced. Vice versa, upon isomerization to the  $[Z_{N=N}, E_{C=C}]$  isomer, the  $\alpha$ -CD ring resides at the stilbene unit, and therefore, the luminescence of the blue emitter is enhanced. If fluorescence intensity is considered as an output channel, the HA-4 molecule behaves as a XOR gate: the  $[E_{N=N}, Z_{C=C}]$  and  $[Z_{N=N}, E_{C=C}]$  isomers are strongly luminescent, while the  $[E_{N=N}, E_{C=C}]$  and  $[E_{N=N}, Z_{C=C}]$  ones emit only weakly. Furthermore, photoisomerization of both units are associated with absorbance changes. The strongest change is observed during concomitant reaction at both centers; therefore, the absorbance channel produces the AND gate.<sup>508</sup>

The photochemically driven multistate [2]rotaxane HA-4 mimics a half-adder with distinct AND and XOR logic gates. The device is reversible and can then be reset with light or heat such that the half-adder can be operated repeatedly. Furthermore, the logic output of the four-state device can be further complicated by discrimination of absorption and emission wavelengths.

A very different approach to molecular computing was reported by Yeow and Steer.<sup>509</sup> The molecular device is composed from two molecules: zinc porphyrin and azulene (HA-5). The operation of this device is based on Förster energy transfer between the two components of the device. Azulene (AZ, Figure 58a) can be pumped to the luminescent excited state ( $S_1$ ) by absorption of a photon with  $\nu_1 \geq 14400 \text{ cm}^{-1}$ . The luminescence of this state is considered as the  $out_1$  output of the device. Absorption of a second photon from the other source ( $\nu_2 \geq 13900 \text{ cm}^{-1}$ ) produces the  $S_2$  excited state. The  $S_2$  state of azulene is an efficient energy donor and transfers electronic energy to the acceptor molecule, in this case to the  $S_2$  state of zinc porphyrin. This

state is luminescent and therefore can be also considered as an output ( $out_2$ ) of the device. Luminescence of azulene ( $11000\text{--}13400 \text{ cm}^{-1}$ ) is observed only upon absorption of one photon ( $h\nu_1$  or  $h\nu_2$ ), while luminescence of porphyrin is observed only upon two-photon excitation of azulene. Therefore, the azulene luminescence can be assigned the XOR function, while the porphyrin luminescence the AND function. Combination of XOR and AND in one molecular system results in the all-optical binary half-adder.

There is, however, a further complication to the logic structure of this device. Not only azulene but also porphyrin can be selectively excited to the  $S_1$  and  $S_2$  states by absorption of one ( $\nu_3$ ) or two ( $\nu_3 + \nu_4$ ) photons of  $\nu \geq 18000 \text{ cm}^{-1}$ , respectively. The  $S_2$  state is luminescent, and its emission is regarded as the  $out_2$  output, while the  $S_1$  state can transfer electronic energy to the azulene molecule, thus producing the azulene  $S_1$  emission. This results in additional gates connected with the half-adder (Figure 58b).

The electronic energy transfer to porphyrin serves as a tool for the detection of the  $S_2$  state of azulene. In principle, any aromatic molecule with easily accessible (and detectable)  $S_1$  and  $S_2$  excited states (cf. Figure 58a) can act as binary half-adder provided that the two excited states can be spectroscopically detected.<sup>510</sup>

### 7.1.3. Mixed Signal Molecular Half-Adders

Implementation of arithmetic function to molecular systems may require the combination of various input signals, e.g., chemical and electrochemical, or chemical and optical. Two examples of such systems are discussed below.

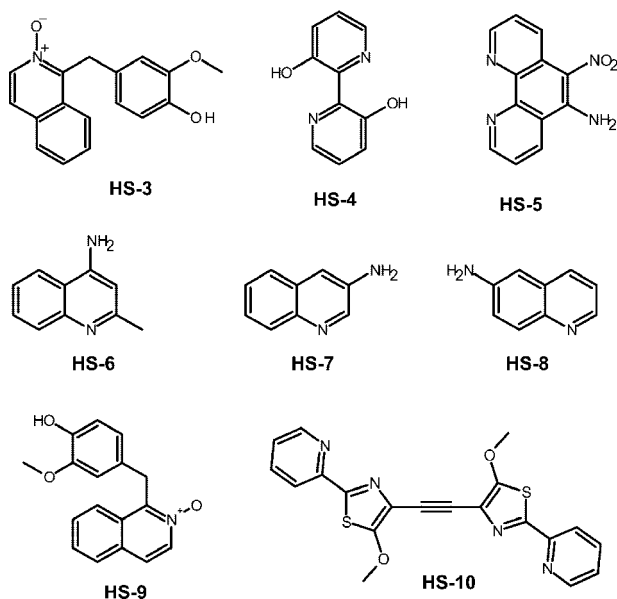
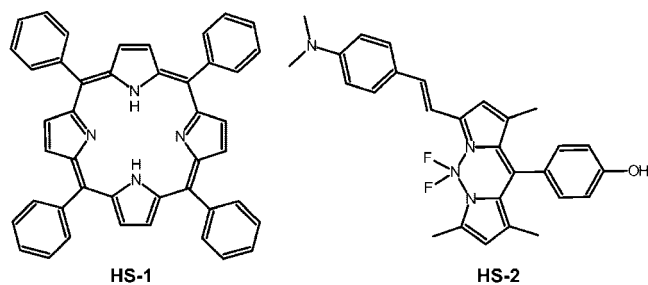
The redox-driven half-adder based on tetrathiafulvalene (HA-6) was reported recently by Zhu et al.<sup>511</sup> The device is based on spectral differenced between TTF and its partially ( $TTF^{+}$ ) and fully oxidized ( $TTF^{2+}$ ) forms. TTF can be oxidized to the cation radical electrochemically (in acetonitrile at +0.65 V vs Ag/AgCl) or by the addition of 1 equivalent of a strong one-electron oxidant, e.g., NOPF<sub>6</sub>. This reaction is accompanied by the formation of an intense absorption band at 435 nm. Further chemical oxidation with another equivalent of NOPF<sub>6</sub> yields the dication characterized by strong absorption at 350 nm (and weak at 435 nm). The same effect can be produced when electrochemically generated radical is reacted with one equivalent of oxidant. Therefore, two inputs of the half-adder are one-electron electrochemical oxidation and one-electron chemical oxidation. Absorbance of the cation radical can be regarded as the XOR gate output and the absorbance of the dication as the AND output. Altogether, the redox-driven binary half-adder is achieved, and its output can be read as absorbance at two different wavelengths.

A molecular binary half-adder based on photochromic ligand HA-7 was reported by Zhu et al.<sup>512</sup> On irradiation with UV light (365 nm), the spirocyanine undergoes ring opening, yielding the colored merocyanine form ( $\lambda_{\text{max}} = 590 \text{ nm}$ ). It can further react with the  $Fe^{3+}$  ions yielding a stable complex characterized by strong absorption at 430 nm. The HA-6 reacts also with  $Fe^{3+}$  in the SP form: the reaction yields the colored cation radical characterized by strong absorption at 500 nm. Absorption at 430 nm thus corresponds to the AND operation with UV light and  $Fe^{3+}$  as arguments, while the absorbance at 550 nm (halfway between the ME and SP cation radical) absorption bands corresponds to the XOR function of the same input data.

## 7.2. Molecular-Scale Half-Subtractors

Molecular implementation of the binary half-subtractor is much more difficult than any of the logic devices discussed so far. There are several molecular half-subtractors reported so far, but some additional tricks have been used to achieve the desired operation, e.g., one input was read in positive, while the other in negative logic. Interestingly, both devices use acids and bases as input signals.

The first binary molecular half-subtractor ever reported comes from the laboratory of S. J. Langford (HS-1).<sup>513</sup> The operation of the device is based on bathochromic shift of the Soret band of tetraphenylporphyrin (H<sub>2</sub>TPP) and changes in energy and intensity of the emission bands on protonation and deprotonation. The Soret band of H<sub>2</sub>TPP is localized at 417 nm; after protonation (H<sub>4</sub>TPP<sup>2+</sup>), it shifts to ~440 nm, and in the presence of strong base (e.g., *t*-BuOK), the TPP<sup>2-</sup> dianion exhibiting a strong band at ~430 nm is formed. Furthermore, only protonated and deprotonated forms are strongly luminescent as compared with the neutral, weakly emitting form (H<sub>2</sub>P). The H<sub>4</sub>TPP<sup>2+</sup> cation emits at 405 nm, while the TPP<sup>2-</sup> dianion at 440 nm. Strong visible absorption at  $\lambda > 425$  nm is observed when one of the inputs is present (i.e., either acid or base); therefore, it corresponds to XOR function. Strong emission at selected wavelength (405 or 440 nm) is present only in the presence of one particular stimuli (acid or base, respectively), therefore luminescence output presents the INHIBIT function. Integration of XOR and INH within one molecule with the same inputs and different output channels results in the molecular scale binary half-subtractor.



The HS-2 molecular device also takes acid and base as input, and the outputs are both in fluorescence channels at different wavelengths.<sup>514</sup> The luminescence of the BDPY central unit is controlled by two processes: PET from the phenol moiety and ICT involving the dimethylaniline moiety. Deprotonation of the phenol moiety results in complete quenching of the fluorescence. However, protonation of the amino group results in a strong hypsochromic shift (from 660 to 565 nm). Emission at 565 nm can be thus regarded as an output of the INH gate, while emission at 660 nm corresponds to XNOR function. Application of positive logic to the INH output and negative logic to the XNOR output results in binary half-subtractor.

The same set of input signals is used in the HS-3 device.<sup>515</sup> The isoquinoline *N*-oxide is characterized by unstructured S<sub>1</sub> fluorescence at 400 nm. Upon protonation the acceptor character of the isoquinoline moiety is enhanced, and fluorescence from the charge transfer excited state can be observed at 491 nm ( $\lambda_{\text{ex}} > 360$  nm, output 1). Furthermore, the S<sub>1</sub> emission shifts hypsochromically to 380 nm (output 2). Deprotonation of the HS-3 molecule, in turn, results in enhanced donor properties of the phenolate, which also switches on the charge transfer emission at 497 nm. Thus, output 1 (S<sub>1</sub> emission from protonated isoquinoline *N*-oxide) corresponds to the INH function and output 2 (charge transfer emission) to the XOR function.

An even simpler switching pattern, but also resulting in implementation of binary half-subtractor, is observed in the case of HS-4.<sup>516</sup> The neutral form of 2,2'-bipyridyl-3,3'-diol is only weakly luminescent. Protonation results in strong luminescence at 494 nm, while the deprotonated form fluoresces at 453 nm. Both emission spectra are broad and show identical intensity at 453 nm (output 1). Emission spectrum of the protonated form extends toward red, and the emission at 500 nm can be taken as the second output. Emission at 453 nm is thus observed for both protonated and deprotonated forms, while the signal at 500 nm is characteristic only for the protonated one. Therefore, the first output can be associated with the XOR gate, while the second with the INH gate; therefore, the HS-4 molecule acts as a binary half-subtractor operating on H<sup>+</sup> and OH<sup>-</sup> inputs.

Simple quinoline derivatives (HS-5, HS-6, HS-7, and HS-8) are also good models of half-subtractors operating with acid and base inputs.<sup>517</sup> Each of these compounds has two protonation sites: the arylamine group and the heterocycle nitrogen atom of very different pK<sub>a</sub> values. Thus, in solutions of variable acidity they can exist as neutral molecules, monocations, and dications. Neutral species are only weakly fluorescent (HS-5 is an exception), and protonation induces strong ICT fluorescence involving the arylamine group as a donor and the protonated heterocyclic group as an acceptor. In the case of doubly protonated forms, the homocyclic ring acts as a donor and the heterocyclic ring as an acceptor. This results in a red shift of the emission line upon the second protonation step. Application of the input/output assignment similar to that applied in the previous case (HS-4) results in half-subtractor behavior.<sup>517</sup> Isoquinoline *N*-oxide (HS-9) is an example of the application of multiple fluorescent states for information processing.<sup>518</sup> Depending on the acidity of the solution, it exists in neutral, cationic, and anionic forms. Independent of acidity, excitation

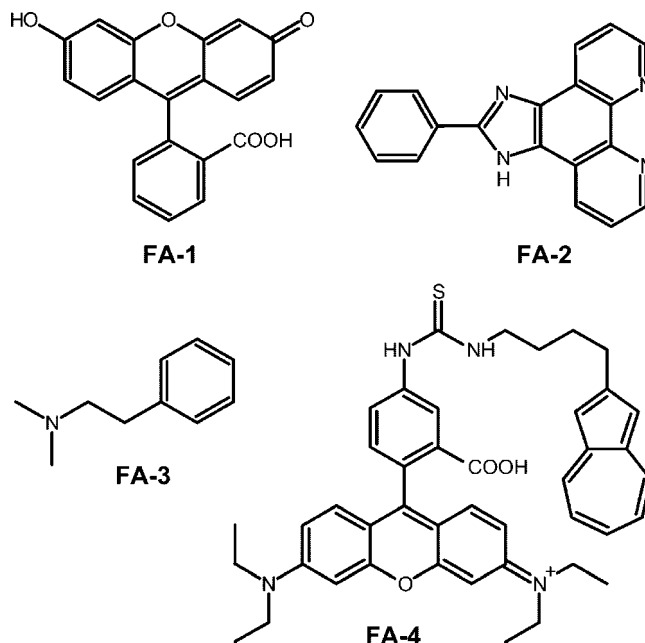
at 330 nm results in the generation of the locally excited (LE) state of isoquinoline. This singlet state emits at 400 nm for the neutral and anionic form, and protonation of the N-oxide moiety results in a small hypsochromic shift (380 nm). Furthermore, low energy excitation ( $>360$  nm) may lead to the ICT excited state as the N-oxide is an acceptor, and electron rich methoxyphenol is an electron donor. Their relative donor and acceptor properties are easily modulated with protonation–deprotonation. Protonated N-oxide is a better acceptor than the neutral one, and phenolate is a better donor than phenol. Therefore, ICT emission at 500 nm can be observed only for cationic and anionic forms of HS-9, while the neutral form shows only LE fluorescence. Blue shifted LE emission is observed only in acidic solutions (INH gate) and ICT emission in acidic or basic but not in neutral solutions. Therefore, if the 380 and 500 nm emissions are considered as outputs and acid and base additions as the inputs, the systems mimicks the binary half-subtractor.

The same inputs are applied to control the HS-10 device reported recently by Yan and co-workers.<sup>519</sup> The fluorescent HS-10 molecule emits at 450 nm excitation, and the dinuclear copper(II) complex is, however, nonluminescent. On addition of acid one copper ion is released, and the luminescent (475 nm)  $\text{CuH}(\text{HA-10})^{3+}$  complex is formed. Further acidification results in the formation of  $\text{H}_2(\text{HA-10})^{2+}$  characterized by 550 nm emission. Addition of a strong base to the starting complex liberated the free ligand, and fluorescence at 450 nm is restored. Therefore, the 475 nm luminescence (present both upon addition of acid and base) can be regarded as an output of the XOR gate and the 550 nm emission (present only in acidic solutions) as an output of the INH gate.

### 7.3. Molecular-Scale Full Adders and Full Subtractors: Toward Arithmetical Processors

The highest complexity of arithmetic operations is achieved in binary full adders and full subtractors. These devices require three input signals and as a result of computation yield two output bits (cf. Figure 8). There are several devices of that kind described in the chemical literature, and the most complex ones include full adder and full subtractor integrated within the same molecular system and sharing the same input data. In most of the cases, various chemical stimuli (acids, bases) are taken as input data, while the output usually involves changes in spectral properties of the molecular computing system. Some other molecular arithmetic systems are based on multiphoton excitation to higher excited states.

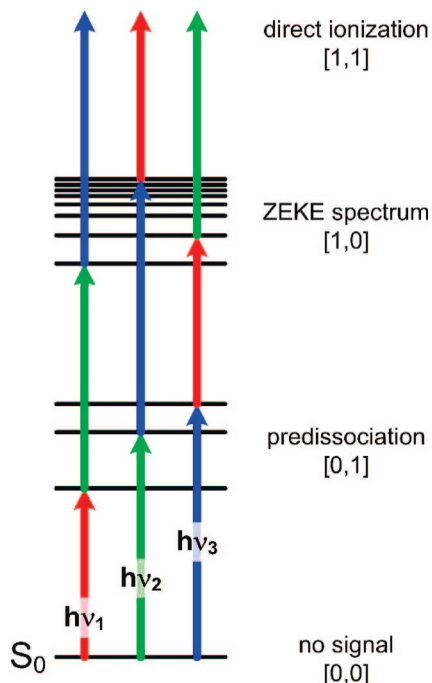
The first complex molecular arithmetic system, integrating full adder and full subtractor within the same molecular system was reported by D. Margulies et al.<sup>502</sup> It is based on a simple, commercially available fluorescent indicator fluorescein (FA-1) and used acids and bases as input signals, while changes in absorbance, transmittance, and fluorescence are used as outputs. Protonation and deprotonation of fluorescein results in changes in its absorption spectrum. Two analytical wavelengths are selected: 447 and 474 nm. The first one is characteristic for both monocation and monoanion of fluorescein, while the second is high only for the monoanion and dianion. The neutral form of fluorescein shows only weak absorption at both analytical wavelengths.



In order to achieve full adder based on fluorescein, the transmittance at 447 nm is assigned to the sum output, while absorbance at 474 nm as carry output. Operation of full adder starts from the monocationic form of FA-1; it corresponds to [0,0,0] set of inputs, and this state is characterized by low transmittance at 447 and low absorption at 474 nm, i.e., it returns the  $[s = 0, c = 0]$  output (i.e.,  $0 + 0 + 0 = 0$ ). Addition of one equivalent of strong base yields the neutral form, which shows low absorbance at both analytical wavelengths (hence high transmittance at 447 nm), which corresponds to the  $[s = 1, c = 0]$  output state (i.e.,  $0 + 0 + 1 = 1$ ). Addition of the second equivalent of the base yields the monoanionic form, characterized by low transmittance at 447 and high absorbance at 474 nm, thus corresponding to the  $[s = 0, c = 1]$  state, i.e.,  $0 + 1 + 1 = 2$ . Introduction of a third  $\text{OH}^-$  input yields the dianion, which show high transmittance at 447 and high absorbance at 474 nm, which corresponds to the  $[s = 1, c = 1]$  state, i.e., the  $1 + 1 + 1 = 3$  operation is performed.

The same chemical systems can also operate as binary full adder. The same analytical wavelengths are used for modeling the full subtractor, but only absorbancies are used as outputs, while both acid and base are used as chemical inputs. The neutral form of fluorescein is set as the initial form corresponding to the [0,0,0] input. The acid input is assigned to the minuend while the base input to the subtrahend and the pay-back values (cf. Figure 8 and Table 4).

Another system based on the same principle was reported by Liu et al.<sup>520</sup> The FA-2 switch operated with acid and base inputs and integrates three devices within one molecule: half-adder, half-subtractor, and comparator. Furthermore, due to the presence of four spectrally different forms (anion, neutral, cation dication) of the FA-2 compound, it is possible to implement binary full adder and full subtractor within this molecule. This problem, however, was not addressed so far in the FA-2 molecular device. Furthermore, this device is the only known example of a molecular binary comparator (cf. Table 3 and Figure 8). Neutral FA-2 upon 335 nm-excitation emits blue fluorescence (423 nm). Application of no inputs ( $x = 0, y = 0$ ) or both acid and base ( $x = 1, y = 1$ ) yields the equality bit of 1 and majority bit of 0 (cf. Table 3 and Figure 8). Addition of strong base results in the

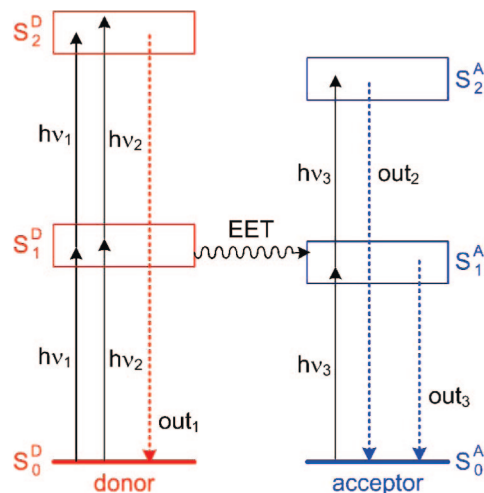


**Figure 59.** Photophysical implementation of a binary full adder. Numbers in brackets indicate carry and sum bits, respectively. Adapted from refs 521 and 522.

formation of the anionic form of FA-2, which is nonfluorescent (equality 0, majority 0), while upon addition of acid green fluorescence of monocation at 513 nm is observed (majority bit set to 1).

All these chemically driven molecular devices require sequential addition of chemicals to perform calculations and to reset the device to the initial state. This is not the most convenient way of computing; therefore, although very interesting, they have no practical significance. Furthermore, the rate of their operation is limited to the time of mixing and recording absorption or emission spectra. Much more promising are systems based on multiphoton photophysical processes in higher excited states. By definition, these processes are very fast and reversible, but unfortunately, their operation requires a lot of energy to provide sufficiently high light flux to achieve multiphoton absorptions. Furthermore, they do not yield output into two channels but to three, and they are assigned to [0,1], [1,0], and [1,1] two-bit states. The simplest molecule on which a binary full adder can be based on is nitric oxide.<sup>521,522</sup> Energies of photons must be tuned to reach low electronic excited states with one photon, near the ionization edge with two photons, and finally induce ionization of a molecule with three photons (Figure 59). Recently, a full adder based on the FA-3 molecule excited with UV and visible photons was reported.<sup>510</sup> Fluorescence ([0,1]), ionization of the amine ([1,0]) group or aromatic moiety ([1,1]) were defined as output signals. These systems are capable of very rapid operation, but disadvantageously molecules are destroyed during the operation of this full adder, and it cannot be reverted to the initial state.

This problem was recently solved by Speiser et al.<sup>523</sup> The bichromophoric system, the rhodamine-azulene conjugate (FA-4), enables the reversible all-optical binary calculation (Figure 60). Excitation of the rhodamine moiety (energy donor) with either  $h\nu_1$  or  $h\nu_2$  photons results in the  $S_1$  excited state, which can efficiently transfer electronic energy to the azulene moiety, which then generates the  $out_3$  signal (sum). The same can be recorded with direct azulene excitation with



**Figure 60.** Photophysical diagram of an all-optical binary full adder based on the rhodamine-azulene conjugate. Adapted from ref 523.

$h\nu_3$  photons (carry in). The second  $h\nu_3$  photon (or concomitant excitation of rhodamine with either  $h\nu_1$  or  $h\nu_2$ ) results in  $S_2$  emission of azulene ( $out_2$ , carry out). Also, concomitant application of  $h\nu_1$  and  $h\nu_2$  photons results in the generation of carry output ( $S_2$  luminescence of rhodamine fragment,  $out_1$ ). This system represents the first molecular, all-optical arithmetic system, which works reversibly. The XOR operations are based on one- versus two-photon excitations of two chromophoric moieties, while communication between individual gates is based on intramolecular electronic energy transfer.

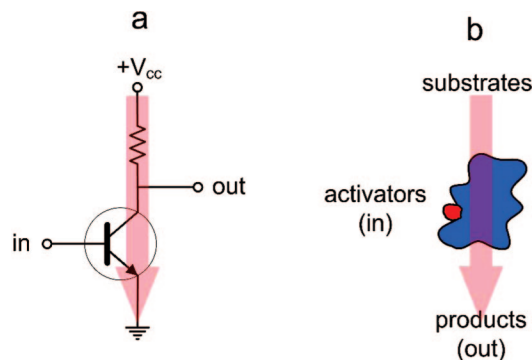
## 8. Logic Devices Based on Biomolecules and Biosystems

Processing of information is one of the most crucial processes in all of the living organisms. It regards not only advanced processes in nervous systems of higher animals, but also a plethora of biomolecular processes involving proteins and nucleic acids. Boolean processes can be observed at all levels of abstraction: large populations of organisms, single organisms, organs, tissues, cells, intracellular structures, and molecules.<sup>120,524–527</sup> Proteins can act as signal receptors, logical gates, or signal transducers between different forms of signaling, including light, electricity, and chemical messenger systems. Nucleic acids mainly act as memory, both for permanent and for short-term applications, although the self-splicing activity of certain RNA molecules means that they can perform information processing as well (see section 8.1).<sup>528</sup>

Diverse and complex chemistry of biomolecules allows the construction of artificial logic systems of unprecedented complexity (cf section 8.3), capable of solving various nontrivial problems.

### 8.1. Boolean Processes in Natural Biosystems

The most important biomolecular processes usually associated with Boolean logic are expression of genes and signal transduction. The latter is not a Boolean process per se, but the mutual interaction of various signals or the choice of signaling pathway is best described by Boolean functions. Even most of the enzymatic reactions can be described in terms of Boolean logic, and electronic equivalents of these processes can be easily found. The



**Figure 61.** Functional analogy between the bipolar transistor (a) and enzyme transistor (b). The current flowing through transistors is a function of gate potential (in), while the rate of product formation is a function of activator concentration. Adapted from ref 526.

basic electronic switching device (a transistor) is easily mimicked by an enzyme converting a substrate into a product in the presence of an activating molecule (Figure 61).<sup>526</sup>

The simplest case of natural logic systems is connected with the control of gene expression. In order to translate DNA into mRNA and hence induce protein synthesis, RNA polymerase must attach to the DNA strand at the promoter site and the repressor site of the DNA must be unoccupied (Figure 62a). Binding of repressor protein to the repressor site inhibits the translation process, and no protein synthesis associated with the output gene is observed (Figure 62b). In the case of more repressor sites within the promoter region, more complex logic functions may be observed (e.g., NOR, Figure 62c).<sup>529</sup> The presence of sites that upon ligation may facilitate binding of RNA polymerase results in higher complexity of the logic response.<sup>530–534</sup>

RNA itself is also capable of performing logic operations, and the so-called riboswitches are crucial elements of the regulatory system of cellular metabolism. The recently discovered RNA-based receptor of glycine can in a concentration-dependent manner switch the cellular metabolism between anabolic (at low concentration) and catabolic (at high concentration) utilization of glycine by bacteria.<sup>535,536</sup>

Signal transduction pathways are governed by processes that are not Boolean in nature, but can be easily described by a series of logic gates (Figure 63).<sup>537,538</sup> These Boolean networks are well accepted models for the description of cellular signaling, especially in the nervous system.<sup>538</sup> Simple gates such as AND and OR are used to describe synergistic and redundant signaling, respectively, while more complex transduction schemes, such as adverse effects, one way suppression, or mutual suppression, require more complex model logic circuits (Figure 63).<sup>537</sup>

## 8.2. Protein-Based Molecular Logic Systems and Devices

Only a few binary logic devices based on proteins are described so far. These devices utilize two different phenomena: changes in the structure of the protein itself or changes in pathways of enzyme-catalyzed reaction.

The first approach to protein-based logic devices was applied by Aida and co-workers.<sup>539</sup> The device is based on the genetically engineered GroEL chaperone protein, with cysteine side chains modified with azobenzene moieties. Under natural conditions, the GroEL chaperone binds de-

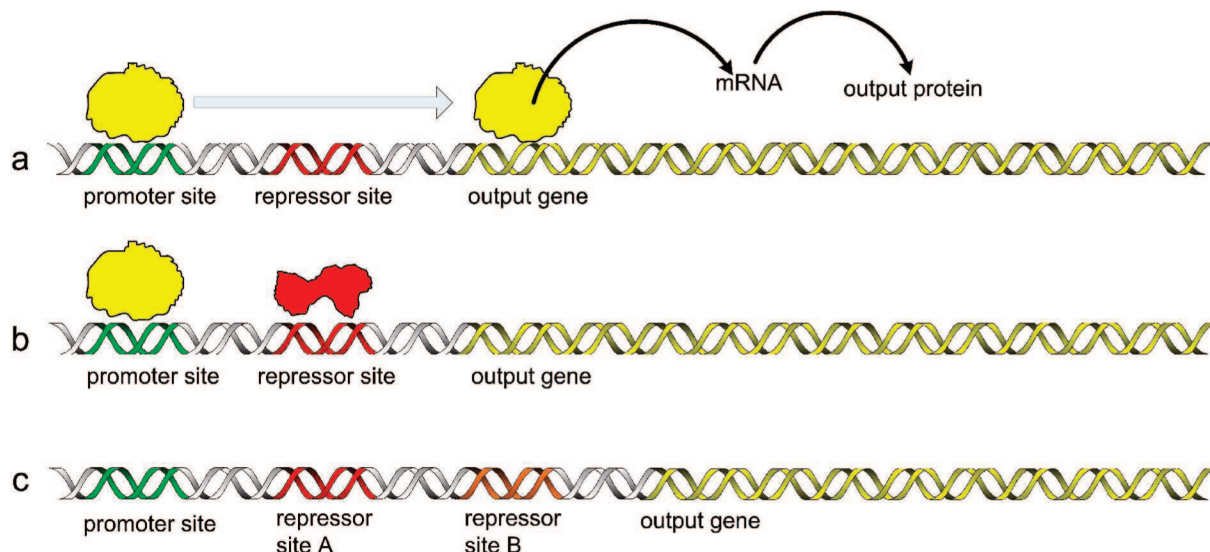
natural proteins inside the cavity and assists their refolding into native forms.<sup>540,541</sup> ATP and GroES capping protein trigger the opening of the GroEL and release of the refolded protein. Therefore, this system can be regarded as an AND logic gate with GroES and ATP as inputs and refolding activity toward denatured proteins as an output. On the basis of that scheme, a semiartificial protein-based device was developed. Photoisomerization of azobenzene moieties is equivalent to binding and releasing of capping protein as it results in closure (*trans*) and opening (*cis*) of the protein cavity (Figure 64). Interaction of ATP is identical in the case of both the native and engineered proteins. When the azo-GroEL protein is reacted with denatured green fluorescent protein (GFP), the fluorescence of GFP is recovered only upon photoisomerization of azobenzene units to *cis* isomer in the presence of ATP, while in the absence of light and ATP, the engineered GroEL prevents GFP refolding. This device is not only a molecular logic gate, but can be also regarded as the molecular-level machine.<sup>539</sup>

Much more versatile logic schemes can be achieved when various enzymatic reaction pathways are considered. The simplest one-input logic gates (YES and NOT) can be easily mimicked with glucose oxidase (GOx) and formaldehyde dehydrogenase (FDH), respectively (Figure 65).<sup>542</sup> The biocatalytic YES gate produces high output signal (gluconic acid) only when glucose is supplied (Figure 65a). The implementation of a NOT gate is more complex. Formaldehyde dehydrogenase is inhibited by hydrogen peroxide. Therefore, in the absence of  $H_2O_2$  (low input), formaldehyde and  $NAD^+$  are converted to formic acid and NADH (high output). Addition of  $H_2O_2$  to the reaction mixture (high input) prevents the production of NADH (low output, Figure 65b).

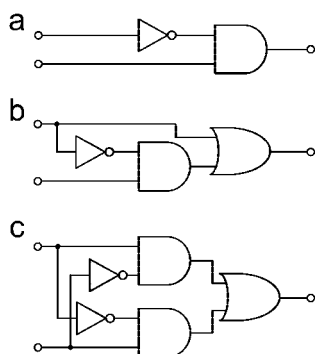
Coupling of two enzymes into catalytic cycles resulted in biochemical mimicking of two-input logic gates (Figure 66).<sup>542,543</sup> The AND gate was implemented in the system composed of two enzymes: catalase (Cat) and glucose oxidase (GOx) under anaerobic atmosphere. The catalase-mediated transformation of input 2 yielded molecular oxygen that was consumed by GOx, catalyzing the oxidation of input 1, glucose, to gluconic acid. The gluconic acid product corresponded to the output (Figure 66a).<sup>542</sup>

Biocatalytic mimicking of the OR gate was more difficult and required the utilization of the modulus of the NADH absorbance change (at 340 nm) as the output. The biocatalytic cycle was composed of two enzymes: GOx and horseradish peroxidase (HRP) and the cofactor NADH (Figure 66b). Upon addition of glucose to the system (input 1), GOx yielded  $H_2O_2$  that was subsequently consumed by HRP with concomitant oxidation of NADH to  $NAD^+$ , resulting in the depletion of NADH and an absorbance change. Upon addition of  $H_2O_2$  (input 2), either in the presence or absence of glucose, the same oxidation of NADH to  $NAD^+$  proceeded, thus resulting in overall OR response.<sup>542</sup>

A very similar approach was applied to the implementation of the XOR gate. The system contains two enzymes: GDH and HRP in the presence of equal amounts of NADH and  $NAD^+$  (Figure 66c).<sup>542</sup> As in the previous case, the output signal is assigned to the absolute value of the variation of NADH absorbance at 340 nm. The highest variations of the NADH concentration are observed in the presence of glucose (input 1) and in the absence of  $H_2O_2$  (input 2), or in the presence of  $H_2O_2$  and in the absence of glucose. Other combinations of input data result in rather constant absorbance at 340 nm. Therefore, this biocatalytic system is



**Figure 62.** DNA expression based logic gates: NOT (a and b) and NOR (c). See text for details. Adapted from ref 529.

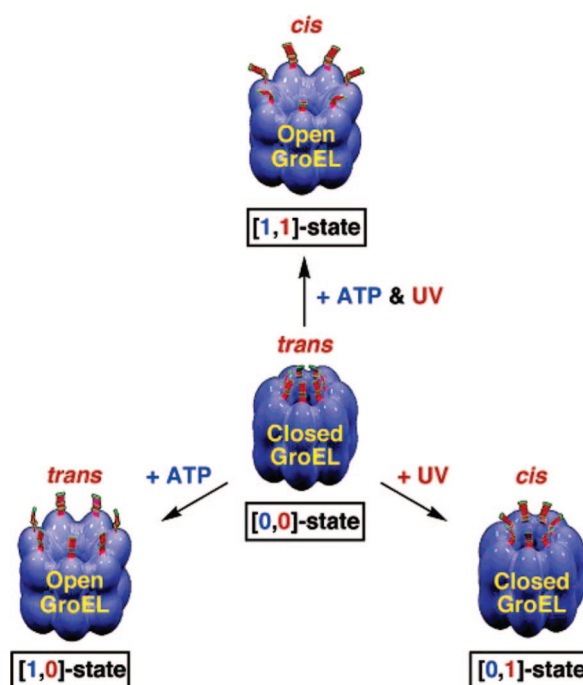


**Figure 63.** Three basic logic circuits used for the description of alternative signaling pathways: adverse effects (a), one-way suppression (b), and mutual suppression (c). Adapted from ref 537.

regarded as a XOR logic gate. The same enzymatic system can also mimic the AND logic gate in the initial absence of  $\text{NAD}^+$  and with gluconic acid as an output (Figure 66c, output 2).<sup>543</sup>

Further complication of biochemical logic systems was achieved in a coupled four-enzyme system reported by Willner and co-workers.<sup>544</sup> The system is constructed from four enzymes: acetylcholine esterase (AChE), choline oxidase (ChOx), microperoxidase-11 (MP-11), and glucose dehydrogenase (GDH) (Figure 67). Information is fed to the system by four different chemical stimuli, which are substrates for these enzymes: acetylcholine (input A), butyrylcholine (input B), molecular oxygen (input C), and glucose (input D). The operation of the logic system is read out by following the NADH concentration changes on the basis of the absorbance at 340 nm. Acetylcholine (input A) or butyrylcholine (input B) are hydrolyzed by AChE to form choline that acts as the output of the first OR gate. Choline generated by the OR gate and  $\text{O}_2$  (input C) activate the AND gate that yields betaine aldehyde and  $\text{H}_2\text{O}_2$  as products. Two enzymes MP-11 and GDH perform the XOR operation on the product of the AND gate ( $\text{H}_2\text{O}_2$ ) and glucose (input D).<sup>544</sup>

The most advanced artificial logic protein-based device, binary half-adder, was reported by Willner et al. in 2006.<sup>545</sup> This biocatalytic system comprises a combination of two enzyme-based logic gates: AND and XOR. The AND gate is based on the GOx-Cat enzyme pair (vide supra) and the XOR gate on the GDH-HRP pair (Figure 68). The inputs

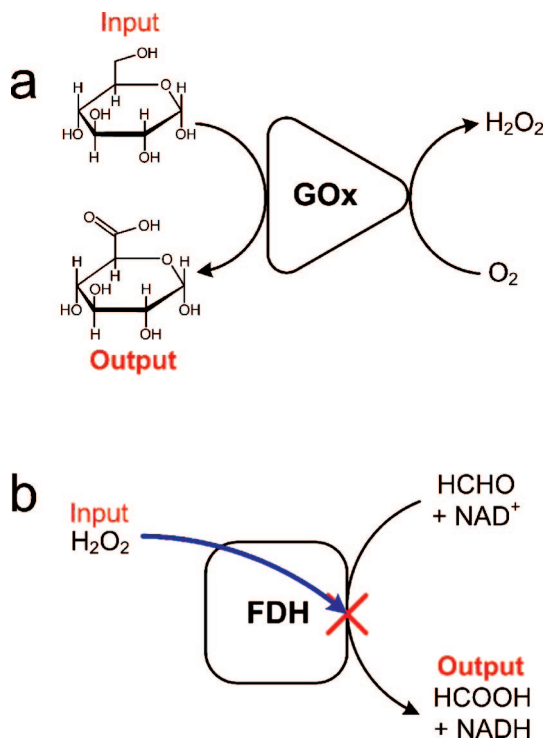


**Figure 64.** Schematic representations of structural changes of the azobenzene-based photomechanical gates of azo-GroEL upon exposure to UV light and ATP. Reprinted from ref 539. Copyright 2006 American Chemical Society.

for both gates are glucose (input 1) and  $\text{H}_2\text{O}_2$  (input 2), while the changes in concentration of gluconic acids and NADH are the outputs.

The same approach can be used to build much more complex logic systems; their complexity in principle is limited only by the number of enzymes involved and the number of independent substrates (acting as input signals), and coupling reagents providing communication between individual enzyme gates.<sup>546–548</sup> Better control over enzymatic logic gates was observed upon immobilization onto electrode surfaces. Coimmobilization of GOx and MP-11 via pyrroloquinoline quinone monolayer resulted in the system, the response of which can be controlled by electrode potential. AND, OR, or XOR functions were computed on chemical inputs ( $\text{H}_2\text{O}_2$  and glucose) depending on electrode potential.





**Figure 65.** Principle of operation of biocatalytic YES and NOT logic gates. Adapted from ref 542.

Interestingly, the output can be recorded as a current generated by the enzymatic electrode.<sup>549</sup>

Enzymatic activity of kinase and phosphatase enzymes on a specially designed oligopeptide with appended SP-MC unit enables the construction of a molecular computing device with integrated memory.<sup>550</sup> The peptide contains two different phosphorylation sites (tyrosine and serine), designed to be phosphorylated by *c*-Src protein tyrosine kinase (SrcN1) and cAMP-dependent protein kinase A (PKA), respectively. These two peptide moieties are separated by xenobiotic 6-aminohexanoic acid (Figure 69a). Phosphorylation changes the net charge of the oligopeptide (nonphosphorylated tetracationic, monophosphorylated dicationic, and diphosphorylated neutral), thus affecting its interaction charged polymers (cationic polylysine and anionic polyaspartate), which in turn affects the formation of the colored merocyanine unit (gate readout). Thermal isomerization of SP into MC is governed by the net charge of the peptide-polymer assembly: positive charge of the system facilitates the formation of the colored merocyanine form. Furthermore, various absorption thresholds can be applied for information readout. In the case of the nonphosphorylated oligopeptide, the SP-to-MC thermal conversion is accelerated by the presence of a cationic polymer and inhibited by an anionic one. Upon phosphorylation, the anionic polymer does not change the conversion rate, while the cationic one inhibits the formation of the colored MC form. Depending on the polymer used and the threshold, the device can mimic the operation of AND, OR, and NOR logic gates (Figure 69b).<sup>550</sup>

### 8.3. Nucleic Acid-Based Molecular Logic Systems

Nucleic acid-based logic devices operate using two different approaches: nonenzymatic Watson-Crick type interaction and enzymatic activity of ribozymes and deoxyribozymes.

The simplest device of the first kind was reported by Ghadiri et al.<sup>551</sup> The device was constructed from 3'-fluorescein-modified DNA hexadecamer (Figure 70). Excitation with 350 nm light does not result in appreciable fluorescein emission at 520 nm. Interaction with a complementary strand or with Hoechst 33342 dye does not change the emission properties of the gate. Only the case of concomitant presence of the complementary strand and the dye excitation at 350 nm result in efficient FRET from the Hoechst dye embedded within the minor groove to the fluorescein reporter (Figure 70a), thus performing the AND operation on two chemical inputs.

Change of one input to ethidium bromide and excitation wavelength to 450 nm results in the NAND gate (Figure 70b). Interaction of the labeled strand with the complementary one does not influence strong fluorescein emission. Upon addition of ethidium bromide to single-stranded labeled DNA, the 520 nm-emission decreases in intensity by approximately 20%. Application of both stimuli (addition of complementary strand and ethidium bromide) results in fluorescence quenching due to the efficient FRET process from fluorescein moiety to ethidium cations intercalated within the double-stranded DNA.<sup>452</sup> Application of three different inputs complementary strand, Hoechst 33342, and ethidium bromide allows molecular implementation of the three-input INH gate.<sup>452</sup>

More universal DNA-based logic gates were reported recently by Fujimoto and co-workers.<sup>552</sup> The described protocol involves photocleavage of cross-linked DNA strands upon hybridization with carbazole-modified cDNA fragments (Figure 71a). The specially designed DNA sequences contain the address part, the gate moiety with cross-linked base pair, and biotin moiety for fluorescent staining. Hybridization with a complementary strand containing the photosensitizer moiety (carbazole) and subsequent irradiation with 366 nm light results in photocleavage of the cross-link. All of the strands are attached to the DNA chip using the address part. The photocleaved strands cannot be labeled with fluorescent avidin label, which corresponds to the logic low state (Figure 71b). An AND gate contains two cross-linked sites, and four different carbazole-modified DNA strands serve as the inputs (Figure 71c). More complex operations are achieved by a combination of larger number of gate strands in solution or by incorporation of a larger number of cross-links in a single strand. Implementation of any more complex function required its decomposition into the sum of products (a disjunction of minterms). Devices such as full adder and full subtractor were easily implemented using this protocol.<sup>552</sup>

An analogous DNA-based logic system was reported recently by Gianneschi and Ghadiri.<sup>553</sup> In this system, one DNA strand is attached covalently to the mutant cereus neutral protease, while input strands may contain the inhibitor moiety (1*H*-indol-3-yl-acetic acid derivative). Enzymatic activity is monitored using fluorogenic protein substrate. This platform allows the construction of elementary OR, AND, and NOR logic gates. A similar approach, but one based on restriction enzymes, was used to solve chess problems<sup>554</sup> and the maximal clique problem.<sup>555</sup>

Introduction of the xenobiotic base (methoxybenzodeazaadenine, <sup>MD</sup>A, Figure 72a) to the DNA strand facilitates control over hole transfer to guanine.<sup>556</sup> This artificial nucleotide forms Watson-Crick pairs with cytidine (Figure 72a) and thymidine (Figure 72b). Depending on the counterpart within the duplex DNA, the efficiency of a hole transfer can be switched on and off. If <sup>MD</sup>A is coupled with

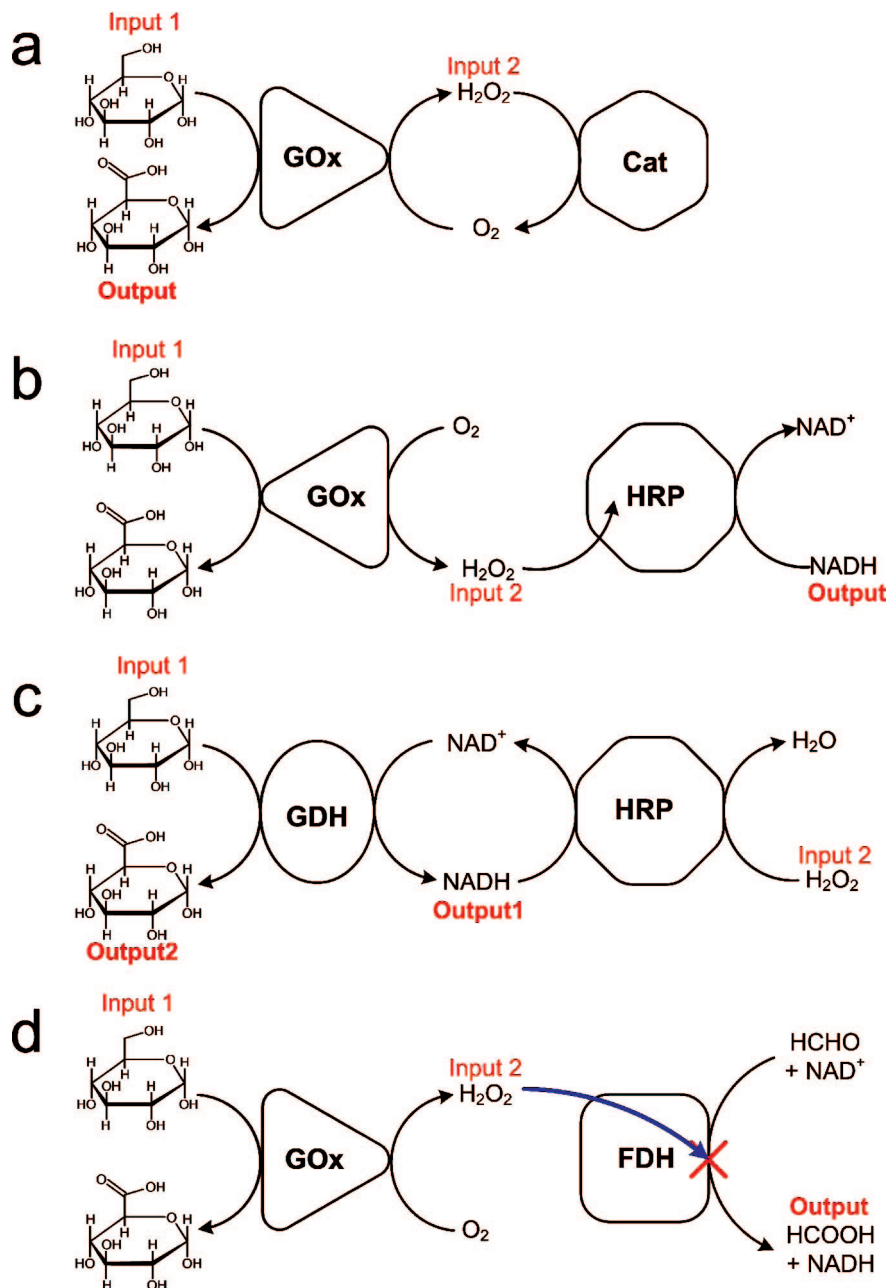


Figure 66. Principle of operation of biocatalytic AND (a), OR (b), XOR (c), and NOR (d) logic gates. Adapted from refs 542 and 543.

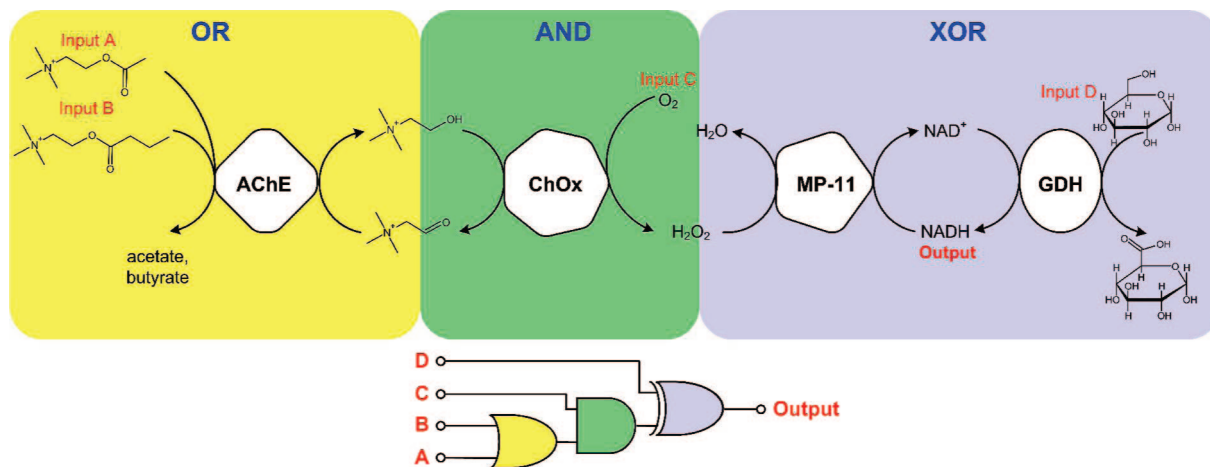
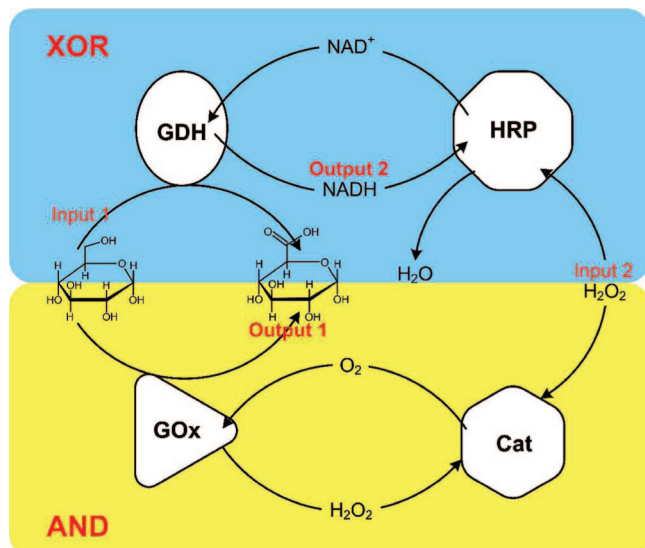
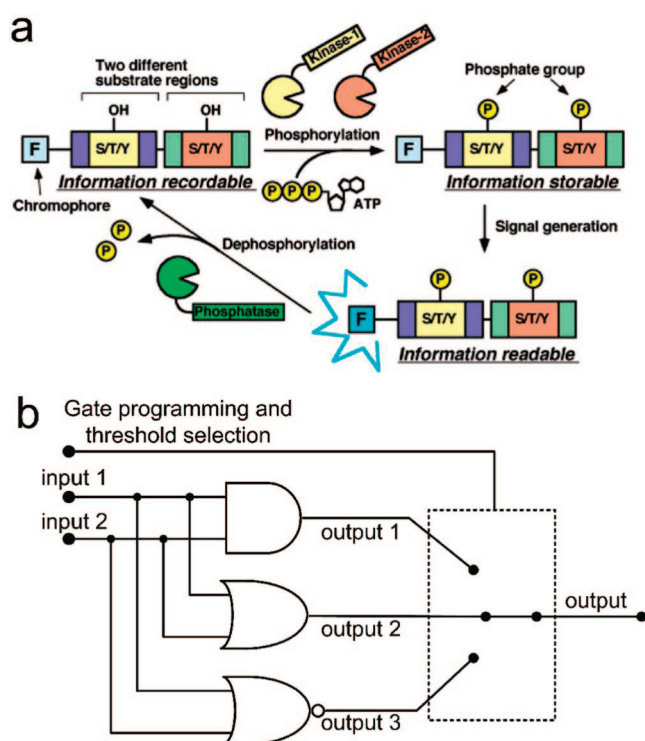


Figure 67. Principle of operation of the concatenated four-enzyme logic system and corresponding electronic circuit. Adapted from ref 544.



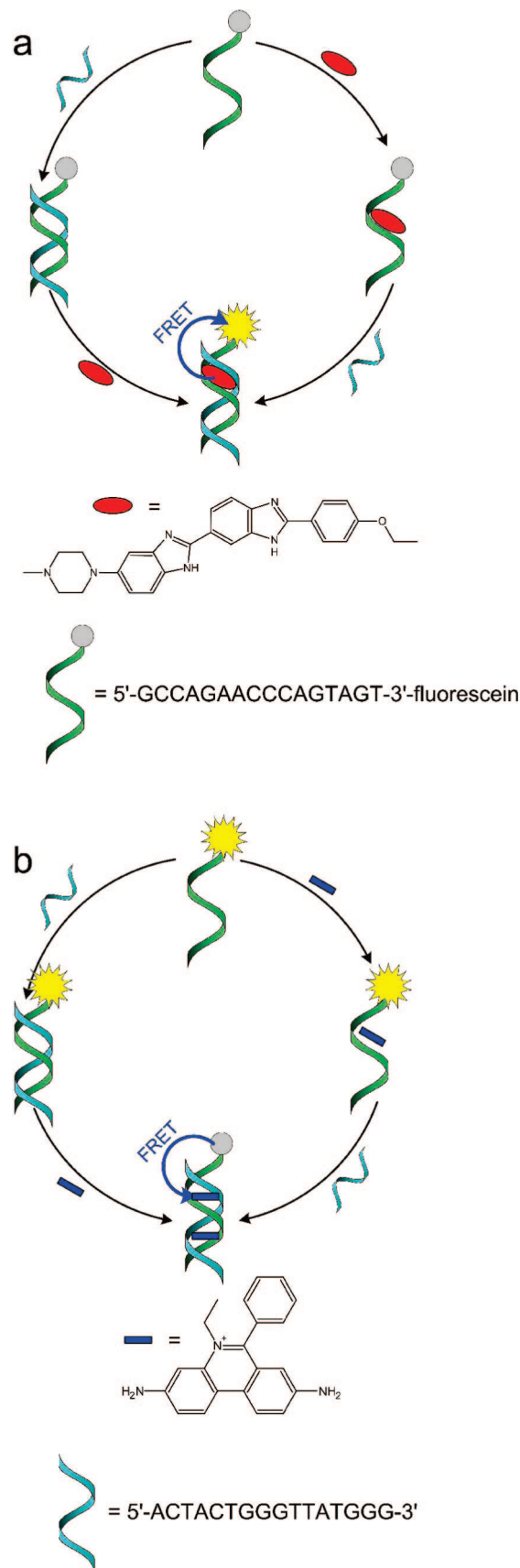
**Figure 68.** Operation of the biocatalytic half adder based on four coupled enzymes. Adapted from ref 545.



**Figure 69.** Schematic illustration of a phosphorylation-based molecular device (a) and its electronic equivalent circuit (b). Reprinted from ref 550. Copyright 2007 American Chemical Society.

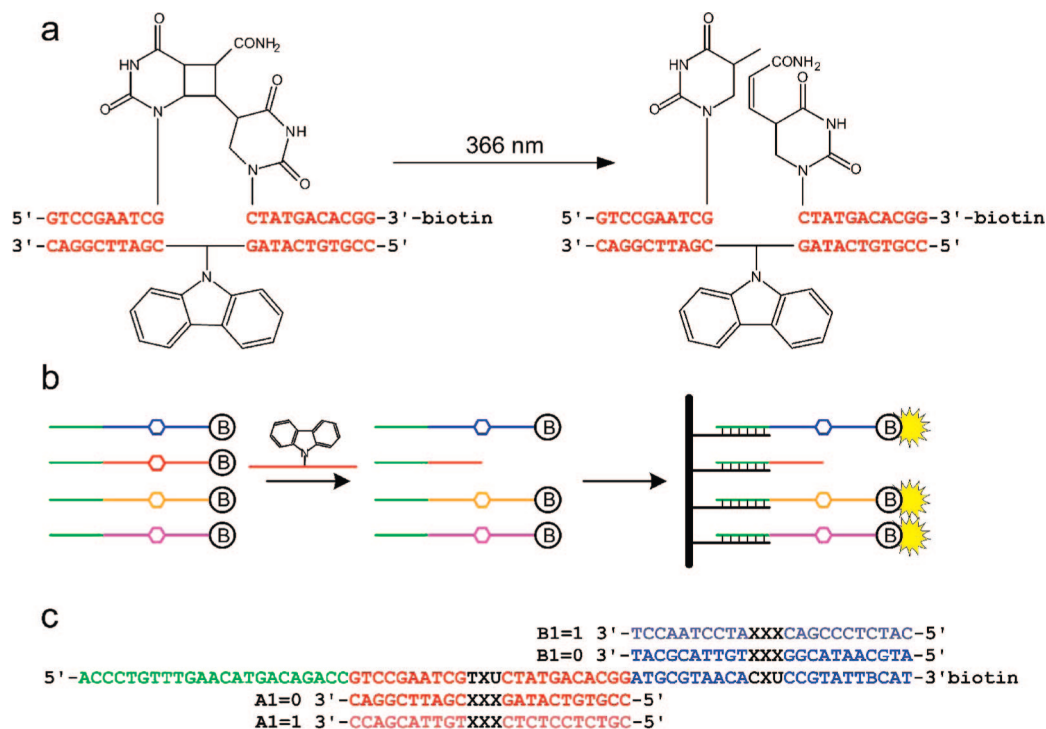
thymidine, the hole transfer is favored, while pairing with cytidine, strongly suppresses the hole transfer. Operation of the device required the photoactive hole generator (uridine with attached cyanobenzophenone photosensitizer, Figure 72c) and hole detection unit (GGG sequence). Any Boolean function that can be represented as a disjunction of minterms can be implemented in this molecular device.

DNA-based logic gates can be also built of the bases of telomere sequences with attached fluorophore and quencher moieties.<sup>557</sup> The efficiency of quenching depends on the DNA structure, which in turn depends on simple chemical inputs ( $H^+$ ,  $Li^+$ , and  $K^+$ ). This device provides much simpler input and output, but its operation is limited to simple logic gates.



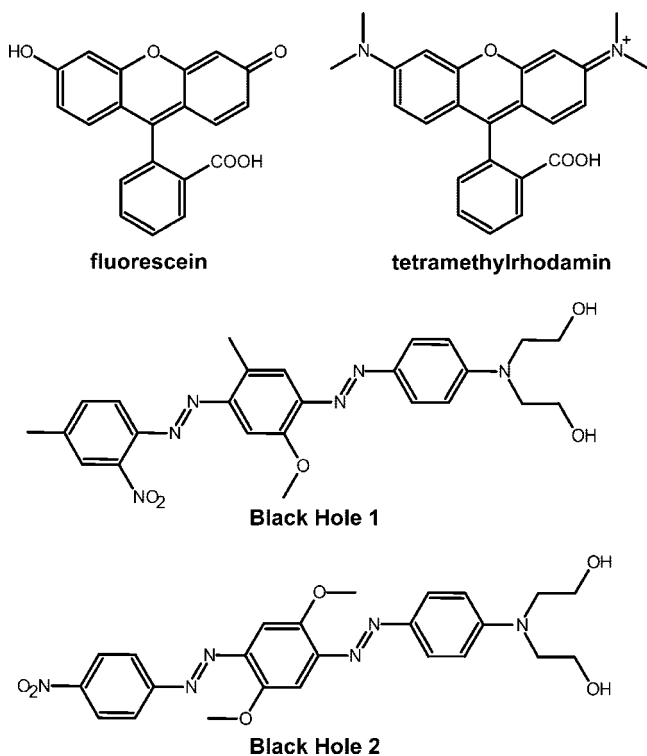
**Figure 70.** Principle of operation of DNA-based AND (a) and NAND (b) logic gates. Adapted from ref 551.

The most versatile and hence the most complex molecular devices known up to date are based on DNA and RNA aptamers and deoxyribozymes. These molecules usually exist in solution as stem-loop structures with both ends modified



**Figure 71.** Schematic representation of carbazole-induced photocleavage of photocross-linked DNA strands (a), the general scheme of operational procedure of the DNA-based logic gates (b), and the design of the DNA-based AND gate (c). Address sequence is marked in green, while the gate sequences are in red and blue. XU stands for 5-carboxyvinyl-2'-deoxyuridine and XXX for the carbazole photosensitizer. Adapted from ref 552.

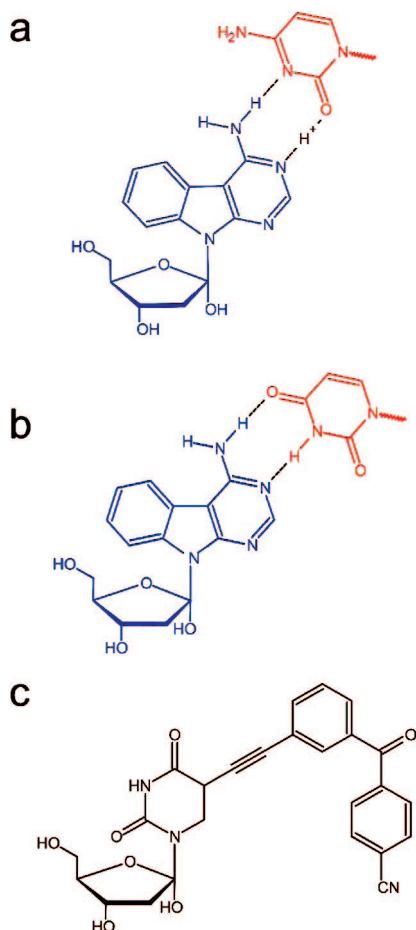
with appropriate labels, e.g., a fluorophore and a quencher. Alternatively, the aptamer may contain the fluorescent molecule bound within its cavity. Such molecular devices were initially designed as molecular sensors<sup>558–562</sup> but later on evolved into complex logic devices<sup>152,563–569</sup> and molecular-scale communication networks.<sup>570</sup>



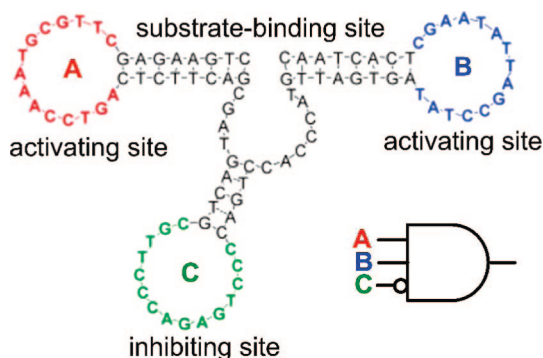
The deoxyribozyme logic devices comprise two parts: the deoxyribozyme module and signaling module. Active form of the deoxyribozyme can catalytically cleave the signaling

DNA molecule and thus trigger the optical output (switch on fluorescence). Signaling DNA strands contain one ribosyladenine, which is the cleavage site, while both ends of this strand are modified with fluorescent labels of different excited-state energies (e.g., fluorescein and tetramethylrhodamine) or fluorescent label and a quencher (e.g., Black Hole). In the initial, uncleaved form, resonant energy transfer results in fluorescence quenching, while deoxyribozyme-catalyzed cleavage on the signaling strands switches on the fluorescence. In order to perform logic operation, the deoxyribozyme strand must be equipped with one or more input-strand binding sites, which modulate its catalytic activity. The most common approach includes deoxyribozymes containing self-complementary fragments, which may form stem-loops. Upon binding of the input strands, the stem-loops open, and this in turn changes the catalytic activity of the deoxyribozyme. If the stem-loop is located next to the substrate binding site, its opening results in activation of the catalyst, while opening of the stem loop located in the central part of the deoxyribozyme results in inhibition that arrests the cleavage reactions. The deoxyribozyme logic gates usually perform NOT, AND, and INH operations, and OR and XOR functions are obtained by combining two or more YES or INH gates, respectively, in one solution.<sup>563,564</sup>

Further development of deoxyribozyme-based logic gates resulted in the construction of binary half-adder.<sup>565</sup> All of the data inputs were encoded in short DNA strands complementary to the loops of the gates, while the response was observed as a fluorescence of cleaved strand containing a fluorophore and a quencher. Depending on the deoxyribozyme gate characteristics, its catalytic activity can be switched on upon the binding of desired combination of input strands (both for AND and only one for INH). On cleavage, the fluorophore and the quenched fall apart, and fluorescence



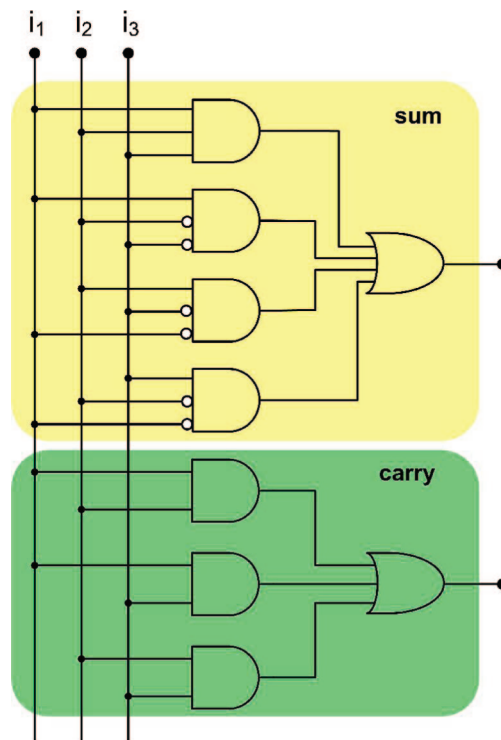
**Figure 72.** Structures of <sup>MD</sup>A/C (a), <sup>MD</sup>A/T (b), and cyanobenzophenone-modified uridine (c).



**Figure 73.** Structure of the three-input, deoxyribozyme-based logic gate and corresponding electronic equivalent. Partially reprinted from ref 568. Copyright 2006 American Chemical Society.

can be recorded. Mixture of three different DNA gates designed to respond to common input strands (one AND and two INH, which constitute for one XOR) results in binary half-adder. The same strategy can be applied to develop logic devices with a larger number of inputs, resulting from implicit-OR tiling of gates around common substrates.<sup>564</sup>

Even higher complexity can be achieved by advanced engineering of DNA strands forming the deoxyribozymes.<sup>568</sup> Larger deoxyribozymes containing three loops may perform complex AND, NAND, and INH functions depending on the interplay between activating and inhibiting receptors (Figure 73). Therefore, mixing of several different AND and INH gates operating on the same input strands allows construction of complex devices, such as full adder (Figure



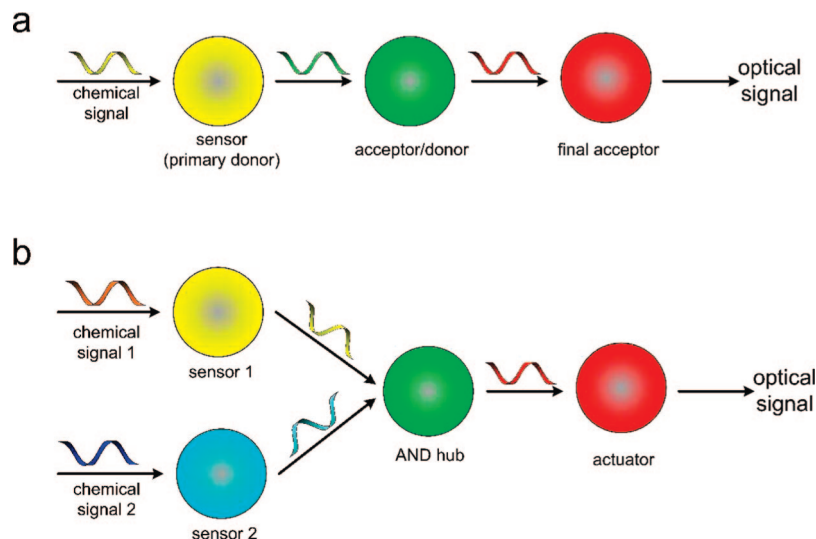
**Figure 74.** Full adder implementation using three-input INH gates and two-input AND gates based on deoxyribozymes. Adapted from ref 568.

74). In principle, there are no obstacles in the construction of logic systems of much higher complexity. It was found, however, that at high concentrations some interactions between individual deoxyribozymes occur, which in turn impairs the functionality of the device.<sup>568</sup>

The most complex deoxyribozyme logic devices were obtained by the combination of 23 different gates in a  $3 \times 3$  well array.<sup>152</sup> This resulted in an automaton named MAYA (Molecular Array of YES and ANDANDNOT gates), which can interactively play tic-tac-toe against the human opponent. The algorithm implemented in this array describes the perfect strategy, and the automaton cannot be defeated. Further development of this device yielded the MAYA-II automaton, the first medium-scale integrated molecular device combining 128 individual logic gates operating on 32 input molecules with two different fluorescent outputs.<sup>569</sup>

The practical applications of this massive parallel integration are more likely in oligonucleotide analysis rather than in competition with silicon devices in high-speed computing. This deoxyribonuclease device has an ability to detect and analyze combinations of multiple DNA sequences. The MAYA-II automaton can analyze the space of 232 possible subsets of the 32 input oligonucleotides and partition it into equivalence classes signaled by unique two-color, eight-well patterns, for a total of up to  $2^{16} = 65536$  patterns. Based on MAYA-II, several systems for multiplex single nucleotide polymorphism detection and viral lineage attribution are currently investigated. These developments should allow for the application of deoxyribozyme logic gate technology in bidirectional signaling events and pave the way for the next generation of fully autonomous molecular devices.<sup>569</sup>

Apart from logic operation, the deoxyribozyme-based systems are the first chemical models of complex information transfer at the molecular level. There are systems utilizing energy,<sup>523</sup> electron,<sup>292</sup> or proton<sup>491</sup> transfer processes (nu-



**Figure 75.** Principle of operation of network arrays of particles (a) and an AND hub (b). Adapted from ref 570.

merous examples can be found in the preceding sections of this review) for information transfer between different chemical entities, but only DNA-based systems provide networking schemes analogous to silicon-based devices.<sup>570</sup> The system comprises a mixture of plastic (polystyrene or latex) beads covered with various deoxyribozymes. The information donor bead collects information (captures the input molecule to the aptamer), processes it according to the Boolean function encoded in its structure, and eventually yields the DNA output strand (a fragment of the input strand or a strand released upon binding of the analyte). This output strand can in turn play a role of the input to the secondary bead containing different active molecules immobilized at the surface. Based on that principle, a three layer cascade (Figure 75a) and an AND hub (Figure 75b) were constructed. It was shown that both mixtures of particles and particles separated with polycarbonate membranes yield identical results. Therefore, it can be concluded that a real molecular level communication between DNA-modified particles has been established. Silicomimetic DNA computing and sensing (based on aptamers and deoxyribozymes) can be adapted to accomplish the integration of microparticles into cascades and networks, and these networks are capable of more complex functions than individual particles. The dynamic networks of beads are of interest not only as a new computing medium but also for their potential in nanomedicine, for example, in molecular computing-controlled drug release. These studies represent a step toward a scenario in which molecular-level networks connect molecular level computing units, thus forming a unique molecular level computing device that conforms with most of the silicon-based computing paradigms. In contrast to most of the molecular level devices, this one has great practical potential. This approach should minimize the side effects of targeted immunotherapy whenever nanoparticles are used. Furthermore, these results represent a step toward a scenario in which networks will be used to assess the presence of multiple tissue markers, or they could assess additional information from the remote positions. There are countless possibilities of constructing more complex systems by loading a single particle with additional functionalities.<sup>570</sup>

## 9. Concluding Remarks

The investigations presented in this review clearly indicate that information processing at the molecular level is possible and that even relatively complex logic devices can be built on the basis of simple chemical systems. At this point, however, these devices cannot compete with classical, semiconductor-based processors, in terms of computational power, efficiency, and user-friendliness. In most cases, only elementary logic gates could be implemented, which is absolutely insufficient for any serious computing applications. It does not mean, however, that all of the effort of many scientists from all over the world is futile. A combination of chemistry with Boolean logic and theory of information may lead to a better understanding of the molecular processes responsible for information processing in natural systems, i.e., in the brain and nervous systems of animals. Furthermore, most of the natural processes are controlled by other processes and parameters of the environment; Boolean analysis of various chemical systems, including those involving the genome, may lead to a better understanding of nature. Moreover, chemical logic devices constitute a new platform for drug activation and delivery, thus limiting the deleterious side effects, especially during antitumor therapy.<sup>128,129</sup> Some molecular logic gates are also useful for diagnostic purposes.<sup>571</sup>

At the present stage of development, the research on molecular logic systems answers the question: Can it be made to work? In the future, chemists and computer engineers together should try to answer another one: If it works, what can we use it for?<sup>572</sup>

## 10. List of Abbreviations

$\Phi$	quantum yield
$\alpha$ -CD	cyclomaltohexaose, $\alpha$ -cyclodextrin
A	electron acceptor
<sup>MD</sup> A	methoxybenzodeazaadenine
abs	absorption
AChE	acetylcholine esterase
ATP	adenosine triphosphate
AZ	<i>N,N</i> -dimethyl-4-[( <i>E</i> )-pyridin-2-ylidiazonyl]aniline ( <i>azopyridine</i> )
BDPY	boron-dipyrrin
BN	binaphthalene
bpy	2,2'-bipyridine

bpy'	2,2'-bipyridine-4,4'-dicarboxylic acid
BT	betaine
Cat	catalase
CD	circular dichroism
CHEMFET	chemical field effect transistor
ChOx	choline oxidase
CMOS	complementary metal-oxide-semiconductor
CPD	cyclophanediene
CT	charge transfer
D	electron donor
DAPI	4',6-diamidino-2-phenylindole
DFT	density functional theory
DFWM	degenerate four wave mixing
DH	dihydroazulene
DHI	dihydroindolizine
DHP	dihydropyrene
DMSO	dimethylsulfoxide
DNA	deoxyribonucleic acid
DPi	<i>N</i> -dodecylpiperidine
DPy	2-dodecylpyridine
DT	dithienylethene
EDTA	ethylenediaminetetraacetate
EET	electronic energy transfer
ethidium	3,8-diamino-5-ethyl-6-phenylphenanthridinium
FDH	formaldehyde dehydrogenase
FG	fulgimide
fl	fluorescence
FRET	Förster resonance energy transfer
GDH	glucose dehydrogenase
GFP	green fluorescent protein
GOx	glucose oxidase
HCF	hexacyanoferrate
Hoechst 33342	2'-(4-ethoxyphenyl)-5-(4-methylpiperazin-1-yl)-2,6'-bi(1 <i>H</i> -benzo[ <i>d</i> ]imidazole)
HOMO	highest occupied molecular orbital
HRP	horseradish peroxidase
ICT	internal charge transfer
IR	infrared radiation
LD-LISC	ligand-driven light induced spin change
LED	light emitting diode
LIESST	light-induced excited spin state trapping
MC	merocyanine
MLCT	metal-to-ligand charge transfer
MMCT	metal-to-metal charge transfer
MP-11	microperoxidase-11
NAD <sup>+</sup>	nicotinamide adenine dinucleotide, oxidized
NADH	nicotinamide adenine dinucleotide, reduced
Nd:YAG	neodymium-doped yttrium aluminum garnet
NMR	nuclear magnetic resonance
OLED	organic light emitting diode
P	porphyrin
PCF	pentacyanoferrate
PCT	photoinduced charge transfer
PDB	Protein Data Bank
PDMS	poly(dimethylsiloxane)
PEDOT	poly(3,4-ethylenedioxythiophene)
PEPS	photoelectrochemical photo current switching
PET	photoinduced electron transfer
PI	perylenebisimide
PPS	poly(styrene sulfonic acid)
PQ	phenoxynaphthacenequinone
PY	perylene
RNA	ribonucleic acid
SCO	spin crossover
SP	spiropyran
TCNE	tetracyanoethene
TCNQ	tetracyanoquinodimethane
TEA	triethanolamine
TTF	2,2'-bis(1,3-dithiolyldiene), "tetrathiafulvalene"
UV	ultraviolet radiation
vis	visible light

## 11. Acknowledgments

I thank Dr. Wojciech Macyk for valuable discussions and comments and Dr. Radim Beránek for assistance with the literature search.

## 12. Note Added after ASAP Publication

There was an error in eq 2 in the version published ASAP June 27, 2008; the corrected version was published ASAP September 10, 2008.

## 13. References

- (1) Cook, N. P. *Introductory Digital Electronics*; Prentice-Hall Inc.: Upper Saddle River, NJ, 1998.
- (2) Floyd, T. L. *Digital Fundamentals*; Prentice-Hall International Inc.: Upper Saddle River, NJ, 1997.
- (3) Hillis, W. D. *The Pattern on the Stone. The Simple Ideas That Make Computers Work*; Perseus Publishing: Boulder, CO, 1999.
- (4) Frank, D. J. *IBM J. Res. Dev.* **2002**, *46*, 235.
- (5) Shahidi, G. G. *IBM J. Res. Dev.* **2002**, *46*, 121.
- (6) Wong, H.-S. P. *IBM J. Res. Dev.* **2002**, *46*, 133.
- (7) Isaac, R. D. *IBM J. Res. Dev.* **2000**, *44*, 369.
- (8) Moore, G. E. *Electronics* **1965**, *38*, 114.
- (9) Grozema, F. C.; Siebbeles, L. D. A.; Gelincik, G. H.; Warman, J. M. *Top. Curr. Chem.* **2005**, *257*, 135.
- (10) James, D. K.; Tour, J. M. *Top. Curr. Chem.* **2005**, *257*, 33.
- (11) Schwab, P. F. H.; Levin, M. D.; Michl, J. *Chem. Rev.* **1999**, *99*, 1836.
- (12) Schwab, P. F. H.; Smith, J. R.; Michl, J. *Chem. Rev.* **2005**, *105*, 1197.
- (13) *Stimulating Concepts in Chemistry*; Vögtle, F., Stoddart, J. F., Shibusaki, M., Eds.; Wiley-VCH: Weinheim, 2000.
- (14) Hoeben, F. J. M.; Jonkheijm, P.; Meijer, E. W.; Schenning, A. P. H. J. *Chem. Rev.* **2005**, *105*, 1491.
- (15) Berresheim, A. J.; Müller, M.; Müllen, K. *Chem. Rev.* **1999**, *99*, 1747.
- (16) Bendikov, M.; Wudl, F.; Perepichka, D. F. *Chem. Rev.* **2004**, *104*, 4891.
- (17) Bunz, U. H. F. *Top. Curr. Chem.* **1999**, *201*, 131.
- (18) Smith, D. K.; Hirst, A. R.; Love, C. S.; Hardy, J. G.; Brignell, S. V.; Huang, B. *Prog. Polym. Sci.* **2005**, *30*, 220.
- (19) Jiang, D.-L.; Aida, T. *Prog. Polym. Sci.* **2005**, *30*, 403.
- (20) Yokoyama, S.; Otomo, A.; Nakahama, T.; Okuno, Y.; Mashiko, S. *Top. Curr. Chem.* **2003**, *228*, 205.
- (21) Inoue, K. *Prog. Polym. Sci.* **2000**, *25*, 453.
- (22) Frauenrath, H. *Prog. Polym. Sci.* **2005**, *30*, 325.
- (23) Li, X.-G.; Huang, M.-R.; Duan, W.; Yang, Y.-L. *Chem. Rev.* **2002**, *102*, 2925.
- (24) Pron, A.; Rannou, P. *Prog. Polym. Sci.* **2002**, *27*, 135.
- (25) Schenning, A. P. H. J.; Meijer, E. W. *Chem. Commun.* **2005**, 3245.
- (26) Perepichka, I. F.; Perepichka, D. F.; Meng, H.; Wudl, F. *Adv. Mater.* **2005**, *17*, 2281.
- (27) Brédas, J.-L.; Beljonne, D.; Coropceanu, V.; Cornil, J. *Chem. Rev.* **2004**, *104*, 4971.
- (28) Meier, H. *Angew. Chem., Int. Ed.* **2005**, *44*, 2482.
- (29) Femoni, C.; Iapaluccia, C.; Kaswalder, F.; Longoni, G.; Zacchini, S. *Coord. Chem. Rev.* **2006**, *250*, 1580.
- (30) Satake, A.; Kobuke, Y. *Tetrahedron* **2005**, *61*, 13.
- (31) Burrell, A. K.; Officer, D. L.; Plieger, P. G.; Reid, D. C. W. *Chem. Rev.* **2001**, *101*, 2751.
- (32) Wojaczyński, J.; Latos-Grazyński, L. *Coord. Chem. Rev.* **2000**, *204*, 113.
- (33) Shanmugathan, S.; Edwards, C.; Boyle, R. W. *Tetrahedron* **2000**, *56*, 1025.
- (34) Rosi, N. L.; Mirkin, C. A. *Chem. Rev.* **2005**, *105*, 1547.
- (35) Mirkin, C. A.; Taton, T. A. *Nature* **2000**, *405*, 626.
- (36) Katz, E.; Willner, I. *Angew. Chem., Int. Ed.* **2004**, *43*, 6042.
- (37) Niemeyer, C. M. *Angew. Chem., Int. Ed.* **2001**, *40*, 4128.
- (38) Katz, E.; Wilner, I.; Wang, J. *Electroanalysis* **2004**, *16*, 19.
- (39) Daniel, M.-C.; Astruc, D. *Chem. Rev.* **2004**, *104*, 293.
- (40) Wilner, I.; Katz, E. *Angew. Chem., Int. Ed.* **2000**, *39*, 1180.
- (41) Cushing, B. L.; Kolesnichenko, V. L.; O'Connor, C. J. *Chem. Rev.* **2004**, *104*, 3893.
- (42) Turco Liveri, V. *Controlled Synthesis of Nanoparticles in Microheterogeneous Systems*; Springer: New York, 2006.
- (43) Veinot, J. G. C. *Chem. Commun.* **2006**, 4160.
- (44) *Nanoparticles: From Theory to Applications*; Schmid, G., Ed.; Wiley-VCH: Weinheim, 2004.
- (45) Terrones, M.; Hsu, W. K.; Kroto, H. W.; R.M. Walton, D. *Top. Curr. Chem.* **1999**, *199*, 189.

- (46) Dai, H. *Surf. Sci.* **2002**, *500*, 218.
- (47) Avouris, P. *Acc. Chem. Res.* **2002**, *35*, 1026.
- (48) Hoenlein, W.; Kreupl, F.; Duesberg, G. S.; Graham, A. P.; Liebau, M.; Seidel, R.; Unger, E. *Mater. Sci. Eng., C* **2003**, *23*, 663.
- (49) Rao, C. N. R.; Deepak, F. L.; Gundiah, G.; Govindaraj, A. *Prog. Solid State Chem.* **2003**, *31*, 5.
- (50) Ozin, G. A.; Arsenault, A. C. *Nanochemistry. A Chemical Approach to Nanomaterials*; The Royal Chemical Society: Cambridge, U.K., 2005.
- (51) Dragoman, M.; Dragoman, D. *Nanoelectronics. Principles and Devices*; Artech House, Inc.: Norwood, MA, 2006.
- (52) *Nanoscale Assembly: Chemical Techniques*; Huck, W. T. S., Ed.; Springer: New York, 2005.
- (53) Tasis, D.; Tagmatarchis, N.; Bianco, A.; Prato, M. *Chem. Rev.* **2006**, *106*, 1105.
- (54) *Nanotubes and Nanofibers*; Gogotsi, Y., Ed.; Taylor&Francis Group, LLC: New York, 2006.
- (55) *Carbon Nanomaterials*; Gogotsi, Y., Ed.; Taylor&Francis Group, LLC: New York, 2006.
- (56) *Nanoscience. Nanotechnologies and Nanophysics*; Dupas, C.; Houdy, P.; Lahmani, M., Eds.; Springer Verlag: Berlin, 2007.
- (57) ter Brake, H. J. M.; Buchholtz, F.-I.; Burnell, G.; Claeson, T.; Crété, D.; Febvre, P.; Gerritsma, G. J.; Hilgenkamp, H.; Humpreys, R.; Ivanov, Z.; Jutzi, W.; Khabipov, M. I.; Mannhart, J.; Meyer, H. G.; Niemeyer, J.; Ravex, A.; Rogalla, H.; Russo, M.; Satchell, J.; Siegel, M.; Töpfer, H.; Uhlmann, F. H.; Villégier, J.-C.; Wikborg, E.; Winkler, D.; Zorin, A. B. *Physica C* **2006**, *439*, 1.
- (58) Jérôme, D. *Chem. Rev.* **2004**, *104*, 5565.
- (59) Kobayashi, H.; Cui, H. B.; Kobayashi, A. *Chem. Rev.* **2004**, *104*, 5265.
- (60) Love, J. C.; Estroff, L. A.; Kriebel, J. K.; Nuzzo, R. G.; Whitesides, G. M. *Chem. Rev.* **2005**, *105*, 1103.
- (61) Garcia, R.; Martinez, R. V.; Martinez, J. *Chem. Soc. Rev.* **2006**, *35*, 29.
- (62) Crespo-Biel, O.; Ravoo, B. J.; Huskens, J.; Reinhoudt, D.N. *Dalton Trans.* **2006**, 2737.
- (63) Henzie, J.; Barton, J. E.; Stender, C. L.; Odom, T. W. *Acc. Chem. Res.* **2006**, *39*, 249.
- (64) Huc, V. *J. Phys.: Condens. Matter* **2006**, *18*, S1909.
- (65) Buriak, J. M. *Chem. Rev.* **2002**, *102*, 1271.
- (66) Waltenburg, H. N., Jr. *J. Chem. Rev.* **1995**, *95*, 1589.
- (67) Leising, G.; Stadlober, B.; Haas, U.; Haase, A.; Palfinger, C.; Gold, H.; Jakopic, G. *Microelectr. Eng.* **2006**, *83*, 831.
- (68) Lin, N.; Stepanow, S.; Vidal, F.; Kern, K.; Alam, M. S.; Strömsdörfer, S.; Dremov, V.; Müller, P.; Landa, A.; Ruben, M. *Dalton Trans.* **2006**, 2794.
- (69) Ruiz, S. A.; Chen, C. S. *Soft Matter* **2007**, *3*, 186.
- (70) *Introduction to Nanoscale Science and Technology*; Di Ventra, M.; Evoy, S.; Heflin, J. R., Jr., Eds.; Kluwer Academic Publishers: New York, 2004.
- (71) Mahalik, N. P. *Micromanufacturing and Nanotechnology*; Springer Verlag: Berlin, Germany, 2006.
- (72) Risch, L. *Solid-State Electron.* **2006**, *50*, 527.
- (73) Yu, B.; Meyyapan, M. *Solid-State Electron.* **2006**, *50*, 536.
- (74) *Nanoelectronics and Information Technology*; Waser, R., Ed.; Wiley-VCH: Weinheim, Germany, 2003.
- (75) Cavin, R. K.; Zhirmov, V. V. *Solid-State Electron.* **2006**, *50*, 520.
- (76) Maruccio, G.; Cingolani, R.; Rinaldi, R. *J. Mater. Chem.* **2004**, *14*, 542.
- (77) Bsiesy, A. *Compt. Rend. Physique* **2005**, *6*, 1022.
- (78) Tanaka, M. *J. Cryst. Growth* **2005**, *278*, 25.
- (79) Lu, J. G.; Chang, P.; Fan, Z. *Mater. Sci. Eng.* **2006**, *R52*, 49.
- (80) Allwood, D. A.; Xiong, G.; Faulkner, C. C.; Atkinson, D.; Petit, D.; Cowburn, R. P. *Science* **2005**, *309*, 1688.
- (81) Das, G. P.; Rao, B. K.; Jena, P.; Kawazoe, Y. *Comput. Mater. Sci.* **2006**, *36*, 84.
- (82) Palacio, F.; Miller, J. S. *Nature* **2000**, *408*, 421.
- (83) Ohno, Y.; Young, D. K.; Beschoten, B.; Matsukura, F.; Ohno, H.; Awschalom, D. D. *Nature* **1999**, *402*, 790.
- (84) Petej, I.; Gregg, J. *In Magnetism: Molecules to Materials III*; Miller, J. S., Drillon, M., Eds.; Wiley-VCH: Weinheim, Germany, 2002.
- (85) Milburn, G. *Quantum Technology*; Allen & Unwin Pty Ltd.: St. Leonards, Australia, 1996.
- (86) Jones, J. A. *Prog. Nucl. Magn. Reson. Spectrosc.* **2001**, *38*, 325.
- (87) Jonhson, G. *A Shortcut through Time. The Path to the Quantum Computer*; Random House, Inc.: New York, 2003.
- (88) *Nano, Quantum and Molecular Computing. Implications to High Level Design and Validation*; Shukla, S. K.; Bahar, R. I., Eds.; Kluwer Academic Publishers: New York, 2004.
- (89) Joachim, C. *J. Phys.: Condens. Matter* **2006**, *18*, S1935.
- (90) Minolli, D. *Nanotechnology Applications to Telecommunications and Networking*; Wiley-Interscience: Hoboken, NJ, 2006.
- (91) Frank, M. P., Jr. *Nanotechnology* **1998**, *9*, 162.
- (92) Keyes, R. W. *Proc. IEEE* **2001**, *89*, 227.
- (93) Meindl, J. D.; Chen, Q.; Davis, J. A. *Science* **2001**, *293*, 2044.
- (94) Waser, R. *In Nanoelectronics and Information Technology*; Waser, R., Ed.; Wiley-VCH Verlag GmbH: Weinheim, Germany, 2003.
- (95) Ugarov, W. A. *Special Theory of Relativity (in Russian)*; Nauka: Moscow, 1977.
- (96) Balzani, V.; Venturi, M.; Credi, A. *Molecular Devices and Machines: A Journey into Nanoworld*; Wiley-VCH: Weinheim, Germany, 2003.
- (97) Zauner, K. P. *Crit. Rev. Solid State Mat. Sci.* **2005**, *30*, 33.
- (98) de Silva, A. P.; McClenaghan, N. D. *Chem. Eur. J.* **2004**, *10*, 574.
- (99) Balzani, V.; Credi, A.; Venturi, M. *ChemPhysChem* **2003**, *3*, 49.
- (100) Balzani, V.; Credi, A.; Venturi, M. *Chem. Eur. J.* **2002**, *8*, 5525.
- (101) Suhir, E. *Microelectronics J.* **2000**, *31*, 839.
- (102) Szaciłowski, K.; Stasiccka, Z. *Coord. Chem. Rev.* **2002**, *229*, 17.
- (103) de Silva, A. P.; Uchiyama, S.; Vance, T. P.; Wannalserse, B. *Coord. Chem. Rev.* **2007**, *251*, 1623.
- (104) de Silva, A. P.; McClenaghan, N. D.; McCoy, C. P. *In Handbook of Electron Transfer*; Balzani, V., de Silva, A. P., Gould, E. J., Eds.; Wiley-VCH: Weinheim, Germany, 2000; Vol. 5.
- (105) de Silva, A. P.; McClenaghan, N. D.; McCoy, C. P. *In Molecular Switches*; Feringa, B. L., Ed.; WILEY-VCH: Weinheim, 2001; Vol. 5.
- (106) *Nano and Molecular Electronics*; Lyshevski, S. E., Ed.; CRC Press: London, 2007.
- (107) Ballardini, R.; Ceroni, P.; Credi, A.; Gandolfi, M. T.; Maestri, M.; Semararo, M.; Venturi, M.; Balzani, V. *Adv. Funct. Mater.* **2007**, *17*, 740.
- (108) Raymo, F. M. *In Springer Handbook of Nanotechnology*, 2nd ed.; Bhushan, B., Ed.; Springer Verlag: Berlin, 2007.
- (109) Simon, J. *C.R. Chimie* **2005**, *8*, 893.
- (110) Penrose, R. *The Large, the Small and the Human Mind*; Cambridge University Press: Cambridge, U.K., 1997.
- (111) Crick, F. *The Astonishing Hypothesis*; Scribner Book Company: New York, 1995.
- (112) Waser, R. *In Nanoelectronics and Information Technology*; Waser, R., Ed.; Wiley-VCH Verlag GmbH: Weinheim, Germany, 2003.
- (113) George A. Philbrick Researches Inc. *Applications Manual for Computing Amplifiers for Modelling, Measuring, Manipulating & Much Else*; Nimrod Press, Inc.: Boston, MA, 1965.
- (114) *The Illustrated Dictionary of Electronics*; Gibilisco S. ed.; McGraw-Hill: New York, 2001.
- (115) Andersen, M. E.; Dennison, J. E.; Thomas, R. S.; Conolly, R. B. *Trends Biotechnol.* **2005**, *23*, 122.
- (116) Cornah, J. E.; Terry, M. J.; Smith, A. G. *Trends Plant Sci.* **2003**, *8*, 224.
- (117) Stock, J.; Da Re, S. *Curr. Biol.* **2000**, *10*, R420.
- (118) Milani, M.; Pesce, A.; Nardini, M.; Ouellet, H.; Ouellet, Y.; Dewilde, S.; Bocedi, A.; Ascenzi, P.; Guertin, M.; Moens, L.; Friedman, J. M.; Wittenberg, J. B.; Bolognesi, M. *J. Inorg. Biochem.* **2005**, *99*, 97.
- (119) Gilles-Gonzalez, M.-A.; Gonzalez, G. J. *Inorg. Biochem.* **2005**, *99*, 1.
- (120) Tsuda, S.; Aono, M.; Gunji, Y.-P. *BioSystems* **2004**, *73*, 45.
- (121) Feynman, R. P. *Eng. Sci.* **1960**, *23*, 22.
- (122) Milburn, G. *The Feynman Processor. An Introduction to Quantum Computation*; Perseus Books: Boulder, CO, 1998.
- (123) Amir, R. J.; Popkov, M.; Lerner, R. A.; Carbas III, C. F.; Shabat, D. *Angew. Chem., Int. Ed.* **2005**, *44*, 4378.
- (124) Broxterman, H. J.; Georgopadakou, N. F. *Drug Resist. Updates* **2005**, *8*, 183.
- (125) de Groot, F. M. H.; Damen, E. W. P.; Scheeren, H. W. *Curr. Med. Chem.* **2001**, *8*, 1093.
- (126) Szaciłowski, K. *Chem. Eur. J.* **2004**, *10*, 2520.
- (127) Szaciłowski, K.; Macyk, W.; Stochel, G.; Sostero, S.; Traverso, O.; Stasiccka, Z. *Coord. Chem. Rev.* **2000**, *208*, 277.
- (128) Szaciłowski, K.; Macyk, W.; Drzewiecka-Matuszek, A.; Brindell, M.; Stochel, G. *Chem. Rev.* **2005**, *105*, 2647.
- (129) Szaciłowski, K. *BioSystems* [Online early access]. DOI: 10.1016/j.biosystems.2007.03.002.
- (130) *Introducing Molecular Electronics*; Cuniberti, G.; Fagas, G.; Richter, K., Eds.; Springer Verlag: Berlin, Germany, 2005.
- (131) Tour, J. M. *Molecular Electronics*; World Scientific: Hackensack, NJ, 2003.
- (132) *Nanotechnology and Nanoelectronics*; Fahrner, W. R., Ed.; Springer Verlag: Berlin, Germany, 2005.
- (133) Aviram, A.; Ratner, M. A. *Chem. Phys. Lett.* **1974**, *29*, 277.
- (134) Metzger, R. M. *J. Mater. Chem.* **1999**, *9*, 2027.
- (135) Metzger, R. M. *Acc. Chem. Res.* **1999**, *32*, 950.
- (136) Gould, P. *Materials Today* **2005**, (07–08), 56.
- (137) Kuhr, W. G. *Electrochem. Soc. Interface* **2004**, *34*.
- (138) Ellenbogen, J. C.; Love, J. C. *Proc. IEEE* **2000**, *88*, 386.
- (139) Mayor, M.; Weber, H. B.; Waser, R. *In Nanoelectronics and Information Technology*; Waser, R., Ed.; Wiley-VCH Verlag GmbH: Weinheim, Germany, 2003.



- (140) de Silva, A. P.; Gunaratne, H. Q. N.; McCoy, C. P. *Nature* **1993**, *364*, 42.
- (141) Pina, F.; Melo, M. J.; Maestri, M.; Passaniti, P.; Balzani, V. *J. Am. Chem. Soc.* **2000**, *122*, 4496.
- (142) Raymo, F. M.; Giordani, S. *J. Am. Chem. Soc.* **2001**, *123*, 4651.
- (143) Pina, F.; Melo, M. J.; Maestri, M.; Passaniti, P.; Camaioni, N.; Balzani, V. *Eur. J. Org. Chem.* **1999**, 3199.
- (144) Raymo, F. R.; Giordani, S. *Proc. Natl. Acad. Sci. U.S.A.* **2002**, *99*, 4941.
- (145) Raymo, F. M. *Adv. Mater.* **2002**, *14*, 401.
- (146) Biancardo, M.; Bignozzi, C.; Doyle, H.; Redmond, G. *Chem. Commun.* **2005**, 3918.
- (147) Szaciłowski, K.; Macyk, W. *Comp. Rend. Chimie* **2006**, *9*, 315.
- (148) Szaciłowski, K.; Macyk, W.; Stochel, G. *J. Am. Chem. Soc.* **2006**, *128*, 4550.
- (149) Furtado, L. F. O.; Alexiou, A. D. P.; Gonçalves, L.; Toma, H. E.; Araki, K. *Angew. Chem., Int. Ed.* **2006**, *45*, 3143.
- (150) Park, W. I.; Kim, J. S.; Yi, G.-C.; Lee, H.-J. *Adv. Mater.* **2005**, *17*, 1393.
- (151) Heo, Y. W.; Norton, D. P.; Tien, L. C.; Kwon, Y.; Kang, B. S.; Ren, F.; Pearton, S. J. *Mater. Sci. Eng.* **2004**, *R47*, 1.
- (152) Stojanović, M. N.; Stefanović, D. *Nat. Biotechnol.* **2003**, *21*, 1069.
- (153) Deonaraine, A. S.; Clark, S. M.; Konermann, L. *Fut. Gener. Comp. Systems* **2003**, *19*, 87.
- (154) Fu, L.; Cao, L.; Liu, Y.; Zhu, D. *Adv. Colloid Interface Sci.* **2004**, *111*, 133.
- (155) Conrad, M.; Kampfer, R. R.; Kirby, K. G.; Rizki, E. N.; Schleis, G.; Smalz, R.; Trenary, R. *BioSystems* **1989**, *23*, 175.
- (156) Epstein, I. R.; Showalter, K. *J. Phys. Chem.* **1996**, *100*, 13132.
- (157) Hegedüs, L.; Kirschner, N.; Wittmann, M.; Simon, P.; Noszticzius, Z. *Chaos* **1999**, *9*, 283.
- (158) Rambidi, N. G. *BioSystems* **2002**, *64*, 169.
- (159) Rambidi, N. G.; Shamayaev, K. E.; Peshkova, G. Y. *Phys. Lett. A* **2002**, *298*, 375.
- (160) Rambidi, N. G. *Microelectr. Eng.* **2003**, *69*, 485.
- (161) Steinbock, O.; Kettunen, P.; Showalter, K. *J. Phys. Chem.* **1996**, *100*, 18970.
- (162) Motoike, I. N.; Yoshikawa, K. *Phys. Rev. E* **1999**, *59*, 5354.
- (163) Siewiesiuk, J.; Górecki, J. *J. Phys. Chem. A* **2001**, *105*, 8189.
- (164) Górecki, J.; Yoshikawa, K.; Igarashi, Y. *J. Phys. Chem. A* **2003**, *107*, 1664.
- (165) Szaciłowski, K. *Wiad. Chem.* **2004**, *58*, 11.
- (166) de Silva, A. P.; Gunaratne, H. Q. N.; Gunnlaugsson, T.; Huxley, A. J. M.; McCoy, C. P.; Rademacher, J. T.; Rice, T. E. *Chem. Rev.* **1997**, *97*, 1515.
- (167) de Silva, A. P.; McClean, G. D.; Moody, T. S. In *Encyclopedia of Supramolecular Chemistry*; Mrcel Dekker Inc.: New York, 2004.
- (168) Bakker, E.; Bühlmann, P.; Pretsch, E. *Chem. Rev.* **1997**, *97*, 3083.
- (169) Yam, V. W.-W.; Lo, K. K.-W. *Coord. Chem. Rev.* **1998**, *184*, 157.
- (170) Bühlmann, P.; Pretsch, E.; Bakker, E. *Chem. Rev.* **1998**, *98*, 1593.
- (171) Pina, F.; Parola, A. *J. Coord. Chem. Rev.* **1999**, *185–186*, 149.
- (172) de Silva, A. P.; Fox, D. A.; Huxley, A. J. M.; McClenaghan, N. D.; Roiron, J. *Coord. Chem. Rev.* **1999**, *185–186*, 297.
- (173) Beer, P. D.; Cadman, J. *Coord. Chem. Rev.* **2000**, *205*, 131.
- (174) Prodi, L.; Boletta, F.; Montalti, M.; Zaccaroni, N. *Coord. Chem. Rev.* **2000**, *205*, 59.
- (175) Keeffe, M. H.; Benkstein, K. D.; Hupp, J. T. *Coord. Chem. Rev.* **2000**, *205*, 201.
- (176) Bargossi, C.; Fiorini, M. C.; Montalti, M.; Prodi, L.; Zaccaroni, N. *Coord. Chem. Rev.* **2000**, *208*, 17.
- (177) Robertson, A.; Shinkai, *Coord. Chem. Rev.* **2000**, *205*, 157.
- (178) Valeur, B.; Leray, I. *Coord. Chem. Rev.* **2000**, *205*, 3.
- (179) de Silva, A. P.; Fox, D. A.; Huxley, A. J. M.; Moody, T. S. *Coord. Chem. Rev.* **2000**, *205*, 41.
- (180) Rurack, K. *Spectrochim. Acta* **2001**, *A57*, 2162.
- (181) Sun, S.-S.; Lees, A. J. *Coord. Chem. Rev.* **2002**, *230*, 171.
- (182) Rogers, C. W.; Wolf, M. O. *Coord. Chem. Rev.* **2002**, *233–234*, 341.
- (183) Faulkner, S.; Matthews, J. L. In *Comprehensive Coordination Chemistry II*; McCleverty, J. A., Meyer, T. J., Eds.; Elsevier: Amsterdam, 2003; Vol. 9.
- (184) Beer, P. D.; Hayes, E. J. *Coord. Chem. Rev.* **2003**, *240*, 167.
- (185) Gale, P. A. *Coord. Chem. Rev.* **2003**, *240*, 191.
- (186) Suksai, C.; Tuntulani, T. *Top. Curr. Chem.* **2005**, *255*, 163.
- (187) Beer, P. D.; Bayly, S. R. *Top. Curr. Chem.* **2005**, *255*, 125.
- (188) Callan, J. F.; de Silva, A. P.; Magria, D. C. *Tetrahedron* **2005**, *61*, 8551.
- (189) Fabbri, L.; Francese, G.; Lichelli, M.; Perotti, A.; Taglietti, A. *J. Chem. Soc., Chem. Commun.* **1997**, 581.
- (190) Fabbri, L.; Lichelli, M.; Rabaioli, G.; Taglietti, A. *Coord. Chem. Rev.* **2000**, *205*, 85.
- (191) Lakowicz, J. R. *Anal. Biochem.* **2001**, *298*, 1.
- (192) Pina, F.; Bernardo, M. A.; García-España, E. *Eur. J. Inorg. Chem.* **2000**, 2143.
- (193) Geue, J. P.; Head, N. J.; Ward, D.; Lincoln, S. F. *Dalton Trans.* **2003**, 521.
- (194) Xue, G.; Bradshaw, J. S.; Dalley, N. K.; Savage, P. B.; Izatt, R. M.; Prodi, L.; Montalti, M.; Zaccaroni, N. *Tetrahedron* **2002**, *58*, 4809.
- (195) Kim, S. K.; Lee, J. H.; Yoon, J. *Bull. Korean Chem. Soc.* **2003**, *24*, 1032.
- (196) Klein, G.; Kaufmann, D.; Schuerch, S.; Reymond, J.-L. *J. Chem. Soc., Chem. Commun.* **2001**.
- (197) Beltramello, M.; Gatos, M.; Mancin, F.; Tecilla, P.; Tonellato, U. *Tetrahedron Lett.* **2001**, *42*, 9143.
- (198) Sauer, M. *Angew. Chem., Int. Ed.* **2003**, *42*, 1790.
- (199) Diaz-Fernandez, Y.; Foti, F.; Mangano, C.; Pallavicini, P.; Patroni, S.; Perez-Gramatges, A.; Rodriguez-Calvo, S. *Chem. Eur. J.* **2006**, *12*, 921.
- (200) Ogoshi, T.; Takashima, Y.; Yamaguchi, H.; Harada, A. *Chem. Commun.* **2006**, 3702.
- (201) Kirkbright, G. F. In *Indicators*; Pergamon: Oxford, U.K., 1972.
- (202) Ros-Lis, J. V.; Martínez-Máñez, R.; Rurack, K.; Salcenón, F.; Soto, J.; Spieles, M. *Inorg. Chem.* **2004**, *43*, 5183.
- (203) Huang, J.-H.; Wen, W.-H.; Sun, Y.-Y.; Chou, P.-T.; Fang, J.-M. *J. Org. Chem.* **2005**, *70*, 5827.
- (204) Ajayaghosh, A.; Arunkumar, E.; Daub, J. *Angew. Chem., Int. Ed.* **2002**, *41*, 1766.
- (205) Arunkumar, E.; Chithra, P.; Ajayaghosh, A. *J. Am. Chem. Soc.* **2004**, *126*, 6590.
- (206) Ajayaghosh, A. *Acc. Chem. Res.* **2005**, *38*, 449.
- (207) Arunkumar, E.; Ajayaghosh, A.; Daub, J. *J. Am. Chem. Soc.* **2005**, *127*, 3156.
- (208) Marsella, M. J.; Swager, T. M. *J. Am. Chem. Soc.* **1993**, *115*, 12214.
- (209) Crawford, K. B.; Goldfinger, M. B.; Swager, T. M. *J. Am. Chem. Soc.* **1998**, *120*, 5187.
- (210) Kim, J.; McQuade, D. T.; McHugh, S. K.; Swager, T. M. *Angew. Chem., Int. Ed.* **2000**, *39*, 3868.
- (211) Boldea, A.; Lévesque, I.; Leclerc, M. *J. Mater. Chem.* **1999**, *9*, 2133.
- (212) Linert, W.; Fukuda, Y.; Camard, A. *Coord. Chem. Rev.* **2001**, *218*, 113.
- (213) Gunnlaugsson, T.; Leonard, J. P. *Chem. Commun.* **2005**, 3114.
- (214) Gunnlaugsson, T.; Leonard, J. P.; Sénéchal, K.; Harte, A. J. *J. Am. Chem. Soc.* **2003**, *125*, 12062.
- (215) de Silva, A. P.; Gunaratne, H. Q. N.; Rise, T. E.; Stewart, S. *Chem. Commun.* **1997**, 1891.
- (216) Tomasulo, M.; Yildiz, I.; Raymo, F. M. *J. Phys. Chem. B* **2006**, *110*, 3853.
- (217) Snee, P. T.; Somers, R. C.; Nair, G.; Zimmer, J. P.; Bawendi, M. G.; Nocera, D. C. *J. Am. Chem. Soc.* **2006**, *128*, 3146.
- (218) Chen, C.-Y.; Cheng, C.-T.; Lai, C.-W.; Wu, P.-W.; Wu, K.-C.; Chou, P.-T.; Chou, Y.-H.; Chiu, H.-T. *Chem. Commun.* **2006**, 263.
- (219) Pradhan, S.; Ghosh, D.; Xu, L.-P.; Chen, S. *J. Am. Chem. Soc.* **2007**, *129*, 10622.
- (220) Kubo, Y.; Yamamoto, M.; Ikeda, M.; Takeuchi, M.; Shinkai, S.; Yamaguchi, S.; Tamao, K. *Angew. Chem., Int. Ed.* **2003**, *42*, 2036.
- (221) Azov, V. A.; Schlegel, A.; Diederich, F. *Angew. Chem., Int. Ed.* **2005**, *44*, 4635.
- (222) Kameta, N.; Nagawa, Y.; Karikomi, M.; Hiratani, K. *Chem. Commun.* **2006**, 3714.
- (223) Paszyc, S. *Introduction to Photochemistry (in Polish)*; Wydawnictwo Naukowe PWN: Warszawa, Poland, 1992.
- (224) Balzani, V.; Gómez-López; Stoddart, J. F. *Acc. Chem. Res.* **1998**, *31*, 405.
- (225) Balzani, V.; Credi, A.; Raymo, F. M.; Stoddart, J. F. *Angew. Chem., Int. Ed.* **2000**, *39*, 3348.
- (226) Liu, J.; Gómez-Kaifer, M.; Kaifer, A. E. *Struct. Bonding (Berlin)* **2001**, *99*, 141.
- (227) Yen, M.-L.; Li, W.-S.; Lai, C.-C.; Chao, I.; Chiu, S.-H. *Org. Lett.* **2006**, *8*, 3223.
- (228) Leray, I.; O'Reilly, F.; Jiwan, J.-L. H.; Soumillon, J.-P.; Valeur, B. *Chem. Commun.* **1999**, 795.
- (229) Albelda, M. T.; Bernardo, M. A.; Díaz, P.; García-España, E.; Seixas de Melo, J.; Pina, F.; Soriano, C.; Luis, S. V. *Chem. Commun.* **2001**, 1520.
- (230) Shiraishi, Y.; Tokitoh, Y.; Nishimura, G.; Hirai, T. *J. Phys. Chem. B* **2007**, *111*, 5090.
- (231) Fujimoto, K.; Shimizu, H.; Inouye, M. *J. Org. Chem.* **2004**, *69*, 3271.
- (232) Brea, R. J.; Vazquez, M. E.; Mosquera, M.; Castedo, L.; Granja, J. R. *J. Am. Chem. Soc.* **2007**, *129*, 1653.
- (233) Elizarov, A. M.; Chiu, S.-H.; Stoddart, J. F. *J. Org. Chem.* **2002**, *67*, 9175.
- (234) Liang, L.; Okano, J.; Orita, A.; Otera, J. *Angew. Chem., Int. Ed.* **2004**, *43*, 2121.
- (235) Badjic, J. D.; Balzani, V.; Credi, A.; Silvi, S.; Stoddart, J. F. *Science* **2004**, *303*, 1845.

- (236) Badjic, J. D.; Serroni, C. M.; Stoddart, J. F.; Balzani, V.; Credi, A. *J. Am. Chem. Soc.* **2006**, *128*, 1489.
- (237) Balzani, V.; Credi, A.; Langford, S. J.; Raymo, F. M.; Stoddart, J. F.; Venturi, M. *J. Am. Chem. Soc.* **2000**, *122*, 3542.
- (238) Kim, K. *Chem. Soc. Rev.* **2002**, *31*, 96.
- (239) Sindelar, V.; Silvi, S.; Kaifer, A. E. *Chem. Commun.* **2006**, 2185.
- (240) Jun, S. I.; Lee, J. W.; Sakamoto, S.; Yamaguchi, K.; Kim, K. *Tetrahedron Lett.* **2000**, *41*, 471.
- (241) Lagona, J.; Mukhopadhyay, P.; Chakrabarti, S.; Isaacs, L. *Angew. Chem., Int. Ed.* **2005**, *44*, 4844.
- (242) Harada, A. *Acc. Chem. Res.* **2001**, *34*, 456.
- (243) Wenz, G.; Han, B.-H.; Müller, A. *Chem. Rev.* **2006**, *106*, 782.
- (244) Baylor, D. *Proc. Natl. Acad. Sci. U.S.A.* **1996**, *93*, 560.
- (245) Hampp, N. *Chem. Rev.* **2000**, *100*, 1755.
- (246) Pandley, P. C. *Anal. Chim. Acta* **2006**, *586*, 47.
- (247) Feringa, B. L.; van Delden, R. A.; Koumura, N.; Geertsema, E. M. *Chem. Rev.* **2000**, *100*, 1789.
- (248) Feringa, B. L. *Acc. Chem. Res.* **2001**, *34*, 504.
- (249) Feringa, B. L.; Koumura, N.; van Delden, R. A.; ter Wiel, M. K. J. *Appl. Phys. A* **2002**, *75*, 301.
- (250) Altoè, P.; Bernardi, F.; Conti, I.; Garavelli, M.; Negri, F.; Orlandi, G. *Theor. Chem. Acc.* **2007**, *117*, 1041.
- (251) Shibaev, V.; Bobrovsky, A.; Boiko, N. *Prog. Polym. Sci.* **2003**, *28*, 729.
- (252) Ichimura, K. *Chem. Rev.* **2000**, *100*, 1847.
- (253) Yerushalmi, R.; Scherz, A.; van der Boom, M. E.; Kraatz, H.-B. *J. Mater. Chem.* **2005**, *15*, 4480.
- (254) Pieroni, O.; Fissi, A.; Angelini, N.; Lenci, F. *Acc. Chem. Res.* **2001**, *34*, 9.
- (255) Conti, I.; Marchioni, F.; Credi, A.; Orlandi, G.; Rosini, G.; Garavelli, M. *J. Am. Chem. Soc.* **2007**, *129*, 3198.
- (256) Murakami, H.; Kawabuchi, A.; Kotoo, K.; Kunitake, M.; Nakashima, N. *J. Am. Chem. Soc.* **1997**, *119*, 7605.
- (257) Tsuda, S.; Aso, Y.; Kaneda, T. *Chem. Commun.* **2006**, 3072.
- (258) Muraoka, T.; Kinbara, K.; Aida, T. *J. Am. Chem. Soc.* **2006**, *128*, 11600.
- (259) Qu, D.-H.; Wang, Q.-C.; Ren, J.; Tian, H. *Org. Lett.* **2004**, *6*, 2085.
- (260) Willner, B.; Pardo-Yissar, V.; Katz, E.; Ranjit, K. T. *J. Electroanal. Chem.* **2001**, *497*, 172.
- (261) Kume, S.; Kurihara, M.; Nishihara, H. *Inorg. Chem.* **2003**, *42*, 2194.
- (262) Kurihara, M.; Hirooka, A.; Kume, S.; Sugimoto, M.; Nishihara, H. *J. Am. Chem. Soc.* **2002**, *124*, 8800.
- (263) Kume, S.; Kurihara, M.; Nishihara, H. *Chem. Commun.* **2001**, 1656.
- (264) Tamai, N.; Masayaka, H. *Chem. Rev.* **2000**, *100*, 1875.
- (265) Rotkin, S. A.; Zharov, I. *Int. J. Nanosci.* **2002**, *1*, 347.
- (266) Gobbi, L.; Seiler, P.; Diederich, F.; Gramlich, V.; Boudon, C.; Gisselbrecht, J.-P.; Gross, M. *Helv. Chim. Acta* **2001**, *84*, 743.
- (267) De Waele, V.; Schmidhammer, U.; Mrozek, T.; Daub, J.; Riedle, E. *J. Am. Chem. Soc.* **2002**, *124*, 2438.
- (268) Irie, M. *Chem. Rev.* **2000**, *100*, 1685.
- (269) Matsuda, K.; Irie, M. *J. Photochem. Photobiol., C* **2004**, *5*, 169.
- (270) Berkovic, G.; Krongauz, V.; Weiss, V. *Chem. Rev.* **2000**, *100*, 1741.
- (271) Tomasulo, M.; Sortino, S.; White, A. J. P.; Raymo, F. M. *J. Org. Chem.* **2005**, *70*, 8180.
- (272) Tomasulo, M.; Sortino, S.; Raymo, F. M. *Org. Lett.* **2005**, *7*, 1109.
- (273) Jockusch, S.; Turro, N. J.; Blackburn, F. R. *J. Phys. Chem. A* **2002**, *106*, 9236.
- (274) Sheepwash, M. A. L.; Mitchell, R. H.; Bohne, C. J. *J. Am. Chem. Soc.* **2002**, *124*, 4693.
- (275) Yokoyama, Y. *Chem. Rev.* **2000**, *100*, 1717.
- (276) Raymo, F. M.; Tomasulo, M. *Chem. Soc. Rev.* **2005**, *34*, 327.
- (277) Raymo, F. M.; Tomasulo, M. *J. Phys. Chem. A* **2005**, *109*, 7343.
- (278) Kawai, T.; Kim, M.-S.; Sasaki, T.; Irie, M. *Opt. Mater.* **2002**, *21*, 275.
- (279) Takeshita, M.; Hayashi, M.; Kadota, S.; Mohammed, K. H.; Yamato, T. *Chem. Commun.* **2005**, 761.
- (280) Alifimov, M. V.; Fedorova, O. A.; Gromov, S. P. *J. Photochem. Photobiol., A* **2003**, *158*, 183.
- (281) Takeshita, M.; Irie, M. *Tetrahedron Lett.* **1998**, *39*, 613.
- (282) Frigoli, M.; Mehl, G. H. *Chem. Eur. J.* **2004**, *10*, 5234.
- (283) Morimoto, M.; Kobatake, S.; Irie, M. *J. Am. Chem. Soc.* **2003**, *127*, 11080.
- (284) Tanaka, M.; Ikeda, T.; Xu, Q.; Ando, H.; Shibutani, Y.; Nakamura, M.; Sakamoto, H.; Yajima, S.; Kimura, K. *J. Org. Chem.* **2002**, *67*, 2223.
- (285) Tanaka, M.; Kamada, K.; Ando, H.; Kitagaki, T.; Shibutani, Y.; Kimura, K. *J. Org. Chem.* **2000**, *65*, 4342.
- (286) Tian, H.; Qin, B.; Yao, R.; Zhao, X.; Yang, S. *Adv. Mater.* **2003**, *15*, 2104.
- (287) Mrozek, T.; Görner, H.; Daub, J. *Chem. Eur. J.* **2001**, *7*, 1028.
- (288) Myles, A. J.; Wigglesworth, T. J.; Branda, N. R. *Adv. Mater.* **2003**, *15*, 745.
- (289) Kawai, T.; Iseda, T.; Irie, M. *Chem. Commun.* **2004**, 72.
- (290) Liddell, P. A.; Kodis, G.; Moore, A. L.; Moore, T. A.; Gust, D. *J. Am. Chem. Soc.* **2002**, *124*, 7668.
- (291) Ramsteiner, I. B.; Hartschuh, A.; Port, H. *Chem. Phys. Lett.* **2001**, *343*, 83.
- (292) Straight, S. D.; Andreasson, J.; Kodis, G.; Moore, A. L.; Moore, T. A.; Gust, D. *J. Am. Chem. Soc.* **2005**, *127*, 2717.
- (293) Benniston, A. C. *Chem. Soc. Rev.* **2004**, *33*, 573.
- (294) Nešpùrek, S.; Toman, P.; Sworakowski, J.; Lipiński, J. *Curr. Appl. Phys.* **2002**, *2*, 299.
- (295) Nešpùrek, S.; Sworakowski, J.; Kadaschuk, A.; Toman, P. *J. Organomet. Chem.* **2003**, *685*, 269.
- (296) Toman, P.; Bartkowiak, W.; Nešpùrek, S.; Sworakowski, J.; Zaleny, R. *Chem. Phys.* **2005**, *316*, 267.
- (297) Kim, E.; Kim, M.; Kim, K. *Tetrahedron* **2006**, *62*, 6814.
- (298) Taniguchi, M.; Nojima, Y.; Yokota, K.; Terao, J.; Sato, K.; Kambe, N.; Kawai, T. *J. Am. Chem. Soc.* **2006**, *128*, 15062.
- (299) Ikeda, M.; Tanifuni, N.; Yamaguchi, H.; Irie, M.; Matsuda, K. *Chem. Commun.* **2007**, 1355.
- (300) Katsonis, N.; Kudernac, T.; Walko, M.; van der Molen, S. J.; van Wees, B. J.; Feringa, B. L. *Adv. Funct. Mater.* **2006**, *18*, 1397.
- (301) Whalley, A. C.; Steigerwald, M. L.; Guo, X.; Nuckolls, C. J. *J. Am. Chem. Soc.* **2007**, *129*, 12590.
- (302) Tanaka, Y.; Inagaki, A.; Akita, M. *Chem. Commun.* **2007**, 1169.
- (303) Staykov, A.; Nozaki, D.; Yashizawa, K. *J. Phys. Chem. C* **2007**, *111*, 3517.
- (304) Ashton, P.; Ballardini, R.; Balzani, V.; Credi, A.; Dress, K. R.; Ishow, E.; Kleverlaan, C. J.; Kocian, O.; Preece, J. A.; Spencer, N.; Stoddart, J. F.; Venturi, M.; Wenger, S. *Chem. Eur. J.* **2000**, *6*, 3558.
- (305) Clemente-León, M.; Marchioni, F.; Credi, A. *Synth. Met.* **2003**, *139*, 773.
- (306) Balzani, V.; Credi, A.; Venturi, M. *Pure Appl. Chem.* **2003**, *75*, 541.
- (307) Abraham, W.; Grubert, L.; Grummt, U. W.; Buck, K. *Chem. Eur. J.* **2004**, *10*, 3562.
- (308) Schmidt-Schäffer, S.; Grubert, L.; Grummt, U. W.; Buck, K.; Abraham, W. *Eur. J. Org. Chem.* **2006**, 378.
- (309) Balzani, V.; Credi, A.; Silvi, S.; Venturi, M. *Chem. Soc. Rev.* **2006**, *35*, 1135.
- (310) Credi, A. *Aust. J. Chem.* **2006**, *59*, 157.
- (311) Balzani, V.; Credi, A.; Venturi, M. *Proc. Natl. Acad. Sci. U.S.A.* **2002**, *99*, 4814.
- (312) Ashton, P.; Balzani, V.; Kocian, O.; Prodi, L.; Spencer, N.; Stoddart, J. F. *J. Am. Chem. Soc.* **1998**, *120*, 11190.
- (313) Winzer, P. *J. Elektrotechnik & Informationsstechnik* **2007**, *124*, 169.
- (314) Nijhuis, C. A.; Ravoo, B. J.; Huskens, J.; Reinhoudt, D. N. *Coord. Chem. Rev.* **2007**, *251*, 1761.
- (315) Kalny, D.; Elhabiri, M.; Moav, T.; Vaskevich, A.; Rubinstein, I.; Shanzer, A.; Albrecht-Gary, A.-M. *Chem. Commun.* **2002**, 1426.
- (316) Chambron, J.-C.; Collin, J.-P.; Dalbavie, J.-O.; Diederich-Buchecker, C. O.; Heitz, V.; Odobel, F.; Soddadié, N.; Sauvage, J.-P. *Coord. Chem. Rev.* **1998**, *178-180*, 1299.
- (317) Jimenez-Molero, M. C.; Dietrich-Buchecker, C.; Sauvage, J.-P. *Chem. Commun.* **2003**, 1613.
- (318) Collier, C. P.; Wong, E. W.; Belohradsky, M.; Raymo, F. M.; Stoddart, J. F.; Kuekes, P. J.; Heath, R. S. W. *R. Science* **1999**, *285*, 391.
- (319) Chen, Y.; Ohlberg, D. A. A.; Li, X.; Stewart, D. R.; Williams, S. *Appl. Phys. Lett.* **2003**, *82*, 1610.
- (320) Mendes, P. M.; Flood, A. H.; Stoddart, J. F. *Appl. Phys. A* **2005**, *80*, 1197.
- (321) Collier, C. P.; Jeppensen, J. O.; Luo, Y.; Perkins, J.; Wong, E. W.; Heath, J. R.; Stoddart, J. F. *J. Am. Chem. Soc.* **2001**, *123*, 12632.
- (322) Collier, C. P.; Mattersteig, G.; Wong, E. W.; Luo, Y.; Beverly, K.; Raymo, F. M.; Stoddart, J. F.; Heath, J. R. *Science* **2000**, *289*, 1172.
- (323) Yu, H.; Luo, Y.; Beverly, K.; Stoddart, J. F.; Tseng, H.-R.; Heath, J. R. *Angew. Chem., Int. Ed.* **2003**, *42*, 5706.
- (324) Kim, Y.-H.; Goddard III, W. A. *J. Phys. Chem. C* **2007**, *111*, 4831.
- (325) Feng, M.; Gao, L.; Du, S.; Deng, Z.; Cheng, Z.; Ji, W.; Zhang, D.; Guo, X.; Lin, X.; Chi, L.; Zhu, D.; Fuchs, H.; Gao, H. *Adv. Funct. Mater.* **2007**, *17*, 770.
- (326) Willner, I.; Basnar, B.; Willner, B. *Adv. Funct. Mater.* **2007**, *17*, 702.
- (327) Star, A.; Steuerman, D. W.; Heath, J. R.; Stoddart, J. F. *Angew. Chem., Int. Ed.* **2002**, *41*, 2508.
- (328) Star, A.; Liu, Y.; Grant, K.; Ridvan, L.; Stoddart, J. F.; Steuerman, D. W.; Diehl, M. R.; Boukai, A.; Heath, J. R. *Macromolecules* **2003**, *36*, 553.
- (329) Diehl, M. R.; Steuerman, D. W.; Tseng, H.-R.; Vignon, S. A.; Star, A.; Celestre, P. C.; Stoddart, J. F.; Heath, J. R. *ChemPhysChem* **2003**, *4*, 1335.
- (330) Luo, Y.; Collier, C. P.; Jeppesen, J. O.; Nielsen, K. A.; Delonno, E.; Ho, G.; Perkins, J.; Tseng, H.-R.; Yamamoto, T.; Stoddart, J. F.; Heath, J. R. *ChemPhysChem* **2002**, *3*, 519.

- (331) Chen, Y.; Jung, G.-Y.; Ohleberg, D. A. A.; Li, X.; Stewart, D. R.; Jeppesen, J. O.; Nielsen, K. A.; Stoddart, J. F.; Williams, R. S. *Nanotechnology* **2003**, *14*, 462.
- (332) Saha, S.; Johansson, E.; Flood, A. H.; Tseng, H.-R.; Zink, J. I.; Stoddart, J. F. *Chem. Eur. J.* **2005**, *11*, 6846.
- (333) Bach, U.; Lupo, D.; Comte, P.; Moser, J. E.; Weissortel, F.; Salbeck, J.; Spreitzer, H.; Grätzel, M. *Nature* **1998**, *395*, 583.
- (334) Moser, J. E.; Bonnote, P.; Grätzel, M. *Coord. Chem. Rev.* **1998**, *171*, 245.
- (335) Saha, S.; Flood, A. H.; Stoddart, J. F.; Impellizzeri, S.; Silvi, S.; Venturi, M.; Credi, A. *J. Am. Chem. Soc.* **2007**, *129*, 12159.
- (336) Browne, W. R.; de Jong, J. J. D.; Kudernac, T.; Walko, M.; Lucas, L. N.; Uchida, K.; van Esch, J. H.; Feringa, B. L. *Chem. Eur. J.* **2005**, *11*, 6414.
- (337) Browne, W. R.; de Jong, J. J. D.; Kudernac, T.; Walko, M.; Lucas, L. N.; Uchida, K.; van Esch, J. H.; Feringa, B. L. *Chem. Eur. J.* **2005**, *11*, 6430.
- (338) Guirado, G.; Coudret, C.; Launay, J.-P. *J. Phys. Chem. C* **2007**, *111*, 2770.
- (339) Gorodetsky, B.; Branda, N. R. *Adv. Funct. Mater.* **2007**, *17*, 786.
- (340) Wagner, R. W.; Lindsey, J. S.; Seth, J.; Palaniappan, V.; Bocian, D. F. *J. Am. Chem. Soc.* **1996**, *118*, 3996.
- (341) Lammi, R. K.; Wagner, R. W.; Ambroise, A.; Diers, J. R.; Bocian, D. F.; Holten, D.; Lindsey, J. S. *J. Phys. Chem. B* **2001**, *105*, 5341.
- (342) Ambroise, A.; Wagner, R. W.; Dharma Rao, P.; Riggs, J. A.; Hascoat, P.; Diers, J. R.; Seth, J.; Lammi, R. K.; Bocian, D. F.; Holten, D.; Lindsey, J. S. *Chem. Mater.* **2001**, *13*, 1023.
- (343) Bonhôte, P.; Gogniat, E.; Campus, F.; Walder, L.; Grätzel, M. *Displays* **1999**, *20*, 137.
- (344) Sonmez, G. *Chem. Commun.* **2005**, 5251.
- (345) Menon, A. K.; Gupta, B. K. *NanoStructured Mater.* **1999**, *11*, 965.
- (346) Menon, A. K.; Gupta, B. K. *NanoStructured Mater.* **1999**, *12*, 1117.
- (347) *Magnetism: Molecules to Materials I: Models and Experiments*; Miller, J. S.; Drillon, M., Eds.; Viley-VCH: Weinheim, Germany, 2002.
- (348) *Magnetism: Molecules to Materials II: Molecule-Based Materials*; Miller, J. S.; Drillon, M., Eds.; Viley-VCH: Weinheim, Germany, 2002.
- (349) *Magnetism: Molecules to Materials III. Nanosized Magnetic Materials*; Miller, J. S.; Drillon, M., Eds.; Viley-VCH: Weinheim, Germany, 2002.
- (350) *Magnetism: Molecules to Materials IV. Nanosized Magnetic Materials*; Miller, J. S.; Drillon, M., Eds.; Viley-VCH: Weinheim, Germany, 2002.
- (351) Létard, J.-F.; Guionneau, P.; Goux-Capes, L. *Top. Curr. Chem.* **2004**, *235*, 221.
- (352) *Spin Crossover in Transition Metal Compounds, in Topics in Current Chemistry*; Gütllich, P.; Goodwin, H. A., Eds., 2004; Vol. 233–235.
- (353) Bousseksou, A.; Molnár, G.; Real, J. A.; Tanaka, K. *Coord. Chem. Rev.* **2007**, *251*, 1822.
- (354) Przychodzeń, P.; Korzeniak, T.; Podgajny, R.; Sieklucka, B. *Coord. Chem. Rev.* **2006**, *250*, 2234.
- (355) Culp, J. T.; Park, J.-H.; Frye, F.; Huh, Y.-D.; Meisel, M. W.; Talham, D. R. *Coord. Chem. Rev.* **2006**, *249*, 2642.
- (356) Gaspar, A. B.; Ksenofontov, V.; Sereyuk, M.; Gütllich, P. *Coord. Chem. Rev.* **2005**, *249*, 2661.
- (357) Krivokapic, I.; Zerara, M.; Daku, M. L.; Vargas, A.; Enachescu, C.; Ambrusc, C.; Tregenna-Piggott, P.; Amstutz, N.; Kraus, E.; Hauser, A. *Coord. Chem. Rev.* **2007**, *251*, 364.
- (358) Hauser, A.; Enachescu, C.; Daku, M. L.; Vargas, A.; Amstutz, N. *Coord. Chem. Rev.* **2006**, *250*, 1642.
- (359) Sato, O.; Tao, J.; Zhang, Y.-Z. *Angew. Chem., Int. Ed.* **2007**, *46*, 2152.
- (360) Sato, O. *J. Photochem. Photobiol., C* **2004**, *5*, 203.
- (361) Einaga, Y. *J. Photochem. Photobiol., C* **2006**, *7*, 69.
- (362) Andruh, M. *Chem. Commun.* **2007**, 2565.
- (363) Gómez-Segura, J.; Veciana, J.; Ruiz-Molina, D. *Chem. Commun.* **2007**, 3699.
- (364) Gütllich, P.; Goodwin, H. A. In *Comprehensive Coordination Chemistry*; McCleverty, J. A., Meyer, T. J., Lever, A. B. P., Eds.; Elsevier, Ltd.: Amsterdam, 2003; Vol. II.
- (365) Hauser, A. *Top. Curr. Chem.* **2004**, *234*, 155.
- (366) Crayston, J. A.; Devine, J. N.; Walton, J. C. *Tetrahedron* **2000**, *56*, 7829.
- (367) Miller, J. S. *Dalton Trans.* **2006**, 2742.
- (368) Larionova, J.; Willemijn, S.; Dannadieu, B.; Henner, B.; Guérin, C.; Gillon, B.; Goujon, A. *J. Phys. Chem. Solids* **2004**, *65*, 677.
- (369) Winpenny, R. E. P. In *Comprehensive Coordination Chemistry II*; McCleverty, J. A., Meyer, T. J., Fujita, M., Powell, A., Creutz, C., Eds.; Elsevier: Amsterdam, 2003; Vol. 9.
- (370) Pilkington, M.; Decurtis, S. In *Comprehensive Coordination Chemistry II*; McCleverty, J. A., Meyer, T. J., Fujita, M., Powell, A., Creutz, C., Eds.; Elsevier: Amsterdam, 2003; Vol. 9.
- (371) Kitagawa, S.; Noro, S. In *Comprehensive Coordination Chemistry II*; McCleverty, J. A., Meyer, T. J., Fujita, M., Powell, A., Creutz, C., Eds.; Elsevier: Amsterdam, 2003; Vol. 9.
- (372) Real, J. A.; Gaspar, A. B.; Niel, V.; Munoz, M. C. *Coord. Chem. Rev.* **2003**, *236*, 121.
- (373) Escax, V.; Bleuzen, A.; Cartier dit Moulin, C.; Villain, F.; Goujon, A.; Varret, F.; Verdaguer, M. *J. Am. Chem. Soc.* **2001**, *123*, 12536.
- (374) Ohkoshi, S.; Machida, N.; Zhong, Z. J.; Hashimoto, K. *Synth. Met.* **2001**, *122*, 523.
- (375) Evangelio, E.; Ruiz-Molina, D. *Eur. J. Inorg. Chem.* **2005**, 2957.
- (376) Hendrickson, D. N.; Pierpont, C. G. *Top. Curr. Chem.* **2004**, *234*, 63.
- (377) Dei, A.; Gatteschi, D.; Sangregorio, C.; Sorace, L. *Acc. Chem. Res.* **2004**, *37*, 827.
- (378) Boillot, M.-L.; Zarembowitch, J.; Sour, A. *Top. Curr. Chem.* **2004**, *234*, 261.
- (379) Negre, N.; Goiran, M.; Bousseksou, A.; Haasnoot, J.; Boukheddaden, K.; Askenazy, S.; Varret, F. *Synth. Met.* **2000**, *115*, 289.
- (380) Brusso, J. L.; Clements, O. P.; Haddon, R. C.; Itkis, M. I.; Leitch, A. A.; Oakley, R. T.; Reed, R. W.; Richardson, J. F. *J. Am. Chem. Soc.* **2004**, *126*, 14692.
- (381) Matsuda, K.; Irie, M. *J. Am. Chem. Soc.* **2000**, *122*, 8309.
- (382) Matsuda, K.; Irie, M. *Polyhedron* **2001**, *20*, 1391.
- (383) Mitchel, R. H.; Ward, T. R.; Wang, Y.; Debbie, P. W. *J. Am. Chem. Soc.* **1999**, *121*, 2601.
- (384) Gobbi, L.; Seiler, P.; Diederich, F. *Angew. Chem., Int. Ed.* **1999**, *38*, 674.
- (385) Nielsen, M. B.; Diederich, F. *Chem. Rev.* **2005**, *105*, 1837.
- (386) Guo, X.; Zhang, D.; Zhu, D. *J. Phys. Chem. B* **2004**, *108*, 12.
- (387) Ohsumi, M.; Fukaminato, T.; Irie, M. *Chem. Commun.* **2005**, 3921.
- (388) Zhou, Y.; Zhang, D.; Zhu, L.; Shuai, Z.; Zhu, D. *J. Org. Chem.* **2006**, *71*, 2123.
- (389) Ziganshina, A. Y.; Ko, Y. H.; Jeon, S. W.; Kim, K. *Chem. Commun.* **2004**, 806.
- (390) Ashton, P. R.; Balzani, V.; Becher, J.; Credi, A.; Fyfe, M. C. T.; Matternsteig, G.; Menzer, S.; Nielsen, M. B.; Raymo, F. M.; Stoddart, J. F.; Venturi, M.; Williams, D. J. *J. Am. Chem. Soc.* **1999**, *121*, 3951.
- (391) Yamazaki, T.; Murata, Y.; Komatsu, K.; Furukawa, K.; Morita, M.; Maruyama, N.; Yamao, T.; Fujita, S. *Org. Lett.* **2004**, *6*, 4865.
- (392) Sporer, C.; Ratera, I.; Ruiz-Molina, D.; Zhao, Y.; Vidal-Gancedo, J.; Wurst, K.; Jaitner, P.; Clays, K.; Persoons, A.; Rovira, C.; Veciana, J. *Angew. Chem., Int. Ed.* **2004**, *43*, 5266.
- (393) Anelli, P. L.; Ashton, P. R.; Ballardini, R.; Balzani, V.; Delgado, M.; Gandolfi, M. T.; Goodnow, T. T.; Kaifer, A. E.; Philp, D.; Pietraszkiewicz, M.; Prodi, L.; Reddington, M. V.; Slawin, A. M. Z.; Spencer, N.; Stoddart, J. F.; Vicent, C.; Williams, D. J. *J. Am. Chem. Soc.* **1992**, *114*, 193.
- (394) Huston, M. E.; Akkaya, E. U.; Czarnik, A. W. *J. Am. Chem. Soc.* **1989**, *111*, 8735.
- (395) de Silva, A. P.; de Silva, S. A.; Dissanayake, A. S.; Sandanayake, K. R. A. S. *J. Chem. Soc., Chem. Commun.* **1989**, 1054.
- (396) de Silva, A. P.; Sandanayake, K. R. A. S. *J. Chem. Soc., Chem. Commun.* **1989**, 1183.
- (397) Hosseini, M. W.; Blacker, A. J.; Lehn, J. M. *J. Am. Chem. Soc.* **1990**, *112*, 3896.
- (398) de Silva, A. P.; Gunaratne, H. Q. N.; Maguire, G. E. M. *J. Chem. Soc., Chem. Commun.* **1994**, 1213.
- (399) Ghosh, P.; Gharadway, P. K.; Roy, J.; Ghosh, S. *J. Am. Chem. Soc.* **1997**, *119*, 11903.
- (400) McSkimming, G.; Tucker, J. H. R.; Bouas-Laurent, H.; Desvergne, J.-P. *Angew. Chem., Int. Ed.* **2000**, *39*, 2167.
- (401) de Silva, A. P.; Gunaratne, H. Q. N.; McCoy, C. P. *J. Am. Chem. Soc.* **1997**, *119*, 7891.
- (402) de Silva, A. P.; Sandanayake, K. R. A. S. *Angew. Chem., Int. Ed.*, *Engl.* **1990**, *29*, 1173.
- (403) Czarnik, A. W. *ACS Symp. Ser.* **1994**, *561*, 314.
- (404) James, T. D.; Sandanayake, K. R. A. S.; Shinkai, S. *Angew. Chem., Int. Ed., Engl.* **1994**, *33*, 2207.
- (405) Uchiyama, S.; McClean, G. D.; Iwai, K.; de Silva, A. P. *J. Am. Chem. Soc.* **2005**, *127*, 8920.
- (406) Callan, J. F.; de Silva, A. P.; McClenaghan, N. D. *Chem. Commun.* **2004**, 2048.
- (407) Ji, H.-F.; Dabestani, R.; Brown, G. M. *J. Am. Chem. Soc.* **2000**, *122*, 9306.
- (408) Sadhu, K. K.; Bag, B.; Bharadwaj, P. K. *J. Photochem. Photobiol., A* **2007**, *185*, 231.
- (409) Koskela, S. J. M.; Fyles, T. M.; James, T. D. *Chem. Commun.* **2005**, 945.
- (410) de Silva, A. P.; McClean, G. D.; Pagliari, S. *Chem. Commun.* **2003**, 2010.
- (411) Lankshear, M. D.; Cowley, A. R.; Beer, P. D. *Chem. Commun.* **2006**, 612.

- (412) Magri, D. C.; Brown, G. J.; McClean, G. D.; de Silva, A. P. *J. Am. Chem. Soc.* **2006**, *128*, 4950.
- (413) Zhang, G.; Zhang, D.; Zhou, Y.; Zhu, D. *J. Org. Chem.* **2006**, *71*, 3970.
- (414) Wang, H.; Zhang, D.; Guo, X.; Zhu, L.; Shuai, Z.; Zhu, D. *Chem. Commun.* **2004**, 670.
- (415) Blough, N. V.; Simpson, D. J. *J. Am. Chem. Soc.* **1988**, 110.
- (416) Kumar, S.; Singh, P.; Kaur, S. *Tetrahedron* **2007**, *63*, 11724.
- (417) Szaciłowski, K.; Stochel, G.; Stasicka, Z.; Kisch, H. *New J. Chem.* **1997**, *21*, 893.
- (418) Credi, A.; Balzani, V.; Langford, S. J.; Stoddart, J. F. *J. Am. Chem. Soc.* **1997**, *119*, 2679.
- (419) Bergamini, G.; Saudan, C.; Ceroni, P.; Maestri, M.; Balzani, V.; Gorka, M.; Lee, S.-K.; van Heyst, J.; Vögtle, F. *J. Am. Chem. Soc.* **2004**, *126*, 16466.
- (420) Ward, M. D. *Coord. Chem. Rev.* **2006**, *250*, 3128.
- (421) Han, M.-J.; Gao, L.-H.; Lü, Y.-Y.; Wang, K.-Z. *J. Phys. Chem. B* **2006**, *110*, 2364.
- (422) Gao, F.; Chao, H.; Zhou, F.; Beng, B.; Ji, L.-N. *Inorg. Chem. Commun.* **2007**, *10*, 170.
- (423) de Silva, A. P.; Gunaratne, H. Q. N.; McCoy, C. P. *Chem. Commun.* **1996**, 2399.
- (424) de Silva, S. A.; Loo, K. C.; Amorelli, B.; Pathirana, S. L.; Nyakirang'ani, M.; Dharmasena, M.; Demarais, S.; Dorcley, B.; Pullay, P.; Salih, Y. A. *J. Mater. Chem.* **2005**, *15*, 2791.
- (425) Li, Y.; Zheng, H.; Li, Y.; Wang, S.; Wu, Z.; Liu, P.; Gao, Z.; Liu, H.; Zhu, D. *J. Org. Chem.* **2007**, *72*, 2878.
- (426) de Silva, A. P.; McClenaghan, N. D. *Chem. Eur. J.* **2002**, *8*, 4935.
- (427) Miyaji, H.; Kim, H.-K.; Sim, E.-K.; Lee, C.-K.; Cho, W.-S.; Sessler, J. L.; Lee, C.-H. *J. Am. Chem. Soc.* **2005**, *127*, 12510.
- (428) Montenegro, J.-M.; Perez-Inestrosa, E.; Collado, D.; Vida, Y.; Suau, R. *Org. Lett.* **2004**, *6*, 2353.
- (429) Miyaji, H.; Collinson, S. R.; Prokes, I.; Tucker, J. H. R. *Chem. Commun.* **2003**, 64.
- (430) Gunnlaugsson, T.; Mac Dónaill, D. A. *Chem. Commun.* **2000**, 93.
- (431) Gunnlaugsson, T.; Mac Dónaill, D. A.; Parker, D. J. *J. Am. Chem. Soc.* **2001**, *123*, 12866.
- (432) Nishimura, G.; Ishizumi, K.; Shirakashi, Y.; Hirai, T. *J. Phys. Chem. B* **2006**, *110*, 21596.
- (433) de Sousa, M.; Kluciar, M.; Abad, S.; Miranda, M. A.; de Castro, B.; Pischel, U. *Photochem. Photobiol. Sci.* **2004**, *3*, 639.
- (434) Park, M. S.; Swamy, K. M. K.; Lee, Y. J.; Lee, H. N.; Jang, Y. J.; Moon, Y. H.; Moon, J. *Tetrahedron Lett.* **2006**, *47*, 8129.
- (435) de Silva, A. P.; Dixon, I. M.; Gunaratne, H. Q. N.; Gunnlaugsson, T.; Maxwell, P. R. S.; Rice, T. E. *J. Am. Chem. Soc.* **1999**, *121*, 1393.
- (436) Leigh, D. A.; Morales, M. A. F.; Pérez, E. M.; Wong, J. K. Y.; Saiz, C. G.; Slawin, A. M. Z.; Carmichael, A. J.; Haddleton, D. M.; Brouwer, A. M.; Buma, W. J.; Wülpel, G. W. H.; León, S.; Zerbetto, F. *Angew. Chem., Int. Ed.* **2005**, *44*, 3062.
- (437) Wang, Z.; Zheng, G.; Lu, P. *Org. Lett.* **2005**, *7*, 3669.
- (438) Parker, D.; Williams, J. A. G. *Chem. Commun.* **1998**, 245.
- (439) Iwata, S.; Tanaka, K. *J. Chem. Soc., Chem. Commun.* **1995**, 1491.
- (440) Baytekin, H. T.; Akkaya, E. U. *Org. Lett.* **2000**, *2*, 1725.
- (441) Chiang, P. T.; Cheng, P.-N.; Lin, C.-F.; Liu, Y.-H.; Lai, C.-C.; Peng, S.-M.; Chiu, S.-H. *Chem. Eur. J.* **2006**, *12*, 865.
- (442) Zong, G.; Xian, L.; Lu, G. *Tetrahedron* **2007**, *48*, 3891.
- (443) Becker, J.; Hartenstein, R. *J. Systems Arch.* **2003**, *49*, 127.
- (444) Lee, S. H.; Kim, J. Y.; Kim, S. K.; Lee, J. H.; Kim, J. S. *Tetrahedron* **2004**, *60*, 5171.
- (445) Alves, S.; Pina, F.; Albelda, M. T.; Garcia-Espana, E.; Soriano, C.; Luis, S. V. *Eur. J. Inorg. Chem.* **2001**, 405.
- (446) Shiraishi, Y.; Tokitoh, Y.; Hirai, T. *Chem. Commun.* **2005**, 5316.
- (447) Rurack, K.; Koval'chuck, A.; Bricks, J. L.; Slominskii, J. L. *J. Am. Chem. Soc.* **2001**, *123*, 6205.
- (448) Petitjean, A.; Kyritsakas, N.; Lehn, J.-M. *Chem. Eur. J.* **2005**, *11*, 6818.
- (449) Straight, S. D.; Andreasson, J.; Kodis, G.; Bandyopadhyay, S.; Mitchell, R. H.; Moore, T. A.; Moore, A. L.; Gust, D. *J. Am. Chem. Soc.* **2005**, *127*, 9403.
- (450) Raymo, F. M.; Tomasulo, M. *Chem. Eur. J.* **2006**, *12*, 3186.
- (451) Straight, S. D.; Liddell, P. A.; Terazono, Y.; Moore, T. A.; Moore, A. L.; Gust, D. *Adv. Funct. Mater.* **2007**, *17*, 777.
- (452) Andreasson, J.; Straight, S. D.; Bandyopadhyay, S.; Mitchell, R. H.; Moore, T. A.; Moore, A. L.; Gust, D. *J. Phys. Chem. C* **2007**, *111*, 14274.
- (453) Andreasson, J.; Straight, S. D.; Bandyopadhyay, S.; Mitchell, R. H.; Moore, T. A.; Moore, A. L.; Gust, D. *Angew. Chem., Int. Ed.* **2007**, *46*, 958.
- (454) Kompa, K. L.; Levine, R. D. *Proc. Natl. Acad. Sci. U.S.A.* **2001**, *98*, 410.
- (455) Witte, T.; Bucher, C.; Remacle, F.; Proch, D.; Kompa, K. L.; Levine, R. D. *Angew. Chem., Int. Ed.* **2001**, *40*, 2512.
- (456) Lukas, A. S.; Bushard, P. J.; Wasielewski, M. R. *J. Am. Chem. Soc.* **2001**, *123*, 2440.
- (457) Essen, L.-O.; Siegert, R.; Lehmann, W. D.; Oesterheld, D. *Proc. Natl. Acad. Sci. U.S.A.* **1998**, *95*, 11673.
- (458) Masthay, M. B.; Sammeth, D. M.; M.C., H.; Buckman, C. B.; Li, W.; Cde-Baca, M. J.; Kofron, J. T. *J. Am. Chem. Soc.* **2002**, *124*, 3418.
- (459) Padney, P. C. *Anal. Chim. Acta* **2006**, *568*, 47.
- (460) Kulcsár, A.; Saltiel, J.; Zimányi, L. *J. Am. Chem. Soc.* **2001**, *123*, 3332.
- (461) Birge, R. R.; Gillespie, N. B.; Izaguirre, E. W.; Kusnetzow, A.; Lawrence, A. F.; Singh, D.; Song, Q. W.; Schmidt, E.; Stuart, J. A.; Seetharaman, S.; Wise, K. J. *J. Phys. Chem. B* **1999**, *103*, 10746.
- (462) Singh, C. P.; Roy, S. *Curr. Appl. Phys.* **2003**, *3*, 163.
- (463) Singh, C. P.; Kulshreshtha, K.; Roy, S. *Optik* **2006**, *117*, 499.
- (464) Rao, D. V. G. L. N.; Aranda, F. J.; Rao, D. N.; Chen, Z.; Akkara, J. A.; Kaplan, D. L.; Nakashima, M. *Opt. Commun.* **1996**, *127*, 193.
- (465) Yang, X.; Zhang, C.; Qi, S.; Chen, K.; Tian, J.; Zhang, G. *Optik* **2005**, *116*, 251.
- (466) Nilsson, D.; Robinson, N.; Berggren; Forchheimer, R. *Adv. Mater.* **2005**, *17*, 353.
- (467) Zhan, W.; Crooks, R. M. *J. Am. Chem. Soc.* **2003**, *125*, 9934.
- (468) Amatore, C.; Thouin, L.; Warkocz, J.-S. *Chem. Eur. J.* **1999**, *5*, 456.
- (469) Matsui, J.; Mitsuishi, M.; Aoki, A.; Miyashita, T. *Angew. Chem., Int. Ed.* **2003**, *42*, 2272.
- (470) Matsui, J.; Mitsuishi, M.; Aoki, A.; Miyashita, T. *J. Am. Chem. Soc.* **2004**, *126*, 3708.
- (471) Yasutomi, S.; Morita, T.; Imanishi, Y.; Kimura, S. *Science* **2004**, *304*, 1944.
- (472) Mandal, H. S.; Burgess, I. J.; Kraatz, H.-B. *Chem. Commun.* **2006**, 4802.
- (473) Nitahara, S.; Akiyama, T.; Inoue, S.; Yamada, S. *J. Phys. Chem. B* **2005**, *109*, 3944.
- (474) Nitahara, S.; Tasaki, N.; Akiyama, T.; Yamada, S. *Thin Solid Films* **2006**, *499*, 354.
- (475) Hebda, M.; Stochel, G.; Szaciłowski, K.; Macyk, W. *J. Phys. Chem. B* **2006**, *110*, 15275.
- (476) Szaciłowski, K.; Macyk, W. *Solid-State Electron* **2006**, *50*, 1649.
- (477) Szaciłowski, K.; Macyk, W.; Hebda, M.; Stochel, G. *ChemPhysChem* **2006**, *7*, 2384.
- (478) Szaciłowski, K.; Macyk, W.; Stochel, G. *J. Mater. Chem.* **2006**, *16*, 4603.
- (479) Macyk, W.; Stochel, G.; Szaciłowski, K. *Chem. Eur. J.* **2007**, *13*, 5676.
- (480) Gawęda, S.; Stochel, G.; Szaciłowski, K. *Chem. Asian J.* **2007**, *2*, 580.
- (481) Gao, G.; Deng, Y.; Kispert, L. D. *J. Chem. Soc., Perkin Trans. 2* **1999**, 1225.
- (482) Harris, J. A.; Trotter, K.; Brunshwig, B. S. *J. Phys. Chem. B* **2007**, *111*, 6695.
- (483) Long, M.; Cai, W.; Kisch, H. *J. Phys. Chem. C* **2008**, *112*, 548.
- (484) Beránek, R.; Kisch, H. *Angew. Chem., Int. Ed.* **2008**, *47*, 1320.
- (485) de Tacconi, N. R.; Chenthamarakshan, C. R.; Rajeshwar, K.; Tacconi, E. J. *J. Phys. Chem. B* **2005**, *109*, 11953.
- (486) Rammelt, U.; Hebestreit, N.; Fikus, A.; Plieth, W. *Electrochim. Acta* **2001**, *46*, 2363.
- (487) Vu, Q.-T.; Pavlik, M.; Hebestreit, N.; Rammelt, U.; Plieth, W.; Pflieger, J. *React. Funct. Polym.* **2005**, *65*, 69.
- (488) Szaciłowski, K.; Macyk, W. *Chimia* **2007**, *61*, 831.
- (489) Guo, X.; Zhang, D.; Zhu, D. *Adv. Mater.* **2004**, *16*, 125.
- (490) Raymo, F. M.; Giordani, S. *Org. Lett.* **2001**, *3*, 3475.
- (491) Raymo, F. M.; Giordani, S. *Org. Lett.* **2001**, *3*, 1833.
- (492) Raymo, F. M.; Giordani, S. *J. Org. Chem.* **2003**, *68*, 4158.
- (493) Raymo, F. M.; Giordani, S. *J. Am. Chem. Soc.* **2002**, *124*, 2004.
- (494) Jiménez, D.; Martínez-Máñez, R.; Sancenón, F.; Ros-Lis, J. V.; Soto, J.; Benito, A.; García-Breijo, E. *Eur. J. Inorg. Chem.* **2005**, 2393.
- (495) Bantia, S.; Samanta, A. *Eur. J. Org. Chem.* **2005**, 4967.
- (496) Zhou, W.; Li, Y.; Liu, H.; Wang, S.; Li, C.; Yuan, M.; Liu, X.; Zhu, D. *Chem. Asian J.* **2006**, *1*, 224.
- (497) Zhao, L.; Sui, D.; Chai, J.; Wang, Y.; Jiang, S. *J. Phys. Chem. B* **2006**, *110*, 24299.
- (498) Szaciłowski, K.; Oszejca, J.; Barbieri, A.; Karocki, A.; Sojka, Z.; Sostero, S.; Boaretto, R.; Stasicka, Z. *J. Photochem. Photobiol., A* **2001**, *143*, 99.
- (499) Szaciłowski, K.; Oszejca, J.; Stochel, G.; Stasicka, Z. *J. Chem. Soc., Dalton Trans.* **1999**, 2353.
- (500) Pischel, U. *Angew. Chem., Int. Ed.* **2007**, *46*, 4026.
- (501) Credi, A. *Angew. Chem., Int. Ed.* **2007**, *46*, 5472.
- (502) Margulies, D.; Melman, G.; Shanzer, A. *J. Am. Chem. Soc.* **2006**, *128*, 4865.
- (503) de Silva, A. P.; McClenaghan, N. D. *J. Am. Chem. Soc.* **2000**, *122*, 3965.

- (504) Brown, G. J.; de Silva, A. P.; Pagliari, S. *Chem. Commun.* **2002**, 2461.
- (505) Margulies, D.; Melman, G.; Felder, C. E.; Arad-Yellin, R.; Shanzer, A. *J. Am. Chem. Soc.* **2004**, *126*, 15400.
- (506) Andréasson, J.; Kodis, G.; Terazono, Y.; Liddell, P. A.; Bandyopadhyay, S.; Mitchell, R. H.; Moore, T. A.; Moore, A. L.; Gust, D. *J. Am. Chem. Soc.* **2004**, *126*, 15926.
- (507) Andréasson, J.; Straight, S. D.; Kodis, G.; Park, C.-D.; Hamburger, M.; Gervald, M.; Albinsson, B.; Moore, T. A.; Moore, A. L.; Gust, D. *J. Am. Chem. Soc.* **2006**, *128*, 16259.
- (508) Qu, D.-H.; Wang, Q.-C.; Tian, H. *Angew. Chem., Int. Ed.* **2005**, *44*, 5296.
- (509) Yeow, E. K. L.; Steer, R. P. *Phys. Chem. Chem. Phys.* **2003**, *5*, 97.
- (510) Remacle, F.; Weinkauff, R.; Levine, R. D. *J. Phys. Chem. A* **2006**, *110*, 177.
- (511) Zhou, Y.; Wu, H.; Qu, L.; Zhang, D.; Zhu, D. *J. Phys. Chem. B* **2006**, *110*, 15676.
- (512) Guo, X.; Zhang, D.; Zhang, G.; Zhu, D. *J. Phys. Chem. B* **2004**, *108*, 11942.
- (513) Langford, S. J.; Yann, T. *J. Am. Chem. Soc.* **2003**, *125*, 11198.
- (514) Coskun, A.; Deniz, E.; Akkaya, E. U. *Org. Lett.* **2005**, *7*, 5187.
- (515) Pérez-Inestrosa, E.; Montenegro, J.-M.; Collado, D.; Suau, R.; Casado, J. *J. Phys. Chem. C* **2007**, *111*, 6904.
- (516) Suresh, M.; Jose, D. A.; Das, A. *Org. Lett.* **2006**, *9*, 441.
- (517) Suresh, M.; Ghosh, A.; Das, A. *Tetrahedron Lett.* **2007**, *48*, 8205.
- (518) Pérez-Inestrosa, E.; Montenegro, J.-M.; Collado, D.; Suau, R.; Casado, J. *J. Phys. Chem. C* **2007**, *111*, 6904.
- (519) Sun, W.; Zheng, Y.-R.; Xu, C.-H.; Fang, C.-J.; Yan, C.-H. *J. Phys. Chem. C* **2007**, *111*, 11706.
- (520) Liu, Y.; Jiang, W.; Zhang, H.-Y.; Li, C.-J. *J. Phys. Chem. B* **2006**, *110*, 14231.
- (521) Remacle, F.; Weinkauff, R.; Steinitz, D.; Kompa, K. L.; Levine, R. D. *Chem. Phys.* **2002**, *281*, 363.
- (522) Remacle, F.; Schlag, E. W.; Selzle, H.; Kompa, K. L.; Even, U.; Levine, R. D. *Proc. Natl. Acad. Sci. U.S.A.* **2001**, *98*, 2973.
- (523) Kuznetz, O.; Salman, H.; Shakkour, N.; Eichen, Y.; Speiser, S. *Chem. Phys. Lett.* **2008**, *451*, 63.
- (524) Hameroff, S. R. *Ultimate Computing. Biomolecular Consciousness and Nanotechnology*; Elsevier Science Publishers B.V., 1987.
- (525) Bähler, J.; Svetina, S. *J. Theor. Biol.* **2005**, *237*, 210.
- (526) Simpson, M. L.; Saylor, G. S.; Fleming, J. T.; Applegate, B. *Trends Biotechnol.* **2001**, *19*, 317.
- (527) Wolf, D. M.; Arkin, A. P. *Curr. Opin. Microbiol.* **2003**, *6*, 125.
- (528) Gramß, T.; Bornholdt, S.; Groß, M.; Mitchell, M.; Pellizzari, T. *Non-Standard Computation*; Wiley-VCH: Weinheim, Germany, 1998.
- (529) Hayes, B. *Amer. Sci.* **2001**, *89*, 204.
- (530) Buchler, N. E.; Gerland, U.; Hwa, T. *Proc. Natl. Acad. Sci. U.S.A.* **2003**, *100*, 5136.
- (531) Kramer, B. P.; Fischer, C.; Fussenegger, M. *Biotechnol. Bioeng.* **2004**, *87*, 478.
- (532) Sharma, V. *BioTeach J.* **2004**, *2*, 53.
- (533) Beneson, Y.; Gil, B.; Ben-Dor, U.; Adar, R.; Shapiro, E. *Nature* **2004**, *429*, 423.
- (534) Egorov, I. K. *Biomol. Eng.* **2007**, *24*, 293.
- (535) Kräutler, B. *Angew. Chem., Int. Ed.* **2005**, *44*, 4288.
- (536) Stoddard, C. D.; Batey, R. T. *ACS Chem. Biol.* **2007**, *1*, 751.
- (537) Gong, Y.; Zhang, Z. *FEBS Lett.* **2005**, *579*, 5265.
- (538) Gupta, S.; Bisht, S. S.; Kukreti, R.; Jain, S.; Brahmachari, S. K. *J. Theor. Biol.* **2007**, *244*, 463.
- (539) Muramatsu, S.; Kinbara, K.; Taguchi, H.; Ishii, N.; Aida, T. *J. Am. Chem. Soc.* **2006**, *128*, 3764.
- (540) Weissman, J. S.; Hohl, C. M.; Kovalenko, O.; Kashi, Y.; Chen, S.; Braig, K.; Saibil, H. R.; Fenton, W. A.; Horwich, A. L. *Cell* **1995**, *83*, 577.
- (541) Mayhew, M.; da Silva, C. R.; Martin, J.; Erdjument-Bromage, H.; Tempst, P.; Hartl, F. U. *Nature* **1996**, *379*, 420.
- (542) Baron, R.; Lioubashevski, O.; Katz, E.; Niazov, T.; Willner, I. *J. Phys. Chem. A* **2006**, *110*, 8548.
- (543) Baron, R.; Lioubashevski, O.; Katz, E.; Niazov, T.; Willner, I. *Org. Biomol. Chem.* **2006**, *4*, 989.
- (544) Niazov, T.; Baron, R.; Katz, E.; Lioubashevski, O.; Willner, I. *Proc. Natl. Acad. Sci. U.S.A.* **2006**, *103*, 17160.
- (545) Baron, R.; Lioubashevski, O.; Katz, E.; Niazov, T.; Willner, I. *Angew. Chem., Int. Ed.* **2006**, *45*, 1572.
- (546) Hjelmfelt, A.; Weinberger, E. D.; Ross, J. *Proc. Natl. Acad. Sci. U.S.A.* **1992**, *89*, 383.
- (547) Niemz, A.; Rotello, V. M. *Acc. Chem. Res.* **1999**, *32*, 44.
- (548) Hjelmfelt, A.; Weinberger, E. D.; Ross, J. *Proc. Natl. Acad. Sci. U.S.A.* **1991**, *88*, 10983.
- (549) Pita, M.; Katz, E. *J. Am. Chem. Soc.* **2008**, *130*, 36.
- (550) Tomizaki, K.-y.; Mihara, H. *J. Am. Chem. Soc.* **2007**, *129*, 8345.
- (551) Saghatelian, A.; Volker, N. H.; Guckian, K. M.; Lin, V. S.-Y.; Ghadiri, M. R. *J. Am. Chem. Soc.* **2003**, *125*, 346.
- (552) Ogasawara, S.; Fujimoto, Y. K. *ChemBioChem* **2007**, *8*, 1520.
- (553) Gianneschi, N. C.; Ghadiri, M. R. *Angew. Chem., Int. Ed.* **2007**, *46*, 3955.
- (554) Faulhammer, D.; Cukras, A. R.; Lipton, R. J.; Landweber, L. F. *Proc. Natl. Acad. Sci. U.S.A.* **2000**, *97*, 1385.
- (555) Ouyang, Q.; Kaplan, P. D.; Liu, S.; Libchaber, A. *Science* **1997**, *278*, 446.
- (556) Okamoto, A.; Tanaka, K.; Saito, I. *J. Am. Chem. Soc.* **2004**, *126*, 9458.
- (557) Miyoshi, D.; Inoue, M.; Sugimoto, N. *Angew. Chem., Int. Ed.* **2006**, *45*, 7716.
- (558) Stojanović, M. N.; de Prada, P.; Lnadry, D. W. *J. Am. Chem. Soc.* **2000**, *122*, 11547.
- (559) Stojanović, M. N.; de Prada, P.; Landry, D. W. *J. Am. Chem. Soc.* **2001**, *123*, 4928.
- (560) Stojanović, M. N.; Landry, D. W. *J. Am. Chem. Soc.* **2002**, *124*, 9678.
- (561) Stojanović, M. N.; Kolpashchikov, D. M. *J. Am. Chem. Soc.* **2004**, *126*, 9266.
- (562) Pei, R.; Stojanović, M. N. *Anal. Bioanal. Chem.* **2008**, *390*, 1093.
- (563) Stojanović, M.; Mitchell, T. E.; Stefanović, D. *J. Am. Chem. Soc.* **2002**, *124*, 3555.
- (564) Stojanović, M.; Nikić, D. B.; Stefanović, D. *J. Serb. Chem. Soc.* **2003**, *68*, 321.
- (565) Stojanović, M. N.; Stefanović, D. *J. Am. Chem. Soc.* **2003**, *125*, 6673.
- (566) Kolpashchikov, D.; Stojanović, M. *J. Am. Chem. Soc.* **2005**, *127*, 11348.
- (567) Stojanović, M.; Semova, S.; Kolpashchikov, D.; Macdonald, J.; Morgan, C.; Stefanović, D. *J. Am. Chem. Soc.* **2005**, *127*, 6914.
- (568) Lederman, H.; Macdonald, J.; Stefanović, D.; Stojanović, M. *Biochemistry* **2006**, *45*, 1194.
- (569) Macdonald, J.; Li, Y.; Sutović, M.; Lederman, H.; Pendri, K.; Lu, W.; Andrews, B. L.; Stefanović, D.; Stojanović, M. *Nano. Lett.* **2006**, *6*, 2598.
- (570) Yashin, R.; Ruschenko, S.; Stojanović, M. N. *J. Am. Chem. Soc.* **2007**, *129*, 15581.
- (571) [http://optimedical.com/products/opti/opti\\_r.htm](http://optimedical.com/products/opti/opti_r.htm).
- (572) Toffoli, T. *Physica D* **1998**, *120*, 1.

CR068403Q